N72-10051
NASCR-72999

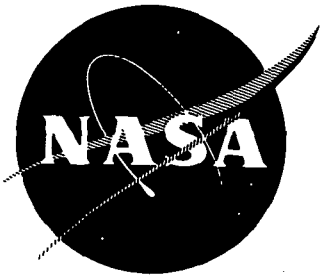

RESEARCH ON RECHARGEABLE OXYGEN ELECTRODES

by

J. Giner
G. Holleck
P.A. Malachesky

Tyco Laboratories, Inc.
Bear Hill
Waltham, Massachusetts 02154

Prepared for

NATIONAL AERONAUTICS AND SPACE ADMINISTRATION

NASA Lewis Research Center

Contract NAS 3-13234

J. Stuart Fordyce, Project Manager

1. Report No.	2. Government Accession No.	3. Recipient's Catalog No.
NASA CR-72999		

4. Title and Subtitle	5. Report Date
Research on Rechargeable Oxygen Electrodes	June 1971
	6. Performing Organization Code

7. Author(s)	8. Performing Organization Report No.
J. Giner, P. A. Malachesky, G. Holleck	C958
	10. Work Unit No.

9. Performing Organization Name and Address	11. Contract or Grant No.
Tyco Laboratories, Inc. Bear Hill Waltham, Massachusetts 02154	NAS3-13234
	13. Type of Report and Period Covered
12. Sponsoring Agency Name and Address	Contractor Report
National Aeronautics and Space Administration Washington, D.C. 20546	14. Sponsoring Agency Code

15. Supplementary Notes

Project Manager, J. Stuart Fordyce, Direct Energy Conversion Division, NASA Lewis Research Center, Cleveland, Ohio.

16. Abstract

Studies have been carried out on a number of factors which may influence the behavior of the platinum electrocatalyst of oxygen electrodes for use in rechargeable metal-oxygen batteries or hydrogen-oxygen fuel cells. The effects of pretreatments at various potentials and added ionic species, which could be present in such systems, have been studied with regard to: (1) the state of surface oxidation, (2) platinum dissolution, (3) the kinetics of oxygen evolution and reduction (including the role of hydrogen peroxide), and (4) changes in porous electrode structure. These studies have been carried out on smooth platinum, platinized platinum, and Teflon-bonded platinum black electrodes in carefully purified electrolyte solutions.

The main factors which appear to affect rechargeable oxygen electrode performance and life are: (1) the buildup of a refractory anodic layer on extended cycling, and (2) the dissolution of platinum. On smooth and platinized platinum electrodes in purified 8.5N KOH, oxygen reduction occurs via hydrogen peroxide as a reactive intermediate. The controlled addition of ionic impurities affects the kinetics of peroxide decomposition. However, these effects do not appear to be important on high surface area fuel cell electrodes. While soluble cadmium species have no significant poisoning effect on oxygen reduction on smooth or platinized platinum electrodes, the precipitation of insoluble cadmium species on the electrode surface does inhibit oxygen reduction. Such precipitation of insoluble cadmium species in porous oxygen electrodes appears to be responsible for effects observed in cadmium-oxygen batteries. Platinum dissolution is enhanced by reduction of the passivating anodic oxygen layer since high anodic potentials alone do not result in significant dissolution. Studies of Teflon-bonded platinum electrodes in half-cells and in full cells have not shown any correlation between decreased performance and changes in electrode structure, aside from loss of electrocatalyst. Periodic high rate discharge to remove the refractory anodic layer formed on cycling seems to be a feasible approach to increasing the performance of

(Abstract continued)

17. Key Words (Suggested by Author(s))	18. Distribution Statement
Oxygen reduction Oxygen evolution Hydrogen Peroxide Decomposition Rotating Ring-Disk Electrodes Teflon-Bonded Platinum Electrodes Anodic Oxygen Layer Platinum Dissolution Fuel Cells Impurity Effects Porous Electrode Theory	Unclassified - unlimited

19. Security Classif. (of this report)	20. Security Classif. (of this page)	21. No. of Pages	22. Price*
Unclassified	Unclassified	236	3.00

* For sale by the National Technical Information Service, Springfield, Virginia 22151

ABSTRACT (continued)

rechargeable oxygen electrodes on extended cycling. Bubbling during gas evolution on charge can disrupt the electrode structure, although theory predicts that this effect is not important with agglomerates less than 1μ in size.

ABSTRACT

Studies have been carried out on a number of factors which may influence the behavior of the platinum electrocatalyst of oxygen electrodes for use in rechargeable metal-oxygen batteries or hydrogen-oxygen fuel cells. The effects of pretreatments at various potentials and added ionic species, which could be present in such systems, have been studied with regard to: (1) the state of surface oxidation, (2) platinum dissolution, (3) the kinetics of oxygen evolution and reduction (including the role of hydrogen peroxide), and (4) changes in porous electrode structure. These studies have been carried out on smooth platinum, platinized platinum, and Teflon-bonded platinum black electrodes in carefully purified electrolyte solutions.

The main factors which appear to affect rechargeable oxygen electrode performance and life are: (1) the buildup of a refractory anodic layer on extended cycling, and (2) the dissolution of platinum. On smooth and platinized platinum electrodes in purified 8.5N KOH, oxygen reduction occurs via hydrogen peroxide as a reactive intermediate. The controlled addition of ionic impurities affects the kinetics of peroxide decomposition. However, these effects do not appear to be important on high surface area fuel cell electrodes. While soluble cadmium species have no significant poisoning effect on oxygen reduction on smooth or platinized platinum electrodes, the precipitation of insoluble cadmium species on the electrode surface does inhibit oxygen reduction. Such precipitation of insoluble cadmium species in porous oxygen electrodes appears to be responsible for effects observed in cadmium-oxygen batteries. Platinum dissolution is enhanced by reduction of the passivating anodic oxygen layer since high anodic potentials alone do not result in significant dissolution. Studies of Teflon-bonded platinum electrodes in half-cells and in full cells have not shown any correlation between decreased performance and changes in electrode structure, aside from loss of electrocatalyst. Periodic high rate discharge to remove the refractory anodic layer formed on cycling seems to be a feasible approach to increasing the performance of rechargeable oxygen electrodes on extended cycling. Bubbling during gas evolution on charge can disrupt the electrode structure, although theory predicts that this effect is not important with agglomerates less than 1μ in size.

Table of Contents

		Page No.
	ABSTRACT	iii
I.	SUMMARY	1
II.	INTRODUCTION	5
III.	PREPARATION OF HIGH PURITY KOH ELECTROLYTE	7
	A. Background	7
	B. Experimental	7
	C. Results and Discussion	11
	D. Conclusions	26
IV.	SURFACE OXIDATION STATE OF PLATINUM IN 8.5N KOH	27
	A. Background	27
	B. Experimental	29
	C. Results and Discussion	29
	D. Conclusions	65
V.	OXYGEN REDUCTION KINETIC STUDIES ON PLATINUM ELECTRODES	67
	A. Background	67
	B. Experimental	73
	C. Results and Discussion	76
	D. Conclusions	146

Table of Contents (Cont.)

		Page No.
VI.	OXYGEN EVOLUTION KINETIC STUDIES	153
	A. Background	153
	B. Experimental	153
	C. Results and Discussion	153
	D. Conclusions	156
VII.	PLATINUM DISSOLUTION STUDIES	157
	A. Background	157
	B. Experimental	158
	C. Results and Discussion	160
	D. Conclusions	165
VIII.	TEFLON-BONDED ELECTRODES	169
	A. Background	169
	B. Experimental	170
	C. Results and Discussion	175
	D. Conclusions	214
IX.	APPLICATION OF THE FLOODED AGGLOMERATE CONCEPT TO RECHARGEABLE O_2 ELECTRODES	221
	A. Introduction	221
	B. The Flooded Agglomerate Model	221
	C. The Anodic Mode of the Oxygen Electrode	226
X.	RECOMMENDATIONS	231
XI.	REFERENCES	233

List of Illustrations

Figure No.		Page No.
1.	Apparatus for Reacting Potassium With Water Vapor	9
2.	Teflon-Quartz Cell for Rotating Ring-Disk Electrode Studies	10
3.	Cyclic Sweep I-E Curves (1 V/Sec-Sweep Rate) Taken at a Smooth Pt Foil Electrode in Unpurified 8.5N KOH (Baker Analyzed Reagent KOH) at 30 °C	12
4.	Cyclic Sweep I-E Curves (1 V/Sec-Sweep Rate) on a Smooth Pt Foil Electrode at 30 °C in Gas Stirred 0.24N KOH Prepared by Reaction of High Purity Potassium Metal with Water Vapor	13
5.	Cyclic Sweep I-E Curves (1 V/Sec-Sweep Rate) on a Smooth Pt Foil Electrode at 30 °C in Gas Stirred 8.5N KOH (Baker Analyzed Reagent)	15
6.	Cyclic Sweeps (1 V/Sec) on a Smooth Pt Foil Electrode in Gas-Stirred 8.5N KOH (Baker Analyzed Reagent) at 30 °C Purified by Treatment With Pt-Black/H_2 for 16 Hr Then Subjected to 32 Hr of Preadsorption at Platinized Platinum	16
7.	Cyclic Sweeps (1 V/Sec) on a Smooth Pt Foil Electrode in Gas-Stirred 8.5N KOH (Baker Analyzed Reagent) at 30 °C After Preadsorption Purification at Platinized Platinum for 120 Hr at 60 °C	17
8.	Cyclic Sweeps (1 V/Sec) on a Rotating Smooth Platinum Disk Electrode (30 rps) in Unpurified 8.5N KOH at 30 °C Prepared From Fluka KOH (Column A) and Baker Analyzed Reagent KOH (Column B)	18
9.	Cyclic Sweep (1 V/Sec) on a Rotating Smooth Platinum Disk Electrode (30 rps) in 8.5N KOH at 30 °C Purified by Preadsorption at Platinized Pt for 16 Hr	19
10.	Cyclic Sweeps (1 V/Sec) on a Rotating Smooth Platinum Disk Electrode (50 rps) in 0.1N KOH	21
11.	Cyclic Sweeps (1 V/Sec) Obtained at a Rotating Smooth Platinum Disk Electrode (50 rps) in 8.5N KOH and 0.1N KOH	22

List of Illustrations (Cont.)

Figure No.		Page No.
12.	Cyclic Sweeps (1 V/Sec) on a Smooth Platinum Disk Electrode (50 rps) in Purified 8.5N KOH After 5 Sec at +0.5 V With Sweeps From +0.5 V to 1.5 V (A) and +0.5 V to +0.9 V (B)	23
13.	Cyclic Sweeps (1 V/Sec) on a Smooth Pt Disk Electrode (30 rps) in Unpurified 8.5N KOH at 30 °C	25
14.	Q_{OX} (μ coul/real cm^2) as a Function of Potential for a Smooth Platinum Foil in Purified 8.5N KOH at 30 °C	31
15.	$Q_{OX}/2Q_H$ as a Function of Potential for a Smooth Platinum Foil in Purified 8.5N KOH at 30 °C After 5 Min at the Potential of Interest	32
16.	Comparison of Q_{OX} (μ coul/real cm^2) Versus Potential Plots on Smooth Platinum Foil in Purified 8.5N KOH Using Galvanostatic and Linear Sweep Stripping Methods	35
17.	Comparison of $Q_{OX}/2Q_H$ Versus Potential Plots on a Smooth Pt Foil in Purified 8.5N KOH Using Galvanostatic and Linear Sweep Stripping Methods	36
18.	Q_{OX} (μ coul/real cm^2) After 2 Min at +1.75 V on a Smooth Platinum Foil in Purified 8.5N KOH at 30 °C as a Function of Time at +1.20 V	38
19.	Current (mA) at +1.75 V Versus Cycle Number for a Smooth Platinum Foil in Purified 8.5N KOH at 30 °C Cycled Under Regime I	40
20.	Current (mA) at +2.0 V Versus Cycle Number for a Smooth Platinum Foil in Purified 8.5N KOH at 30 °C Cycled Under Regime II	44
21.	Q_{OX} and Q_H as a Function of Potential for a Platinized Platinum Foil in Purified 8.5N KOH at 30 °C After 2 Min Anodization	46
22.	$Q_{OX}/2Q_H$ as a Function of Potential for a Platinized Pt Foil in Purified 8.5N KOH at 30 °C After 2 Min Anodization	47
23.	Galvanostatic Potential-Time Curves for a Platinized Platinum Foil in Purified 8.5N KOH at 30 °C After Treatment at +1.75 V for 2 Min (A) and Immediately After 254 Cycles Under Regime I (B)	49
24.	Scanning Electron Micrographs Comparing an Uncycled Pt-Pt Electrode and a Pt-Pt Electrode Cycled 254 Times Under Regime I	51
25.	Further Micrographs of a Scanning Electron Comparing an Uncycled Pt-Pt Electrode and a Pt-Pt Electrode Cycled 254 Times Under Regime I	54
26.	Current (mA) at +1.75 V Versus Cycle Number at a Platinized Platinum Foil in Purified 8.5N KOH at 30°C Cycled Under Regime I	56
27.	Scanning Electron Micrographs Comparing an Uncycled Pt-Pt Electrode and a Pt-Pt Electrode Cycled 254 Times Under Regime II	61

List of Illustrations (Cont.)

Figure No.		Page No.
28.	Further Scanning Electron Micrographs Comparing an Uncycled Pt-Pt Electrode and a Pt-Pt Electrode Cycled 254 Times Under Regime II	63
29.	Current (mA) at +2.0 V Versus Cycle Number at a Platinized Platinum Foil in Purified 8.5N KOH at 30 °C Cycled Under Regime II	66
30.	Rotating Ring-Disk Electrode Assembly	74
31.	Schematic Representation of the Electronic Assembly for Ring-Disk Electrode Voltammetry	75
32.	I_d at E_d = +0.6 V as a Function of Time on a Prereduced Smooth Pt Disk Electrode (60 rps) in Unpurified and Purified 8.5N KOH at 30 °C	78
33.	I_r at E_r = +1.2 V and E_d = +0.6 V as a Function of Time on a Prereduced Smooth Pt Disk Electrode (60 rps) in Unpurified and Purified 8.5N KOH	79
34.	Composite I_d-I_r Versus E_d Curves Obtained by Sweeping From +1.2 to 0.0 V (Forward) Then 0.0 to +1.2 V (Reverse) at 100 mV/Min on a Smooth Pt Disk Electrode (66 rps) at 30 °C in O_2-Saturated 0.1N KOH Which had not Been Purified	80
35.	Composite I_d-I_r Versus E_d Curves Obtained by Sweeping From +1.2 to 0.0 V (Forward) Then 0.0 to +1.2 V (Reverse) at 100 mV/Min on a Smooth Pt Disk Electrode (66 rps) at 30 °C in O_2-Saturated 0.1N KOH Which has Been Subjected to Purification by Preadsorption for 16 hr	81
36.	Composite I_d-I_r Versus E_d Curves Obtained by Sweeping From +1.2 to 0.0 V (Forward) then 0.0 to +1.2 V (Reverse) at 100 mV/Min on a Smooth Pt-Disk Electrode (66 rps) at 30 °C in O_2-Saturated 0.1N KOH Which had Been Subjected to Purification by Preadsorption for 190 hr	82
37.	Composite I_d-I_r Versus E_d Curves Obtained by Sweeping From +1.2 to 0.0 V (Forward) Then 0.0 to +1.2 V (Reverse) at 100 mV/Min on a Smooth Pt Disk Electrode (66 rps) at 30 °C in O_2-Saturated 8.5N KOH Which had not Been Purified	83
38.	Composite I_d-I_r Versus E_d Curves Obtained by Sweeping from +1.2 to 0.0 V (Forward) Then 0.0 to +1.2 V (Reverse) at 100 mV/Min on a Smooth Pt Disk Electrode (65 rps) at 30 °C in O_2-Saturated 8.5N KOH Which Had Been Purified by Preadsorption	84
39.	Steady-State I_d/I_r Versus E_d Curves Obtained During O_2 Reduction at a Prereduced Smooth Platinum Disk Electrode at 64 rps in Purified 8.5N KOH at 30 °C	86

List of Illustrations (Cont.)

Figure No.		Page No.
40.	Steady-State I_d-I_r Versus E_d Curves Obtained During O_2 Reduction at a Preoxidized Smooth Platinum Disk Electrode at 64 rps in Purified 8.5N KOH at 30 °C	87
41.	I_d/I_r Versus $\omega^{-1/2}$ Plots for O_2 Reduction at a Prereduced Smooth Pt Disk Electrode, E_d = +0.85 V, in Unpurified and Purified 8.5N KOH at 30 °C, With E_r = +1.2 V	89
42.	I_d/I_r Versus $\omega^{-1/2}$ Plots for O_2 Reduction at a Prereduced Smooth Pt Disk Electrode, E_d = +0.65 V, in Unpurified and Purified 8.5N KOH at 30 °C, With E_r = +1.2 V	90
43.	I_d/I_r Versus $\omega^{-1/2}$ Plots for O_2 Reduction at a Prereduced Smooth Pt Disk Electrode, E_d = +0.45 V, in Unpurified and Purified 8.5N KOH at 30 °C, With E_r = +1.2 V	91
44.	I_d/I_r Versus $\omega^{-1/2}$ Plots for O_2 Reduction at a Prereduced Smooth Pt Disk Electride, E_d = +0.25 V, in Unpurified and Purified 8.5N KOH at 30 °C, With E_r = +1.2 V	92
45.	I_d/I_r Versus $\omega^{-1/2}$ Plots for O_2 Reduction at Prereduced Smooth Platinum in Purified 8.5N KOH at 30 °C	94
46.	I_d/I_r Versus $\omega^{-1/2}$ Plots for O_2 Reduction at Prereduced Smooth Platinum in Purified 8.5N KOH at 30 °C	95
47.	I_d/I_r Versus $\omega^{-1/2}$ Plots for O_2 reduction at Prereduced and Preoxidized Smooth Pt Disk Electrodes in Purified 8.5N KOH at 30 °C for E_d = +0.45 V	98
48.	I_d Versus $\omega^{1/2}$ Plots for O_2 Reduction at Prereduced and Preoxidized Smooth Pt Disk Electrodes in Purified 8.5N KOH at 30 °C for E_d = +0.45 V	99
49.	I_d/I_r Versus $\omega^{-1/2}$ Plots for O_2 Reduction in Preoxidized Smooth Platinum in Purified 8.5N KOH at 30 °C	101
50.	Plot of the Reciprocal of the Corrected Disk Current, 1/J, Versus $\omega^{-1/2}$ for Prereduced and Preoxidized Smooth Pt Disk Electrodes in Purified 8.5N KOH at 30 °C for E_d = +0.85 V	102
51.	I_d/I_r Versus $\omega^{-1/2}$ Plots for O_2 Reduction at Prereduced and Preoxidized Smooth Pt Disk Electrodes in Purified 0.1N KOH at 30 °C	104
52.	Steady-State I_d-I_r Versus E_d Curves for O_2 Reduction on a Prereduced Platinized Platinum Disk Electrode at 65 rps in Purified 8.5N KOH at 30 °C	106
53.	I_d/I_r Versus $\omega^{-1/2}$ Plots for O_2 Reduction at Prereduced and Preoxidized Smooth Pt Disk Electrodes in Purified 8.5N KOH at 30 °C	117
54.	I_d/I_r Versus $\omega^{-1/2}$ Plots for O_2 Reduction at Prereduced and Preoxidized Smooth Pt Disk Electrodes in Purified 8.5N KOH Saturated With CdO at 30 °C	118

List of Illustrations (Cont.)

Figure No.		Page No.
55.	I_d/I_r Versus $\omega^{-1/2}$ Plots for O_2 Reduction at Prereduced and Preoxidized Smooth Pt Disk Electrodes in Purified 8.5N KOH Saturated with ZnO at 30 °C	119
56.	I_d/I_r Versus $\omega^{-1/2}$ Plots for O_2 Reduction at Prereduced and Preoxidized Smooth Pt Disk Electrodes in Purified 8.5N KOH +0.02M KCl at 30 °C	120
57.	I_d/I_r Versus $\omega^{-1/2}$ Plots for O_2 Reduction at Prereduced and Preoxidized Smooth Pt Disk Electrodes in Purified 8.5N KOH + 0.02M K_2SO_4 at 30 °C	121
58.	I_d/I_r Versus $\omega^{-1/2}$ Plots for O_2 Reduction at Prereduced and Preoxidized Smooth Pt Disk Electrodes in Purified 6.5N KOH+ 1M K_2CO_3 at 30 °C	122
59.	I_d/I_r Versus $\omega^{-1/2}$ Plots for O_2 Reduction at Prereduced and Preoxidized Smooth Pt Disk Electrodes in Purified 8.5N KOH Saturated With Johns-Manville Fuel Cell Asbestos at 30 °C	123
60.	I_d/I_r Versus $\omega^{-1/2}$ Plots for O_2 Reduction at Prereduced and Preoxidized Smooth Pt Disk Electrodes in Purified 8.5N KOH + 100 ppm Fe^{+3} at 30 °C	124
61.	Effects of Cationic Species on the Rate Constant for H_2O_2 Reduction on Prereduced Smooth Platinum as Reflected in the Slopes of I_d/I_r Versus $\omega^{-1/2}$ Plots for O_2 Reduction in KOH Electrolytes at 30 °C	128
62.	Effects of Cationic Species on the Rate Constant for H_2O_2 Reduction on Preoxidized Smooth Platinum as Reflected in the Slopes of I_d/I_r Versus $\omega^{-1/2}$ Plots for O_2 Reduction in KOH Electrolytes at 30 °C	129
63.	Effects of Anionic Species on the Rate Constant for H_2O_2 Reduction on Prereduced Smooth Platinum as Reflected in the Slopes of I_d/I_r Versus $\omega^{-1/2}$ Plots for O_2 Reduction in KOH Electrolytes at 30 °C	130
64.	Effects of Anionic Species on the Rate Constant for H_2O_2 Reduction on Preoxidized Smooth Platinum as Reflected in the Slopes of I_d/I_r Versus $\omega^{-1/2}$ Plots for O_2 Reduction in KOH Electrolytes at 30 °C	131
65.	Composite I_d-I_r Versus E_d Curves Obtained by Sweeping From +1.2 V to 0.0 V (Forward), Then 0.0 V to +0.02 V (Reverse) at 100 mV/Min on a Smooth Pt Disk Electrode (66 rps) at 30 °C in O_2-Saturated Unpurified 0.1N KOH Which Has Been Saturated With CdO	136
66.	Variation in I_d With Cycle Number for a Smooth Pt Disk Electrode Under Regime I (+1.75 V V/10 Min, +0.85 V/ 5 Min) in Purified 8.5N KOH at 30 °C	137

List of Illustrations (Cont.)

Figure No.		Page No.
67.	Variation in I_d With Cycle Number for a Smooth Pt Disk Electrode Under Regime I (+1.75 V/10 Min, +0.85 V/5 Min) in Purified 8.5N KOH Saturated With CdO at 30 °C	138
68.	Variation in I_d With Cycle Number for a Smooth Pt Disk Electrode Under Regime I (+1.75 V/10 Min, +0.85 V/5 Min) in Purified 8.5N KOH Saturated With ZnO at 30 °C	139
69.	Variation in I_d With Cycle Number for a Smooth Pt Disk Electrode Under Regime I (+1.75 V/10 Min, +0.85 V/5 Min) in Purified 8.5N KOH +0.02M KCl at 30 °C	140
70.	Variation in I_d With Cycle Number for a Smooth Pt Disk Electrode Under Regime I (+1.75 V/10 Min, +0.85 V/5 Min) in Purified 8.5N KOH = 0.02M K_2SO_4 at 30 °C	141
71.	Variation in I_d With Cycle Number for a Smooth Pt Disk Electrode Under Regime I (+1.75 V/10 Min, +0.85 V/5 Min) in Purified 6.5N KOH + 1M K_2CO_3 at 30 °C	142
72.	Variation in I_d With Cycle Number for a Smooth Pt Disk Electrode Under Regime I (+1.75 V/10 Min, +0.85 V/5 Min) in Purified 8.5N KOH Saturated With Johns-Manville Fuel Cell Asbestos at 30 °C	143
73.	Variation in I_d With Cycle Number for a Smooth Pt Disk Electrode Under Regime I (+1.75 V/10 Min, +0.85 V/5 Min) in Purified 8.5N KOH Containing 100 ppm Fe^{3+} at 30 °C	144
74.	Variation in I_d During Cycling of a Platinized Platinum Disk Electrode Under Regime I (+1.75 V/10 Min, +0.85 V/5 Min) in O_2-Saturated 8.5N KOH at 30 °C	147
75.	Variation in I_d/I_r During Cycling of a Platinized Platinum Disk Electrode Under Regime I (+1.75 V/10 Min, +0.85 V/5 Min) in O_2-Saturated 8.5N KOH at 30 °C	148
76.	Variation in I_d and I_d^c (the Disk Current Corrected for H_2O_2 Production, $I_d^c = I_d + I_r/N$) During Cycling of a Platinized Platinum-Disk Electrode Under Regime I (+1.75 V/10 Min, +0.85 V/5 Min) in O_2-Saturated 8.5N KOH at 30 °C	149
77.	Variation in I_d During Cycling of a Platinized Platinum Disk Electrode Under a Modified Cycle Regime I Wherein a 30 Sec Pulse to +0.65 V is Inserted Between the +1.75 V and +0.85 V Portions of the Cycle	150
78.	Tafel Plot for Oyxgen Evolution on a Smooth Platinum Disk Electrode in Purified 8.5N KOH at 30 °C	154
79.	Calibration Curve of Optical Absorbance at 394 mμ Versus Concentration of Pt (IV) Using the Stannous Chloride Method	159
80.	Ring Current-Disk Potential Curves for a Gold Ring-Platinum Disk Electrode at 30 rps in H_2-Saturated 8.5N KOH at 30 °C	161

List of Illustrations (Cont.)

Figure No.		Page No.
81.	Experimental Configuration for Platinum Dissolution Studies in 8.5N KOH	163
82.	Ring Current-Disk Potential Curves for a Gold Ring-Platinum Disk Electrode at 60 rps in Argon-Saturated 8.5N KOH After Varying Times at -0.2 V	166
83.	Ring Current-Disk Potential Curve for a Gold Ring-Platinum Disk Electrode at 60 rps in Argon-Saturated 8.5N KOH After 2 hr at -0.2 V	167
84.	Floating Electrode Test Cell	171
85.	Floating Electrode Test Cell Apparatus	172
86.	Testing Rig for Full Fuel Cells	174
87.	Dependence of Q_{ox} and Q_H on Potential For a Teflon-Bonded Platinum Black Electrode in the Floating Electrode Configuration in 8.5N KOH at 30 °C	176
88.	$Q_{ox}/2Q_H$ as a Function of Potential for a Teflon-Bonded Platinum Black Electrode in the Floating Electrode Configuration in 8.5N KOH at 30 °C	177
89.	Oxygen Electrode Potential During Cycling of a (60 Min Charge at 25 mA/cm^2, 30 Min Discharge at 50 mA/cm^2) Teflon-Bonded Platinum Black Electrode in the Floating Electrode Configuration in 8.5N KOH (Cell No. 1) at 30 °C	180
90.	Oxygen Electrode Potential During Cycling (60 Min Charge at 25 mA/cm^2, 30 Min Discharge at 50 mA/cm^2 of a Teflon-Bonded Platinum Black Electrode in the Floating Electrode Configuration in 8.5N KOH Saturated With Johns-Manville Fuel Cell Asbestos (Cell No. 2) at 30 °C	181
91.	Oxygen Electrode Potential During Cycling (60 Min Charge at 25 mA/cm^2, 30 Min Discharge at 50 mA/cm^2) of a Teflon-Bonded Platinum Black Electrode in the Floating Electrode Configuration in 8.5N KOH Saturated with Fe_2O_3 (Cell No. 3) at 30 °C	182
92.	Oxygen Electrode Potential During Cycling (60 Min Charge at 25 mA/cm^2, 30 Min Discharge at 50 mA/cm^2) of a Teflon-Bonded Platinum Black Electrode in the Floating Electrode Configuration in 6.5N KOH/1M K_2CO_3 (Cell No. 4) at 30 °C	183
93.	Oxygen Electrode Potential During Cycling (60 Min Charge at 25 mA/cm^2, 30 Min Discharge at 50 mA/cm^2) of a Teflon-Bonded Platinum Black Electrode in 8.5N KOH (Cell No. 5) at 30 °C	184
94.	Potential-Time Behavior During Cycling of a Teflon-Bonded Platinum Black Oxygen Electrode in the Floating Electrode Configuration in 8.5N KOH (Cell No. 1) at 30 °C for Specified Cycle Numbers	185

List of Illustrations (Cont.)

Figure No.		Page No.
95.	Potential-Time Behavior During Cycling of a Teflon-Bonded Platinum Black Oxygen Electrode in the Floating Electrode Configuration in 6.5N KOH/1M K_2CO_3 (Cell No. 4) at 30 °C for Specified Cycle Numbers	186
96.	Oxygen Electrode Potential During Discharge for Cycles 525-650 for Cells 2 and 4 in the Floating Electrode Configuration	188
97.	Polarization Behavior of Teflon-Bonded Platinum Black Floating Electrodes in 8.5N KOH (Cell No. 1) After Cycling	192
98.	Polarization Behavior of Teflon-Bonded Platinum-Black Floating Electrodes in 8.5N KOH Saturated With Johns-Manville Fuel Cell Asbestos (Cell No. 2) After Cycling	193
99.	Polarization Behavior of Teflon-Bonded Platinum Black Floating Electrodes in 8.5N KOH Saturated With Fe_2O_3 (Cell No. 3) After Cycling	194
100.	Polarization Behavior of Teflon-Bonded Platinum Black Floating Electrodes in 6.5N KOH/1M K_2CO_3 (Cell No. 4) After Cycling	195
101.	Polarization Behavior of Teflon-Bonded Platinum Black Floating Electrodes in 8.5N KOH (Cell No. 5) After Cycling	196
102.	End-of-Charge and Discharge Voltage for a H_2/O_2 Fuel Cell (Cell No. 12) Operating Under a Cycle Regime of a 60 Min Charge Period at 25 mA/cm^2 Followed by a 30 Min Discharge Period at 50 mA/cm^2 in a 8.5N KOH Electrolyte at 30 °C	198
103.	Voltage-Time Curves for Various Cycles During Operation of a H_2/O_2 Fuel Cell (Cell No. 12) Under a Cycle Regime of a 60 Min Charge Period at 25 mA/cm^2 Followed by a 30 Min Discharge Period at 50 mA/cm^2 in a 8.5N KOH Electrolyte at 30 °C	199
104.	End-of-Charge and Discharge Voltages for a H_2/O_2 Fuel Cell. (Cell No. 15) Operating Under a Cycle Regime of a 60 Min Charge Period at 25 mA/cm^2 Followed by a 30 Min Discharge Period at 50 mA/cm^2 in a 8.5N KOH Electrolyte at 30 °C	200
105.	Voltage-Time Curves for Various Cycles During Operation of an H_2/O_2 Fuel Cell (Cell No. 15) Under a Cycle Regime of a 60 Min Charge Period at 25 mA/cm^2 Followed by a 30 Min Discharge Period at 50 mA/cm^2 in a 8.5N KOH Electrolyte at 30 °C	201
106.	End-of-Charge and Discharge Voltages for a H_2/O_2 Fuel Cell (Cell No. 18) Operating Under a Cycle Regime of a 60 Min Charge Period at 25 mA/cm^2 Followed by a 30 Min Discharge Period at 50 mA/cm^2 in a 8.5N KOH Electrolyte Saturated With Fe_2O_3 at 30 °C	202

List of Illustrations (Cont.)

Figure No.		Page No.
107.	Voltage-Time Curves for Various Cycles During Operation of a H_2/O_2 Fuel Cell (Cell No. 18) Under a Cycle Regime of a 60 Min Charge Period at 25 mA/cm^2 Followed by a 30 Min Discharge Period at 50 mA/cm^2 With an 8.5N KOH Electrolyte Saturated With Fe_2O_3 at 30 °C	203
108.	End-of-Charge and Discharge Voltages for a H_2/O_2 Fuel Cell (Cell No. 21) Operating Under a Cycle Regime of a 60 Min Charge Period at 25 mA/cm^2 Followed by a 30 Min Discharge Period at 50 mA/cm^2 With a 6.5N KOH/1M K_2CO_3 Electrolyte at 30 °C	204
109.	Voltage-Time Curves for Various Cycles During Operation of a H_2/O_2 Fuel Cell (Cell No. 21) Under a Cycle Regime of a 60 Min Charge Period at 25 mA/cm^2 Followed by a 30 Min Discharge Period at 50 mA/cm^2 With a 6.5N KOH/1M K_2CO_3 Electrolyte at 30 °C	205
110.	Pore Size Distribution of Uncycled Teflon-Bonded Platinum Black Electrode Material	206
111.	Pore Size Distribution of Teflon-Bonded Platinum Black Electrode Material After 100 Cycles	207
112.	Pore Size Distribution of Teflon-Bonded Platinum Black Electrode Material After 500 Cycles	208
113.	Scanning Electron Microscope Views of American Cyanamid Fuel Cell Electrode Material (AB-40) Sectioned at Room Temperature	210
114.	Scanning Electron Microscope Views of Teflon-Bonded Platinum Black Electrode Material (11 mg Pt/cm^2) Cracked Under Liquid Nitrogen	211
115.	Scanning Electron Microscope Views of Uncycled Teflon-Bonded Platinum Black Electrode Material (11 mg Pt/cm^2) Sectioned Under Liquid Nitrogen	212
116.	Scanning Electron Microscope Views of Teflon-Bonded Platinum Black Electrodes Material After 500 Cycles, Sectioned Under Liquid Nitrogen	214
117.	Photographs of Asbestos Separator From a Shorted-Out H_2/O_2 Fuel Cell	217
118.	Photographs of a Sectioned Asbestos Separator From a Shorted-Out H_2/O_2 Fuel Cell at a Magnification of 50X	218
119.	Effect of Temporarily Short-Circuiting Operating H_2/O_2 Fuel Cells	219
120.	Schematic Representation of a Flooded Cylinder	222

List of Tables

Table No.		Page No.
I	Specifications of KOH Pellets	14
II	Effect of Sweep Rate on the Current Peak at +0.8 V, i_p, and the Ratio of the Anodic Charge, Q_a, to the Cathodic Charge, Q_c, Passed During Cyclic Sweeps from +0.5 to +0.9 V on Smooth Platinum in 8.5N KOH at 30 °C	24
III	Cation Analytical Data for 8.5N KOH	24
IV	Anion Analytical Data for 8.5N KOH	26
V	*Values of Q_{ox}, the Charge Required to Reduce the* Oxygen Layer and $Q_{ox}/2$ Q_H for a Smooth Pt Foil Electrode in Purified 8.5N KOH at 30 °C	30
VI	Comparison of Galvanostatic Stripping at 15 mA/r cm^2 (I) and Linear Sweep Voltammetric Stripping at 1 V/Sec (E) Methods for Determination of Q_{ox} as a Function of Potential for a Smooth Platinum Foil in Purified 8.5N KOH at 30 °C	34
VII	Changes in Q_{ox}, Q_H, and Q_{total} for a Smooth Pt Foil Electrode After Cycling in 8.5N KOH at 30 °C Under Regime I	37
VIII	Changes in Q_{ox}, Q_H, and Q_{total} for a Smooth Pt Electrode After Cycling in 8.5N KOH at 30 °C Under Regime I	39
IX	Results of Extended Anodization (1.75 V/17 Hr) of Platinum Electrodes in Purified 8.5N KOH at 30 °C	41
X	Results of Cycling Under Regime II for Smooth Pt Electrodes in 8.5N KOH at 30 °C	42
XI	Values of Q_{ox}, the Charge Required to Reduce the Oxygen Layer, Q_H, the Charge Required to Deposit a Monolayer of Chemisorbed Hydrogen, and the Ratio $Q_{ox}/2$ QH as a Function of Potential for a Platinized Platinum Foil in Purified 8.5N KOH at 30 °C Using Galvanostatic Pulse of 50 mA	45

List of Tables (Cont.)

Table No.		Page No.
XII	Results of Cycling Under Regime I (10 Min at +1.75 V, Followed by 5 Min at +0.85 V) for Pt-Pt Electrodes in 8.5N KOH at 30 °C	48
XIII	Results of Cycling Eight Different Platinized Platinum Electrodes in Purified 8.5N KOH at 30 °C Under Regime II (10 Min at +2.0 V, Followed by 5 Min at +0.4 V) for Various Number of Cycles	57
XIV	Comparison of the Average Crystallite Size as Determined By X-Ray Diffraction for a Platinized Platinum Electrode Before and After 254 Cycles Under Regime II (10 Min at +2.0 V, Followed by 5 Min at +0.40 V) in 8.5N KOH at 30 °C	60
XV	Ring Current as a Function of Ring Potential for Oxygen Reduction at E_d = +0.6 V on Smooth Pt in 8.5N KOH at 30 °C.	76
XVI	Comparison of I_d/i_r Value at Prereduced and Preoxidized Smooth Platinum Electrodes for Oxygen Reduction in Purified 8.5N KOH at 30 °C	88
XVII	Rotating Ring-Disk Electrode Data for O_2 Reduction on Prereduced Smooth Pt in Purified 8.5N KOH at 30 °C	96
XVIII	Rotating Ring-Disk Electrode Data for Oxygen Reduction on Prereduced Smooth Pt in Purified 8.5N KOH at 30 °C	96
XIX	Summary of Least-Squares Values of the Slope and Intercept of I_d/I_r Versus $\omega^{-1/2}$ Plots Using Data of Table XVII	97
XX	Summary of Least-Squares Values of the Slope and Intercept of I_d/I_r Versus $\omega^{-1/2}$ Plots Using Data of Table XVIII	97
XXI	Rotating Ring-Disk Electrode Data for Oxygen Reduction of Prereduced Smooth Pt in Purified 0.1N KOH at 30 °C	103
XXII	Rotating Ring-Disk Electrode Data for Oxygen Reduction on Preoxidized Smooth Pt in Purified 0.1N KOH at 30 °C	103
XXIII	Rotating Ring-Disk Electrode Data for O_2 Reduction on Prereduced Platinized Platinum in Purified 8.5N KOH at 30 °C	107
XXIV	Rotating Ring-Disk Electrode Data for O_2 Reduction on Preoxidized Platinized Platinum in Purified 8.5N KOH at 30 °C	107
XXV	Rotating Ring-Disk Electrode Data for Oxygen Reduction on Prereduced Smooth Pt in 8.5N KOH Saturated with CdO at 30 °C	108
XXVI	Rotating Ring-Disk Electrode Data for Oxygen Reduction on Preoxidized Smooth Pt in 8.5N KOH Saturated with CdO at 30 °C	109

List of Tables (Cont.)

Table No.		Page No.
XXVII	Rotating Ring-Disk Electrode Data for Oxygen Reduction on Prereduced Smooth Pt in 8.5N KOH Saturated with ZnO at 30 °C	110
XXVIII	Rotating Ring-Disk Electrode Data for Oxygen Reduction on Prereduced Smooth Pt in 8.5N KOH at 30 °C	111
XXIX	Rotating Ring-Disk Electrode Data for Oxygen Reduction on Prereduced Smooth Pt in 6.5N KOH with 1M K_2CO_3 Added at 30 °C	112
XXX	Rotating Ring-Disk Electrode Data for Oxygen Reduction on Preoxidized Smooth Pt in 6.5N KOH with 1M K_2CO_3 Added at 30 °C	112
XXXI	Rotating Ring-Disk Electrode Data for Oxygen Reduction on Prereduced Smooth Pt in 8.5N KOH with 0.02M KCl Added At 30 °C	113
XXXII	Rotating Ring-Disk Electrode Data for Oxygen Reduction on Preoxidized Smooth Pt in 8.5N KOH with 0.02M KCl Added At 30 °C	113
XXXIII	Rotating Ring-Disk Electrode Data for Oxygen Reduction on Prereduced Smooth Pt in 8.5N KOH with 0.02M K_2SO_4 Added at 30 °C	114
XXXIV	Rotating Ring-Disk Electrode Data for Oxygen Reduction on Preoxidized Smooth Pt in 8.5N KOH with 0.02M K_2SO_4 Added at 30 °C	114
XXXV	Rotating Ring-Disk Electrode Data for Oxygen Reduction on Preoxidized Smooth Pt in Purified 8.5N KOH Saturated with Johns-Manville "Fuel Cell Asbestos" at 30 °C	115
XXXVI	Rotating Ring-Disk Electrode Data for Oxygen Reduction on Preoxidized Smooth Pt in Purified 8.5N KOH Saturated with Johns-Manville "Fuel Cell Asbestos" at 30 °C	115
XXXVII	Rotating Ring-Disk Electrode Data for Oxygen Reduction On Prereduced Smooth Pt in Purified 8.5N KOH Containing 100 ppm Fe^{3+}	116
XXXVIII	Rotating Ring-Disk Electrode Data for Oxygen Reduction on Preoxidized Smooth Pt in Purified 8.5N KOH Containing 100 ppm Fe^{3+}	116
XXXIX	Least-Squares Calculated Intercepts of I_d/I_r Versus $\omega^{-1/2}$ Plots in Electrolytes E-1 Through E-8 on Prereduced Smooth Pt	125
XL	Least-Squares Calculated Intercepts of I_d/I_r Versus $\omega^{-1/2}$ Plots in Electrolytes E-1 Through E-8 on Preoxidized Smooth Pt	125

List of Tables (Cont.)

Table No.		Page No.
XLI	Least-Squares Calculated Slopes of I_d/I_r Versus $\omega^{-1/2}$ Plots in Electrolytes E-1 Through E-8 on Prereduced Smooth Pt	126
XLII	Least-Squares Calculated Slopes of I_d/I_r Versus $\omega^{-1/2}$ Plots in Electrolytes E-1 Through E-8 on Preoxidized Smooth Pt	126
XLIII	Rotating Ring-Disk Electrode Data for O_2 Reduction on Prereduced Platinized Platinum in Purified 8.5N KOH Saturated With CdO at 30 °C	132
XLIV	Rotating Ring-Disk Electrode Data for O_2 Reduction on Preoxidized Platinized Platinum Purified 8.5N KOH Saturated With CdO at 30 °C	132
XLV	Rotating Ring-Disk Electrode Data for O_2 Reduction on Prereduced Platinized Platinum in Purified 8.5N KOH Saturated With ZnO at 30 °C	133
XLVI	Rotating Ring-Disk Electrode Data for O_2 Reduction on Preoxidized Platinized Platinum in Purified 8.5N KOH Saturated With ZnO at 30 °C	133
XLVII	Rotating Ring-Disk Electrode Data for O_2 Reduction on Prereduced Platinized Platinum in Purified 8.5N KOH Containing Fe^{3+} (100 ppm) at 30 °C	134
XLVIII	Rotating Ring-Disk Electrode Data for O_2 Reduction on Preoxidized Platinized Platinum in Purified 8.5N KOH Containing Fe^{3+} (100 ppm) at 30 °C	134
XLIX	Percentage Change in Oxygen Reduction Current at +0.85 V and Oxygen Evolution Current at +1.75 V After ~15 Cycles Under Cycle Regime I at 30 °C for Various Electrolytes	145
L	Summary of Tafel Data for O_2 Evolution on Smooth Pt in Various Electrolytes	155
LI	Tafel Parameters for Oxygen Evolution on Platinized Platinum in 8.5N KOH Containing Various Additives at 30 °C	156
LII	Results of Dissolution Studies on Smooth Platinum Foil Electrodes in 8.5N KOH for Various Cycle Regimes	164
LIII	Comparison of Q_{ox} and Q_H After Various Times at +1.05 V for Submerged and Floating Teflon-Bonded Platinum Black Electrodes in 8.5N KOH at 30 °C	178
LIV	Effect of Holding Time at +1.2 V on Measurement of State of Surface Oxidation of a Teflon-Bonded Platinum Black Electrode After 1 Min at +1.70 V	179

List of Tables (Cont.)

Table No.		Page No.
LV	Concentration of Dissolved Platinum in Floating Electrode Cells After Cycling	187
LVI	Concentration of Dissolved H_2O_2 in Floating Electrode Cells After Cycling	189
LVII	Summary of Weight Losses of Teflon-Bonded Platinum Black Electrodes After 680 Cycles	189
LVIII	State of Surface Oxidation Data for Teflon-Bonded Platinum Electrodes After Cycling	190
LIX	State of Surface Oxidation Measurement After 650 Cycles	190
LX	Comparison of Surface Area Measurements on Floating Electrodes Before and After 650 Cycles	191
LXI	BET Surface Area of Uncycled Teflon-Bonded Platinum Electrode Material and Electrodes Cycled 100 and 500 Times	209
LXII	Results of X-Ray Line Broadening Average Particle Size Measurements on Uncycled Teflon-Bonded Platinum Electrode Material and Electrodes Cycles 100 and 500 Times	209

I. SUMMARY

Studies have been carried out on the electrochemical and structural factors influencing the behavior of the platinum electrocatalyst in oxygen electrodes of rechargeable H_2-O_2 fuel cells or metal-air batteries. The areas of study reported here include: (1) the surface oxidation state of smooth and platinized platinum electrodes in 8.5N KOH, including the effect of two cycling regimes on the surface oxidation state, (2) the kinetics and path of oxygen reduction and evolution on smooth and platinized platinum electrodes of different surface oxidation state. in prepurified 8.5N KOH and 0.1N KOH to which controlled additions of ionic species were made, (3) the dissolution of smooth platinum in 8.5N KOH, and (4) factors influencing Teflon-bonded platinum black electrodes operating as rechargeable oxygen electrodes.

Adsorption of impurities at low anodic potentials (+0.1 V) on high surface area platinum black electrodes is an effective purification technique for KOH electrolytes. Metal ions such as Fe^{3+} and Cu^{2+} are removed by this procedure along with adsorbable organic species. Cyclic sweeps on smooth platinum electrodes in prepurified 0.1N KOH show less definition than in prepurified 8.5N KOH. In prepurified 8.5N KOH, a sharply defined current peak is observed at +0.8 V which appears to be related to reversible hydroxyl ion adsorption.

Based on coulometric measurements of the charge equivalent, Q_{ox}, of the anodic platinum-oxygen surface layer, a Pt/O stoichiometry of 1:1 is reached at ~+1.6-1.7 V on both smooth and platinized platinum. No limiting oxygen coverage was found at potentials up to +2.0 V. Potential cycling of smooth platinum under a regime (Cycle Regime I) similar to that encountered by rechargeable oxygen electrodes (10 min at +1.75 V, 5 min at +0.85 V) does not result in any appreciable change in surface oxidation state. Extended anodization at +1.75 V/17 hr results in a small variable (12-27%) increase in Q_{ox}. When platinized platinum is cycled under Regime I, the buildup of a Pt-O layer which is more difficult to reduce than that formed at short times (2 min at +1.75 V) is observed. Removal of this Pt-O layer by cathodic reduction restores the electrode to its original condition, i.e., no change in surface area. Cycling of smooth platinum under a regime of 10 min at +2.0 V followed by 5 min at +0.40 V (Cycle Regime II) leads to an increase of real surface area of up to 95%. However, cycling of a freshly prepared platinized platinum electrode under Regime II leads to a decrease in real surface area apparently due to mechanical loss of platinum black by gas evolution.

Studies of oxygen reduction kinetics and path on preoxidized and prereduced smooth platinum electrodes using the rotating ring-disk electrode technique have been carried out in: (1) 8.5N KOH, (2) 0.1N KOH, (3) 8.5N KOH saturated with CdO, (4) 0.1N KOH saturated with CdO, (5) 8.5N KOH saturated with ZnO, (6) 6.5N KOH containing 1M K_2CO_3, (7) 8.5N KOH containing 0.02M KCl, (8) 8.5N KOH containing 0.02M K_2SO_4, (9) 8.5N KOH saturated with Johns-Manville Fuel Cell Asbestos, and (10) 8.5N KOH containing 100 ppm Fe^{3+}.

The reduction of oxygen on platinum electrodes in the pure KOH electrolytes appears to proceed mainly via hydrogen peroxide as a reactive intermediate. At potentials less than +0.8 V, the observation of hydrogen peroxide is related to the impurity content of the electrolyte. The effect of impurities appears to be primarily on the rate of reduction of H_2O_2. Above +0.8V, even under conditions of high purity and/or high surface area platinized platinum electrodes, H_2O_2 can be observed, presumably due to insufficient overpotential for further H_2O_2 reduction. No conclusive evidence for the presence of a parallel path of oxygen reduction, i.e., the direct four-electron reduction to water, has been obtained, although the presence of the heterogeneous catalytic decomposition of H_2O_2 may be inferred.

The influence of various ionic additives is reflected primarily in terms of hydrogen peroxide accumulation, i.e., peroxide decomposition kinetics, with no mechanistic changes apparent. Cadmium species tend to inhibit H_2O_2 formation while $Zn(OH)_4^{2-}$ and Fe^{3+} apparently inhibit H_2O_2 decomposition. Anionic species such as chloride and sulfate enhance H_2O_2 decomposition whereas carbonate and impurities leached from Johns-Manville Fuel Cell Asbestos tend to inhibit H_2O_2 decomposition. It was observed that soluble cadmiate species do not intrinsically poison oxygen reduction on smooth or platinized platinum. Thus cadmium poisoning of air cathodes in metal-air cells appears to be related to precipitation of insoluble cadmium species.

It has been shown that cycling platinum electrodes under cycle regime I, which is typical of rechargeable oxygen electrodes, leads to marked decreases in oxygen reduction and evolution activity. Since it has been pointed out that preoxidized electrodes have lower O_2 reduction activity than prereduced electrodes, the effects of anodic pretreatment on O_2 reduction are not surprising. However, it is possible by a relatively short time cathodic pulse to restore or maintain oxygen electrode activity. Further work is still needed on the practical implications of this technique over extended periods of cycling.

There does not appear to be any significant effects of the various ionic additives studied on O_2 evolution in 8.5N KOH. I° values are on the order of 10^{-11} A/real cm^2 with Tafel slopes of approximately 100 mV/(~ 2 RT/F).

Under constant potential conditions in the region of +0.85 V to +1.75 V, the corrosion current of smooth Pt electrodes in 8.5N KOH is on the order of 10^{-8} A/cm^2. Potential cycling regimes lead to more dissolution than static potential treatment, especially with a regime of +2.0 V/10 min followed by +0.4 V/5 min. Dissolution seems to be favored by cycling regimes which allow reduction of the Pt-O layer to occur.

The deterioration in performance of rechargeable Teflon-bonded platinum-black oxygen electrodes on extended cycling appears to be largely due to the buildup of a refractory anodic layer. Removal of this anodic layer by cathodic polarization restores electrode activity. Some decrease in performance may be due to loss of platinum electrocatalyst as observed with electrodes tested in the floating electrode configuration, where a 10-20% loss of the catalyst over a period of ~750 hr was found. Platinum which is lost from the oxygen electrode appears to migrate through the separator to the hydrogen side of the separator and can cause short-circuits during full cell operation. No measurable changes in catalyst crystallite size with cycling have been observed, although a BET surface area increase has been observed for an electrode cycled for ~900 hr. There is no appreciable accumulation of hydrogen peroxide, while the controlled addition of impurities such as carbonate and ferric ion has no deleterious effect on cycle life.

A mathematical analysis of the porous Teflon-bonded electrode has shown that the agglomerate size is an important consideration with regard to bubbling during gas evolution on charge. Such bubbling can occur in agglomerates greater than 1 μ and can disrupt the electrode structure. Thus it appears that the homogeneity of the electrode with regard to agglomerate size is more important for rechargeable oxygen-electrodes than for nonrechargeable oxygen cathodes.

Page Intentionally Left Blank

II. INTRODUCTION

Secondary hydrogen - oxygen fuel cells and metal-oxygen batteries are among the most promising high energy density rechargeable power sources under development at the present time. Although the Teflon-bonded platinum electrode originally developed for primary fuel cells has served well as a rechargeable oxygen electrode, it appears for these batteries that it is this electrode which ultimately limits the life of rechargeable hydrogen - oxygen or metal-oxygen cells.[1,2]

There are a number of possible failure modes for such rechargeable oxygen electrodes. One can postulate that extensive cycling leads to the buildup of a refractory oxide layer on the platinum electrocatalyst. In addition, there can be adsorption at the electrode of soluble species, such as impurities arising from the electrolyte or the separator, for example CO_3^{2-}, Cl^-, SO_4^{2-}, and Fe^{3+}, or active material proceeding from the negative electrode, i.e., $Cd(OH)_3^-$ For example, Wagner has reported that soluble cadmiate species poison the air electrode in cadmium-air cells.[3] As a consequence of oxide buildup or impurity adsorption, the overvoltage of O_2-evolution and/or oxygen reduction may increase beyond tolerable limits. In addition, the efficiency of oxygen reduction may decrease, leading to high concentrations of H_2O_2.

Another failure mechanism is platinum dissolution.[4] This Pt dissolution can be affected again by oxide formation (increased overpotential during O_2-evolution, passivation, etc.) and by the presence of impurities (for instance, Cl^- ions, which may have the tendency to complex Pt into solution). As a consequence of Pt dissolution from the cathode, deposition of Pt at the anode can occur which can cause a dendrite short through the separator or decrease the hydrogen overvoltage when working with such a negative material as Zn, or both. Thacker has shown that the cycling at high temperatures of a zinc-oxygen cell with a platinum black positive electrode can lead to the formation of a highly divided platinum black deposit on the zinc electrode which results in a lowered efficiency of the zinc electrode.[5]

There can also be changes in electrode structure which can result in failure due to decreased gas transport, etc. These structural changes can be caused by platinum oxide formation, finite Pt-solubility, with dissolution from some highly energetic surface sites and deposition on other sites (this would result in an increase of crystallite size) and purely mechanical stresses, as would be found during formation of O_2-bubbles as they form inside of the flooded Pt agglomerate. Finally, another failure mechanism can be electrolyte migration as a

consequence of "electrode weeping." This is a phenomenon, not fully understood, by which electrolyte is pumped from the electrolyte side into the back side of the electrode during discharge.

The approach followed in this work is aimed at determining the failure mechanism(s) of rechargeable oxygen electrodes and proposing remedial solutions. It consists of studying the effects of electrode cycling in very pure KOH solutions without and with controlled additions of impurities on: (1) oxide formation, (2) oxygen evolution kinetics, (3) oxygen reduction kinetics (including hydrogen peroxide formation), (4) platinum dissolution, and (5) changes of electrode structure. The total program includes studies on bright platinum, platinized platinum, and Teflon-bonded platinum black electrodes. In a program with such a broad scope, it was at times required to limit the depth of our efforts concerning some areas so that attention could be given to all possible aspects of the problem. Thus one of the purposes of this work has been to define those problem areas of prime importance in oxygen electrode performance.

In Section III of this report, we discuss the preparation of very high purity 8.5N KOH electrolyte. The use of an electrolyte of high purity was necessary in these studies in order to eliminate impurity effects and to help clarify the effect of controlled additions of selected ionic species. Section IV presents a study of the state of surface oxidation of smooth and platinized platinum electrodes under static oxidation conditions and under two different potential cycling regimes. In Section V, a study of the kinetics and path of oxygen reduction on smooth and platinized platinum by the rotating ring disk electrode technique is presented for 0.1N KOH, 8.5N KOH, and 8.5N KOH-based electrolytes containing controlled additions of ionic species. The kinetics of oxygen evolution on smooth and platinized platinum electrodes in various KOH electrolytes are discussed in Section VI. The dissolution of platinum under conditions of potential cycling is considered in Section VII. Section VIII presents a study of the Teflon-bonded platinum black oxygen electrode operating in the rechargeable mode in both the "floating electrode" configuration and in a typical fuel cell configuration. Section IX discusses the use of a mathematical model in considering bubble formation in the agglomerates of the Teflon-bonded oxygen electrode during charge and the effects of changing the physical characteristics of the electrodes on activity. Section X discusses some recommendations for improvements in the construction and operation of fuel cells with rechargeable oxygen electrodes.

III. PREPARATION OF HIGH PURITY KOH ELECTROLYTE

A. Background

In order to carry out meaningful measurements of electrode kinetics and surface state on smooth electrodes, it is necessary to use electrolytes of high purity. The importance of solution purity in studies of oxygen reduction was demonstrated by Damjanovic, et al., who showed that hydrogen peroxide is not formed in the reduction of oxygen in highly purified sulfuric acid.[6,7] The formation of H_2O_2 had been reported by several authors working in the same electrolyte which had not been purified under the same stringent conditions.[8,9] Since we planned to use the rotating ring-disk electrode (RRDE) technique in our studies of oxygen electrode behavior on smooth platinum electrodes, it was imperative to use high-purity electrolytes since, under conditions of convective mass transport at the RRDE, impurity effects are magnified.

B. Experimental

1. Methods of monitoring solution purity

It was necessary to have a method to monitor the purity of the electrolyte to be used in the studies to follow. The method we have used is the measurement of the ability of a smooth platinum electrode to adsorb hydrogen under conditions of forced convection. The following potential sequence is applied to a smooth platinum electrode:

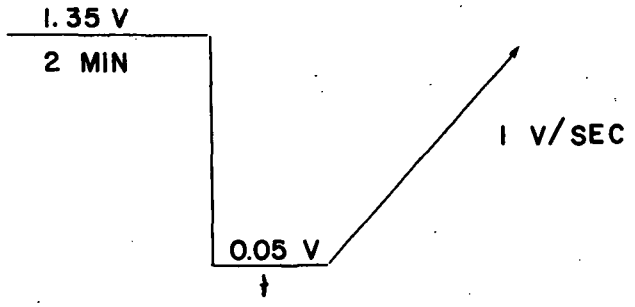

The step at 1.35 V versus RHE for 2 min serves to oxidize or desorb any adsorbed impurities; it also forms a protective oxygen layer. On pulsing the electrode to +0.05 V versus RHE, the oxygen layer is removed (reduced) and at this potential a monolayer of adsorbed hydrogen would be deposited on the platinum surface in an amount corresponding to 210 μcoul/r cm^{2*}

*Real cm^2.

in the absence of impurities. In the presence of impurities, the formation of this layer of adsorbed hydrogen is reduced by a certain fraction corresponding to that portion of the surface now occupied by impurities. The amount of adsorbed hydrogen formed is determined by applying a triangular sweep of 1 V/sec to the electrode and a cyclic I-E curve is oscilloscopically obtained. In a pure electrolyte, the current peaks arising from oxidation of adsorbed hydrogen should be very distinct and independent of the time at +0.05 V. In an impure electrolyte, the hydrogen dissolution peaks become smaller and less distinct.

We have supplemented this electrochemical technique of monitoring solution purity with chemical analysis for metals such as copper, mercury, and iron, and anions such as chloride, sulfate, and carbonate.

2. Method of preparation of high purity KOH electrolyte

We have used two methods to prepare pure KOH electrolytes: (1) the reaction of water with high purity potassium metal, and (2) preadsorption electrolysis at high surface area platinum electrodes.

Fig. 1 shows an all quartz apparatus for the reaction of pure potassium metal with water. Purified argon is saturated with water vapor (CO_2-free, triply-distilled water was used) and passed over potassium in the quartz reaction vessel (second from left). The next vessel is a trap, while a water seal completes the system. The quartz reaction vessel was filled with potassium inside a Vacuum Atmospheres Glove Box.

The technique of preadsorption electrolysis has been used successfully at Tyco previously and consists of adsorbing impurities on a high surface area platinum electrode held at a low anodic potential of +0.1 V versus RHE. While Teflon-bonded platinum black electrodes had been used previously in purification of acid electrolytes, we did not have sufficient initial success with them in highly alkaline KOH and have used a platinized platinum mesh or gauze as a preadsorption electrode in the major portion of our work. This difficulty in using Teflon-bonded electrodes was later traced to the presence of leachable impurities in the electrode. It was found that boiling the fuel cell electrode material in distilled water, followed by cathodic, then anodic polarization in dilute KOH prior to inserting it in the cell eliminated this problem. We have used American Cyanamid AB-4X (9 mg Pt/cm^2) and our own specially prepared Teflon-bonded platinum black on platinum screen electrode material with equal success. Two alternatives are possible as to the cell arrangement. We have carried out preadsorption in the actual cell used in further electrochemical experimentation and also have used a 1-ℓ quartz reaction vessel for the purification of larger quantities of KOH.

3. Electrochemical cell

For the studies of solution purity and also for the study of platinum surface oxidation state and O_2 electrode kinetics, we have used a simple thermostatted cell, made of pure fused quartz of ~ 100-ml capacity. Fig. 2 shows the cell arrangement, as typically used for rotating disk voltammetry. Only quartz and Teflon are in contact with electrolyte. The dynamic hydrogen

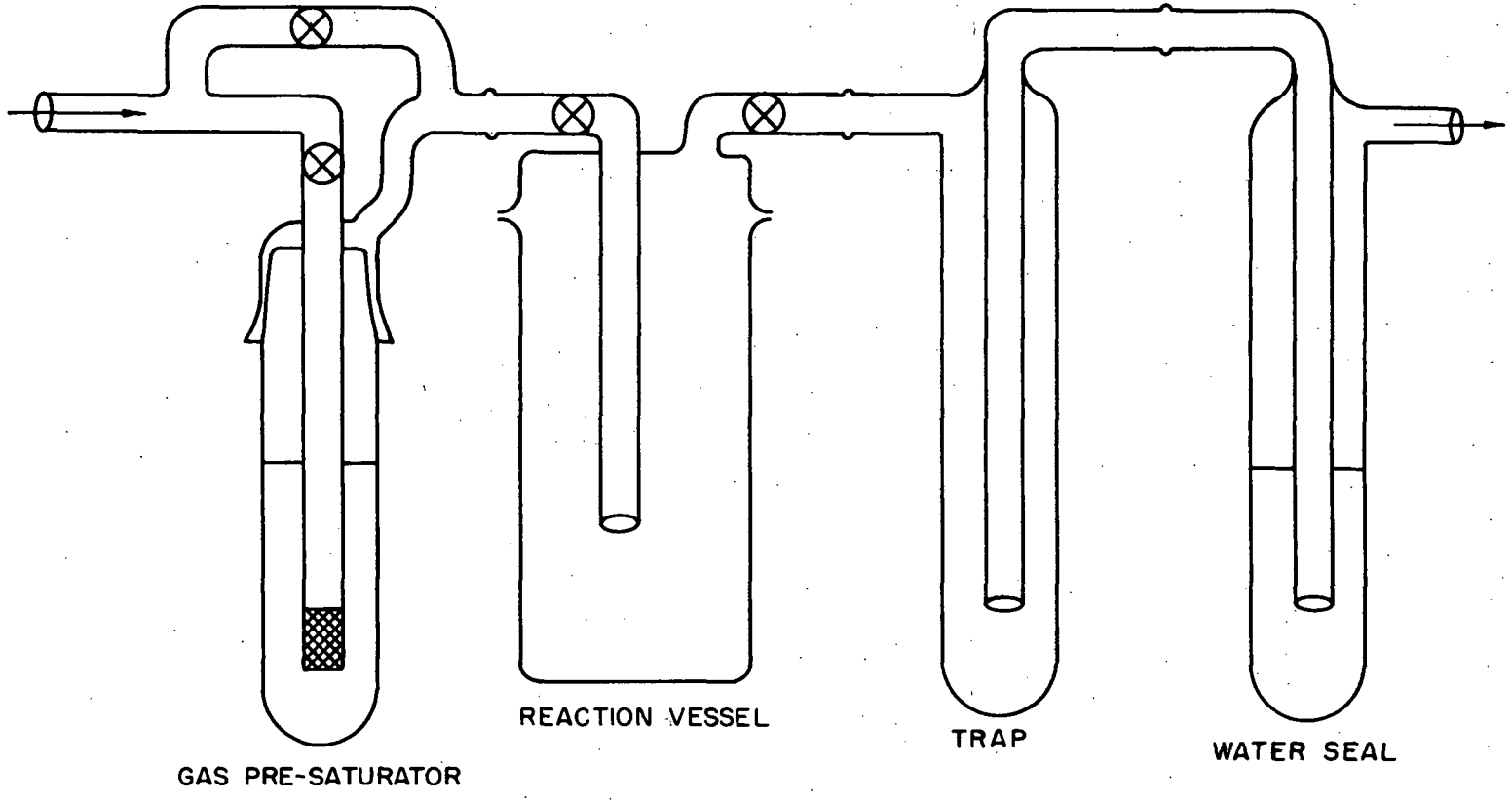

Fig. 1. Apparatus for reacting potassium with water vapor

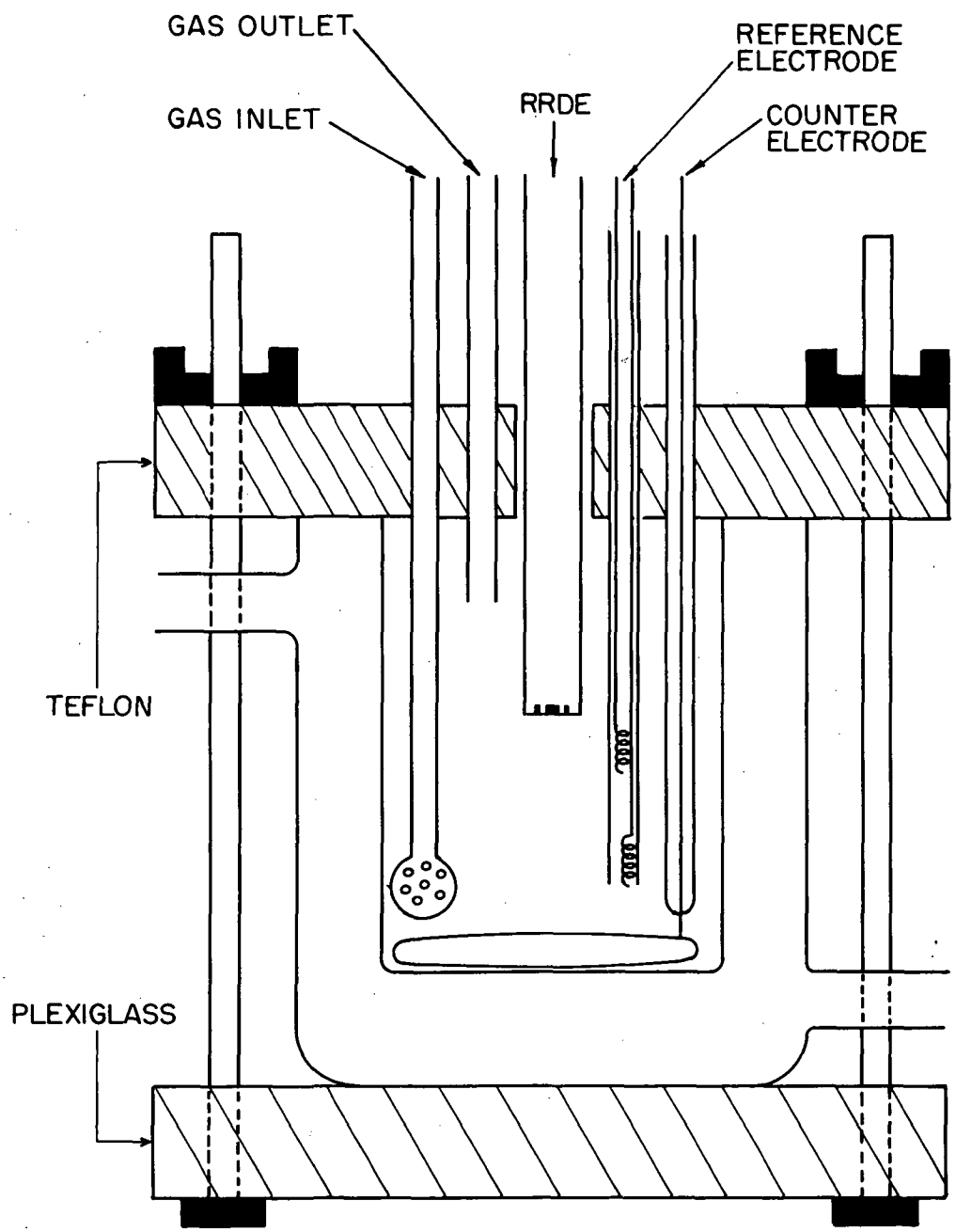

Fig. 2. Teflon-quartz cell for rotating ring-disk electrode studies

electrode (DHE) of Giner served as the reference electrode.[10] Under these conditions, the DHE was found to be -50 mV versus RHE. All potentials have been corrected and are reported versus RHE. Platinized platinum was used for the counterelectrode. All work was carried out at 30 °C.

C. Results and Discussion

In order to establish a baseline to compare the behavior of smooth platinum electrodes in pure 8.5N KOH and impure 8.5N KOH, we made a series of measurements of solution purity using the electrochemical technique described above in 8.5N KOH prepared from Baker Analyzed Reagent KOH and triply-distilled water. Fig. 3 shows the cyclic I-E curves obtained. Fig. 3(a) shows that the hydrogen adsorption region is quite distinct after adsorbing at +0.05 V for 5 sec. Fig. 3(b) shows the cyclic sweep after 5 min at +0.05 V with no stirring of the electrolyte. The hydrogen peaks have decreased and are less distinct. Fig. 3(c) shows the cyclic sweep after 5 min at +0.05 V with stirring by helium gas. Note that the current in the hydrogen region has become much less and that the current in the double layer region, +0.4 to +0.7 V, has increased. Our data show that in this electrolyte complete poisoning of the platinum electrode occurs after 30 min at +0.05 V without gas stirring. In a stirred electrolyte, where mass transport of impurities to the electrode is much greater, complete poisoning occurs in 5 min.

Our initial attempts at preparing a high purity KOH electrolyte were via the reaction of high purity potassium metal (99.99%K, obtained from the High Purity Metals Division of Poly-Research Corporation) with CO_2-free, triply-distilled H_2O in the all quartz apparatus pictured above. A 0.24N KOH solution was obtained and subjected to electrochemical testing of purity.

Fig. 4, column A shows the variation in the cyclic sweeps on a smooth platinum electrode in the stirred 0.24 N KOH electrolyte after various times at +0.05 V. There is a decrease in the magnitude of the hydrogen oxidation current even after 1 min at +0.05 V. After 10 min, the hydrogen region is completely smeared out, while at high potentials, a considerable increase in current can be seen. This electrolyte was then subjected to preadsorption at a platinized platinum foil held at +0.1 V for 16 hr. Fig. 4, column B, shows a definite improvement in solution purity. A further 16-hr preadsorption period gave an electrolyte of high purity, as evidenced from the cyclic sweeps of Fig. 4, column C. These sweeps showed very little difference between adsorption times of 5 sec and 5 min. Using potassium metal supplied by Mine Safety Appliance Company of very high quality (obtained from NASA Lewis) in further work, we found that this method of preparing KOH from pure potassium and water vapor did not lead to very pure material as evidenced from cyclic I-E curves.

These measurements indicated that, although reaction of pure potassium with CO_2-free water appeared to be the best method to eliminate carbonate, preadsorption was still needed to effectively purify the KOH electrolyte thus formed. Therefore, we concentrated our further efforts on preadsorption purification of 8.5N KOH.

In order to have a very high surface area electrode with good mass transport characteristics, we investigated the use of a high surface area Pt black dispersed in the KOH electrolyte

a

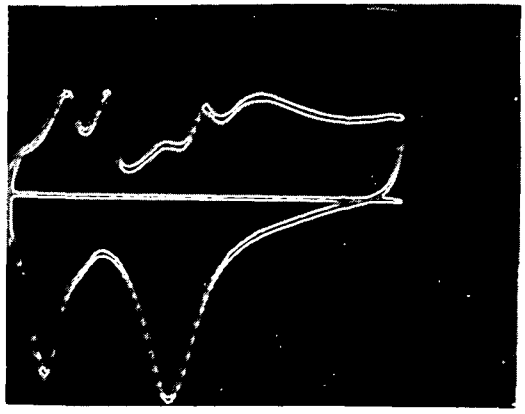

b

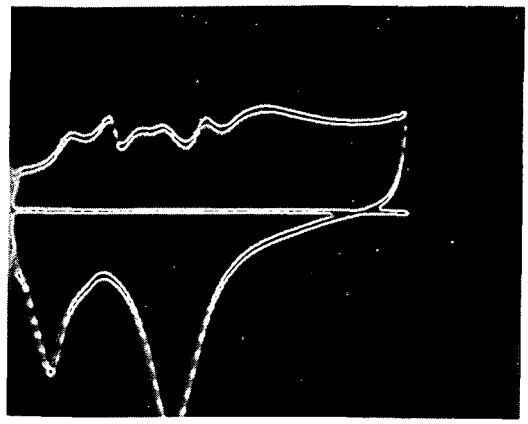

c

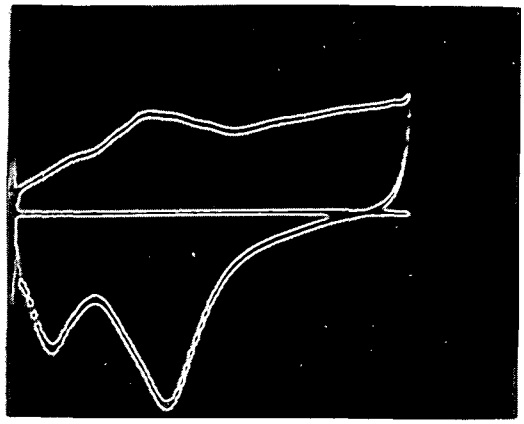

Fig. 3. Cyclic sweep I-E curves (1 V/sec-sweep rate) taken at a smooth Pt foil electrode in unpurified 8.5N KOH (Baker Analyzed Reagent KOH) at 30 °C after: (a) 5 sec at +0.05 V; (b) 5 min at +0.05 V without gas stirring; and (c) 5 min at +0.05 V with gas stirring

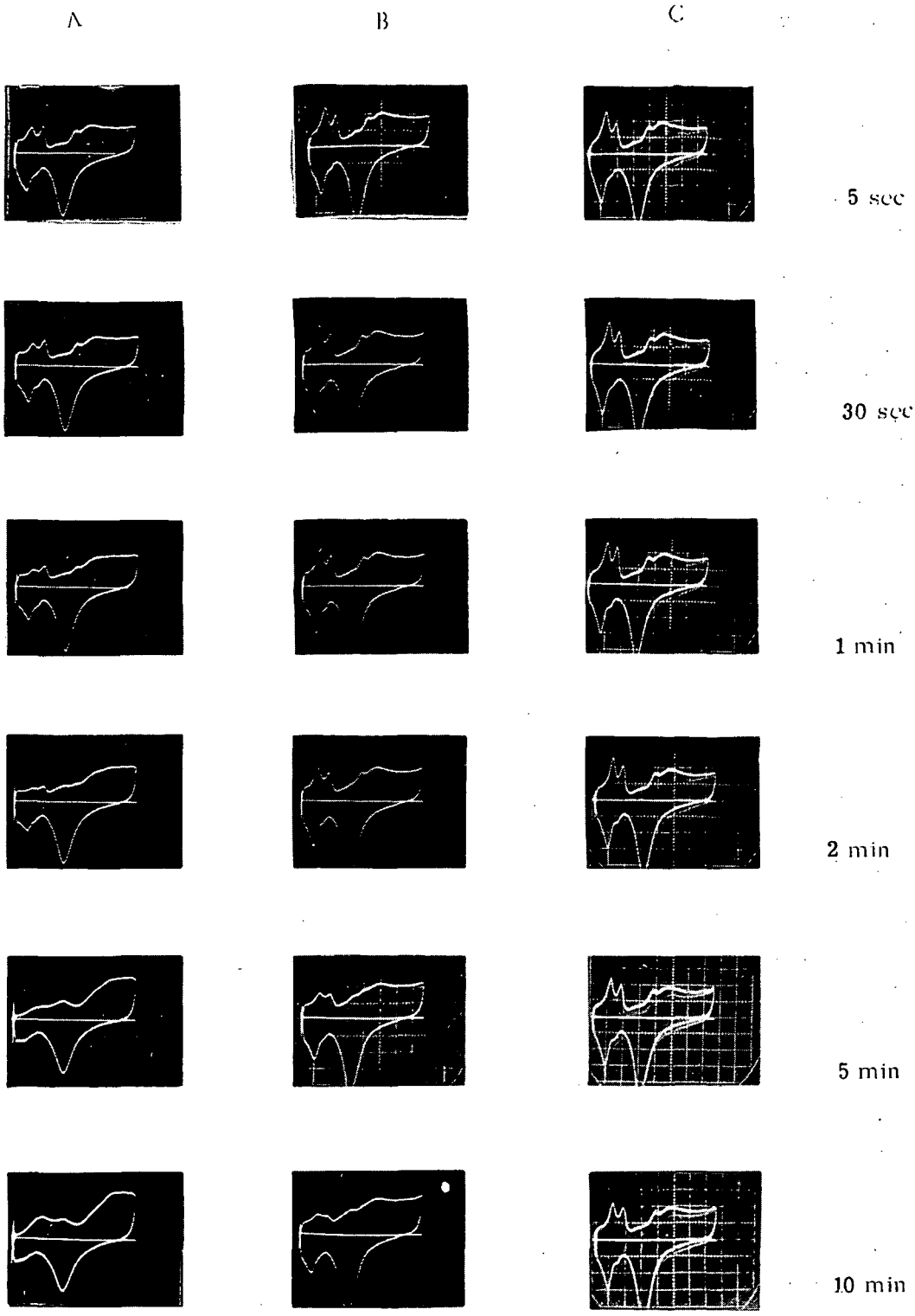

Fig. 4. Cyclic sweep I-E curves (1 V/sec-sweep rate) on a smooth Pt foil electrode at 30 °C in gas stirred 0.24N KOH prepared by reaction of high purity potassium metal with water vapor, after various times at +0.05 V (column A refers to sweeps obtained in the original 0.24N KOH electrolyte, column B depicts sweeps obtained after 16 hr pre-adsorption at +0.1 V using a platinized platinum gauze electrode, and column C refers to sweeps obtained after 32 hr preadsorption)

held at a potential in the hydrogen region by stirring the electrolyte-platinum black mixture with hydrogen gas. Fig. 5(a) shows the cyclic sweep obtained after 5 min at +0.05 V with stirring in an untreated 8.5N KOH electrolyte. Fig. 5(b) depicts the cyclic sweep under the same conditions after a 16-hr treatment with Pt black/H_2. Some improvement can be observed. The Pt black was then removed from the electrolyte by filtration. This electrolyte was then pretreated by preadsorption at a platinized platinum foil at +0.10 V for 16 hr. After this period, the cyclic sweep of Fig. 5(c) was obtained. There is a definite improvement in solution purity after this preadsorption period. A further preadsorption period of 16 hr gave a solution of a very high degree of purity as is shown in Fig. 5(d). Fig. 6 shows cyclic sweeps obtained in this purified electrolyte after various times at +0.05 V with gas stirring. Note that there is still good definition and current level in the hydrogen region after 30 min at +0.05 V.

It was found that a 3- or 4-day period of preadsorption at elevated temperatures (ca. 60° C) was sufficient to eliminate treatment of the 8.5N KOH electrolyte with Pt black at the hydrogen potential. Fig. 7 shows a series of cyclic sweeps carried out in a purified 8.5N KOH prepared by preadsorption at a platinized platinum gauze for 120 hr at 60° C.

At this stage, it was decided to investigate the use of a very pure KOH supplied by Fluka (Kalium hydroxide puriss. p.a.). Table I compares the specifications of Fluka and Baker Analyzed Reagent KOH pellets.

Table I. Specifications of KOH Pellets

	BAR	Fluka
Assay (as KOH)	86.9	$\geq$ 86
K_2CO_3	0.6	$\leq$ 0.6
Chloride	0.003	$\leq$ 0.001
Sulfate	0.001	$\leq$ 0.001
Fe	0.0003	$\leq$ 0.0005

It should be noted here that the impurity levels quoted for the Baker Analyzed Reagent (BAR) KOH pellets are actual lot analysis values, while those given for the Fluka material are maximum impurity limits. It can be seen from Table I that Fluka KOH is lower in chloride. We compared cyclic sweeps on a smooth Pt rotating disk electrode at 30 rps in unpurified 8.5N KOH electrolyte prepared from these two materials. In Fig. 8, unpurified 8.5N KOH prepared from Fluka materials is noticeably "cleaner" than 8.5N KOH prepared from (BAR) material. This difference in initial levels, not obvious from Table II, is substantiated by our finding that a 16-hr preadsorption period at a platinized platinum gauze electrode was sufficient to allow the preparation of 8.5N KOH of high purity using Fluka KOH. Fig. 9 shows cyclic sweeps on a smooth Pt disk electrode at 30 rps in nonpurified 8.5N KOH prepared with Fluka KOH and the same electrolyte purified for 16 hr by preadsorption at a platinized platinum gauze electrode. From sweep 9(C), obtained after 30 min at +0.05 V, it can be observed that a very pure electrolyte can be obtained. Our final procedure for electrolyte purification involved a preadsorption period of 60 hr at +0.1 V. This procedure resulted in a highly purified 8.5N KOH electrolyte

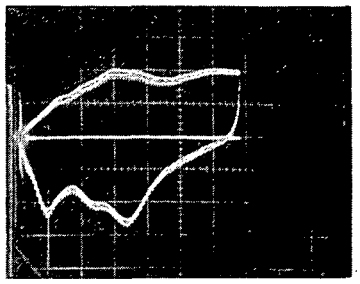

a. Not pre-electrolyzed

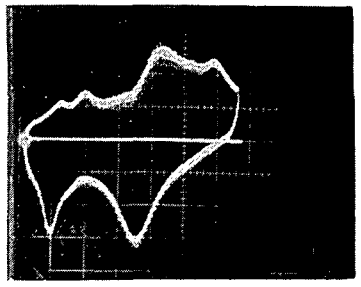

b. Pt black/H_2 for 16 hr

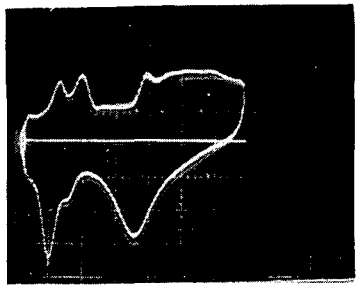

c. Pre-electrolyzed 16 hr at Pt-Pt

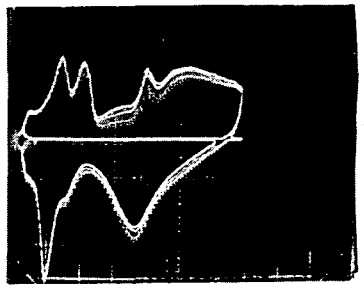

d. Pre-electrolyzed 32 hr at Pt-Pt

Fig. 5. Cyclic sweep I-E curves (1 V/sec-sweep rate) on a smooth Pt foil electrode at 30 °C in gas stirred 8.5N KOH (Baker Analyzed Reagent) after 5 min at +0.05 V

a

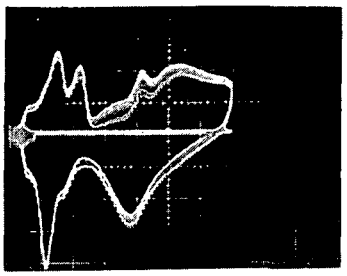

b

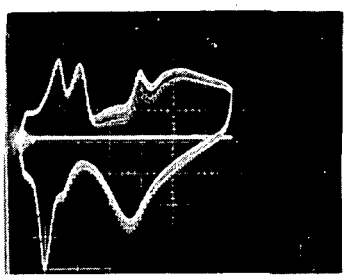

c

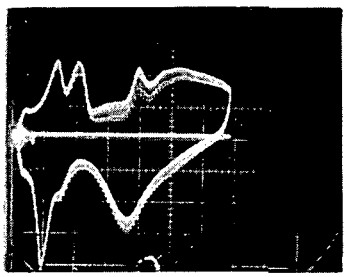

d

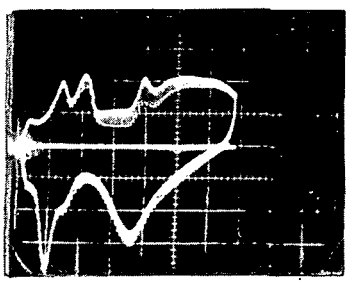

Fig. 6. Cyclic sweeps (1 V/sec) after various times at +0.05 V on a smooth Pt foil electrode in gas-stirred 8.5N KOH (Baker Analyzed Reagent) at 30 °C purified by treatment with Pt black/H_2 for 16 hr then subjected to 32 hr of preadsorption at platinized platinum with times at +0.05 V of: (a) 5 sec; (b) 5 min; (c) 10 min; and (d) 30 min

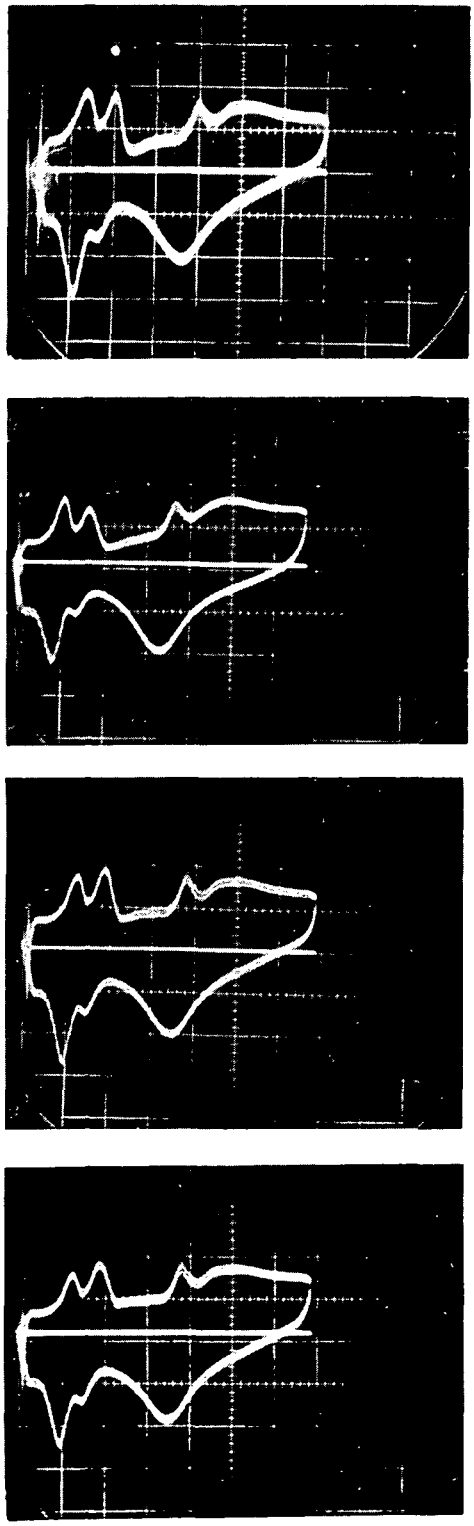

Fig. 7. Cyclic sweeps (1 V/sec) after various times at +0.05 V on a smooth Pt foil electrode in gas-stirred 8.5N KOH (Baker Analyzed Reagent) at 30 °C after preadsorption purification at platinized platinum for 120 hr at 60 °C with times at +0.05 V of: (a) 5 sec; (b) 5 min; (c) 10 min; and (d) 30 min

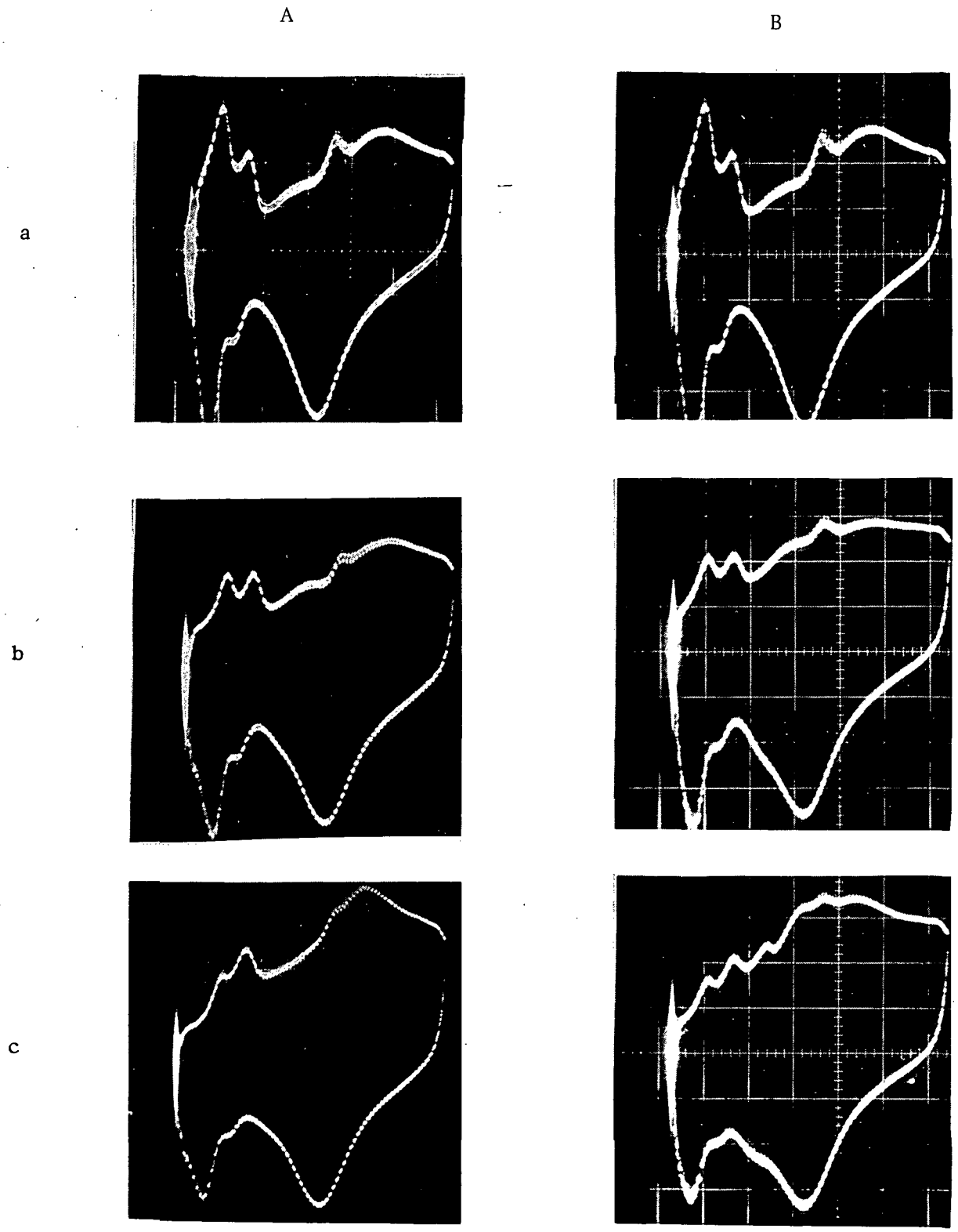

Fig. 8. Cyclic sweeps (1 V/sec) after various times at +0.05 V on a rotating smooth platinum disk electrode (30 rps) in unpurified 8.5N KOH at 30 °C prepared from Fluka KOH (column A) and Baker Analyzed Reagent KOH (column B) after times at +0.05 V of: (a) 5 sec; (b) 5 min; and (c) 30 min

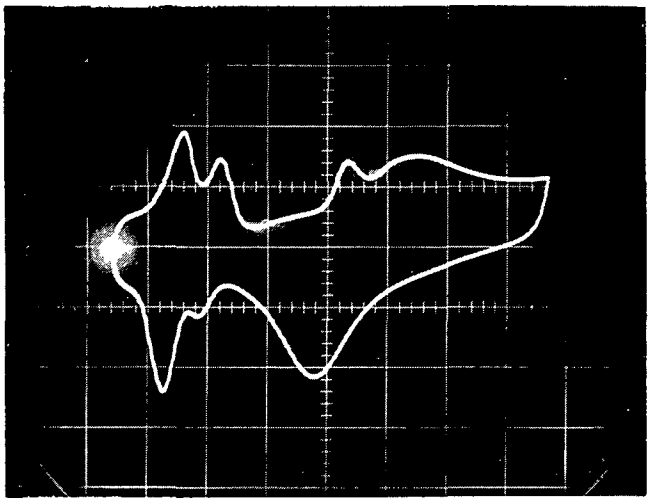

a

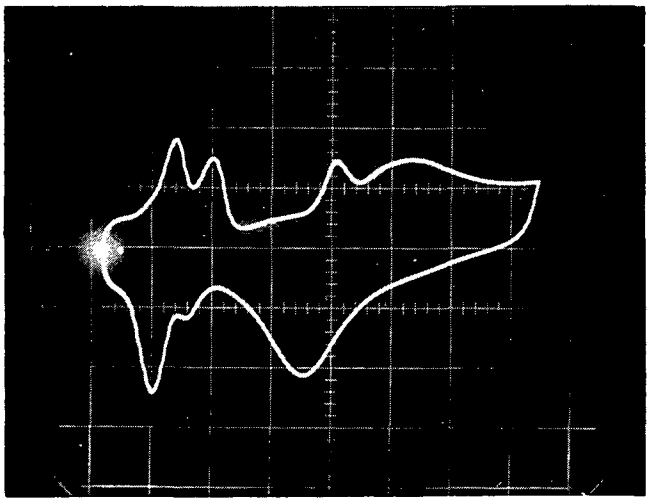

b

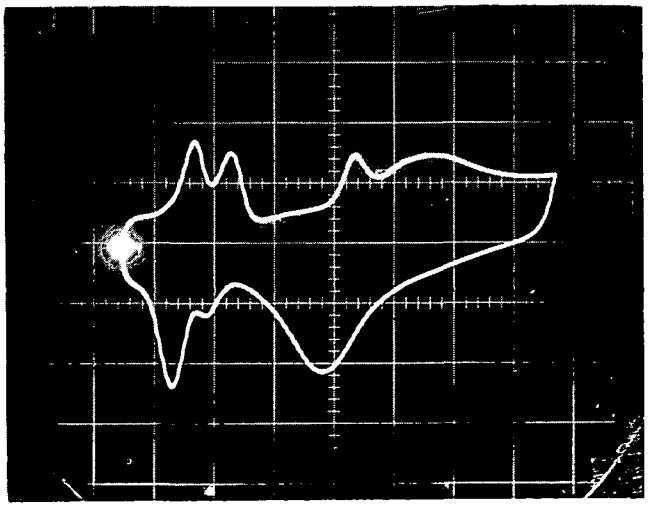

c

Fig. 9. Cyclic sweeps (1 V/sec) after various times at +0.05 V on a rotating smooth platinum disk electrode (30 rps) in 8.5N KOH at 30 °C purified by preadsorption at platinized platinum for 16 hr with times at +0.05 V of: (a) 5 sec; (b) 5 min; and (c) 30 min

which shows identical cyclic sweeps after 5 sec and 30 min at +0.05 V using a smooth Pt disk electrode at 30 rps.

We have also purified 0.1N KOH using the electrochemical preadsorption technique and have found some distinct differences in behavior. Fig. 10 shows the cyclic sweep (1 V/sec) obtained in 0.1N KOH (prepared from Fluka KOH) using a smooth Pt rotating disk electrode at 50 rps. Sweeps a and a' were obtained in the unpurified electrolyte after 5 sec and 30 min at +0.05 V, respectively. Sweeps b and b' were obtained after 16 hr preadsorption, while sweeps c and c' were obtained after a total of 190 hr of preadsorption. Even after this extended preadsorption period, the 0.1N KOH electrolyte does not appear to reach the state of cleanliness observed in 8.5N KOH as evidenced by the decrease in the current corresponding to Pt-H oxidation after 30 min at +0.05 V. This somewhat surprising result may be due to stronger OH^- adsorption in the concentrated KOH which precludes impurity adsorption.

Some features of the cyclic I-E curves presented here for 0.1N KOH and 8.5N KOH merit some discussion. In contrast to the cyclic sweep on smooth platinum in 0.1N KOH reported by Bold and Breiter,[11] two peaks are observed in the hydrogen region. Shumilova, et al., showed cyclic sweeps on platinum electrodes of roughness factor 13 to 18 in preelectrolyzed 1N KOH and 10N KOH.[12] In agreement with our results for 0.1N KOH and 8.5N KOH, the cyclic sweeps obtained by Shumilova in 1N KOH showed less definition than those obtained in 10N KOH. For ease of comparison, Fig. 11 shows cyclic sweeps (1 V/sec) obtained in purified 0.1N KOH and 8.5N KOH on a smooth Pt rotating disk electrode (50 rps) after 5 sec, 5 min, and 30 min at +0.05 V. In the hydrogen region, the anodic peaks for Pt-H are much more defined in the 8.5N KOH electrolyte. More striking is the development of a sharply defined peak at +0.8 V in 8.5N KOH which is quite ill-defined in 0.1N KOH. This "prewave" in the region of Pt-O formation was studied in more detail.

Fig. 12 shows cyclic sweeps (at 0.5 V/sec) on smooth platinum in 8.5N KOH from +0.50 to +1.50 V (sweep A) and +0.50 to +0.9 V (sweep B). The electrode was held at +0.50 V for 5 sec before initiating the sweep. In sweep A, the ratio of the anodic charge to the cathodic charge was 0.96 while in sweep B the corresponding ratio was 1.02. This value of Q_a/Q_c of approximately unity is indicative of complete charge balance as would arise from the formation and dissolution of an adsorbed layer. Table II summarizes the dependence of the peak current, i_p, at +0.8 V and the Q_a/Q_c ratio on the sweep rate for cyclic sweeps from +0.50 to 0.90 V. The i_p/V ratio is essentially independent of sweep rate, V, over two orders of magnitude variation in V, which negates the possibility of a diffusion controlled process such as the deposition and removal of a trace metallic impurity which would show a $V^{1/2}$ dependence. The Q_a/Q_c ratio is also independent of sweep rate. Thus this "prewave" appears to be a "reversible" oxygen or hydroxyl ion adsorption-desorption phenomena in contrast to the irreversible behavior of the oxygen layer formed at potentials greater than 1 V.

Breiter postulated the presence of "reversibly bound oxygen" on platinum in acid solution on the basis of ac capacity measurements.[13] During the anodic portion of a cyclic sweep, large low-frequency capacities were observed by Breiter and were interpreted as a pseudocapacity corresponding to the reaction:

$$Pt + H_2O \rightleftharpoons Pt\,OH + H^+ + e^-$$

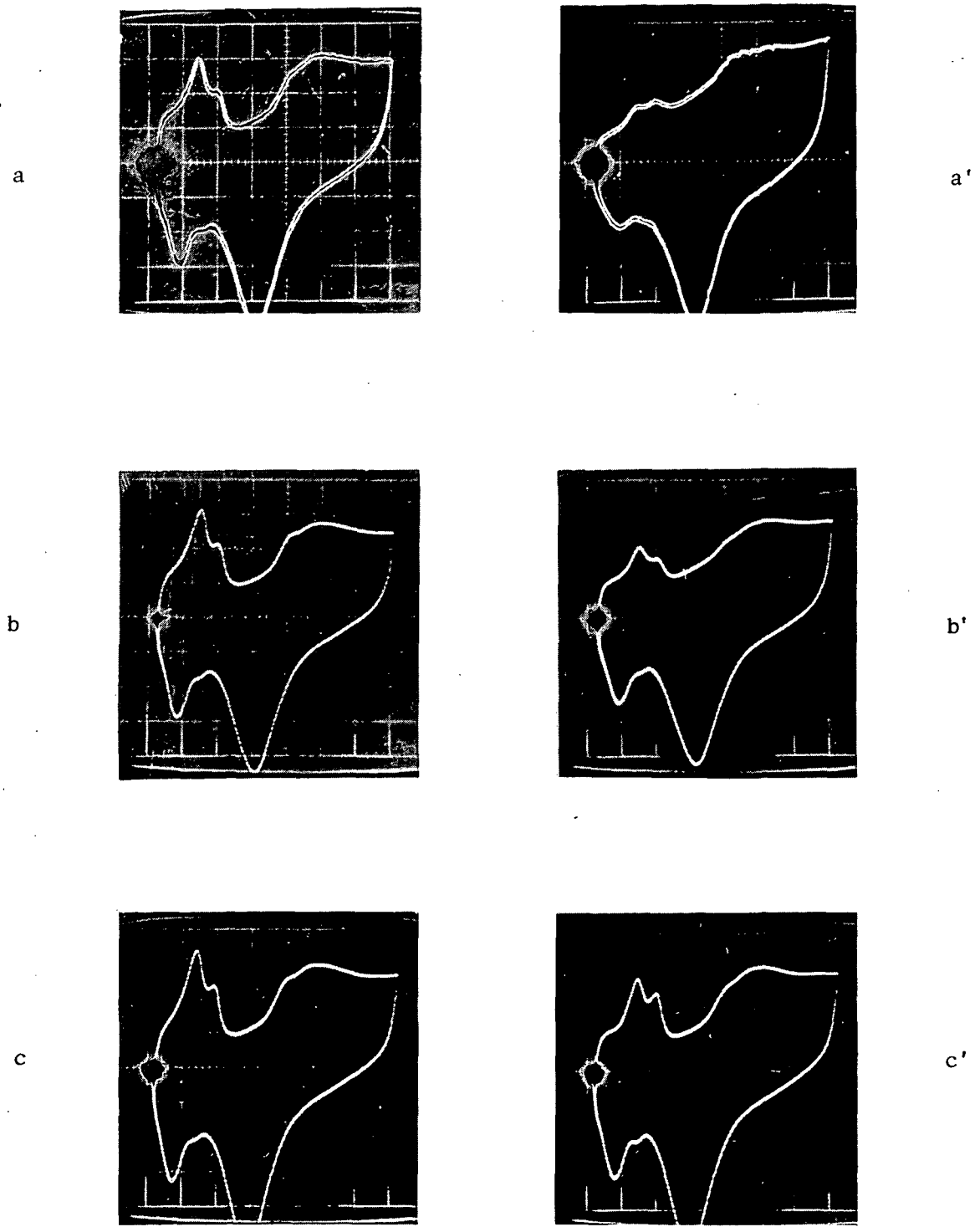

Fig. 10. Cyclic sweeps (1 V/sec) after various times at +0.05 V on a rotating smooth platinum disk electrode (50 rps) in 0.1N KOH prepared from Fluka KOH (sweeps a and a' were obtained in the unpurified electrolyte after 5 sec and 30 min at +0.05 V; sweeps b and b' were obtained after 16 hr preadsorption at a Teflon-bonded Pt black electrode after 5 sec and 30 min at +0.05 V; sweeps c and c' were obtained after 190 hr of preadsorption at a Teflon-bonded Pt black electrode after 5 sec and 30 min at +0.05 V)

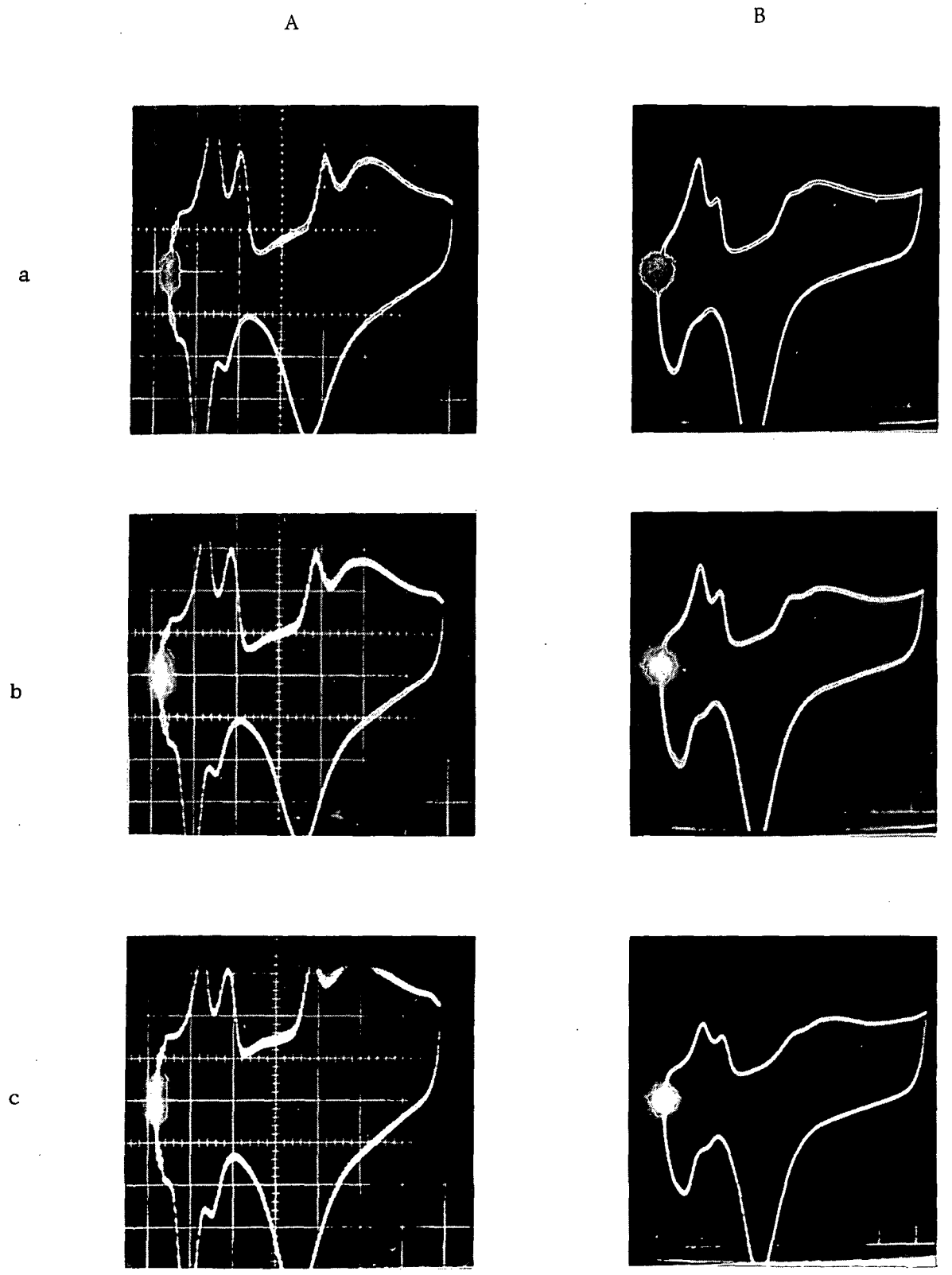

Fig. 11. Cyclic sweeps (1 V/sec) after various times at +0.05 V obtained at a rotating smooth platinum disk electrode (50 rps) after (a) 5 sec; (b) 5 min; and (c) 30 min at +0.05 V in purified 0.1N KOH (column A) and 8.5N KOH (column B)

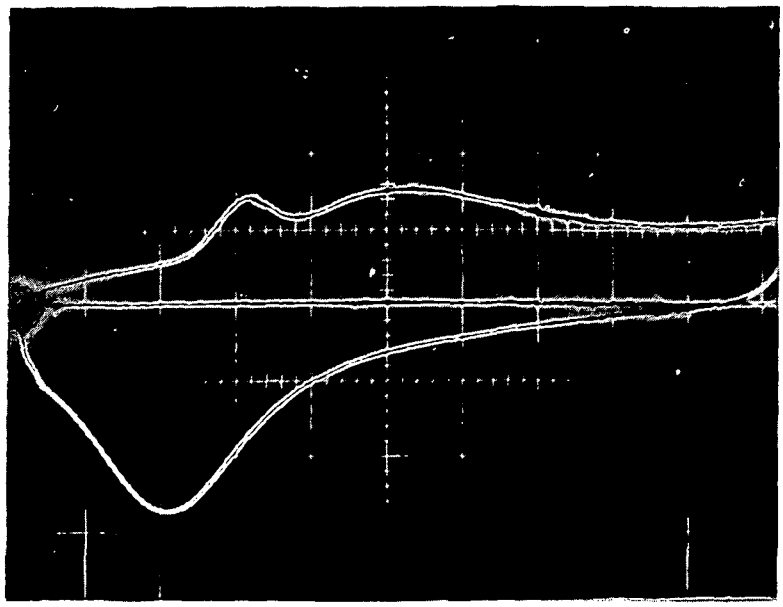

A

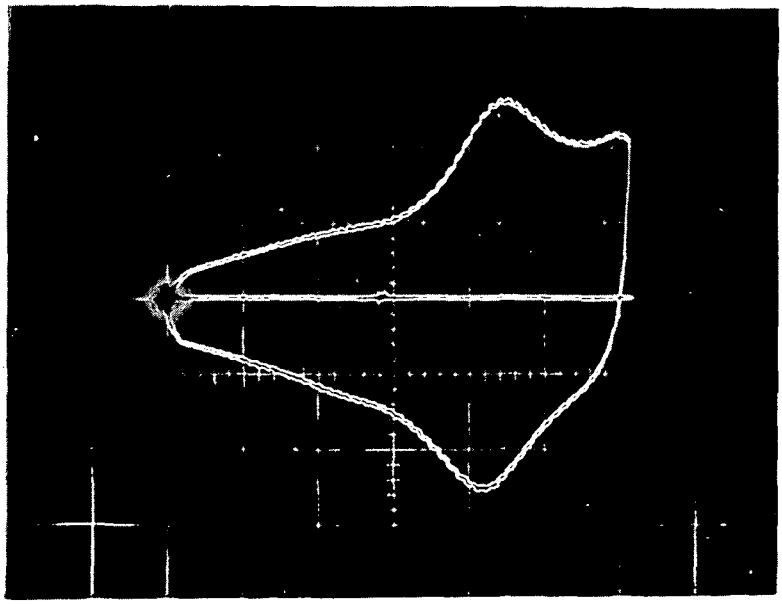

B

Fig. 12. Cyclic sweeps (1 V/sec) after various times at +0.05 V on a smooth platinum disk electrode (50 rps) in purified 8.5N KOH after 5 sec at +0.5 V with sweeps from +0.5 V to +1.5 V (A) and +0.5 V to +0.9 V (B)

that is, to a small concentration of reversibly bound hydroxyl radicals. Also, it has been observed in purified acidic electrolytes that two peaks develop at +0.97 and +1.07 V at the beginning of oxygen deposition.[14] In basic electrolytes, this peak separation may be magnified to give peaks at +0.8 and +1.0 V. However, the broadness of the peak at +1.0 V suggests that it too may be the result from the merger of two peaks. Further work in this area is needed before a definite explanation can be given.

Table II. Effect of Sweep Rate on the Current Peak at +0.8 V, i_p, and the Ratio of the Anodic Charge, Q_a, to the Cathodic Charge, Q_c, Passed During Cyclic Sweeps from +0.5 to +0.9 V on Smooth Platinum in 8.5N KOH at 30° C

V, V/sec	i_p, mA	i_p/V, mA sec/V	Q_a/Q_c
0.05	0.025	0.50	0.91
0.50	0.260	0.52	0.96
5.00	2.00	0.40	0.88

In an impure 8.5N KOH electrolyte, the behavior of cyclic sweeps is of some interest, particularly in the double layer region. Fig. 13 shows a series of cyclic I-E curves taken after various times at +0.5 V. After 5 sec, there is a current peak in the double layer region at +0.65 V. As the time at +0.05 V is increased, this peak grows at the expense of the hydrogen peaks. After 1 min at +0.05 V, there is a splitting of this current peak into two peaks at +0.6 and +0.5 V. This behavior seems to be characteristic of the stripping of metal impurities rather than organic contaminants since most organic species are not chemisorbed at such low potentials.

Quantitative and qualitative analyses have been performed on nonpurified and purified 8.5N KOH. Semiqualitative emission spectroscopy (performed by the Jarrell-Ash Division, Fisher Scientific Company, Waltham, Massachusetts) revealed that iron was the only detectable impurity in the KOH samples tested. Quantitative analyses for Fe, Cu, and Hg performed by atomic absorption (also carried out by Jarrell-Ash Division, Fisher Scientific Company), gave the results of Table III

Table III. Cation Analytical Data For 8.5N KOH (Fluka)*

Sample	Fe*	Cu	Hg	Treatment
1	0.23	0.03	0.25	Purified
2	0.93	0.05	0.34	Nonpurified
3	0.31	0.02	0.37	Purified
4	1.28	0.04	0.45	Nonpurified

* All results in ppm.

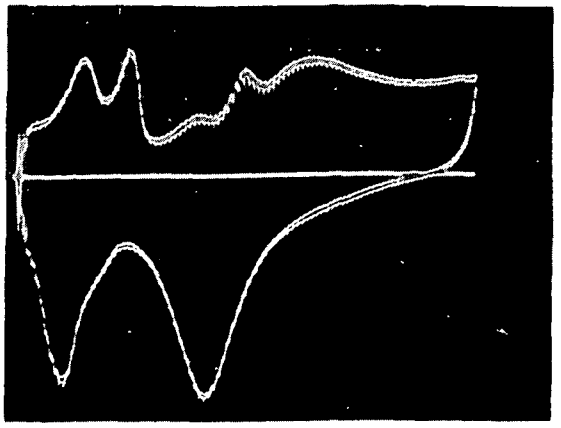

a

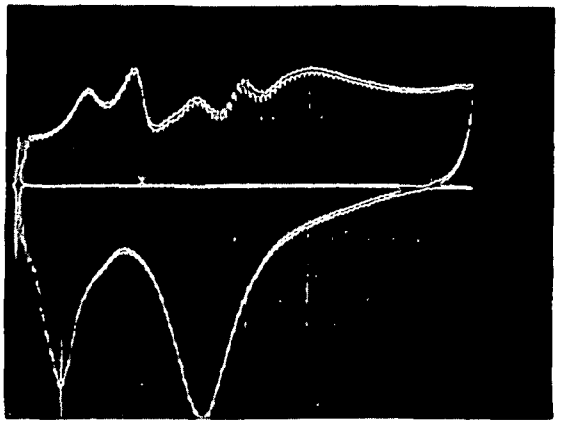

b

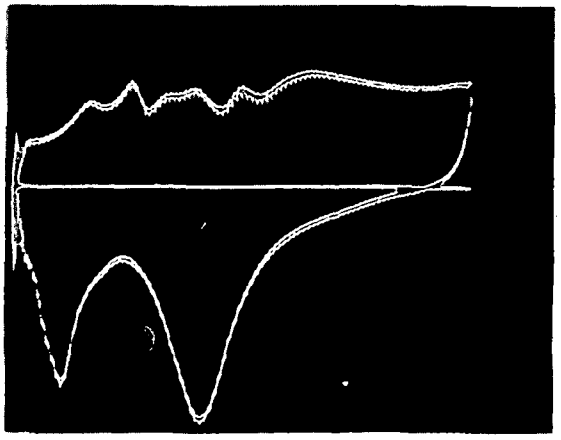

c

Fig. 13. Cyclic sweeps (1 V/sec) after various times at +0.05 V on a smooth Pt disk electrode (30 rps) in unpurified 8.5N KOH at 30 °C after (a) 5 sec; (b) 30 sec; and (c) 60 sec at +0.05 V

From Table III, it can be seen that the concentration levels of Fe, Cu, and Hg are below 1 ppm. Also, preadsorption does appear to be effective in reducing the iron content from ca. 1 ppm to 0.2 to 0.3 ppm.

We have used the chlorite catalyzed reduction of Fe(III) at a dropping mercury electrode in basic media[15] to semiquantitatively estimate the iron content of our 8.5N KOH electrolyte before and after purification by controlled potential adsorption at platinized platinum. With a chlorite concentration of 5×10^{-3}M, the limiting current due to the catalyzed Fe(III) reduction in nonpurified 8.5N KOH (diluted to 0.85N) was 2.43 μA. This current corresponds to an Fe(III) concentration of $\sim 10^{-5}$M prior to dilution. An 8.5N KOH electrolyte (diluted to 0.85N) subjected to purification by preadsorption gave an Fe(III) limiting current of 0.43 μA. This corresponds to an Fe(III) concentration of $\sim 2 \times 10^{-6}$M prior to dilution. Thus, our nonpurified 8.5N KOH electrolyte has an Fe content of $\sim$ 0.4 ppm which can be reduced to less than 0.1 ppm by purification. These results are in agreement with the more quantitative results presented above.

Table IV lists the determined concentration levels (in ppm) for nonpurified and purified 8.5N KOH (Fluka), for chloride, sulfate, and carbonate (analyses performed at Skinner and Sherman, Inc., Newton, Massachusetts). Although our technique of preadsorption does result in removal of Fe and Cu and presumably organic impurities, it does not have a major effect on the concentration levels of these anions. However, except for CO_3^{2-}, their concentration levels are quite low. The carbonate concentration is on the order of 5mM.

Table IV. Anion Analytical Data For 8.5N KOH (Fluka)*

Sample	Cl^-	SO_4^{2-}	CO_3^{2-}	Treatment
1	14	3.2	841	Nonpurified
2	7	<1	561	Nonpurified
3	7	1.6	561	Purified
4	7	<1	561	Purified

*All results in ppm.

D. Conclusions

Adsorption of impurities at low anodic potentials (+0.1 V) on high surface area platinum black electrodes is an effective purification technique for KOH electrolytes. Metal ions such as Fe^{3+} and Cu^{2+} are removed by this procedure along with adsorbable organic species. Cyclic sweeps on smooth platinum electrodes in prepurified 0.1N KOH show less definition than in prepurified 8.5N KOH. In prepurified 8.5N KOH, a sharply defined current peak is observed at +0.8 V which appears to be related to reversible hydroxyl ion adsorption.

IV. SURFACE OXIDATION STATE OF PLATINUM IN 8.5N KOH

A. Background

The subject of the surface state of platinum electrodes has been a favorite subject of controversy among electrochemists. This subject is of considerable importance to the behavior of the rechargeable oxygen electrode since oxygen reduction and evolution occur primarily in a potential region (+0.7 to +1.75 V) where there is an oxygen layer on the platinum electrode surface. There has been much debate on the nature of this oxygen layer. In particular, the primary question has been whether the anodic film on platinum is a monolayer of chemisorbed oxygen or a definite platinum oxide. Most of the evidence on this subject has been obtained using charging curves and cyclic voltammetry and most of the systematic work has been carried out in acidic solutions. The brief discussion of the literature which follows is not intended to be comprehensive but just summarizes several aspects of the nature of the anodic platinum film. More detailed treatments can be found in the article of Gilman[16] and the book of Hoare.[17]

A discussion of the evidence for oxide or chemisorbed oxygen layers on platinum, in acidic solution, with reasons for the latter, was given by Giner.[18] Following this work, Enke and Laitinen and Gilman confirmed this point of view and considerably expanded on the subject.[19,20] The finding by Giner that oxidation of oxalic acid is completely inhibited as soon as Q_{ox} corresponding to the saturation of the Pt-surface with oxygen is reached (but not before) speaks for an even distribution of the oxygen as a monolayer.[21] The controversy has been revived frequently and, in addition, the problem of the ratio of $Q_{ox}/2\ Q_H$ (where Q_{ox} is the measured surface oxidation charge and Q_H is the saturation coverage of the surface with hydrogen) has been added. Part of the difficulties arise from the use of impure solutions and/or the lack of sufficient care in removing gaseous hydrogen and oxygen from the solution close to the working electrode.

With regard to the $Q_{ox}/2\ Q_H$ ratio, it has been reported that the ratio of $Q_{ox}/2\ Q_H$ is close to one when measurements were made in both acidic and basic solutions.[22,23] This ratio corresponds to that commonly measured for hydrogen and oxygen uptake in the gas phase and has bolstered the idea of a chemisorbed film (Pt/O stoichiometry of 1) formed under these conditions. Increases in $Q_{ox}/2\ Q_H$ from unity could be attributed to contamination, since Q_H would decrease and be accompanied by an increase in apparent Q_{ox}, if the contaminants were oxidizable.

However, it should be cautioned that, while the amount of oxygen, Q_{ox}, increases only very slightly with time at potentials below 2 V, at higher potentials the charge equivalent of the film increases progressively until it compares to more than 1 monolayer of chemisorbed oxygen and makes an oxide structure a very reasonable possibility.

Reddy, et al., have interpreted ellipsometry data as indicating a linear increase of the oxygen film with potential up to 1.6 V.[24] This linear increase of thickness goes hand in hand with the observed linear increase of charge. However, this information seems to us of doubtful value since ellipsometry cannot distinguish between chemisorbed oxygen and a phase oxide, especially when the total amount studied is equivalent to a small fraction of a monolayer.

A number of proponents of the "oxide" theory have pointed out that inflections in the anodic charging curves occur which appear to correspond to redox potentials of Pt/Pt-oxide couples. However, Giner showed that such comparisons were based on the appropriate selection of the values of E° for the Pt/Pt-O reaction, and there is considerable doubt about these old measurements on the Pt/Pt-O system and their interpretation.[18]

Mayell and Langer have proposed that there are very definite stoichiometric ratios of oxygen to platinum leading to the formulation of such compounds as $Pt(OH)_2$, PtO_2, PtO, etc.[25] Various potentials were associated with these oxide forms. However, due to the experimental arrangement of Mayell and Langer (a shielded linear diffusion electrode), their results are suspect due to the probable presence of dissolved oxygen.

The latest study of this type by Biegler and Woods supports a model in which oxygen atoms are chemisorbed onto the platinum surface and can be accommodated up to a coverage of about 2.66 oxygen atoms per Pt atom.[26] A limiting coverage, independent of potential and time, was observed which can be taken as evidence for a monolayer of oxygen atoms.

Much of the work which has been discussed concerning the anodic film on Pt electrodes has been done in acidic solutions. Shumilova, et al., studied the coverage of oxygen on Pt in alkaline solutions.[12] At their anodic limit of 1.5 V, Shumilova, et al., found a surface coverage of about 1.5 oxygen monolayers. Sabol and Podlovchenko also studied the properties of the anodic film in basic solutions, with particular reference to the kinetics of film reduction.[27]

The question of impurities arises in considering the nature of the anodic film on platinum electrodes in basic solutions, since cyclic voltammetric curves in alkaline solution do not display the well-reported hydrogen, double-layer, and oxygen film regions as clearly as in acid. This can be attributed to the particular purity problems encountered in alkaline solutions, i.e., carbonate, or to the presence of heavy metals resulting from the attack by the alkaline solution on the conventionally used all glass cells as discussed above.

We have investigated the state of surface oxidation of smooth and platinized platinum electrodes in highly purified 8.5N KOH in fused quartz apparatus as a function of potential. In addition, we have monitored the surface oxidation state changes occurring on smooth and platinized platinum electrodes under these two cycling regimes:

1. Cycle Regime I = 10 min at +1.75 V followed by 5 min at +0.85 V
2. Cycle Regime II =10 min at +2.00 V followed by 5 min at +0.40 V

B. Experimental

The smooth platinum electrodes used here were smooth Pt foils which were flamed to red heat to minimize surface roughness. The "real" electrode area was measured by cathodic H-atom deposition, based on 210 μcoul/cm^2 of hydrogen charge as discussed by Brummer.[28] Platinized platinum electrodes were prepared by deposition onto Pt foils from 5% H_2PtCl_6 solution containing 0.03% lead acetate using a current density of 170 mA/cm^2 in three alternate anodic-cathodic cycles.

Electrochemical measurements were made using a Wenking fast rise potentiostat (Model 61RS) and a laboratory built galvanostat. The potential step generator used to generate the appropriate potential-time relationship has been described elsewhere.[29] For switching from potentiostatic to galvanostatic operation the counter-electrode line was switched with a Hg-wetted relay. For measurement of the charge required to reduce the surface layer by voltammetric stripping, an operational amplifier-based electronic integrator was used. Potential sweeps were obtained using a Hewlett-Packard 202A function generator modified for single shot operation. Potential-time readings were made with a Tektronix Dual Beam Oscilloscope(Model 565) with type 2A63 plugins or a Houston Instruments Recorder (Model 98T), depending on the time scale involved.

All measurements were made in 8.5N KOH purified by the preadsorption technique described previously. High purity argon was used for deaeration and also for stirring.

C. Results and Discussion

1. Surface oxidation state of smooth Pt

Our initial studies of the state of surface oxidation of smooth Pt were carried out by oxidizing a smooth Pt foil at specified potentials in the region of +0.25 to 1.75 V for 5 sec, 1 min, and 5 min. A constant current pulse of 10 mA (5.3 mA/r cm^2) was used to reduce the oxygen layer and the potential-time curve obtained oscilloscopically and photographed. The charge required to reduce the oxygen layer was calculated using the time elapsed from the application of the current pulse to the time required for the Pt electrode potential to reach +0.4 V. Table V gives the measured values of Q_{ox}, the charge required to reduce the oxygen layer, as a function of potential. Fig. 14 shows Q_{ox} as a function of potential for the three times used. Appreciable formation of an oxygen layer does not occur before +0.70 V. There is an almost linear increase in Q_{ox} with increasing E. By comparing Q_{ox} with 2 Q_H (the charge required to deposit a monolayer of chemisorbed hydrogen), after 5 min we can estimate the state of oxidation of the Pt surface. Such a plot of $Q_{ox}/2Q_H$ appears in Fig. 15. The ratio $Q_{ox}/2Q_H$ reaches 1.0 at ~1.60 V. This would correspond to a Pt/O stoichiometry of 1:1. We then made a more detailed study of the state of surface oxidation of smooth Pt in purified 8.5N KOH electrolyte. In particular, we were interested in comparing data obtained using

Table V. Values of Q_{ox}, the Charge Required to Reduce the Oxygen Layer and $Q_{ox}/2\ Q_H$ for a Smooth Pt Foil Electrode in Purified 8.5N KOH at 30 °C

E, Volts*	t, sec	Q_{ox}, μ coul/r cm^2	$Q_{ox}/2\ Q_H$
+0.45	6	3.2	<0.01
	60	2.1	<0.01
	300	1.6	<0.01
+0.60	6	16	0.04
	60	12	0.03
	300	7	0.02
+0.70	6	34	0.08
	60	30	0.07
	300	21	0.05
+0.80	6	70	0.17
	60	72	0.17
	300	63	0.15
+0.90	6	123	0.20
	60	128	0.30
	300	124	0.30
+1.00	6	174	0.41
	60	177	0.42
	300	181	0.43
+1.20	6	252	0.60
	60	259	0.62
	300	275	0.65
+1.40	6	320	0.76
	60	344	0.82
	300	365	0.87
+1.60	6	411	0.98
	60	435	1.04
	300	455	1.08
+1.75	6	548	1.30
	60	556	1.32
	300	545	1.30

*Versus RHE.

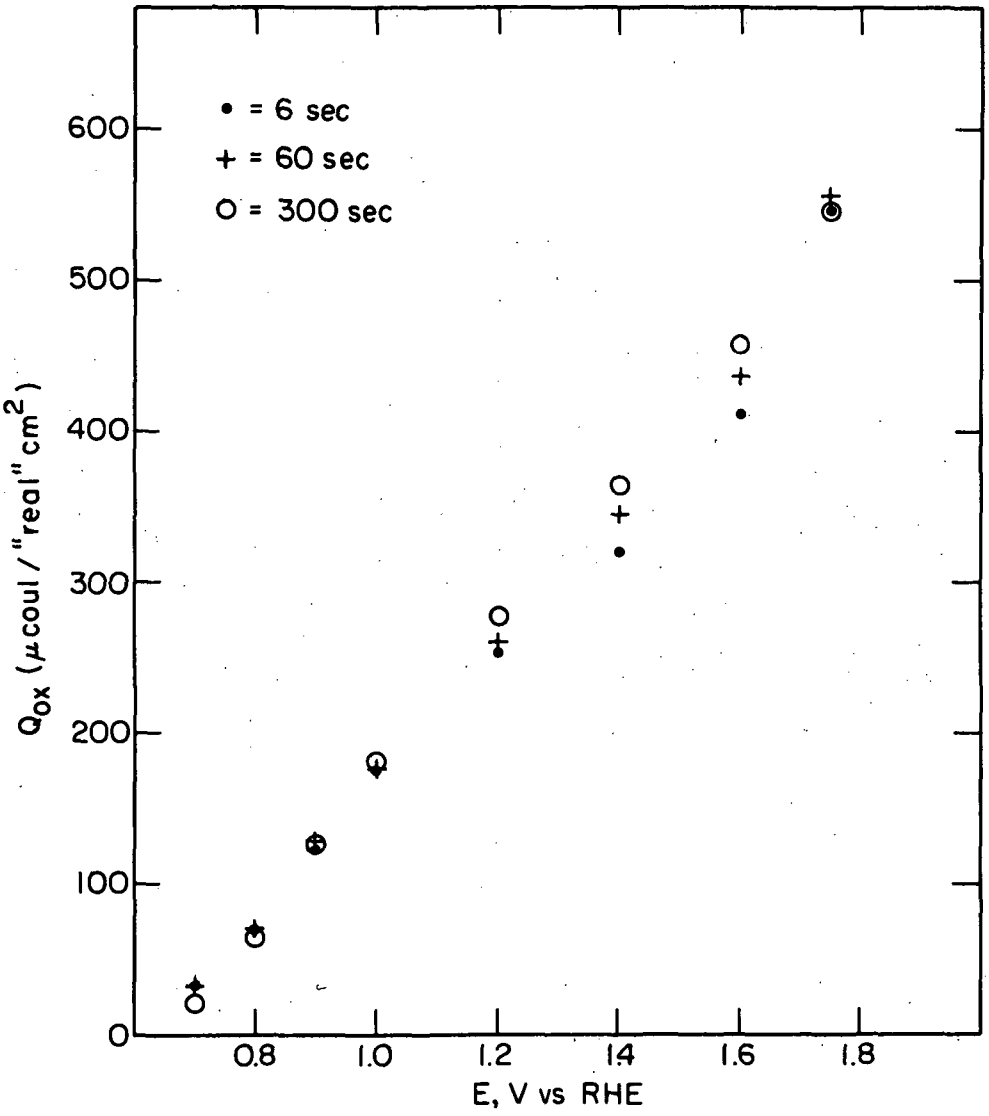

Fig. 14. Q_{ox} (μcoul/real cm^2) as a function of potential for a smooth platinum foil in purified 8.5N KOH at 30 °C

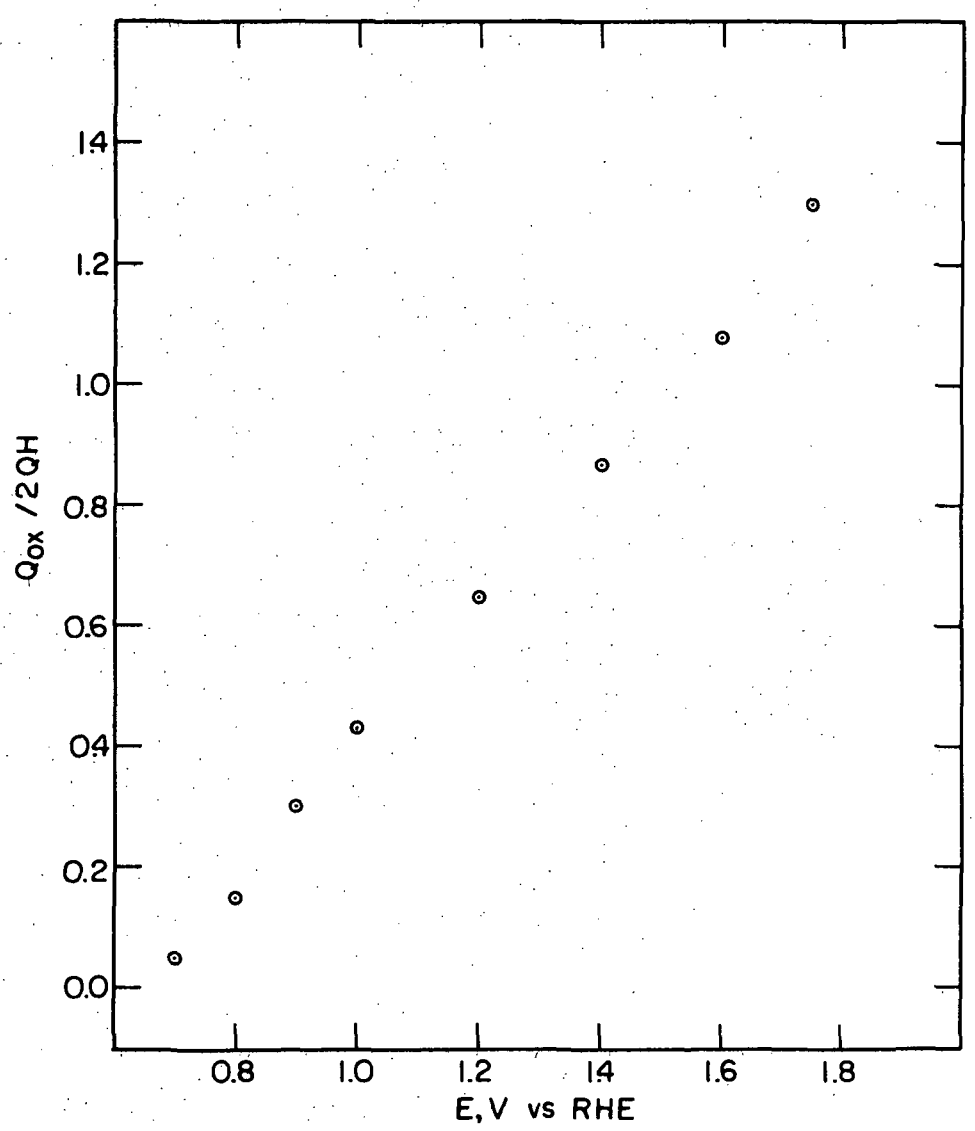

Fig. 15. $Q_{ox}/2Q_H$ as a function of potential for a smooth platinum foil in purified 8.5N KOH at 30 °C after 5 min at the potential of interest

galvanostatic reduction of the oxygen layer with similar data obtained during linear potential sweep voltammetry with current integration giving the charge equivalent of the Pt-oxygen layer. The use of the galvanostatic technique may lead to underestimation of the charge required to reduce the Pt-oxygen layer since some surface reduction may be carried over into the hydrogen region of the cathodic charging curve. In addition, we extended our studies up to +2.0 V.

Table VI compares the charge required to reduce the Pt-oxygen layer as a function of Pt electrode potential using a galvanostatic current pulse (15 mA/r cm^2) and a linear potential sweep technique (1 V/sec) with current integration. In both cases, the charge was calculated to +0.40 V. Q_{ox} versus E and $Q_{ox}/2Q_H$ versus E plots are shown in Figs. 16 and 17 comparing the two techniques. From the data of Table V, Q_{ox} values as measured by the galvanostatic technique are lower which is consistent with our hypothesis of the extension of surface layer reduction into the hydrogen region during a galvanostatic pulse of this magnitude. For measurements at potentials more anodic than +1.5 V, at which considerable molecular oxygen can be evolved, the Pt electrode was brought to +1.0 V for 30 sec to alloy molecular oxygen to be removed. The effect of this change in procedure is reflected as a discontinuity in the plots of Fig. 16. It should be noted that this discontinuity is much larger in the galvanostatically obtained data. This effect is more noticeable because the times required to reduce the surface layer are much shorter in the galvanostatic technique (30 msec) than in the potential sweep technique (1 sec) and thus residual molecular oxygen reduction contributes more charge during the galvanostatic method because sufficient time for O_2-removal is not allowed.

However, it should be mentioned that Biegler and Woods,[26] Becker and Breiter,[30] and Gilman[20] also have reported an "inflexion" at ~1.6 V in plots of Q_{ox} versus E for smooth Pt in acidic solution. Based on the linear sweep results, the stoichometry of the platinum-oxygen layer reached 1 at ~1.6 to 1.7 V. However, no limiting coverage was found at potentials up to +2.0 V.

We then turned to an examination of a suitable procedure for the determination of the state of surface oxidation of smooth platinum after cycling under Regime I (10 min at +1.75 V, 5 min at +0.85 V). Since considerable molecular oxygen is evolved at +1.75 V, its effect must be minimized. By introducing a period at a lower potential before the state of oxidation determination is made, this molecular oxygen should be removed from the immediate vicinity of the electrode. However, there is the possibility that some of the platinum-oxygen layer can be decomposed or reduced simultaneously. Therefore, the potential and duration of this step prior to determination of the surface oxidation state is important. In addition, the current density or rate of potential sweep used to sample the platinum surface oxygen layer is also important since at high current densities or sweep rates the charge contribution of the surface oxygen layer is much more important than any charge from diffusing species, i.e., O_2. On the other hand, high current densities tend to displace surface oxygen layer reduction into the region of hydrogen adsorption and cause some charge arising from surface oxygen layer reduction to be lost.

The first procedure evaluated involved the use of a variable time at open circuit after the 1.75 V step before imposing a galvanostatic measuring pulse. This procedure led to values

Table VI. Comparison of Galvanostatic Stripping at 15 mA/r cm^2 (I) and Linear Sweep Voltammetric Stripping at 1 V/sec (E) Methods for Determination of Q_{ox} as a Function of Potential for a Smooth Platinum Foil in Purified 8.5N KOH at 30 °C

E, volts	I Q_{ox} μcoul/"r" cm^2	E Q_{ox} μcoul/"r" cm^2	I Q_{ox}/Q_H	E Q_{ox}/Q_H
+0.8	66	82	0.16	0.20
+0.9	121	145	0.29	0.35
+1.0	164	205	0.39	0.49
+1.1	204	234	0.48	0.56
+1.2	232	290	0.55	0.69
+1.3	271	327	0.65	0.78
+1.4	312	376	0.75	0.90
+1.5	385	414	0.92	0.99
+1.6	326	409	0.78	0.96
+1.7	360	455	0.86	1.10
+1.8	380	481	0.90	1.15
+1.9	409	516	0.98	1.24
+2.0	431	534	1.03	1.27

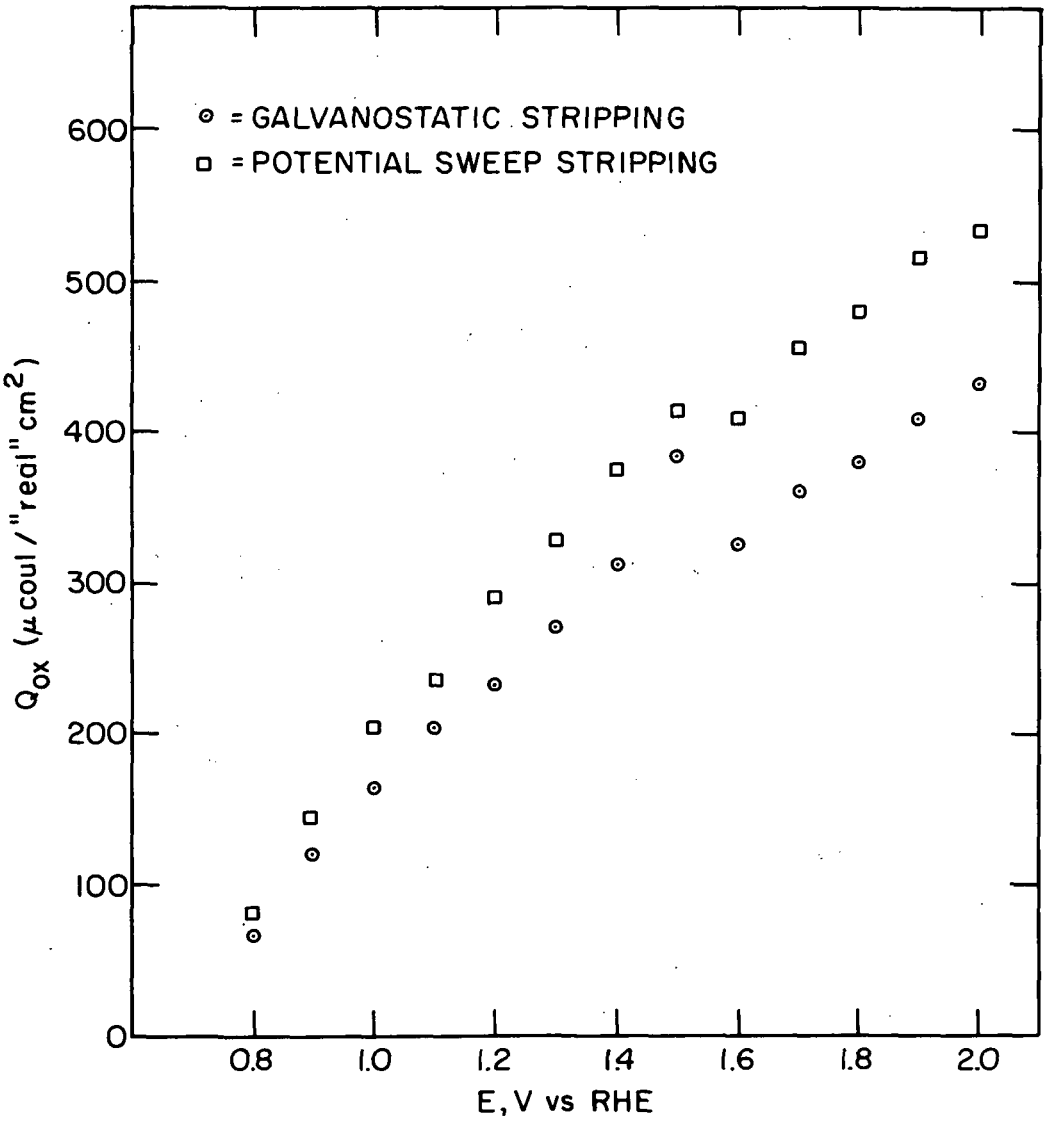

Fig. 16. Comparison of Q_{ox} (μcoul/real cm^2) versus potential plots on smooth platinum foil in purified 8.5N KOH using galvanostatic stripping (⊙) at 15 mA/real cm^2 and linear sweep stripping (□) at 1 V/sec

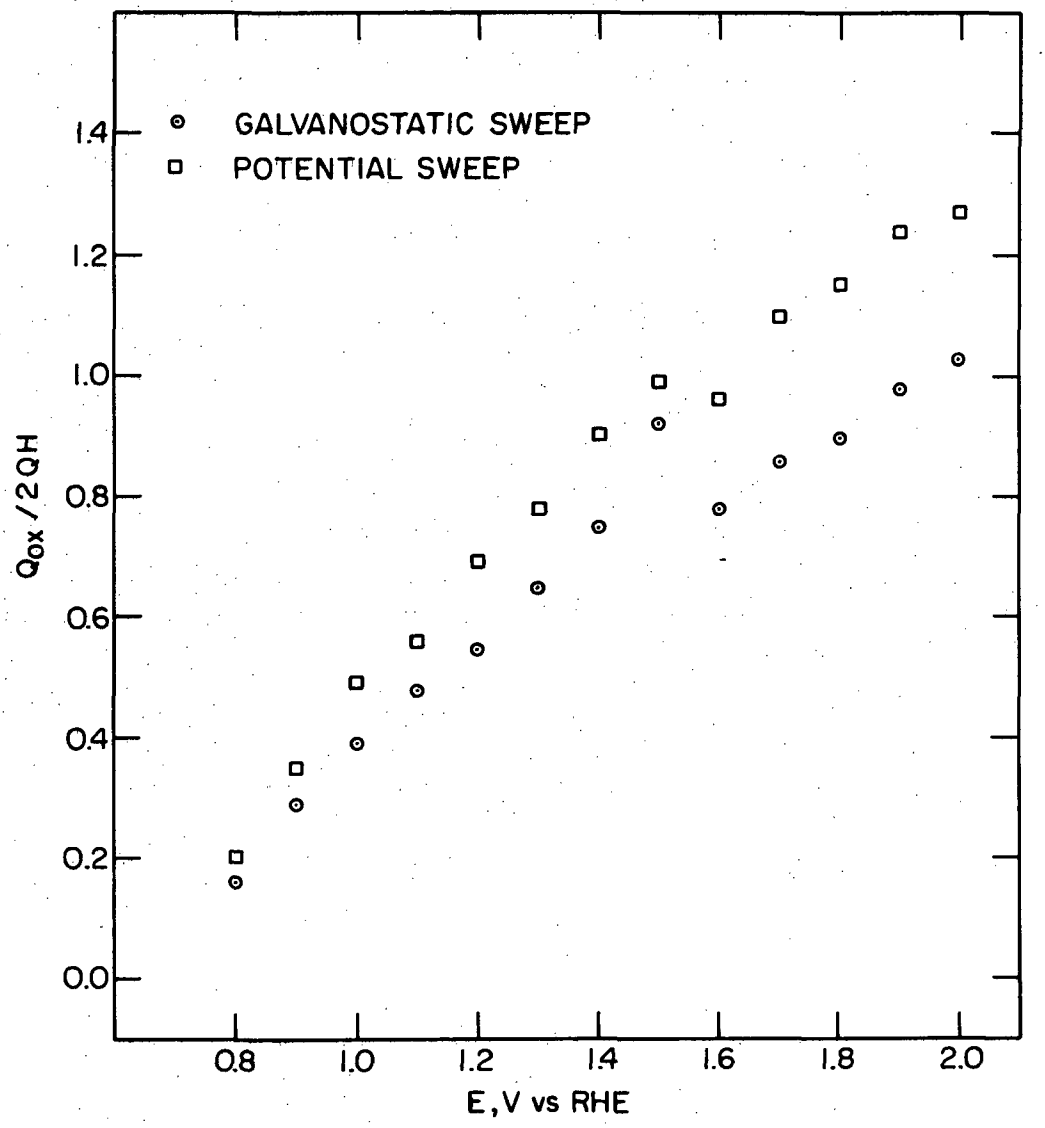

Fig. 17. Comparison of $Q_{ox}/2Q_H$ versus potential plots on a smooth platinum foil in purified 8.5N KOH using galvanostatic and linear sweep stripping methods (O) at 15 mA/real cm^2 and linear sweep stripping (□) at 1 V/sec

of Q_{ox} which were very irreproducible. This method was discarded, and we investigated the effects of a potential step in the region of +1.40 to +1.00 V for various times on Q_{ox} measurements using the galvanostatic technique.

Fig. 18 shows the dependence of Q_{ox} on the potential and the time of this step after a period of 2 min at +1.75 V. A current density of 10 mA/r cm^2 was used to obtain Q_{ox}. Q_{ox} decreases with decreasing potential. However, a 1-min step at +1.20 V leads to a decrease of 20 μcoul or approximately 5% in Q_{ox}. We felt that this error was tolerable since it was within the precision of the measurement. Therefore, we imposed a 1-min potential step to +1.20 V to allow removal of molecular O_2 prior to measurement of the surface oxidation state changes occurring at +1.75 V. A current density of 10 mA/r cm^2 was chosen since it appeared to be high enough to minimize diffusional effects and yet low enough to prevent surface layer reduction from being carried over into the hydrogen region of the galvanostatic charging curve.

2. Surface oxidation state changes of smooth platinum electrodes under potential cycling

Cycle Regime I: The potentials used in Cycle Regime I are typical of those found for oxygen electrodes operating in the rechargeable mode, i.e., +0.85 V is the normal discharge potential, while +1.75 V is a typical oxygen electrode potential during charge. We have investigated the effects of cycling smooth platinum electrodes in 8.5N KOH at 30 °C under a regime of +1.75 V for 10 min followed by +0.85 V for 5 min.

Table VII shows the change in Q_{ox}, Q_H (the hydrogen charge), and Q_{total} obtained after a smooth Pt foil had been cycled 59 times under Regime I.

Table VII. Changes in Q_{ox}, Q_H, and Q_{total} for a Smooth Pt Foil Electrode After Cycling in 8.5N KOH at 30 °C Under Regime I (10 Min at 1.75 V, Followed by 5 Min at +0.85 V)

Cycle No.	Q_{ox}*	Q_H	Q_{total}
1	530	370	900
6	550	340	890
59	610	290	900

*All Q's in μcoul.

Table VIII shows another set of data for a smooth Pt foil which had been cycled for 202 times under Regime I.

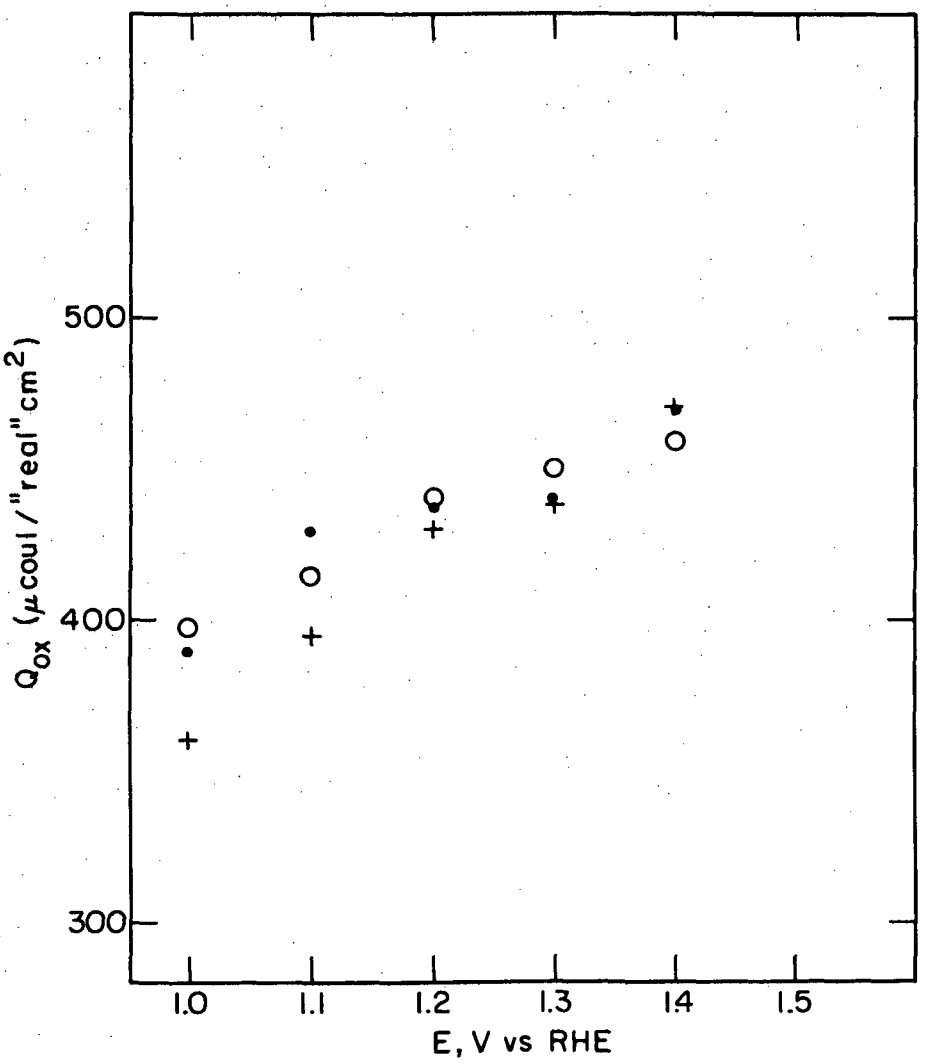

Fig. 18. Q_{ox} (μ coul/real cm^2) after 2 min at +1.75 V on a smooth platinum foil in purified 8.5N KOH at 30 °C as a function of time at +1.20 V times: (•) 6 sec; (o) 60 sec; (+) 120 sec; at various potentials prior to estimation of the state of surface oxidation with a galvanostatic pulse (10 mA/real cm^2)

Table VIII. Changes in Q_{ox}, Q_H, and Q_{total} for a Smooth Pt Electrode After Cycling in 8.5N KOH at 30 °C Under Regime I (10 Min at +1.75 V Followed by 5 Min at 0.85 V)

Cycle No.	Q_{ox}*	Q_H	Q_{total}
1	510	350	860
5	520	330	850
10	540	330	870
202	470	400	870

*All Q's in μ coul

The data of these previous Tables does not show any marked effects on Q_{ox} or Q_H. While Table VII shows an increase in Q_{ox} accompanied by a decrease in Q_H, Table VIII shows little change in Q_{ox} or Q_H for the first ten cycles but Q_H does increase somewhat after 202 cycles. More important is the relative constancy of Q_{total} for both data sets which would indicate that very little change in the Pt surface area has occurred. Measurements of the area of the Pt foil electrode used to obtain the data of Table VIII showed an increase of ~10% after cycling. The measured current values at the end of the +1.75 V portion of the cycle are plotted in Fig. 19. The current at +1.75 V seems to decrease somewhat with cycling from ~6 mA to a value in the vicinity of 4 mA after more than 200 cycles. Thus, it appeared that the effects on the surface state of smooth platinum electrodes under Cycle Regime I were minor.

In an effort to examine the effects of cycling under Regime I more closely, it was decided to subject smooth platinum electrodes to extended anodization at +1.75 V. Table IX presents data obtained from different foil electrodes held for 17 hr at +1.75 V. For comparison, the appropriate values of Q_{ox}, Q_H and Q_{total} after 2 min at +1.75 V before and after the 17-hr period are also included. There is a small variable (12-27%) increase in Q_{ox} which appears to be real and is not due to accumulation of O_2 or H_2O_2, since a 68-hr anodization at +1.75 V (which should lead to more O_2 or H_2O_2) gave an increase of 14% in Q_{ox}, comparable to values obtained after 17-hr anodization. However, this increase in Q_{ox} after the 17-hr period does not lead to a permanent change in electrode surface area as comparison of the 2-min data at +1.75 V before and after the 17-hr period demonstrate.

Cycle Regime II: Cycle Regime II is a more severe treatment than Regime I, and involves a 10-min treatment at +2.0 V followed by a 5-min period at +0.4 V. It is significantly more different than Regime I in that the +0.4 V step allows reduction of the surface layer to occur. We have used a 2-min treatment at +2.0 V before and after cycling to examine any permanent changes in the electrodes studied. Table X summarizes state of oxidation data obtained for different smooth Pt foil electrodes after various number of cycles under Regime II in purified 8.5N KOH. There are definite increases in surface area ranging from 20% to more than 100%. This variation in roughening no doubt reflects variations in the initial surface state of the electrodes. Biegler also observed similar variations in measurements of the roughening of smooth

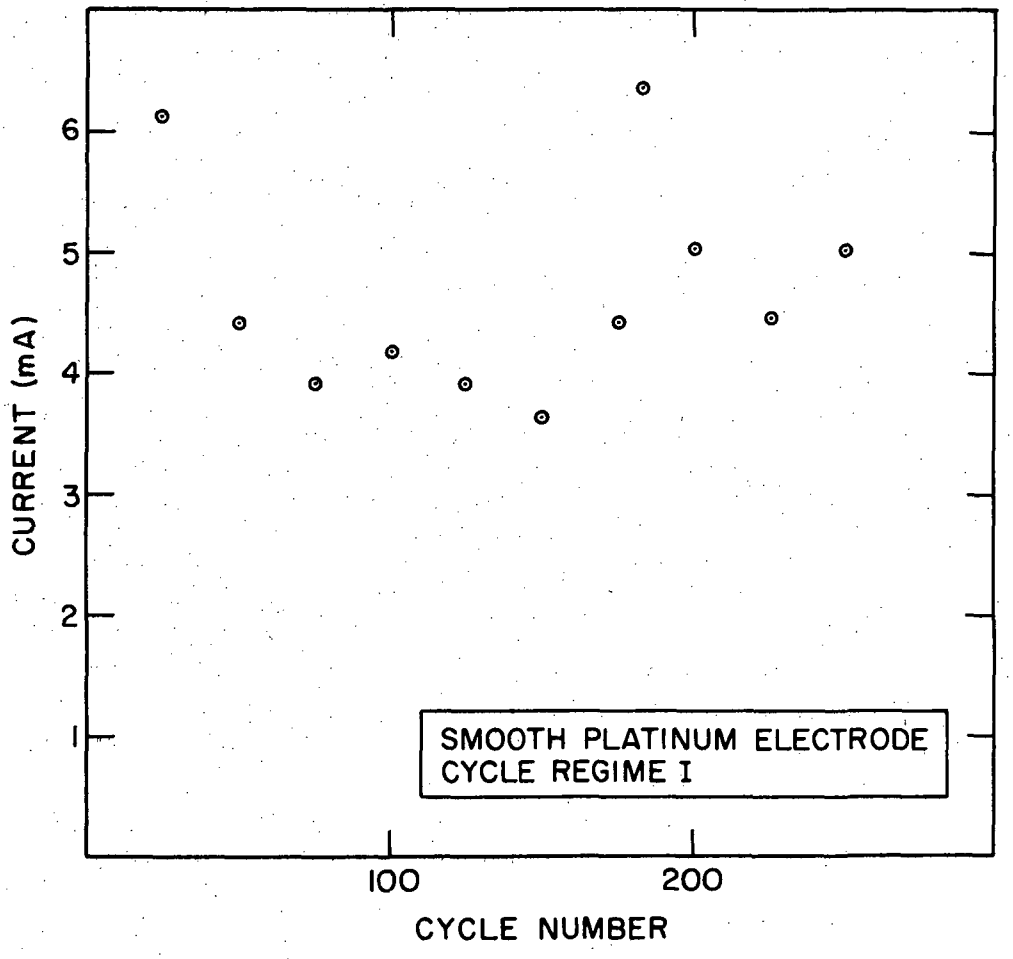

Fig. 19. Current (mA) at +1.75 V versus cycle number for a smooth platinum foil in purified 8.5N KOH at 30 °C cycled under Regime I (+1.75 V/10 min, +0.85 V/5 min)

Table IX. Results of Extended Anodization (1.75 V/17 hr) of Smooth Platinum Electrodes* in Purified 8.5N KOH at 30 °C

Electrode No.	Before Cycling†			After 17 hr at 1.75 V			After Measurement of Surface State†		
	Q_{ox}	Q_H	Q_{total}	Q_{ox}	Q_H	Q_{total}	Q_{ox}	Q_H	Q_{total}
1	1440	1300	2740	1730	1320	3050	—	—	—
2	1780	1610	3390	1990	1550	3540	1760	1470	3230
3	1370	1280	2650	1630	1210	2840	1360	1265	2625
4	1320	1202	2522	1200	1200	2880	1400	1118	2518

*All Q's in μcoul.

†1.75 V for 2 min.

Table X. Results of Cycling Under Regime II (10 Min at +2.00 V, Followed by 5 Min at +0.4 V) for Smooth Pt Electrodes in 8.5 KOH at 30°C*

Electrode No.	Area Before Cycling, r cm^2	Cycle	Q_{ox}	Q_H	Q_{total}	Area After Cycling, r cm^2
1	3.28	1	573	414	987	4.14
		2	585	414	999	
		3	585	414	999	
		4	597	402	999	
		5	597	402	999	
		69	1060	–	–	
2	3.14	1	598	458	1056	5.33
		5	611	458	1069	
		10	611	445	1056	
		87	1184	764	1948	
3	3.42	0	513	421	934	4.57
		1	538	444	982	
		5	573	421	994	
		10	561	444	1005	
		78	982	690	1672	
		79†	941	658	1599	
4	3.42	0	549	468	1017	5.33
		1	596	467	1063	
		5	620	432	1052	
		10	620	468	1088	
		74	1263	702	1965	
		75†	1152	698	1850	
5	3.52	0	556	409	965	6.09
		1	568	409	977	
		5	568	443	1011	
		10	590	443	1033	
		82	1136	614	1750	
		83†	1000	625	1625	
6	3.71	0	517	452	969	7.23
		1	549	464	1013	
		5	571	474	1045	
		10	593	474	1067	
		83	1448	–	–	
		84†	1348	916	2264	
7	3.61	0	576	476	1052	6.1
		1	565	443	1008	
		5	587	476	1063	
		10	670	465	1135	
		278	3878	–	–	
		279†	3074	1495	4569	
8	3.61	0	554	443	997	6.85
		1	587	487	1074	
		5	598	496	1094	
		10	642	510	1152	
		71	1806	–	–	
		72†	1357	941	2298	

*All Q's in μcoul/r cm^2.

†2.0 V for 2 min.

Pt electrodes in acidic solutions.[31] By comparison of the data for the last cycle with the 2 min/2.0 V data obtained immediately after the last cycle, it can be seen that the only affect of cycling smooth Pt under Regime II is the increase in real surface of these electrodes.

As expected from this increase in surface area, the measured O_2 evolution current at +2.0 V also increases. This is shown graphically in Fig. 20. This increase in current corresponds well to the measured increase in surface area of 2.9 to 4.4 cm^2 after 275 cycles.

3. Surface oxidation state of platinized platinum

We have determined the state of oxidation of a platinized platinum electrode as a function of potential in purified 8.5N KOH. The electrode was subjected to a pretreatment sequence of +1.35 V for 2 min, then to +0.05 V for 1 min prior to imposing the desired potential. After 2 min at this potential for surface layer formation, a cathodic current pulse of 50 mA was applied to reduce the surface and an E-t curve recorded to hydrogen evolution. For potentials more anodic than +1.5 V, a 1-min step at +1.2 V was inserted to allow removal of molecular O_2 prior to imposing the cathodic galvanostatic pulse.

Table XI presents the charge required to reduce the electrode surface, Q_{ox} (measured to +0.4 V) and Q_H, the charge equivalent of the chemisorbed hydrogen deposited as a function of anodization potential, and the ratio $Q_{ox}/2Q_H$. Q_H is relatively independent of the anodization potential which is good evidence that no interferences from molecular O_2 reduction or incomplete surface layer reduction are present. Fig. 21 plots Q_{ox} and Q_H as a function of potential. Fig. 22 plots $Q_{ox}/2Q_H$ which gives us a measure of the state of surface oxidation. Above +1.0 V, the state of surface oxidation is a linear function of potential and reaches 1.0 at +1.7 V, approximately the same behavior as described earlier for smooth Pt.

4. Surface oxidation state changes of platinized platinum electrodes under potential cycling

Cycle Regime I: We have cycled platinized platinum electrodes under Regime I in purified 8.5N KOH. Table XII shows the values of Q_{ox}, Q_H, and Q_{total} for five different platinized platinum electrodes for various numbers of cycles up to 268. In general, there is an increase in Q_{ox} with cycling. For example, electrode no. 3 shows an increase of 70 mcoul from cycle 1 to cycle 268, while Q_H increased from 90 to 140 mcoul. However, no permanent change is effected in the electrode, since measurements of Q_{ox}, Q_H, and Q_{total} after 2 min at +1.75 V following the measurements after the final cycle give approximately the same values obtained prior to cycling.

We have observed that the shape of the E-t curve during the reduction of the surface layer before and after extended cycling is different. This is depicted in Fig. 23 which shows E-t curves obtained before cycling (after 2 min at +1.75 V) and immediately after 254 cycles. It can be seen that the transition from the oxide region to the hydrogen region becomes ill defined. Since there is no permanent change in electrode area, the changes observed in Q_H are presumably due to the formation of a Pt-O layer on extended cycling which is more difficult to reduce than that formed during 2 min at +1.75 V and therefore, the reduction of this layer is carried over into the hydrogen region of the charging curve. Also, in Fig. 23, it can be observed that the potential region

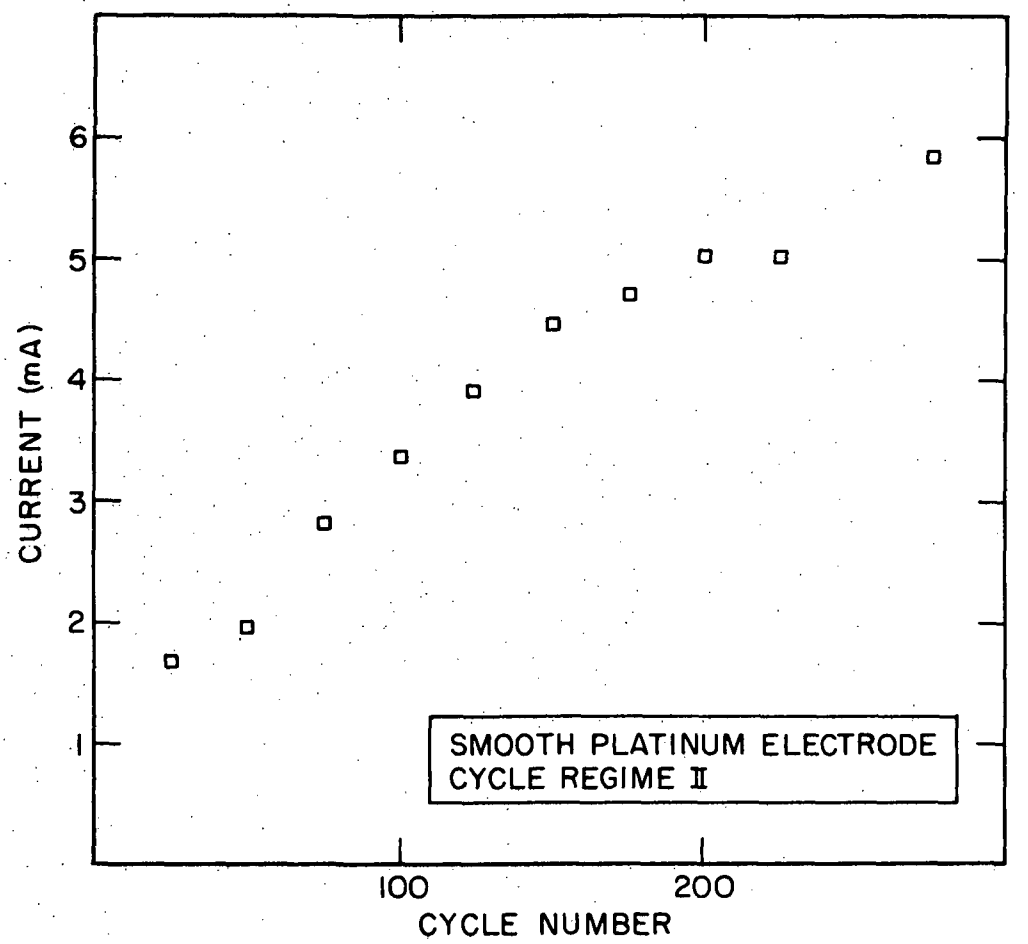

Fig. 20. Current (mA) at +2.0 V versus cycle number for a smooth platinum foil in purified 8.5N KOH at 30 °C cycled under Regime II (+2.0 V/ 10 min, +0.4 V/5 min)

Table XI. Values of Q_{ox}, the Charge Required to Reduce the Oxygen Layer, Q_H, the Charge Required to Deposit a Monolayer of Chemisorbed Hydrogen, and the Ratio $Q_{ox}/2\ Q_H$ as a Function of Potential for a Platinized Platinum Foil in Purified 8.5N KOH at 30 °C Using a Galvanostatic Pulse of 50 mA

E, V versus RHE	Q_{ox}	Q_H	$Q_{ox}/2\ Q_H$
+0.5	10	180	0.03
+0.6	15	187	0.04
+0.7	30	192	0.08
+0.8	70	185	0.19
+0.9	115	200	0.29
+1.0	175	185	0.53
+1.1	220	190	0.58
+1.2	260	200	0.65
+1.3	300	210	0.72
+1.4	335	215	0.78
+1.5	390	220	0.89
+1.6	385	205	0.94
+1.7	410	205	1.00
+1.8	425	200	1.06
+1.9	465	180	1.29

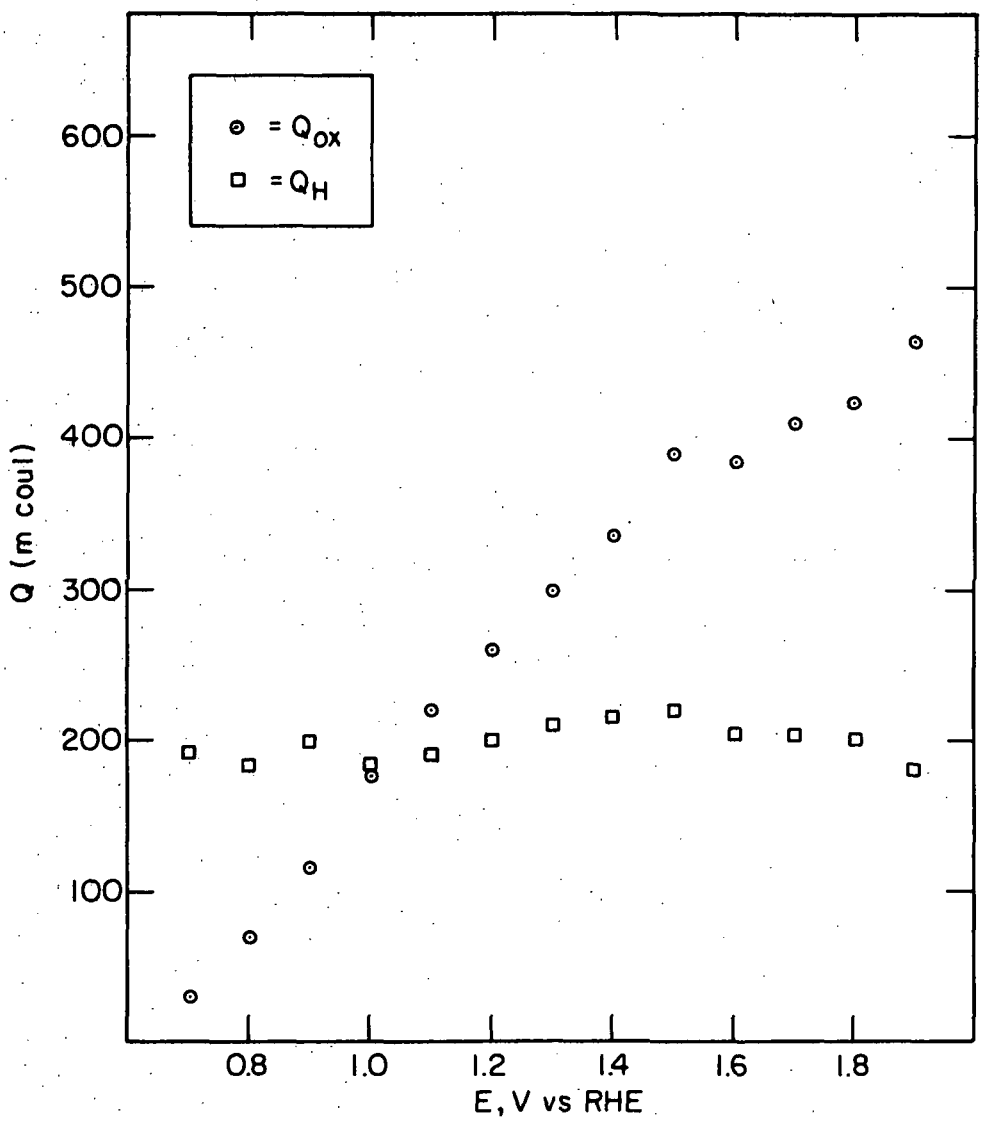

Fig. 21. Q_{ox} and Q_H as a function of potential for a platinized platinum foil in purified 8.5N KOH at 30 °C after 2 min anodization

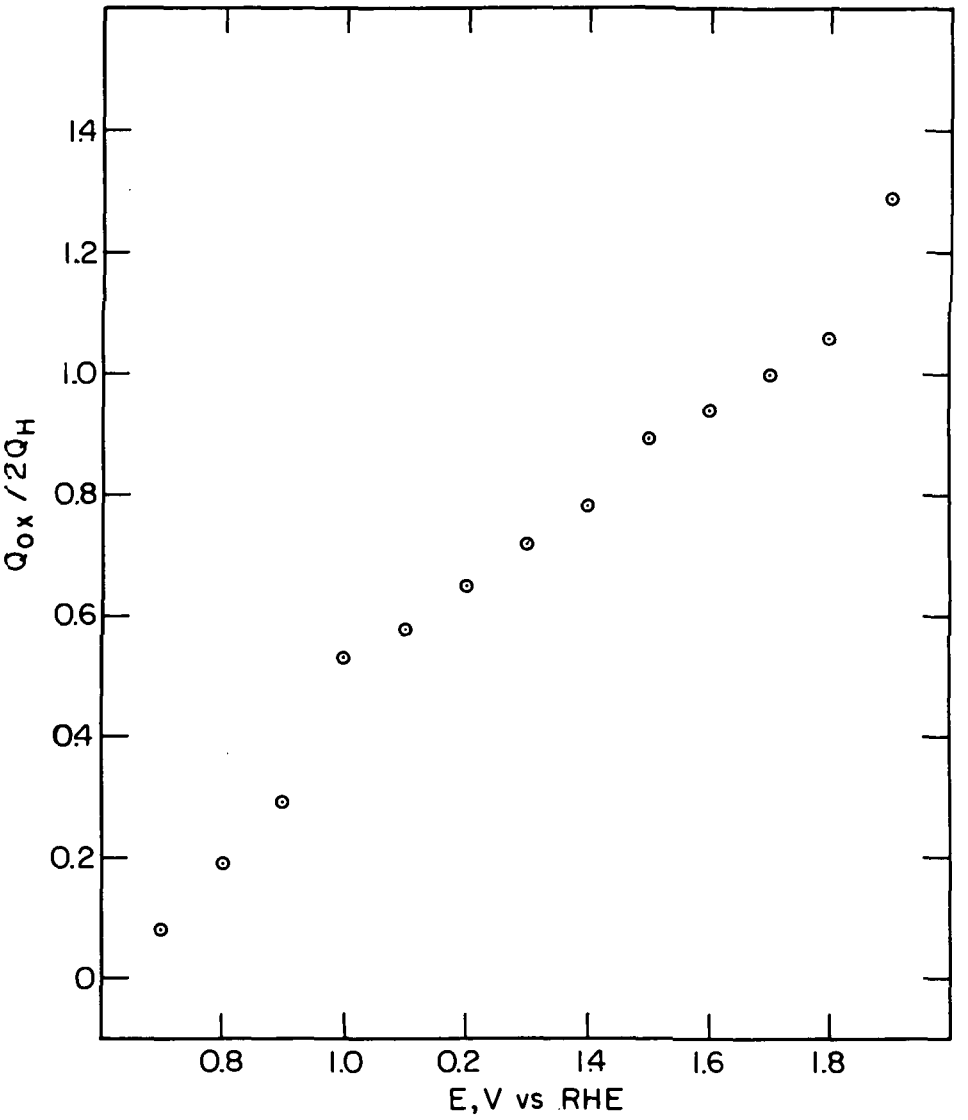

Fig. 22. $Q_{ox}/2Q_H$ as a function of potential for a platinized platinum foil in purified 8.5N KOH at 30 °C after 2 min anodization

Table XII. Results of Cycling Under Regime I (10 min at +1.75 V, followed by 5 min at +0.85 V) for Pt-Pt Electrodes in 8.5N KOH at 30 °C*

Electrode No.	Cycle	Q_{ox}	Q_H	Q_{total}
1	0	450	210	660
	1	530	210	740
	5	570	220	790
	10	600	210	810
	72	710	370	1080
	73†	450	190	640
2	0	310	135	445
	1	360	135	495
	5	390	135	525
	27	450	165	615
	28†	290	132	422
3	0	425	190	615
	1	490	210	700
	38	540	400	940
	39†	430	180	610
4	0	530	230	760
	1	630	230	860
	254	870	420	1290
	255†	540	220	760
5	0	207	95.5	300
	1	245	90	335
	5	260	90	350
	10	262	93	355
	268	315	140	455
	269†	195	90	285

*All Q's in mcoul.

†1.75 V for 2 min.

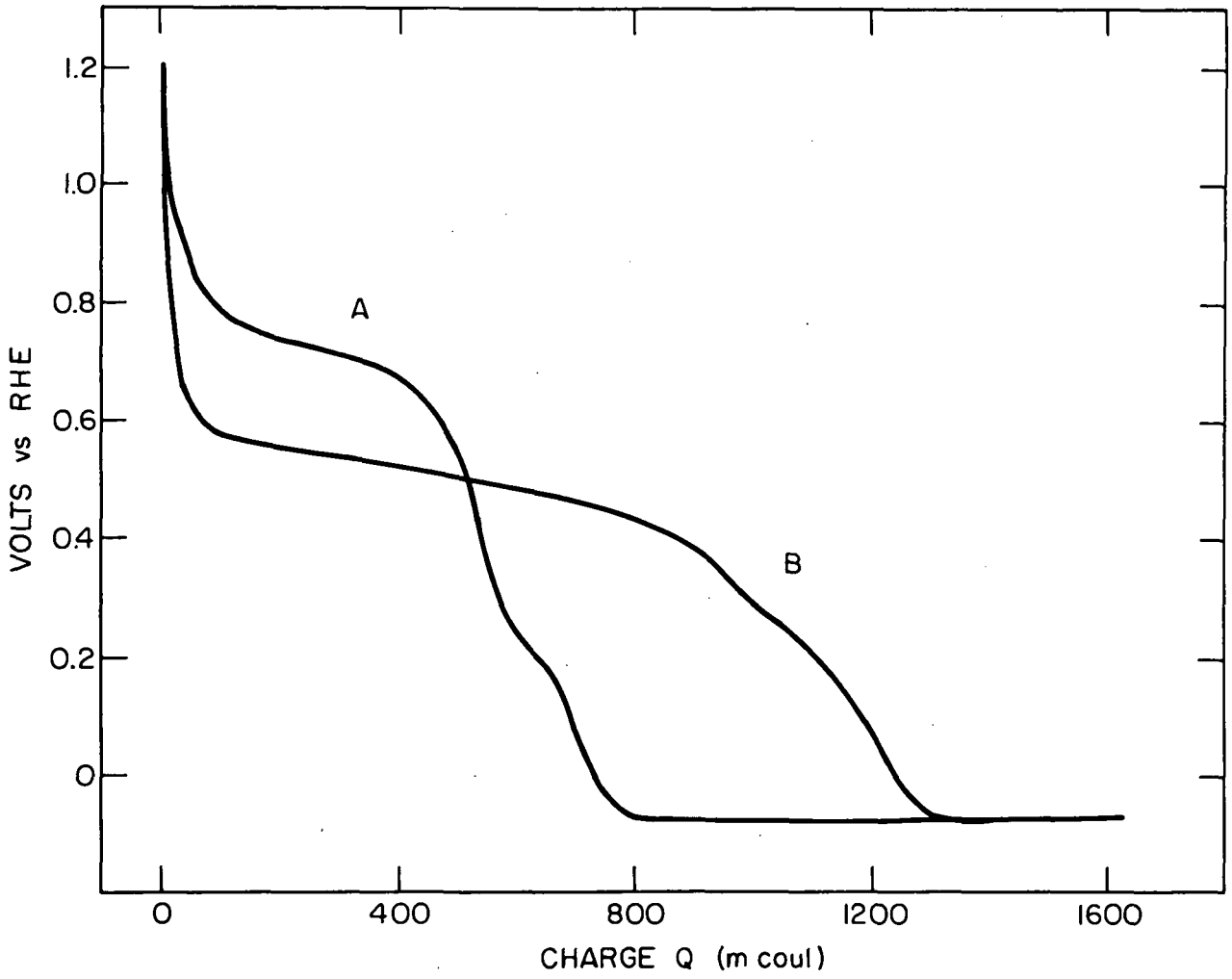

Fig. 23. Galvanostatic potential-time curves for a platinized platinum foil in purified 8.5N KOH at 30 °C after treatment at +1.75 V for 2 min (A) and immediately after 254 cycles under Regime I (B)

of Pt-O reduction is shifted cathodically by 200 mV, again demonstrating that extended cycling under Regime I produces a Pt-O layer significantly different than that produced at short times.

James has recently described the formation of a multilayer oxide film on anodized platinum confirming the earlier work of Shibata and Kozawa.[32, 33, 34] He reported that on extended anodization of smooth Pt in 2N sulfuric acid at 10 A/cm^2, three current peaks could be distinguished in linear voltammetric sweep stripping patterns of oxidized Pt electrodes. The first peak, at +0.6 V, corresponds to that commonly observed. He observed a peak at +0.3 V which he attributed to a monolayer type of oxide comparable in abundance to the normally observed species which reduces at +0.6 V. The reduction charge of the third species, which reduced at +0.2 V reached 25 mcoul/r cm^2 and apparently is a thick, bulk oxide film. We can rule out the possibility of the thick bulk-type of oxide which may reduce at +0.2 V according to James, since this leads to increases in electrode surface area. A species, similar to that found by James to reduce at +0.3 V, seems more probable.

We have used the scanning electron microscope in an attempt to investigate the changes occurring at platinized platinum electrodes under Cycle Regime I. Fig. 24 is a series of micrographs which compares an uncycled Pt-Pt electrode with a Pt-Pt electrode cycled 254 times under Regime I. Fig. 25 is a similar series of micrographs at higher magnifications. Although the quality of the micrographs of the uncycled material is not as good as those of the cycled material, there does not appear to be any observable difference between the uncycled and cycled electrodes, apart from a more noticeable "treeing" or dendrite-type clusters in the cycled electrode views, which is probably due to the better quality of these pictures. This lack of noticeable difference between a cycled and uncycled electrode is not unexpected, since the electrochemical measurements did not reveal any permanent changes in these electrodes.

Fig. 26 shows typical current values during the +1.75 V portion of the cycle for a platinized platinum electrode cycling under Regime I. There is a decrease in O_2 evolution current from a value of 9 to 3.5 mA after 250 cycles. This decrease in O_2 evolution current is presumably due to the build up of Pt-O layer on extended cycling which hinders O_2 evolution and is not related to a surface area decrease.

Cycle Regime II: Table XIII shows state of oxidation data for eight different platinized platinum electrodes cycled under Regime II. (+2.0 V/10 min, +0.4 V/5 min.) The prime electrode numbers refer to electrodes which were returned to cycling after a surface oxidation state measurement was made on them and state of oxidation data after 2 min at +2.0 V had been obtained. For example, electrode 2' had previously been cycled 69 times and had been held at +2.0 V for 2 min to obtain state of oxidation data. It was then cycled for an additional 82 cycles.

The data of Table XIII show that there is a decrease in Q_{ox} and Q_{total} for Pt-Pt electrodes under Cycle Regime II. This decrease in Q_{ox} can be traced to a loss of surface area since the data obtained after 2 min at +2.0 V before and after cycling show a decrease in Q_{ox} and Q_H indicative of a decrease in surface area. This loss of surface area parallels the observed

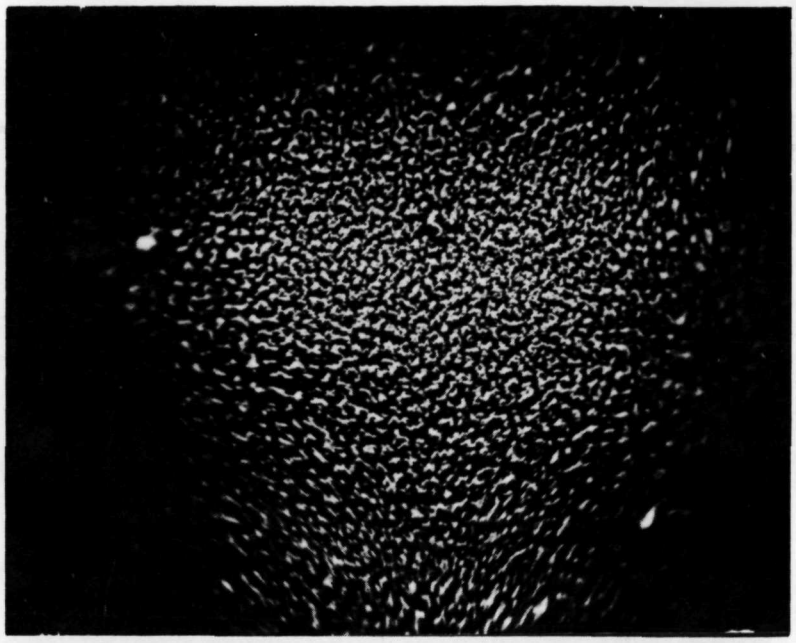

(a) 100X

(b) 100X

Fig. 24. Scanning electron micrographs comparing an uncycled Pt-Pt electrode (a) and a Pt-Pt electrode cycled 254 times under Regime I (b)

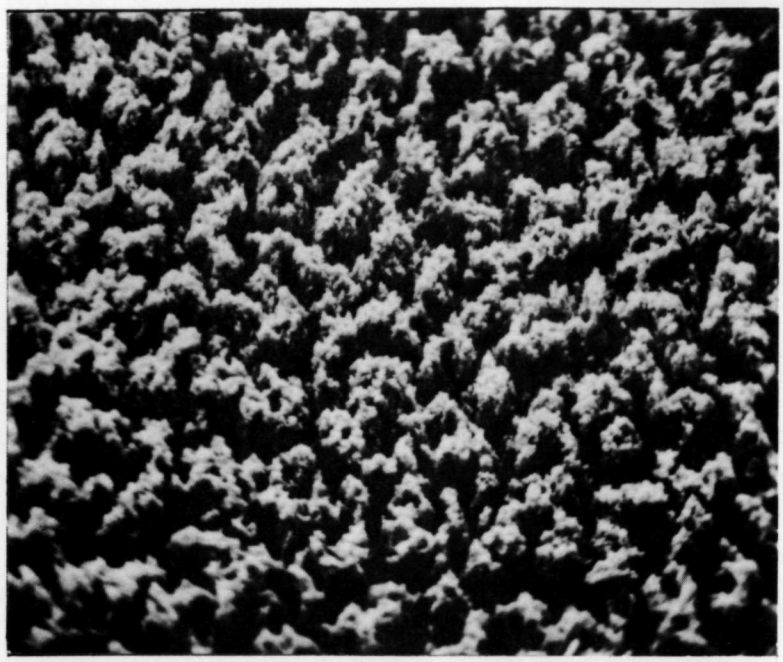

(c) 500X

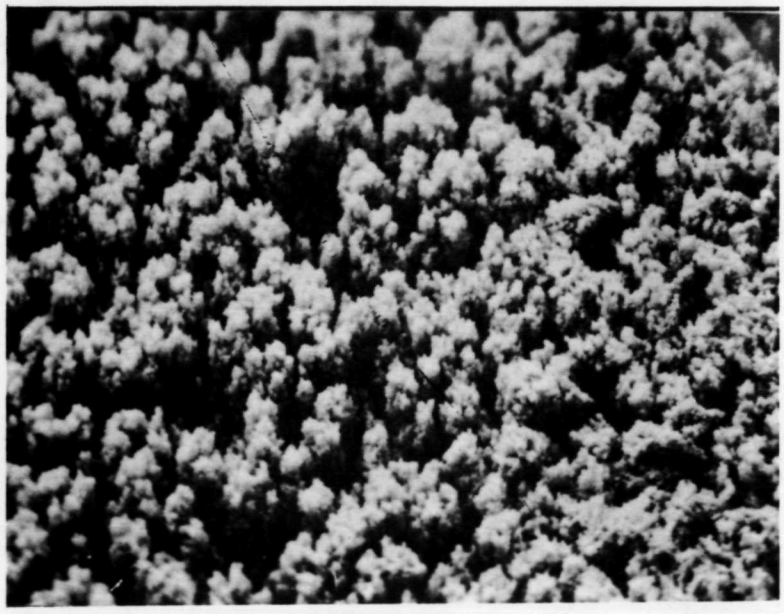

(d) 500X

Fig. 24. Scanning electron micrographs comparing an uncycled Pt-Pt electrode (c) and a Pt-Pt electrode cycled 254 times under Regime I (d)

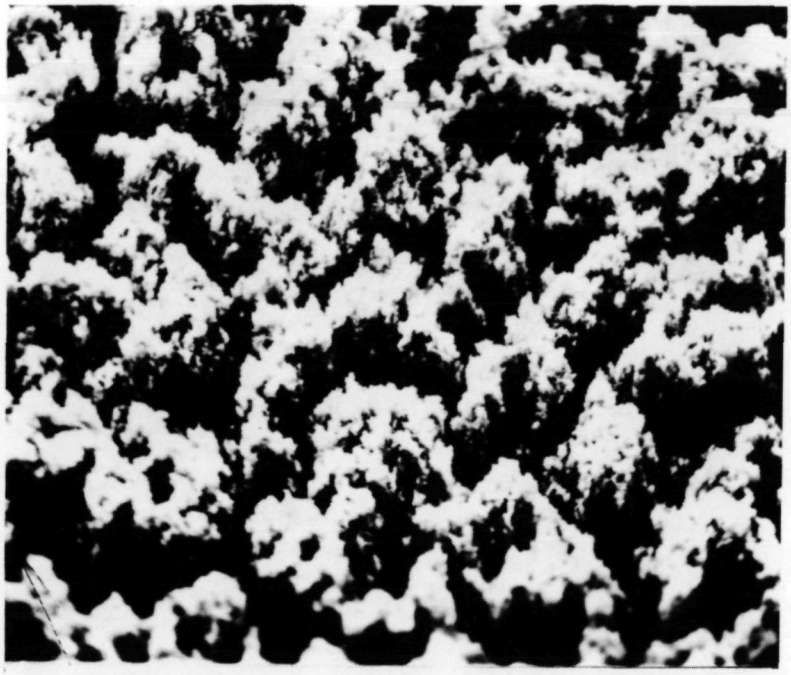

(e) 1000X

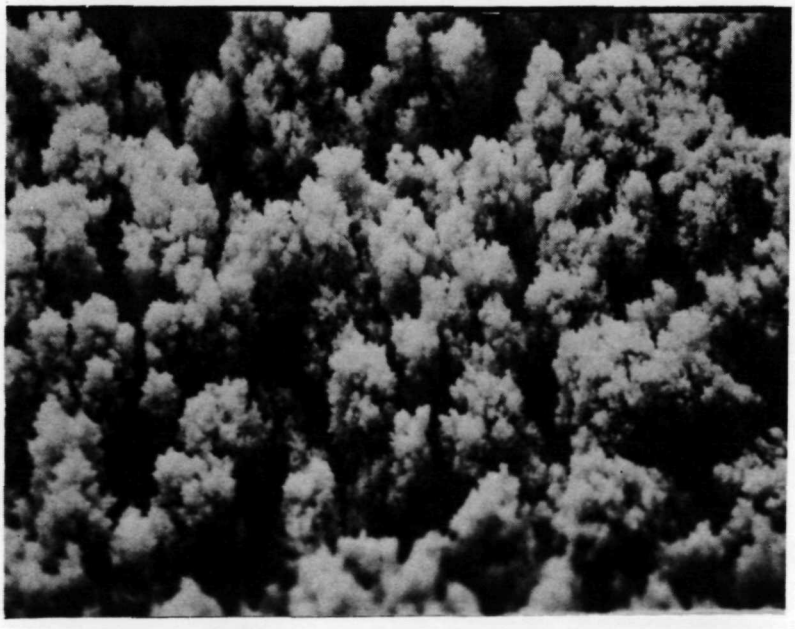

(f) 1000X

Fig. 24. Scanning electron micrographs comparing an uncycled Pt-Pt electrode (e) and a Pt-Pt electrode cycled 254 times under Regime I (f)

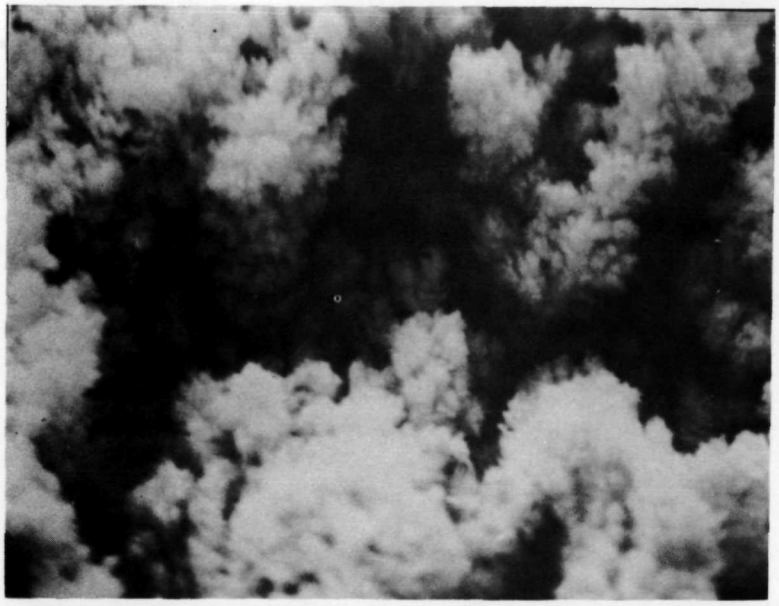

(a) 5000X

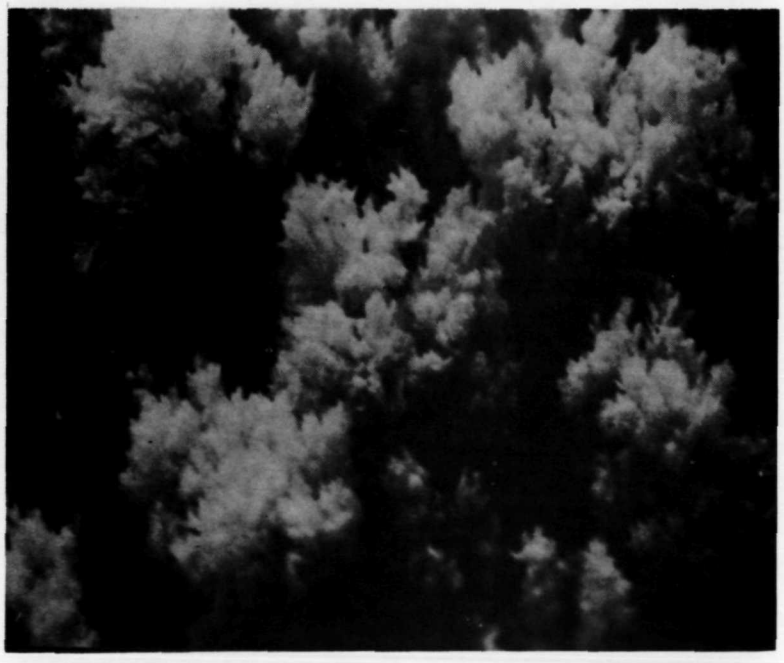

(b) 5000X

Fig. 25. Further micrographs of a scanning electron comparing an uncycled Pt-Pt electrode (a) and a Pt-Pt electrode cycled 254 times under Regime I (b)

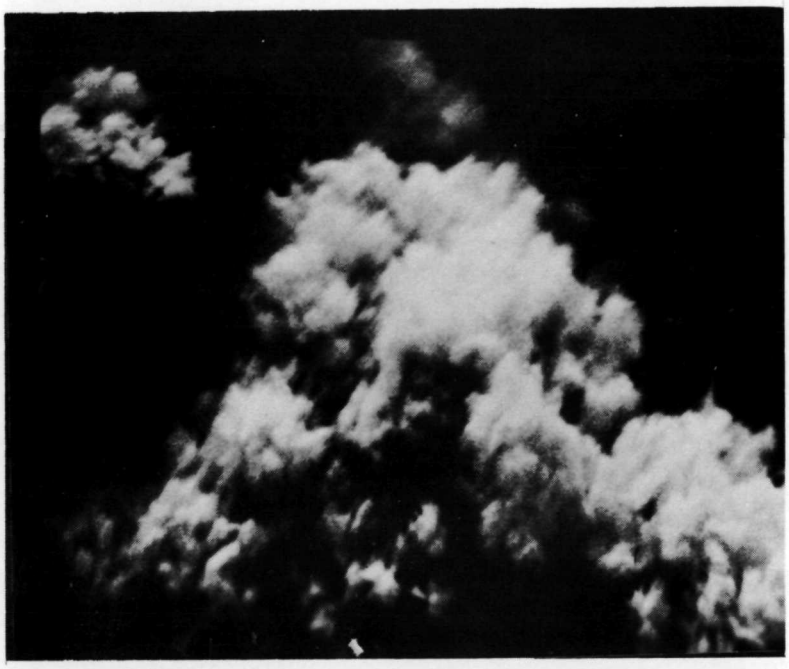

(c) 10,000X

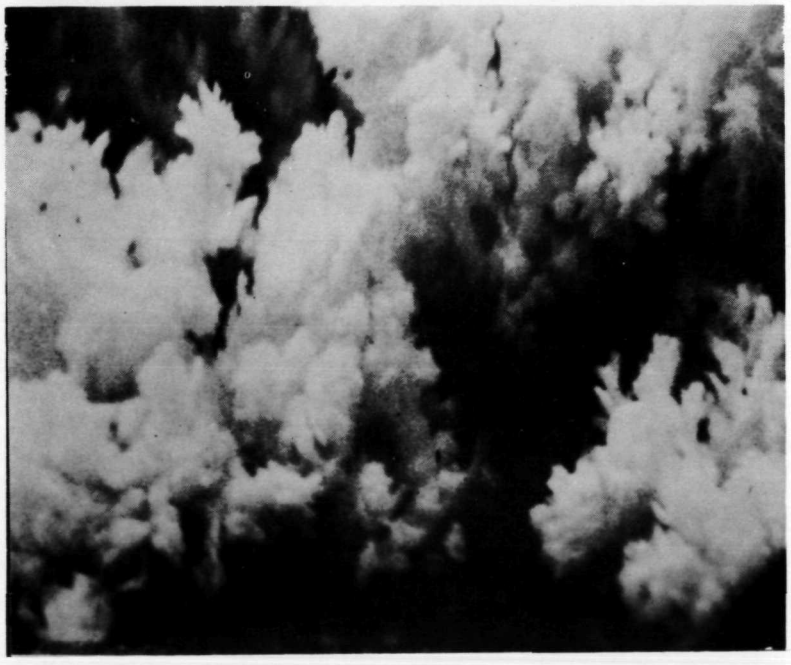

(d) 10,000X

Fig. 25. Further micrographs of a scanning electron comparing an uncycled Pt-Pt electrode (c) and a Pt-Pt electrode cycled 254 times under Regime I (d)

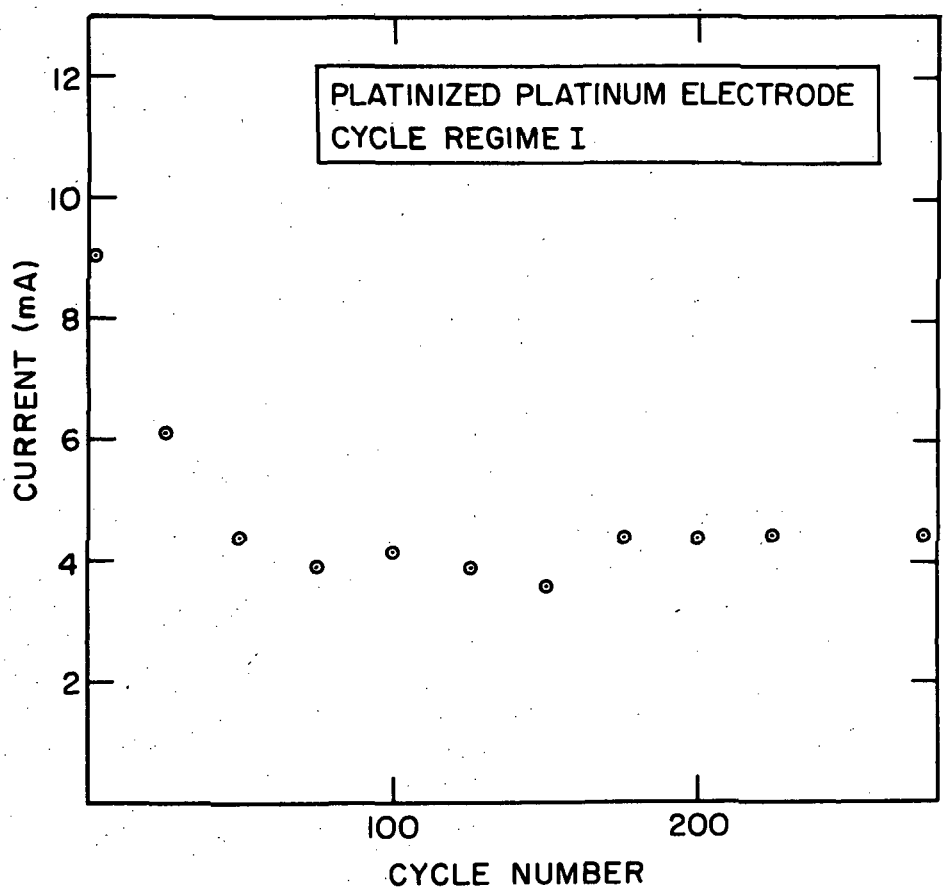

Fig. 26. Current (mA) at +1.75 V versus cycle number at a platinized platinum foil in purified 8.5N KOH at 30 °C cycled under Regime I (+1.75 V/10 min, +0.85 V/5 min)

Table XIII. Results of Cycling Eight Different Platinized Platinum Electrodes in Purified 8.5N KOH at 30 °C Under Regime II (10 min at +2.0 V, Followed by 5 min at +0.4 V) for Various Number of Cycles

Electrode 1

Cycle No.	Q_{ox}	Q_H	Q_{total}
0	152	57	227
1	157	52	209
255	85	32	117
256	75	30	105

Electrode 2

Cycle No.	Q_{ox}	Q_H	Q_{total}
0	135	56	191
1	132	48	180
5	102	42	144
69	102	42	144
70	87	42	129

Electrode 2'

Cycle No.	Q_{ox}	Q_H	Q_{total}
0	92	38	130
1	101	40	141
5	100	39	139
10	100	39	139
82	100	40	140
83	89	36	125

Electrode 3

Cycle No.	Q_{ox}	Q_H	Q_{total}
0	115	45	160
1	115	45	160
5	105	40	145
10	101	39	140
82	85	34	119
83	75	34	109

Electrode 3'

Cycle No.	Q_{ox}	Q_H	Q_{total}
0	74	31	105
1	82	32	114
5	84	31	115
10	81	32	113
90	80	30	110
91	70	29	99

Table XIII (Cont.)

Electrode 4

Cycle No.	Q_{ox}	Q_H	Q total
0	147	82	229
1	140	52	192
5	130	50	180
10	122	44	166
82	98	42	140
83	82	38	120

Electrode 4'

Cycle No.	Q_{ox}	Q_H	Q total
0	90	40	130
1	95	40	135
5	98	40	138
10	95	40	135
86	88	35	123
87	78	32	110

Electrode 5

Cycle No.	Q_{ox}	Q_H	Q total
0	130	55	185
1	130	50	180
5	120	45	165
10	112	42	154
264	75	28	128
265	66	26	92

Electrode 5'

Cycle No.	Q_{ox}	Q_H	Q total
0	64	29	93
1	71	28	99
5	71	28	99
10	72	29	101
81	66	28	84
82	60	25	85

Electrode 6

Cycle No.	Q_{ox}	Q_H	Q total
0	132	52	184
1	142	50	192

Table XIII. (Cont.)

Cycle No.	Q_{ox}	Q_H	Q total
5	132	48	180
10	122	42	164
74	100	38	138
75	92	35	127

Electrode 6'

Cycle No.	Q_{ox}	Q_H	Q total
0	89	38	127
1	98	38	136
5	99	38	137
10	99	38	137
90	97	35	132
91	84	34	118

Electrode 7

Cycle No.	Q_{ox}	Q_H	Q total
0	162	62	224
1	168	58	226
5	158	55	213
10	150	55	205
202	105	42	147
203	95	40	135

Electrode 8

Cycle No.	Q_{ox}	Q_H	Q total
0	170	62	232
1	168	55	223
5	155	45	200
261	102	40	142
262	92	58	150

decrease in Q_{ox}, Q_H, and Q_{total} with extended cycling. The loss of surface area is not a continual process since for electrode 5, which had been cycled 264 times, no further significant loss in surface area was observed after an additional 81 cycles (see electrode 5').

Since we have observed platinum black particles in cells where Pt-Pt electrodes were cycled according to Regime II, we believe that this loss in surface area is due to mechanical loss of Pt particles from the surface due to vigorous O_2 evolution at +2.0 V. This hypothesis has been strengthened by scanning electron microscopy of cycled Pt-Pt electrodes and X-ray diffraction studies.

Fig. 27 is a series of photographs which compares an uncycled platinized platinum electrode with a platinized platinum electrode which had been subjected to 254 cycles of Regime II. Fig. 28 is a similar series of photographs at higher magnification. There is a definite difference in the texture of these two Pt-Pt surfaces, although both have visible patches which have not been plated with Pt black. Note that the uncycled Pt-Pt surface possesses a considerable number of platinum crystallites projecting from the surface. In contrast the surface of the cycled electrode is rather level and is lacking in these surface projections. This "leveling" of the surface of the cycled Pt-Pt electrode is consistent with our hypothesis that the loss of surface area is due to mechanical loss of Pt black due to gas evolution at +2.0 V. It seemed reasonable to assume that the Pt-black crystallites which project from the surface were subject to removal. However, in order to eliminate the possibility that recrystallization of the Pt-black caused this loss of surface area and change of surface texture, X-ray diffraction was used to estimate the average particle size of the Pt-Pt electrode before and after cycling.

Table XIV compares the average crystallite size of a platinized platinum electrode before and after 254 cycles of Regime II. Little or no change in crystallite size is observed which confirms our hypothesis that the decrease in electrode area is indeed due to mechanical loss of platinum black by gas evolution.

Table XIV. Comparison of the Average Crystallite Size as Determined By X-Ray Diffraction for a Platinized Platinum Electrode Before and After 254 Cycles Under Regime II (10 Min at +2.0 V, Followed by 5 Min at +0.40 V) in 8.5N KOH at 30 °C

	Average Crystallite Size, Å	
Reflecting Plane	Before Cycling	After Cycling
<111>	140	140
<200>	90	95
<220>	380	380
<311>	305	305

(a) 100X

(b) 100X

Fig. 27. Scanning electron micrographs comparing an uncycled Pt-Pt electrode (a) and Pt-Pt electrode cycled 254 times under Regime II (b)

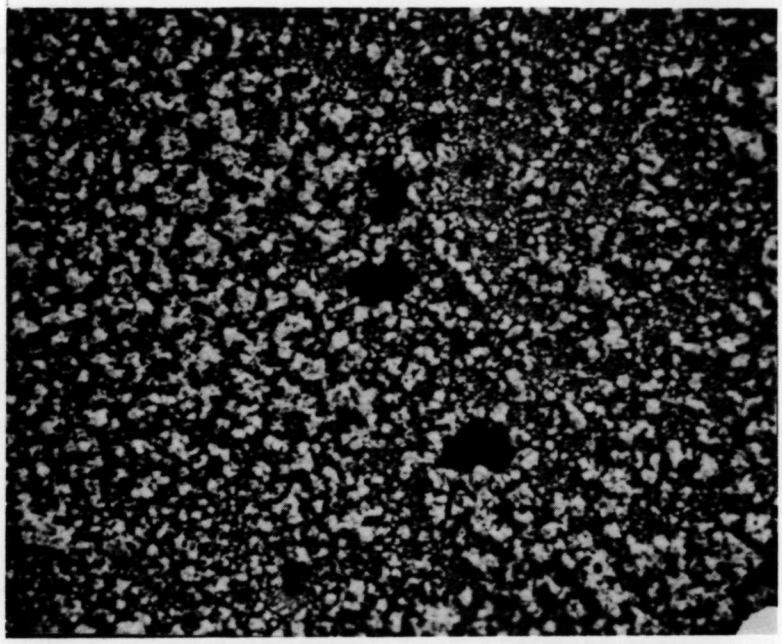

(c) 500X

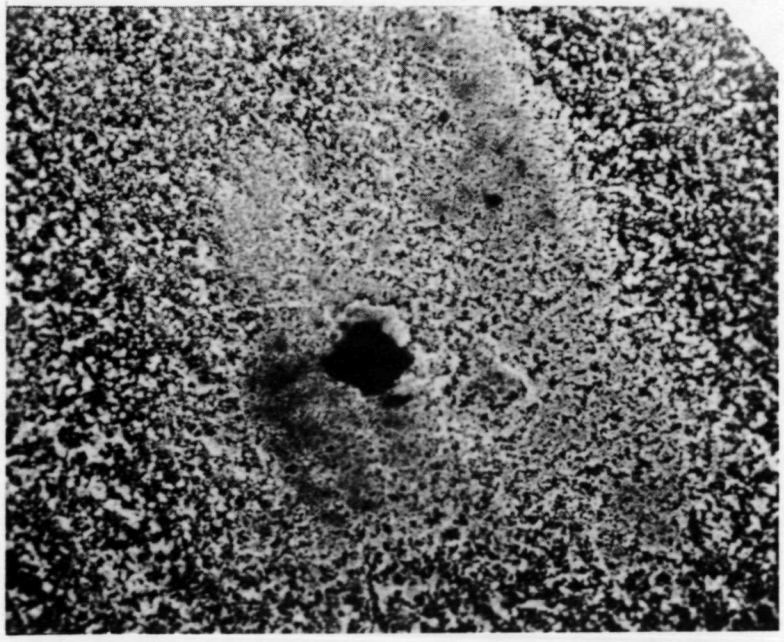

(d) 500X

Fig. 27. Scanning electron micrographs comparing an uncycled Pt-Pt electrode (c) and a Pt-Pt electrode cycled 254 times under Regime II (d)

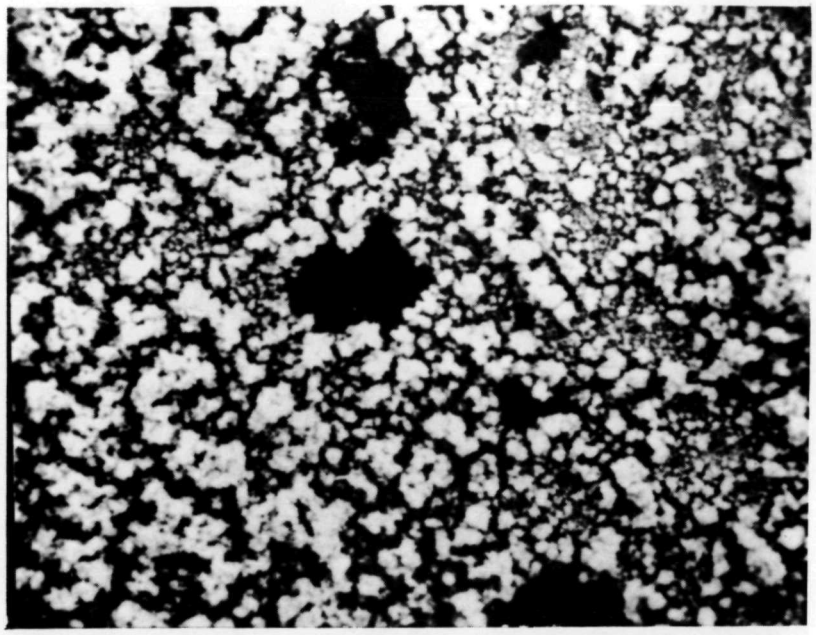

(a) 1000X

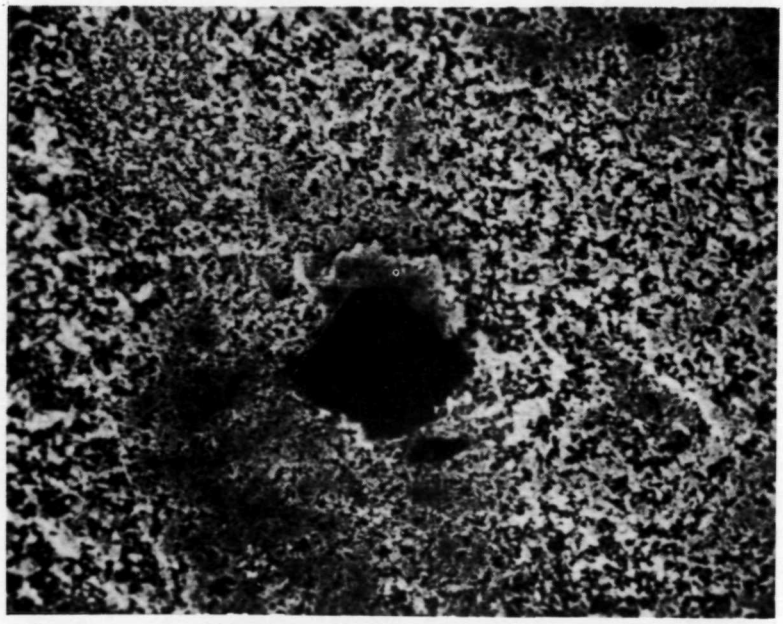

(b) 1000X

Fig. 28. Further scanning electron micrographs comparing an uncycled Pt-Pt electrode (a) and a Pt-Pt electrode cycled 254 times under Regime II (b)

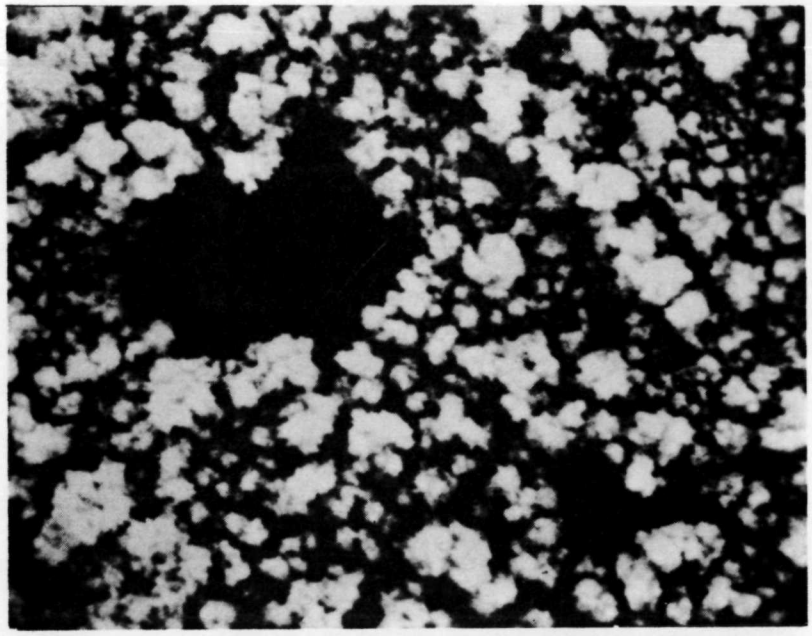

(c) 2000X

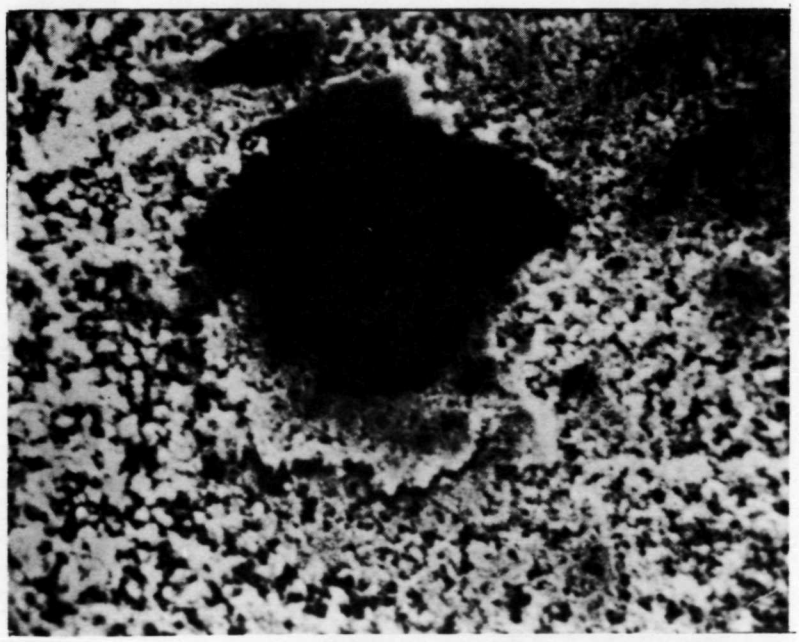

(d) 2000X

Fig. 28. Further scanning electron micrographs comparing an uncycled Pt-Pt electrode (c) and a Pt-Pt electrode cycled 254 times under Regime II (d)

Measurement of the O_2 evolution current at +2.0 V during cycling of Pt-Pt electrodes under Regime II shows typical decreases in current with cycle number as shown in Fig. 29. The 26% decrease in current after 200 cycles correlates very well with the observed decrease of 31% in surface area measured for this electrode after cycling.

D. Conclusions

Based on coulometric measurement of the charge equivalent, Q_{ox}, of the anodic platinum-oxygen surface layer, a Pt/O stoichiometry of 1:1 is reached at ~ +1.6-1.7 V on both smooth and platinized platinum. No limiting oxygen coverage was found at potentials up to +2.0 V. Potential cycling of smooth platinum under a regime (Cycle Regime I) similar to that encountered by rechargeable oxygen electrodes (10 min at +1.75 V, 5 min at +0.85 V) does not result in any appreciable changes in surface oxidation state. Extended anodization at +1.75 V/17 hr results in a small variable (12-27%) increase in Q_{ox}. When platinized platinum is cycled under Regime I, the buildup of a Pt-O layer which is more difficult to reduce than that formed at short times (2 min at +1.75 V) is observed. Removal of this Pt-O layer by cathodic reduction restores the electrode to its original condition, i.e., no change in surface area. Cycling of smooth platinum under a regime of 10 min at +2.0 V followed by 5 min at +0.40 V (Cycle Regime II) leads to an increase of real surface area of up to 95%. However, cycling of a freshly prepared platinized platinum electrode under Regime II leads to a decrease in real surface area apparently due to mechanical loss of platinum black by gas evolution.

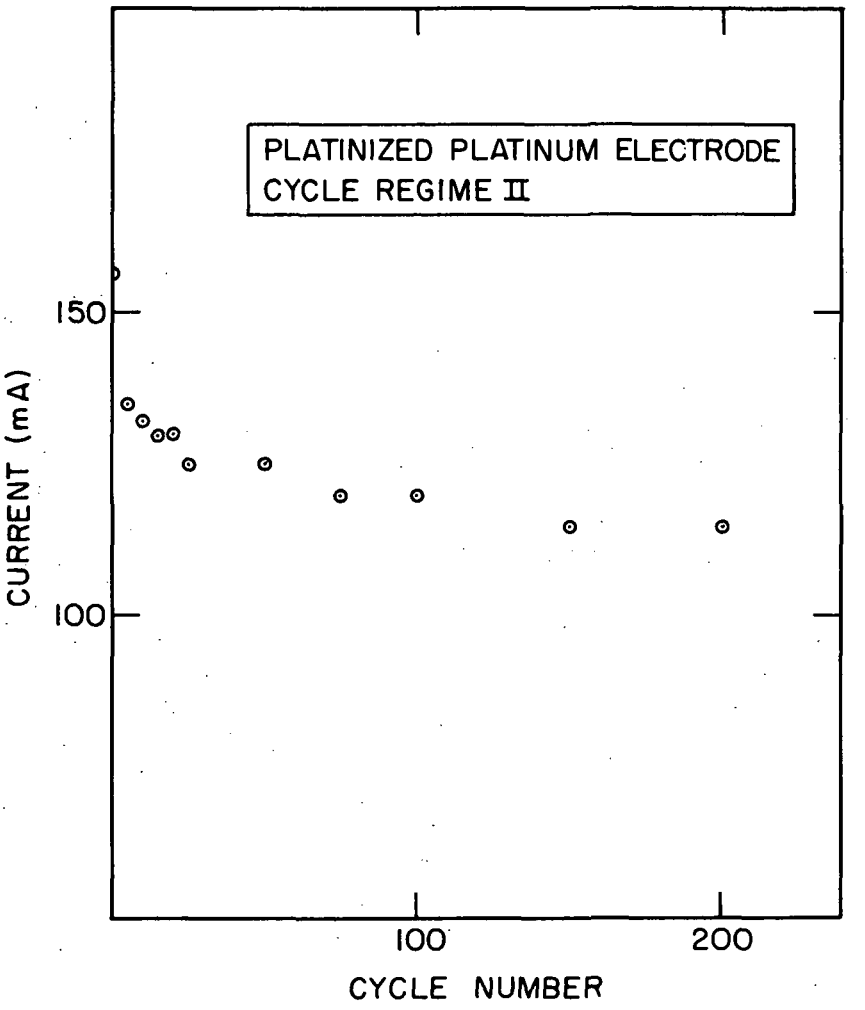

Fig. 29. Current (mA) at +2.0 V versus cycle number at a platinized platinum foil in purified 8.5N KOH at 30 °C cycled under Regime II (+2.0 V/10 min, +0.4 V/5 min)

V. OXYGEN REDUCTION KINETIC STUDIES ON PLATINUM ELECTRODES

A. Background

The kinetics and mechanism of oxygen reduction and evolution on platinum electrodes has been the subject of a very large number of papers. However, the lack of consideration, in most cases, of the presence of Pt-O surface layers and impurity effects has resulted in a considerable amount of confusion and contradictory statements in the literature. For example, the formation of H_2O_2 had been reported by several authors in the reduction of O_2 in sulfuric acid solution.[8,9] Damjanovic, et al., showed that H_2O_2 was not formed in O_2 reduction on smooth Pt if highly purified sulfuric acid was used.[6,7]

By far, the most informative technique which has been used in O_2 reduction studies is the rotating ring-disk electrode (RRDE) method. The use of the RRDE is appealing since it not only allows the establishment of a rigidly controlled mass transport regime, but allows quantitative determination of dissolved intermediates such as H_2O_2, without requiring the sophistication and experimental expertise of electrochemical transient techniques.

Müller and Nekrasov first used the RRDE in a study of the electrochemical reduction of O_2 in both alkaline and acidic solutions.[35] By holding the disk electrode at various potentials along the limiting current plateau for O_2-reduction, they were able to show that the current at the ring electrode, which resulted from oxidation of H_2O_2, a dissolved intermediate, was a function of potential. Significant amounts of H_2O_2 were detected at the ring electrode only at disk potentials at which there was no coverage by platinum surface oxide. This behavior was confirmed in a later report which demonstrated that the presence of surface oxide on platinum retards the formation of H_2O_2 from O_2 in alkaline solutions.[36]

Damjanovic, et al., originally presented diagnostic criteria for the RRDE which allowed the distinction to be made between an intermediate formed in the main reaction path and a product formed in a path parallel to the main reaction, i.e.,[37]

$$Ox \xrightarrow{I_1} Red \qquad (1)$$

$$Ox \xrightarrow{I_2} Int \xrightarrow{I_3} Red \qquad (2)$$

$$Int \xrightarrow{I_4} Solution$$

For the particular case of O_2 reduction, I_1 corresponds to the current arising from the $4e^-$ reduction of oxygen to water without a hydrogen peroxide intermediate. I_2 is the current arising from the $2e^-$ reduction of oxygen to H_2O_2 which could be further reduced to H_2O giving rise to I_3. I_4 expresses the loss of peroxide by diffusion, counted in electrical units. For oxygen reduction in alkaline solution, we can write:

$$O_2 + 2H_2O + 4\,e^- \xrightarrow{k_1} 4OH^- \qquad (3)$$

$$O_2 + H_2O + 2\,e^- \xrightarrow{k_2} OH^- + HO_2^- \qquad (4)$$

$$HO_2^- + H_2O + 2\,e^- \xrightarrow{k_3} 3\,OH^- \qquad (5)$$

Damjanovic, et al., derived the following relationship between I_d/I_r and $\omega^{-1/2}$

$$\frac{I_d}{I_r} = \frac{x+1}{N} + \frac{(x+2)\,k'}{N\,\omega^{1/2}} \qquad (6)$$

where k' stands for:

$$k' = 1.61\,D^{-2/3}\,\nu^{1/6}\,k_3 \qquad (7)$$

and

$$x = I_1/I_2 \qquad (8)$$

In (6), x and k' (k_3) are unknown qualities. They can be obtained from a plot of I_d/I_r versus $\omega^{-1/2}$ since straight lines with an intercept of $(x+1)/N$ and a slope of $[(x+2)k']/N$ are predicted from Eq. (6). Therefore, x and k_3 can be determined. This equation is is a diagnostic one as it enables analysis to be made with regard to the role of the intermediate as will be discussed.

Plots of I_d/I_r were used by Damjanovic, et al., to evaluate the relative role reactions (1), (2), and (3) in O_2 reduction. Five cases were distinguished here. These are:

1. Only reaction (3) occurs, therefore no peroxide intermediate is produced and $I_r = 0$.

2. Only reaction (4) occurs with no further reduction of peroxide via reaction (5). Therefore $k_1 = 0$ and $k_3 \cong 0$ and I_d/I_r is a straight line parallel to the $\omega^{-1/2}$ axis at $I_d/I_r = 1/N$.

3. Only reactions (4) and (5) occur, thus no parallel reaction is present and $x = 0$. The plot of I_d/I_r versus $\omega^{-1/2}$ gives straight lines of the form:

$$\frac{I_d}{I_r} = \frac{1}{N} + \frac{2k'}{N\omega^{1/2}} \qquad (9)$$

Hence, a family of straight lines should be obtained at different potentials with a slope determined by k' with a constant intercept of 1/N.

4. Only reactions (3) and (4) occur, but (5) does not. Hence $k' = 0$ in equation (6) and it reduces to:

$$\frac{I_d}{I_r} = \frac{x + 1}{N} \qquad (10)$$

Thus, the intercept is dependent on x and should be dependent on potential since reactions (3) and (4) will most likely have different potential dependence. A family of lines parallel to the $\omega^{-1/2}$ axis would be expected at I_d/I_r values greater than 1/N.

5. All these reactions occur. Hence, equation (6) must be used in its entirety. A family of straight lines should result with varying slope and intercept since k' and x will be potential dependent.

Based on this theoretical treatment, Damjanovic, et al., studied the reduction of O_2 on smooth platinum in 0.1N H_2SO_4 and 0.1N KOH. In impure 0.1N H_2SO_4, it was found that a series of lines parallel to the $\omega^{-1/2}$ axis was obtained with an intercept greater than 1/N.[6,7] This indicated that reactions (3) and (4) were occurring but that (5) did not occur. However, in highly purified 0.1N H_2SO_4, no peroxide was detected ($I_r \cong 0$) and thus only reaction (3) seems to occur.

In 0.1N KOH, I_d/I_r versus $\omega^{-1/2}$ plots had varying slopes and also had intercepts greater than 1/N.[38] Therefore, Damjanovic, et al., concluded that O_2 reduction in alkaline solution proceeded along two parallel reaction paths with comparable rates. In one of these paths, hydrogen peroxide is a reaction intermediate which is partially reduced to water. In the other, oxygen is reduced to water without the formation of H_2O_2 as an intermediate.

Tarasevich and Bagotskii, et al., later presented more complete theoretical analyses of the oxygen reduction process in terms of parameters obtainable with the RRDE.[39-42] The basic difference in their treatment and that of Damjanovic, et al., was the inclusion of such processes as the electrochemical oxidation of hydrogen peroxide and its heterogeneous catalytic decomposition in a scheme as shown below:

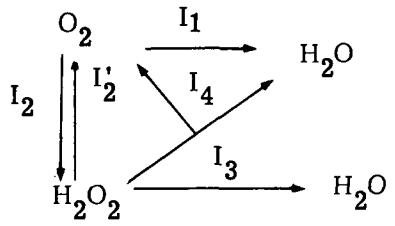

(11)

The following treatment of this reaction scheme is based on that of Bagotskii, Tarasevich, and Filinovskii.[42]

Assuming first order reaction kinetics, we may express the individual currents in terms of their rate constants as:

$$I_1 = 4 F k_1 C_A \tag{12}$$

$$I_2 = 2 F k_2 C_A \tag{13}$$

$$I_2' = 2 F k_2' C_B \tag{14}$$

$$I_3 = 2 F k_3 C_B \tag{15}$$

$$I_4 = 2 F k_4 C_B \tag{16}$$

Here C_A and C_B are the surface concentrations of oxygen and hydrogen peroxide respectively. In addition to Eqs. (12-16) we can write the following two equations describing the diffusion kinetics:

$$I_A = 4 F m_A (C_A^0 - C_A) \tag{17}$$

$$I_B = 2 F m_B (C_B^0 - C_B) \tag{18}$$

where m_A and m_B are the respective mass transfer coefficients given by:

$$m_A = 0.62 D_A^{2/3} \nu^{-1/6} \omega^{1/2} \tag{19}$$

$$m_B = 0.62 D_B^{2/3} \nu^{-1/6} \omega^{1/2} \tag{20}$$

and C_A^0 and C_B^0 refer to the bulk concentration of O_2 and H_2O_2.

Under steady-state conditions, mass balance for oxygen requires that:

$$I_A + I_4 + 2I_2' = I_1 + 2I_2 \tag{21}$$

or

$$m_A (C_A^0 - C_A) + \frac{1}{2} k_4 C_B + k_2' C_B = k_1 C_A + k_2 C_A \tag{22}$$

In the absence of hydrogen peroxide in the bulk of the solution, we have the mass balance for for H_2O_2 as:

$$I_2 = I_B + I_2' + I_3 + I_4 \qquad (23))$$

or:

$$k_2 C_A = m_B C_B + k_2' C_B + k_3 C_B + k_4 C_B \qquad (24)$$

The observed disk current, I_d, is given by:

$$I_d = I_1 + (I_2 - I_2') + I_3 \qquad (25)$$

or,

$$I_d = 4 F k_1 C_A + 2F (k_2 - k_2') C_A + 2F k_3 C_B \qquad (26)$$

According to the original theory of Ivenov and Levich, the ring current, I_r, is given by: [43,44]

$$I_r = N I_B \qquad (27)$$

where N is the collection efficiency and is dependent only on the electrode dimensions.

Appropriate substitutions in (26) yields the ratio:

$$\frac{I_d}{I_B} = 1 + 2\frac{k_1}{k_2} + \left[\left(1 + 2\frac{k_1}{k_2}\right)(k_2' + k_3 + k_4) + (k_3 - k_2')\right]\frac{1}{m_B} \qquad (28)$$

or in terms of I_d/I_r:

$$\frac{I_d}{I_r} = \frac{1}{N}\left(1 + 2\frac{k_1}{k_2}\right) + \frac{1}{N m_B}\left[\left(1 + 2\frac{k_1}{k_2}\right)(k_2' + k_3 + k_4) + (k_3 - k_2')\right] \qquad (29)$$

One can also derive the following relationship:

$$\frac{I_d^{\ell} - I_d}{I_r} = \frac{1}{N}\left[1 + 2\left(\frac{k_3 + k_4 + k_2}{k_2}\right)\frac{D_A^{2/3}}{D_B^{2/3}} + \frac{2m_A}{k_2}\right] \qquad (30)$$

where I_d^{ℓ} is the limiting oxygen reduction current equal to $4 F m_A C_A^0$.

Using (29) and (30), k_2 and k_1 may be obtained explicitly from experimental data. However, k_2', k_3, and k_4 may be obtained only as the combinations:

$$k_a = k_3 - k_2' \qquad (31)$$

$$k_b = k_4 + 2k_3 \qquad (32)$$

$$k_c = 2k_2' + k_4 \qquad (33)$$

k_2', k_3 and k_4 may be estimated from thermodynamic considerations, since k_2 and k_2' are related by:

$$k_2' = k_2 \exp\left[\frac{2F}{RT}(E - E^{0'})\right] \qquad 34$$

where $E^{0'}$ is the formal potential of the O_2/H_2O_2 redox system.

It should be mentioned here that Eq. (29) reduces to the original relationship derived by Damjanovic, et al.,[37] that is:

$$\frac{I_d}{I_r} = \frac{x+1}{N} + \frac{x+2k'}{N\omega^{1/2}} \qquad (35)$$

if we let $2\,k_1/k_2 = x$, and with k_2' and k_4 equal to zero. ($k' = 1.61\,D^{-2/3}\,\nu^{1/6}\,k_3$)

Tarasevich, Burshtein, and Radyashkina applied the treatment of Bagotskii, et al., to the reduction of oxygen in 0.1N KOH.[45] Since the use of Eqs. (29) and (30) require experimental data of high accuracy and reproducibility, special experimental care was taken. Measurements were made from open circuit (10 min) and also on prereduced smooth platinum (0.0 V/5 min). Limiting currents corresponded to a four-electron process, but the prereduced electrode gave higher disk currents at more positive potentials accompanied by lower ring current values. On the prereduced surface, I_d/I_r values were time dependent and changes in intercept and slope of I_dN/I_r plots were observed. On the nonreduced electrode surface, I_dN/I_r versus $\omega^{-1/2}$ plots had intercepts of ~3 indicating that both the two-electron and four-electron processes were occurring simultaneously. The slopes of the I_dN/I_r plots decreased with increasing cathodic polarization for $E_d > +0.8$ V, then increased for $E_d < +0.8$ V. From plots of $(k_3 - k_2')$, $(2k_2' + k_4)$, and $(2k_3 + k_4)$ versus E_d, it was inferred that, at $E_d > +0.85$ V, electrochemical oxidation of H_2O_2 was predominant. At $E_d = +0.85$ V, the electrochemical and catalytic decomposition proceeded at comparable rates. As the potential decreases, catalytic decomposition became less predominant until it ceased at $E_d < +0.65$ V, whereafter electrochemical reduction of H_2O_2 alone was observed.

Breiter commented on the conclusions reached by Damjanovic, et al.[46] He pointed out that, from an experimental viewpoint, such conclusions are critically dependent on maintaining the same surface state at different angular velocities and on the accuracy of the determination of I_d/I_r along with that of the extrapolation of the I_d/I_r versus $\omega^{-1/2}$ plots. In this light, Breiter did not consider the accuracy of the determination of the intercept sufficient to separate the contribution of reaction (3) from that of (4) and (5) if the intercept was less than 2/N. Such values were reported for Pt and for Rh in a large potential range for basic electrolytes.[38, 47] The same comment seems to apply to the work of Taresevich, et al.[45]

Blurton and McMullin also studied the reduction of O_2 using the RRDE technique but in 6.9N KOH at 70 °C.[48] They found that I_d/I_r values for oxygen reduction under their conditions were greater than 1/N (ca. 5) and were independent of rotation speed and of potential between +0.8 and 0.4V. They preferred a mechanism whereby oxygen is electrochemically reduced to hydrogen peroxide which then decomposes by a second order surface catalyzed chemical reaction to form oxygen and water according to the following equations:

$$O_2 + H_2O + 2e^- \rightarrow HO_2^- + OH^- \quad (36)$$

$$2HO_2^- \xrightarrow{k_h} O_2 + 2OH^- \quad (37)$$

Their conclusion was based on the curvature of I_d versus $\omega^{1/2}$ plots as described by McIntyre for such a mechanism.[49] According to Blurton and McMullin, the presence of a second order heterogeneous reaction decreases the dependence of I_d/I_r on $\omega^{-1/2}$ from that originally predicted by Damjanovic, et al. However, it should be mentioned that the curvature in the plots of I_d versus $\omega^{1/2}$ can also be explained by an increased mass transport of impurities to the disk electrode which could cause mechanism changes due to poisoning of surface sites.

McIntyre has also treated in some detail the similarity between a heterogeneous catalytic electrode reaction (HCER) and a reaction involving parallel paths.[50] He concluded that the plots of I_d/I_r versus $\omega^{-1/2}$ for a HCER bear a close resemblance to those for the simple parallel path especially in the restricted range of rotational speeds commonly employed in kinetic studies with the RRDE. The characteristic curvature of HCER can only be revealed properly by obtaining data over a wide range of disk angular velocities (rotation speeds of 100 to 10,000 rpm).

We have used the ring-disk electrode technique in a study of the mechanism of oxygen reduction in highly purified 0.1N KOH and 8.5N KOH on both smooth and platinized platinum electrodes. We have also studied the effects of controlled addition of a number of ionic species which may be present in rechargeable oxygen battery systems and the effects of cycling under Regime I on oxygen reduction and evolution.

B. Experimental

The rotating ring-disk electrode apparatus was supplied by R. Disantis, (Willowick, Ohio), and is schematically depicted in Fig. 30. The rotation rate was monitored via the photoconductive cell with readout to a digital frequency counter.

While our original intent was to use a ring-disk potentiostat of the design of Miller using operational amplifiers,[45] the low ring current levels observed and the inability to accurately measure ring background currents with the disk electrode at open circuit due to electronic problems in this circuit required the use of a more conventional arrangement schematically pictured in Fig. 31. Here the disk is under potentiostatic control via a Wenking potentiostat (Model 61RS). The potential of the disk is modulated using a Tyco-constructed step function generator for electrode pretreatment potential sequence generation. Disk currents have been converted to a suitable voltage for recording with an operational amplifier current-to-voltage converter in the working electrode line or with a Keithly Electrometer (Model 150A or Model 610B). The ring electrode potential was controlled by means of a bias box versus the reference electrode with current measurement and conversion to voltage via a Keithly electrometer. Disk current and ring current versus time curves were recorded simultaneously with a Hewlett-Packard Model 7100B Dual Channel strip chart recorder.

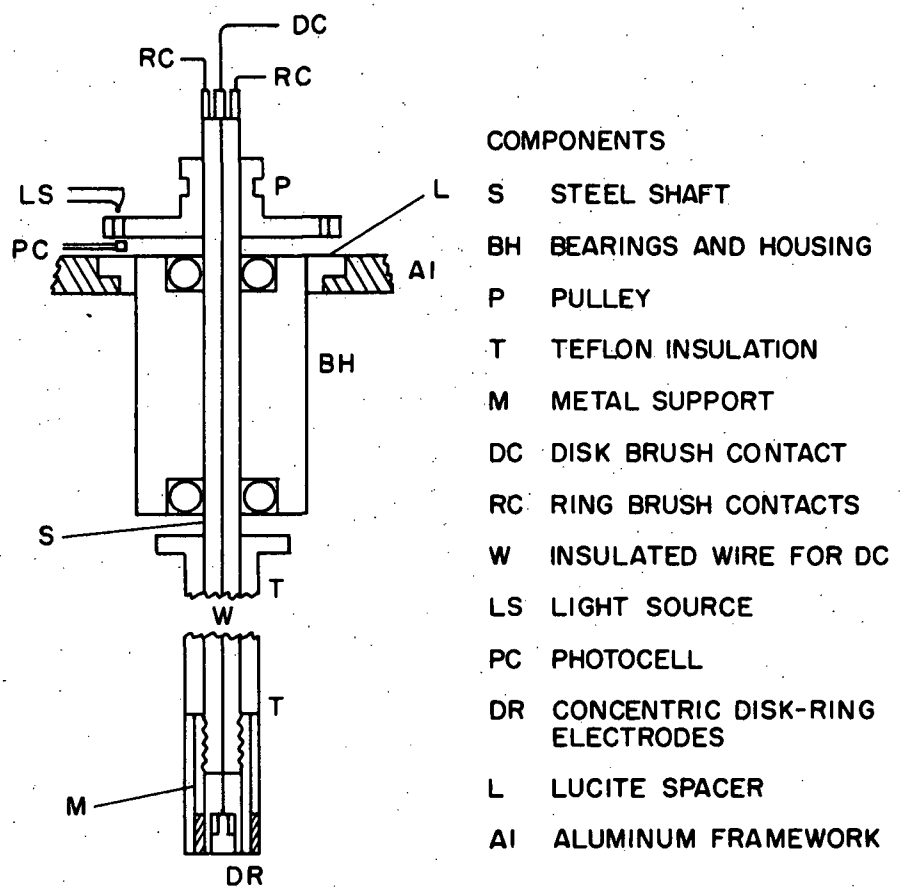

Fig. 30. Rotating ring-disk electrode assembly

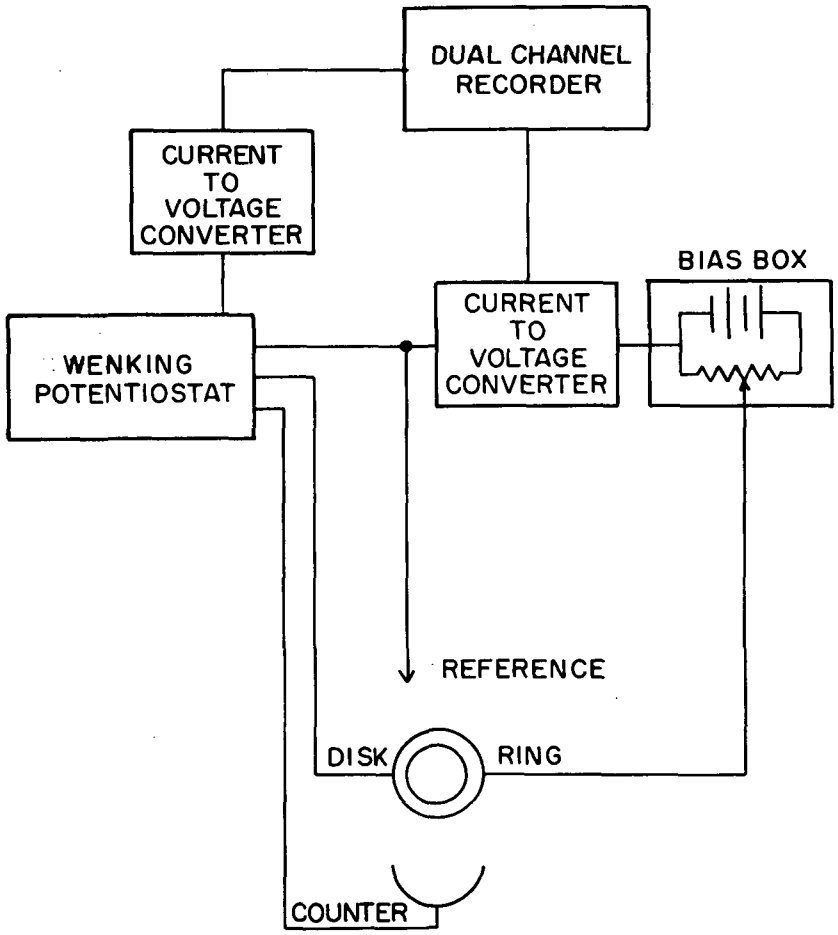

Fig. 31. Schematic representation of the electronic arrangement for rotating ring-disk electrode voltammetry

The ring electrode was lightly platinized before use. The collection efficiency of the ring-disk electrodes used was determined by using the reversible oxidation of ferrocene to ferricinium cation in acetonitrile with 0.2N tetra-ethylammonium perchlorate as the supporting electrolyte. An average value of 0.41 was observed in good agreement with that calculated from geometric parameters of 0.39.

The preparation of pure 8.5N KOH has been described in Section III. The polarographically measured concentrations of Cd^{2+} and $Zn(OH)_4^{2-}$ in 8.5N KOH saturated with CdO and ZnO were 1.8×10^{-4} M (Cd^{2+}) and 5.4×10^{-1} [$Zn(OH)_4^{2-}$]. The carbonate containing electrolyte was 1 M K_2CO_3 in 6.5N KOH. All measurements were made at 30 °C.

C. Results and Discussion

1. O_2 reduction in pure KOH electrolytes

We have spent a considerable amount of effort in obtaining consistent, reproducible data for O_2 reduction in the pure KOH electrolytes. Two problems encountered here were: (1) the low current levels observed because of low oxygen solubility in 8.5N KOH (6×10^{-5} moles/ℓ), and (2) the very marked effects of solution purity.

The main difficulty in obtaining reproducible I_d/I_r measurements was traced to problems in measuring I_r. In order to accurately measure I_r, it was necessary to correct for the ring background current. Originally, we attempted to measure the ring-background current, I_r^b, with the disk at +1.4 V. However, this led to irreproducible results. Measurement of the ring-background current with the disk at open circuit led to more consistent results. The ring background current is a function of potential and becomes greater at $E_r > +1.3$ V. I_r^b is slightly dependent on electrode rotation rate which is indicative of a some diffusion-controlled faradaic process, i.e., oxidation of solution impurities.

Table XV shows the behavior of I_r for differing E_r with E_d = +0.6 V in O_2-saturated 8.5N KOH at a rotation speed of 30 rps. The corrected ring current is relatively independent of E_r which substantiates that we are in the limiting current region of H_2O_2 oxidation at the ring electrode. However, the precision of these measurements is quite poor since the average I_d/I_r values from the four measurements in Table XV is 10.1 ± 0.9. Although the corrected I_r is independent of potential we have used E_r = +1.2V to minimize contributions from background currents.

Table XV. Ring Current as a Function of Ring Potential for O_2 Reduction at E_d = +0.6 V on Smooth Pt in 8.5N KOH at 30 °C

E_r, V	I_r^b, μA	I_r^{obs}, μA	I_r^{corr}, μA	I_d/I_r
1.1	+0.3	- 1.8	- 2.1	11.3
1.2	- 0.2	- 2.5	- 2.3	9.3
1.3	- 0.7	- 2.9	- 2.2	9.9
1.4	- 1.9	- 4.3	-2.4	10.0

We have observed that the state of the solution purity has a major influence on the values of I_d and the I_d/I_r ratio in both 0.1N KOH and 8.5N KOH. These finding are in disagreement with those of Damjanovic, et al., who found no time dependent effects attributable to residual solution impurities on such measurements in 0.1N KOH.[38] However, Tarasevich, et al., did report time-dependent I_d/I_r readings on prereduced smooth platinum during O_2 reduction in 0.1N KOH.[45] Also, Damjanovic, et al., in another paper, found that H_2O_2 was only produced during O_2 reduction on smooth platinum in insufficiently purified 0.1N H_2SO_4.

Figs. 32 and 33 show the time dependence of I_d and I_r during O_2 reduction in purified and nonpurified 8.5N KOH at E_d = +0.6 V and 60 rps. Fig. 32 shows that the disk current is much higher in the purified 8.5N KOH where it decreases rather slowly and true steady state is not achieved even after 30 min. In contrast, the disk current in the purified electrolyte decreases rather rapidly to a nominally steady-state value. I_r data plotted in Fig. 33 show much less peroxide formation in the purified electrolyte. I_d/I_r values (at 30 min) are 4.4 in the nonpurified electrolyte as compared to 21 in the purified electrolyte.

Figs. 34, 35, and 36 show slow-sweep (100 mV/min) composite I_d-I_r versus E curves from +1.2 to 0.0 V and returning to 1.2 V on a smooth Pt rotating ring-disk electrode at 65 rps in 0.1N KOH electrolyte at different levels of purity. The ring was held at +1.2 V to detect H_2O_2. The sweeps of Fig. 34 were obtained in unpurified 0.1N KOH. Figs. 35 and 36 present comparable sweeps for 0.1N KOH purified by a preadsorption for 16 hr and a total of 190 hr. (The corresponding cyclic sweeps for these electrolytes appeared in Fig. 10.) It can be seen that there is a marked effect of electrolyte purity on I_r. As the electrolyte becomes "cleaner," the amount of H_2O_2 production decreases accordingly. Figs. 37 and 38 show similar composite I_d-I_r versus E curves for smooth Pt in unpurified and purified 8.5N KOH at 30 °C. From these I-E curves, in 8.5N KOH, H_2O_2 production is seen to be a maximum at ~+0.8 V. There is also a tendency for H_2O_2 production to increase again at +0.4 V. Again the very marked influence of solution purity can be seen.

In order to make more detailed study of O_2 reduction by diagnostic plots of I_d/I_r versus $\omega^{-1/2}$, we adopted the following procedure, since the use of a slow potential sweep introduces some problems with regard to the exact state of the electrode surface. We felt it preferable to use a constant potential technique, especially in assessing the effect of surface state, e.g., the presence of the platinum-oxygen layer. We obtained an oxygen layer-free Pt surface, which we will term "prereduced," by holding at +1.4 V for 1 min, then reducing at +0.0 V for 1 min before imposing the potential of interest. A Pt surface with an oxygen layer, which we will term "preoxidized," was obtained by holding at +1.75 V for 2 min prior to imposing the potential of interest. The electrode was pretreated as just described before I_d and I_r versus time curves were obtained at constant potential using rotation rates from 5 to 65 rps. The I_d and I_r versus time curves were followed for 30 min and the ratio I_d/I_r calculated from the corresponding current values at 30 min. In an unpurified electrolyte the I_d and I_r values

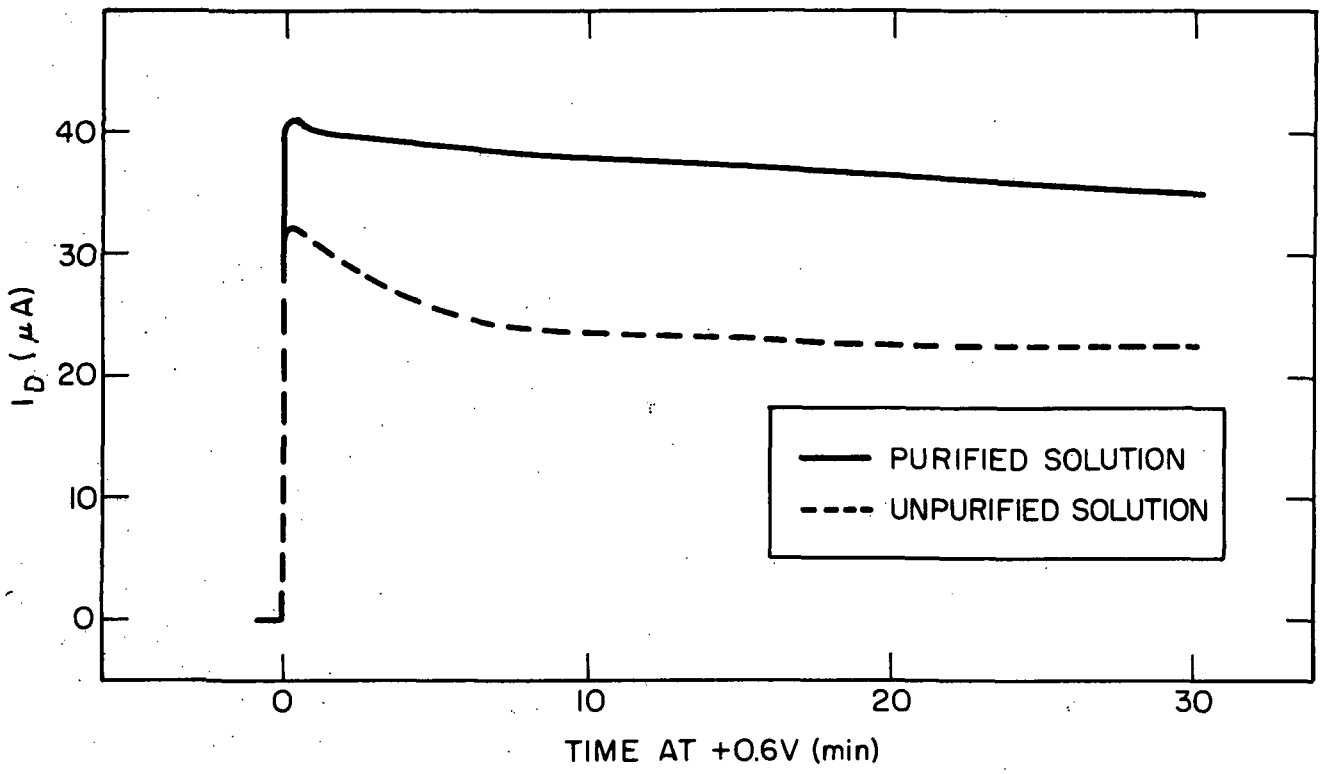

Fig. 32. I_d at E_d = +0.6 V as a function of time on a prereduced smooth Pt disk electrode (60 rps) in unpurified and purified 8.5N KOH at 30 °C

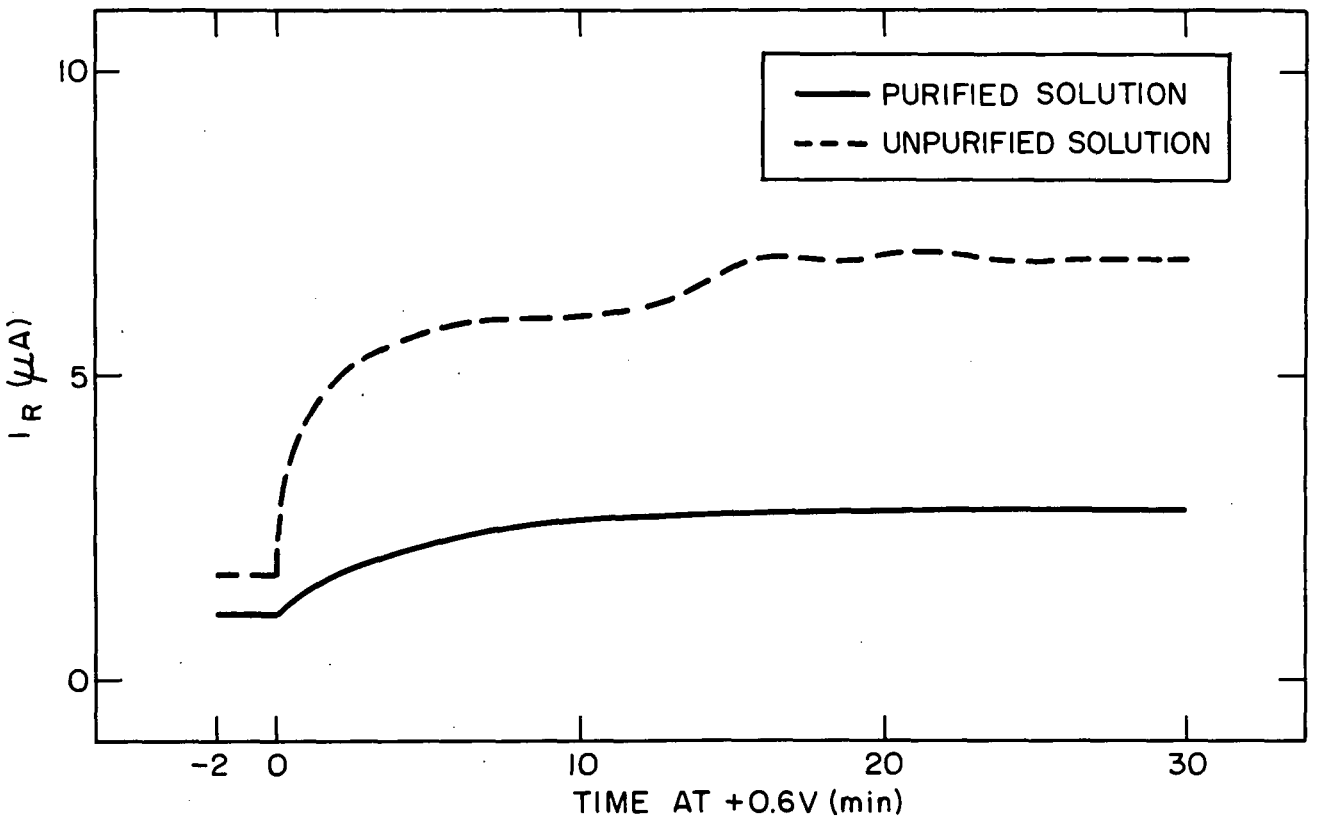

Fig. 33. I_r at E_r = +1.2 V and E_d = +0.6 V as a function of time on a pre-reduced smooth Pt disk electrode (60 rps) in unpurified and purified 8.5N KOH

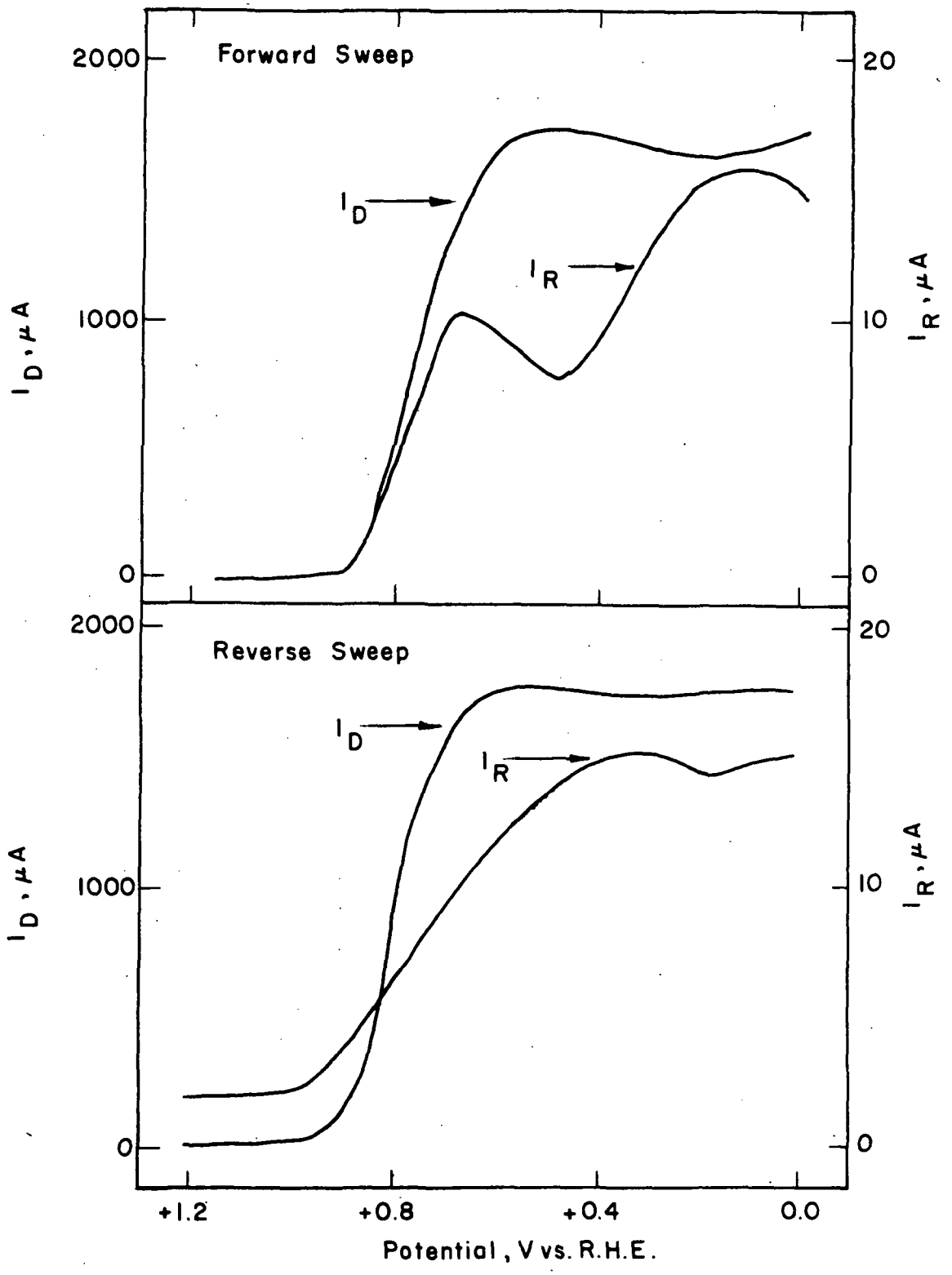

Fig. 34. Composite I_d-I_r versus E_d curves obtained by sweeping from +1.2 to 0.0 V (forward) then 0.0 to +1.2 V (reverse) at 100 mV/min on a smooth Pt disk electrode (66 rps) at 30 °C in O_2-saturated 0.1N KOH which had not been purified (E_r was held at +1.2 V)

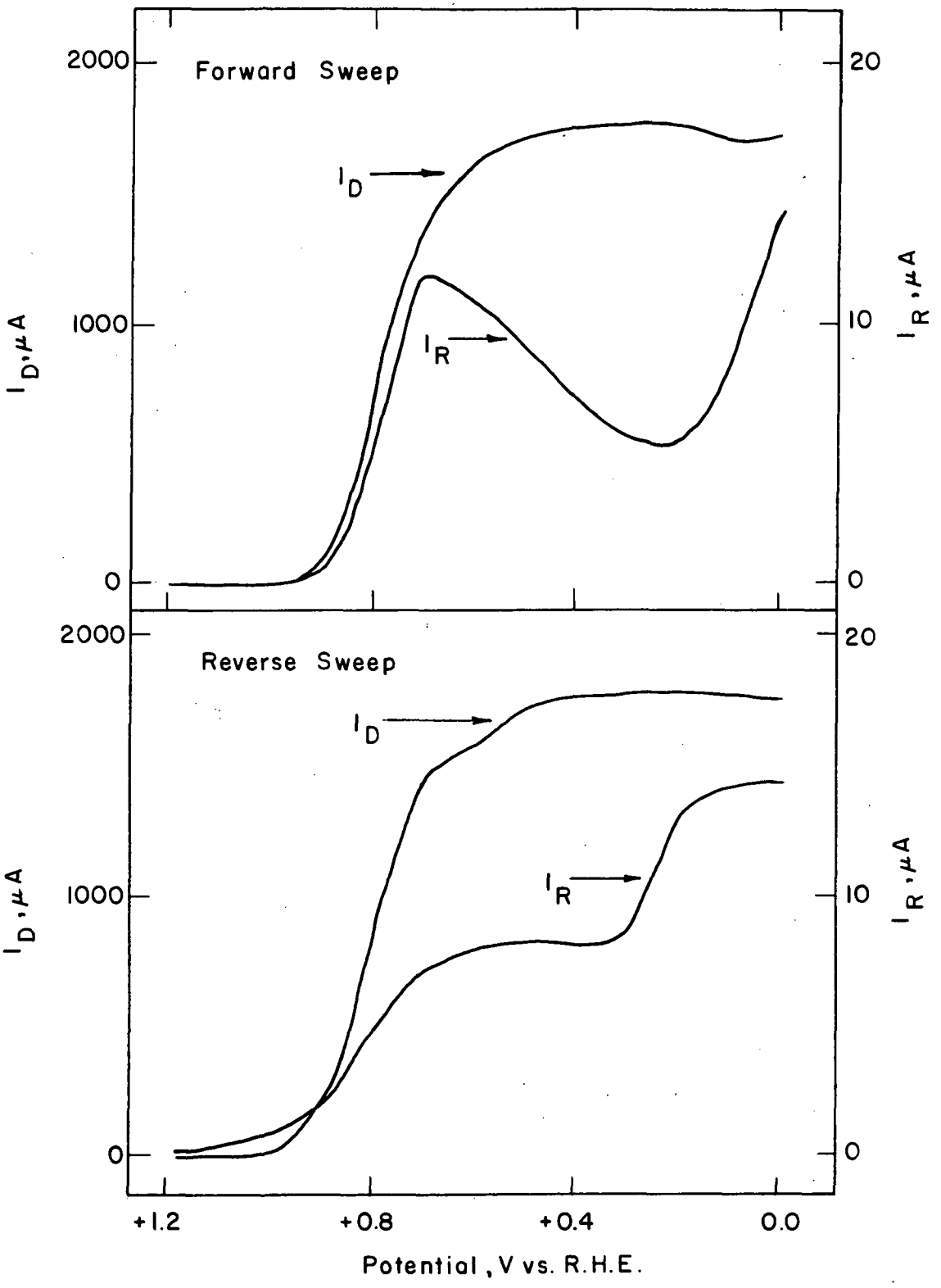

Fig. 35. Composite I_d-I_r versus E_d curves obtained by sweeping from +1.2 to 0.0 V (forward) then 0.0 to +1.2 V (reverse) at 100 mV/min on a smooth Pt disk electrode (66 rps) at 30 °C in O_2-saturated 0.1N KOH which had been subjected to purification by preadsorption for 16 hr (E_r was held at +1.2 V)

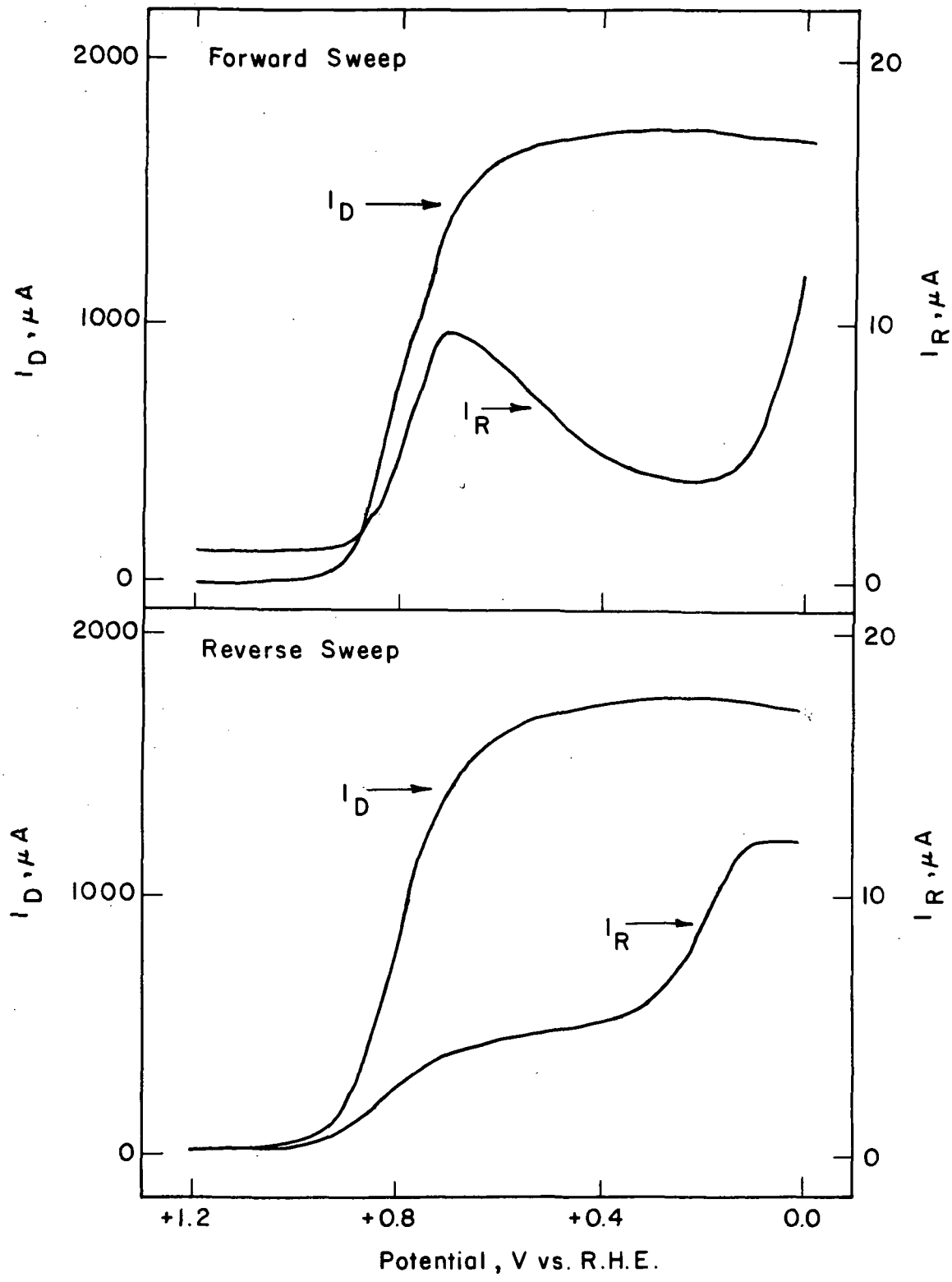

Fig. 36. Composite I_d-I_r versus E_d curves obtained by sweeping from +1.2 to 0.0 V (forward) then 0.0 to +1.2 V (reverse) at 100 mV/min on a smooth Pt disk electrode (66 rps) at 30 °C in O_2-saturated 0.1N KOH which had been subjected to purification by preadsorption for 190 hr (E_r was held at +1.2 V)

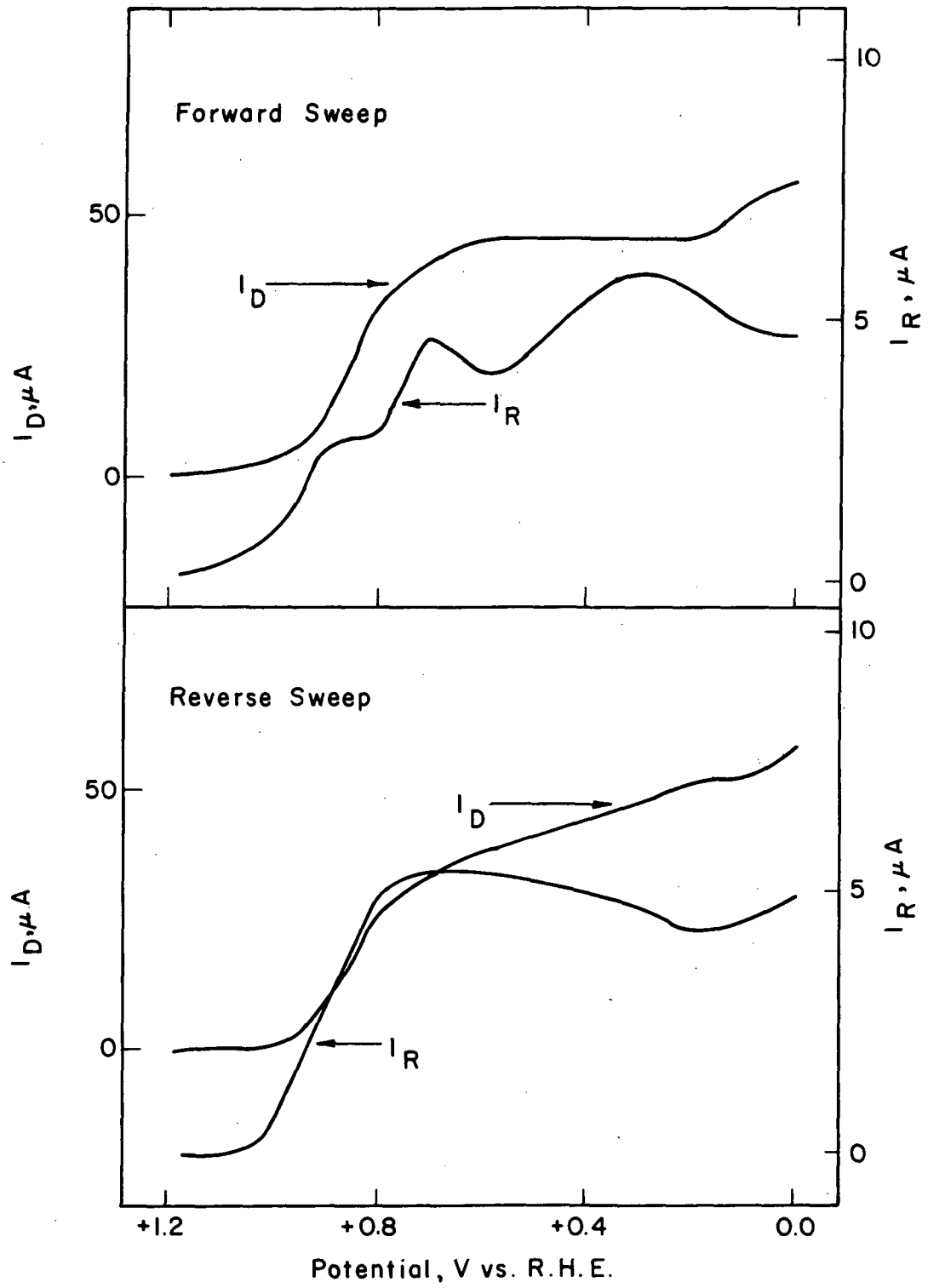

Fig. 37. Composite I_d-I_r versus E_d curves obtained by sweeping from +1.2 to 0.0 V (forward) then 0.0 to +1.2 V (reverse) at 100 mV/min on a smooth Pt disk electrode (66 rps) at 30 °C in O_2-saturated 8.5N KOH which had not been purified (E_r was held at +1.2 V)

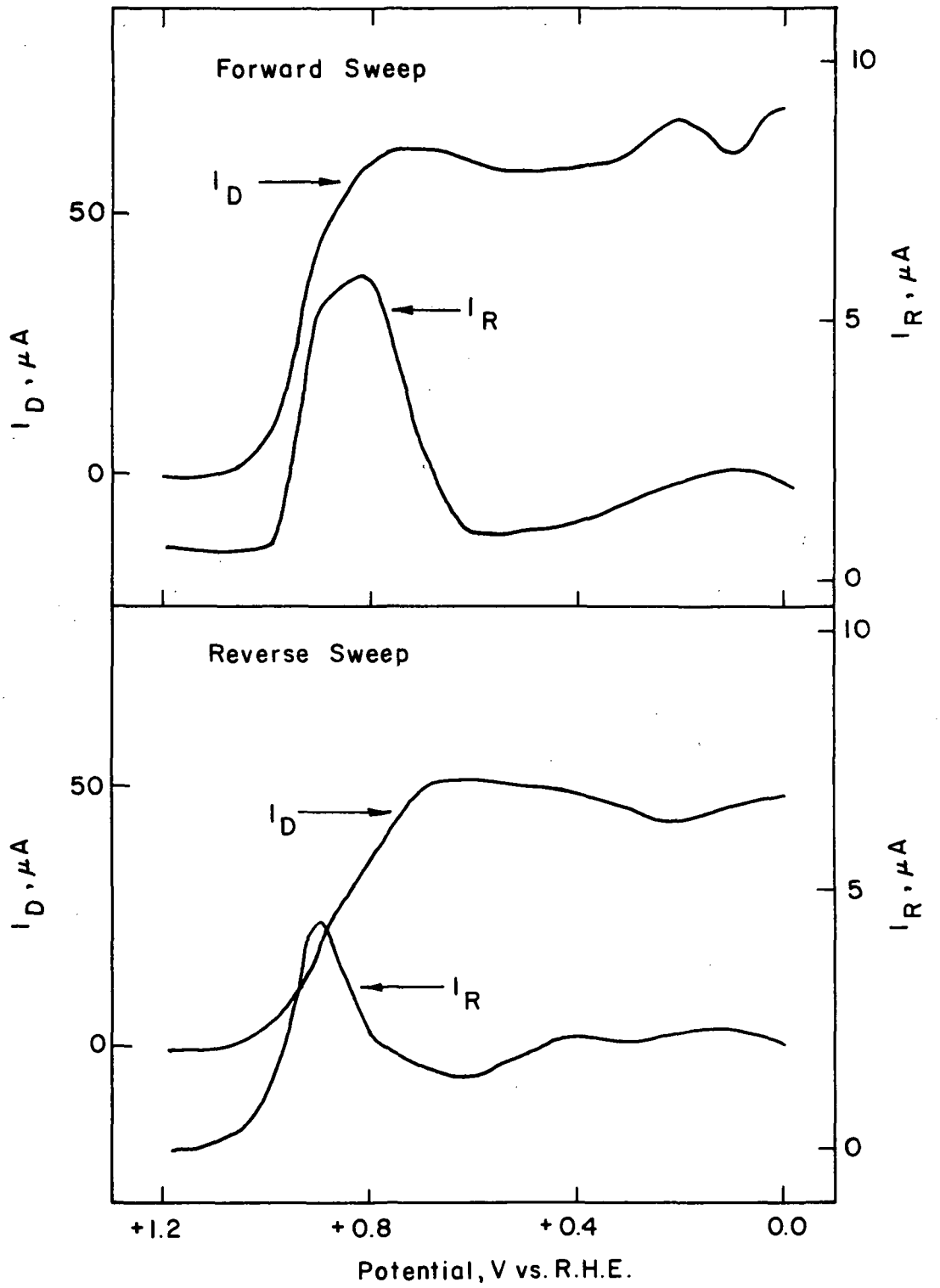

Fig. 38. Composite I_d-I_r versus E_d curves obtained by sweeping from +1.2 to 0.0 V (forward) then 0.0 to +1.2 V (reverse) at 100 mV/min on a smooth Pt disk electrode (65 rps) at 30 °C in O_2-saturated 8.5N KOH which had been purified by preadsorption (E_r was held at +1.2 V)

reached a steady-state value in less than 5 min. However, in purified KOH, I_d decreased rather slowly, and this was accompanied by increasing I_r values.

Figs. 39 and 40 compare composite I_d-I_r versus E_d curves for O_2 reduction of prereduced and preoxidized smooth Pt in 8.5N KOH of a high degree of purity (see Fig. 9, Section III for the corresponding cyclic I-E curves for this particular electrolyte). These points were obtained after 30 min at the potential of interest at a rotation rate of 64 rps. There is a well-defined maximum in I_r at +0.8 to +0.9 V. As E_d becomes more cathodic, peroxide production decreases, then shows a tendency to increase at $E_d < +0.4$ V. Table XVI gives the corresponding I_d/I_r values as a function of E_d. It appears that peroxide formation is favored on the preoxidized surface at $E_d \geq 0.8$ V. At $E_d \leq 0.6$ V, the prereduced and preoxidized surfaces show quite similar I_d/I_r values. This is not too surprising since at these potentials the oxygen layer formed at +1.75 V can be reduced, and the two electrode surfaces become equivalent.

Figs. 41 through 44 compare I_d/I_r versus $\omega^{-1/2}$ plots for O_2 for reduction on a prereduced smooth Pt surface in unpurified and purified 8.5N KOH at 30 °C. It can be seen that, in unpurified 8.5N KOH, a series of lines parallel to the $\omega^{-1/2}$ axis is obtained, while in purified 8.5N KOH a series of straight lines with a positive slope is observed. Based on the original diagnostic criteria of Damjanovic, et al., it would appear that in unpurified 8.5N KOH we are dealing with the case of H_2O_2 production as a species which cannot be reduced further.[37] Implicit in this argument of Damjanovic, et al., then, is that the four-electron process of O_2 reduction to water also occurs in parallel with the two-electron reduction of O_2 to H_2O_2 since the I_d/I_r values are greater than 1/N (~2.5). However, for O_2 reduction in the purified 8.5N KOH, we have observed $\omega^{-1/2} = 0$ intercepts at I_d/I_r ~1/N. This finding of I_d/I_r intercepts of ~1N is indicative of a two-step reduction of O_2 to H_2O via H_2O_2 as a reactive intermediate, without any contribution of the four-electron process.

It is difficult to rationalize the presence of the four-electron process in unpurified 8.5N KOH and its absence in purified 8.5N KOH. There is, however, an alternate explanation. From Figs. 41-44, the unpurified 8.5N KOH shows I_d/I_r values on the order of ~10, independent of $\omega^{-1/2}$ and E_d. It seems unlikely that k_1 and k_2 would be independent of potential. If in Eq. (29), we assume $k_1 << k_2$ then we obtain:

$$\frac{I_d}{I_r} = \frac{1}{N} + \frac{1}{m_B N}(2k_3 + k_4) \qquad (38)$$

or

$$\frac{I_d}{I_r} = \frac{1}{N} + \frac{1}{\gamma_B N \omega^{1/2}}(2k_3 + k_4) \qquad (39)$$

For 8.5N KOH, $\gamma_B \cong 5 \times 10^{-4}$; therefore, for an I_d/I_r of ~10, $2k_3 + k_4 = 3 \times 10^{-2}$ cm/sec at $\omega^{1/2} = 20$ and 0.8×10^{-2} at $\omega^{1/2} = 5$. Therefore, a factor of four variation in the sum, $2k_3 + k_4$,

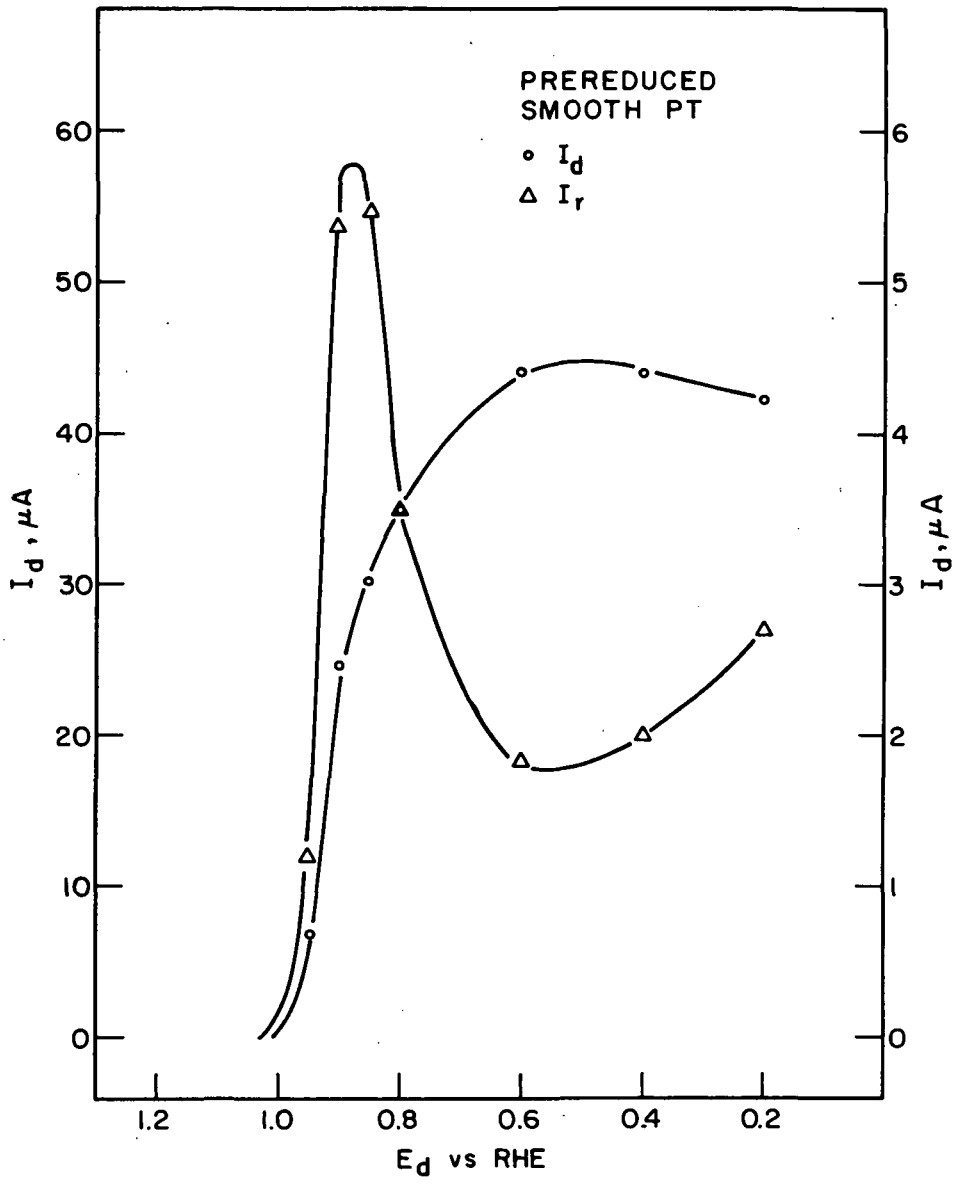

Fig. 39. Steady-state I_d-I_r versus E_d curves obtained during O_2 reduction at a prereduced smooth platinum disk electrode at 64 rps in purified 8.5N KOH at 30 °C

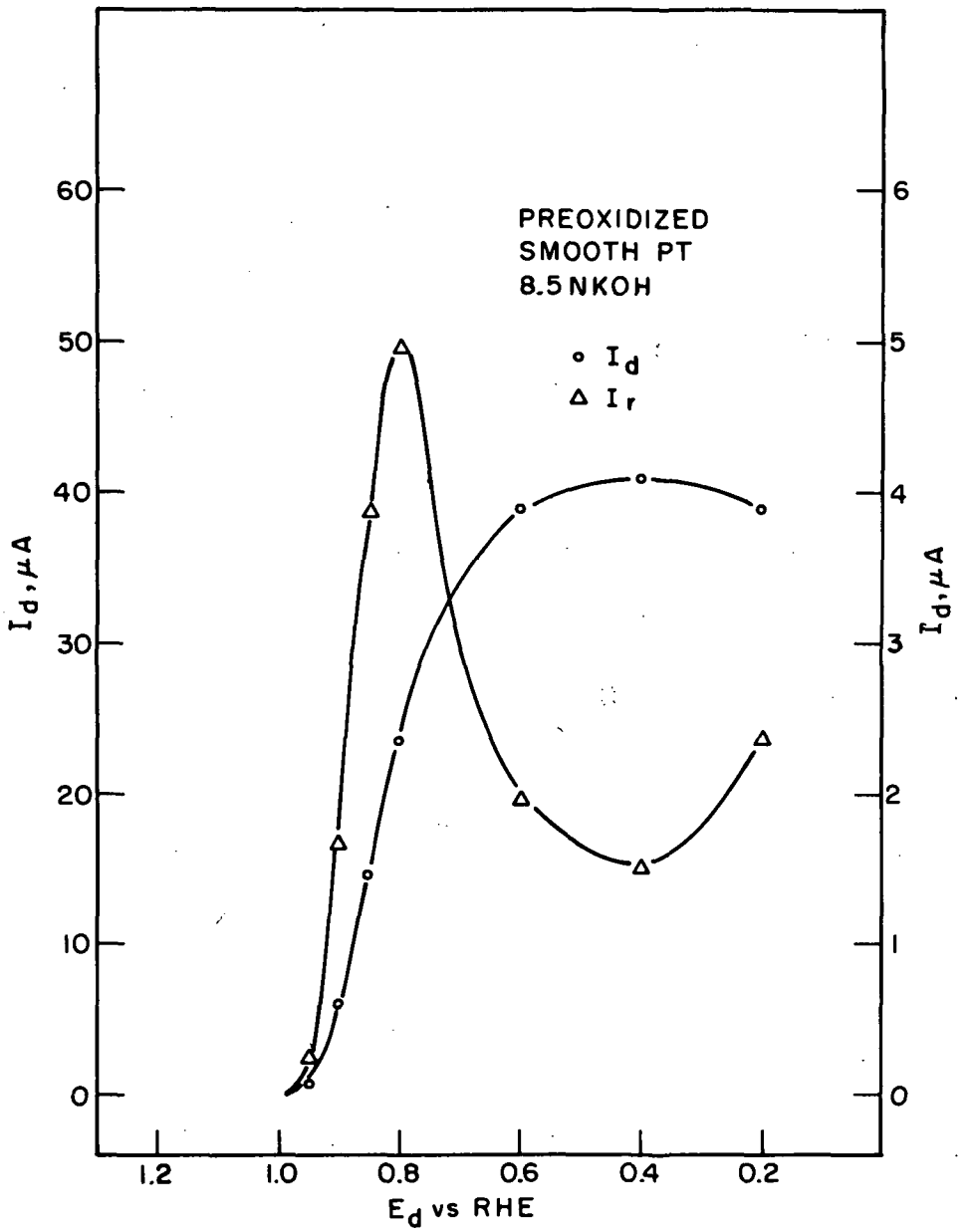

Fig. 40. Steady-state I_d-I_r versus E_d curves obtained during O_2 reduction at a preoxidized smooth platinum disk electrode at 64 rps in purified 8.5N KOH at 30 °C

Table XVI. Comparison of I_d/I_r Values at Prereduced and Preoxidized Smooth Platinum Electrodes For Oxygen Reduction in Purified 8.5N KOH at 30 °C

E_d	I_d/I_r	
	Preoxidized	Prereduced
0.95	2.6	5.8
0.90	3.7	4.6
0.85	3.8	5.5
0.80	4.8	10
0.60	20	24
0.40	27	22
0.20	16	16

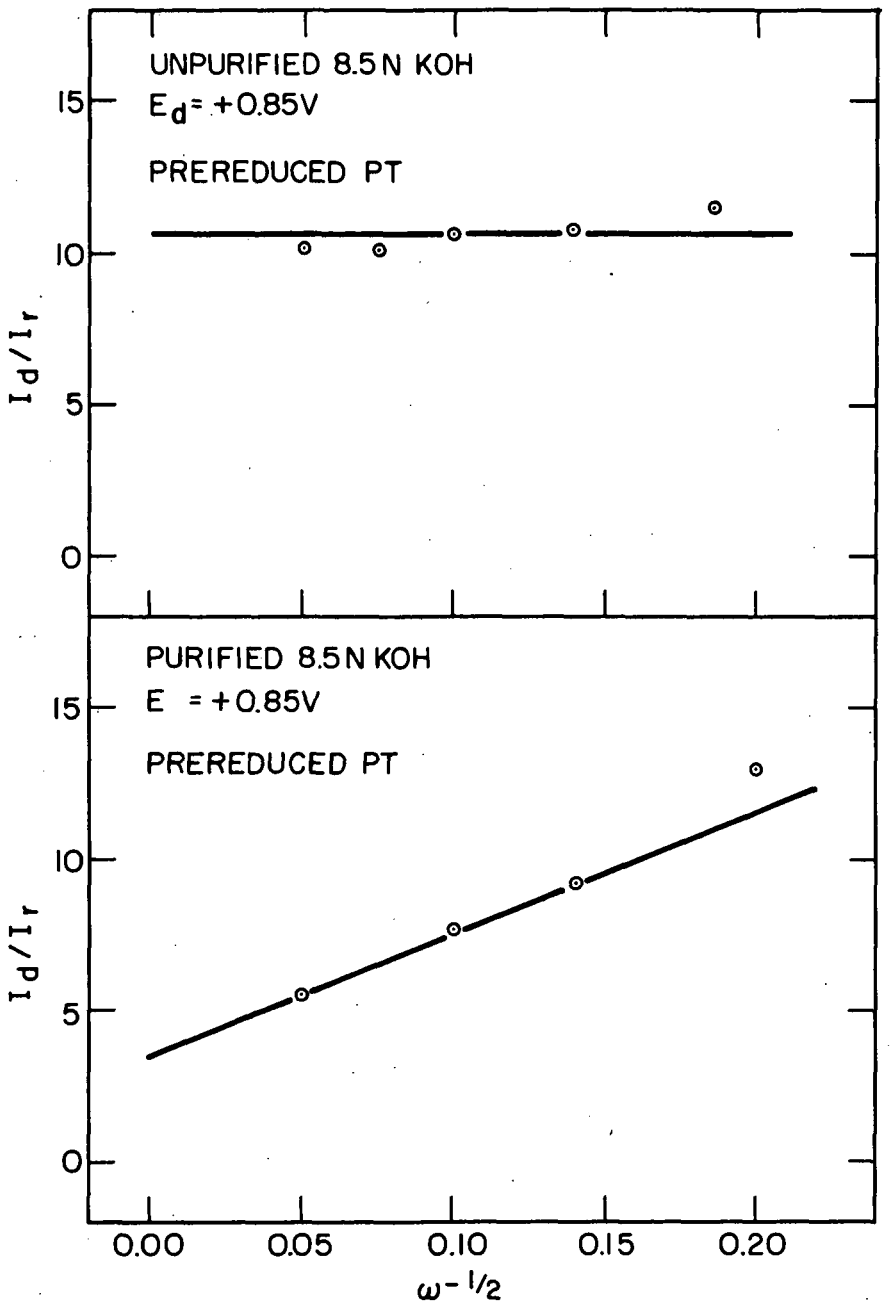

Fig. 41. I_d/I_r versus $\omega^{-1/2}$ plots for O_2 reduction at a prereduced smooth Pt disk electrode, E_d = +0.85 V, in unpurified and purified 8.5N KOH at 30 °C, with E_r = +1.2 V

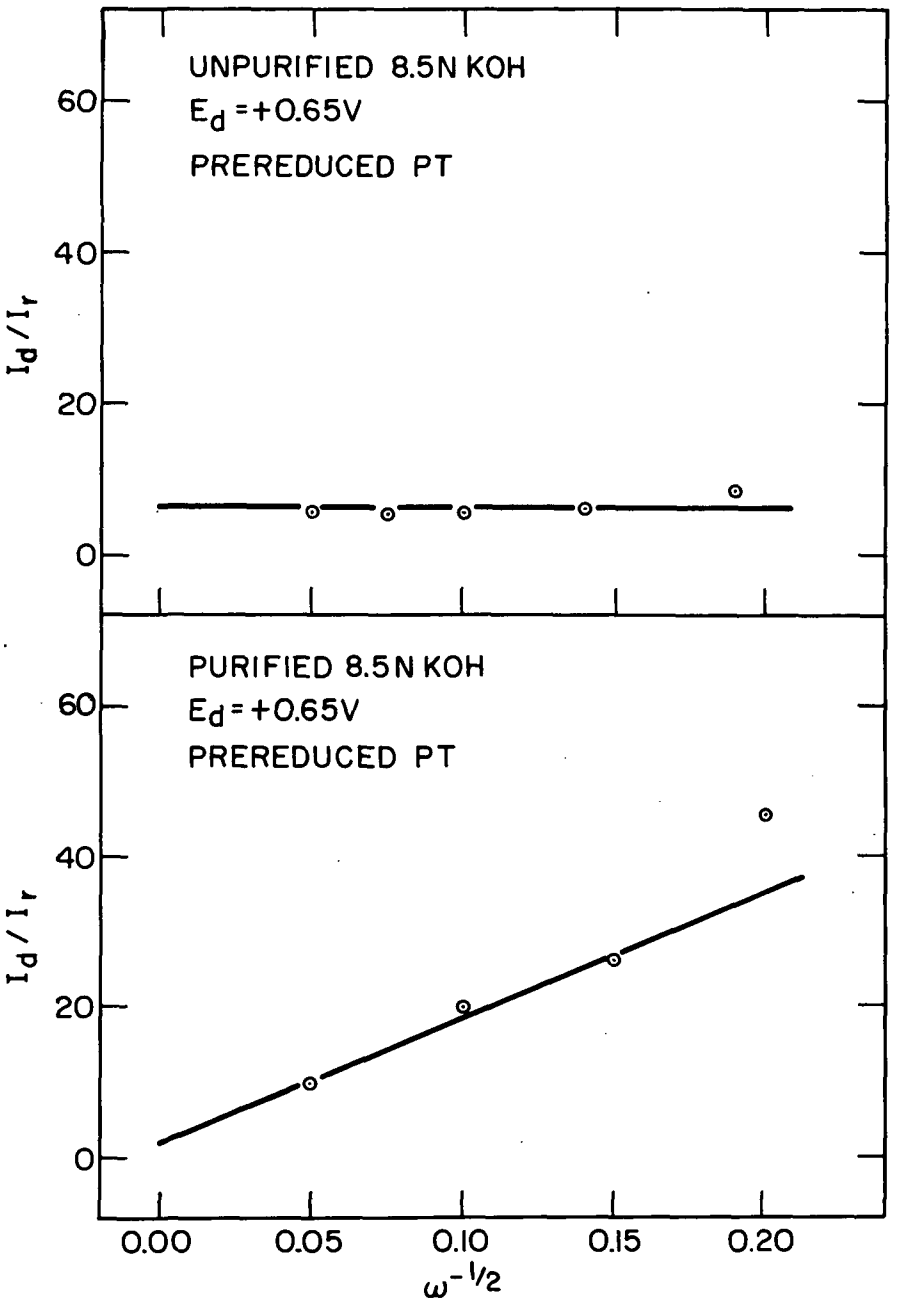

Fig. 42. I_d/I_r versus $\omega^{-1/2}$ plots for O_2 reduction at a prereduced smooth Pt disk electrode, E_d = +0.65 V, in unpurified and purified 8.5N KOH at 30 °C, with E_r = +1.2 V

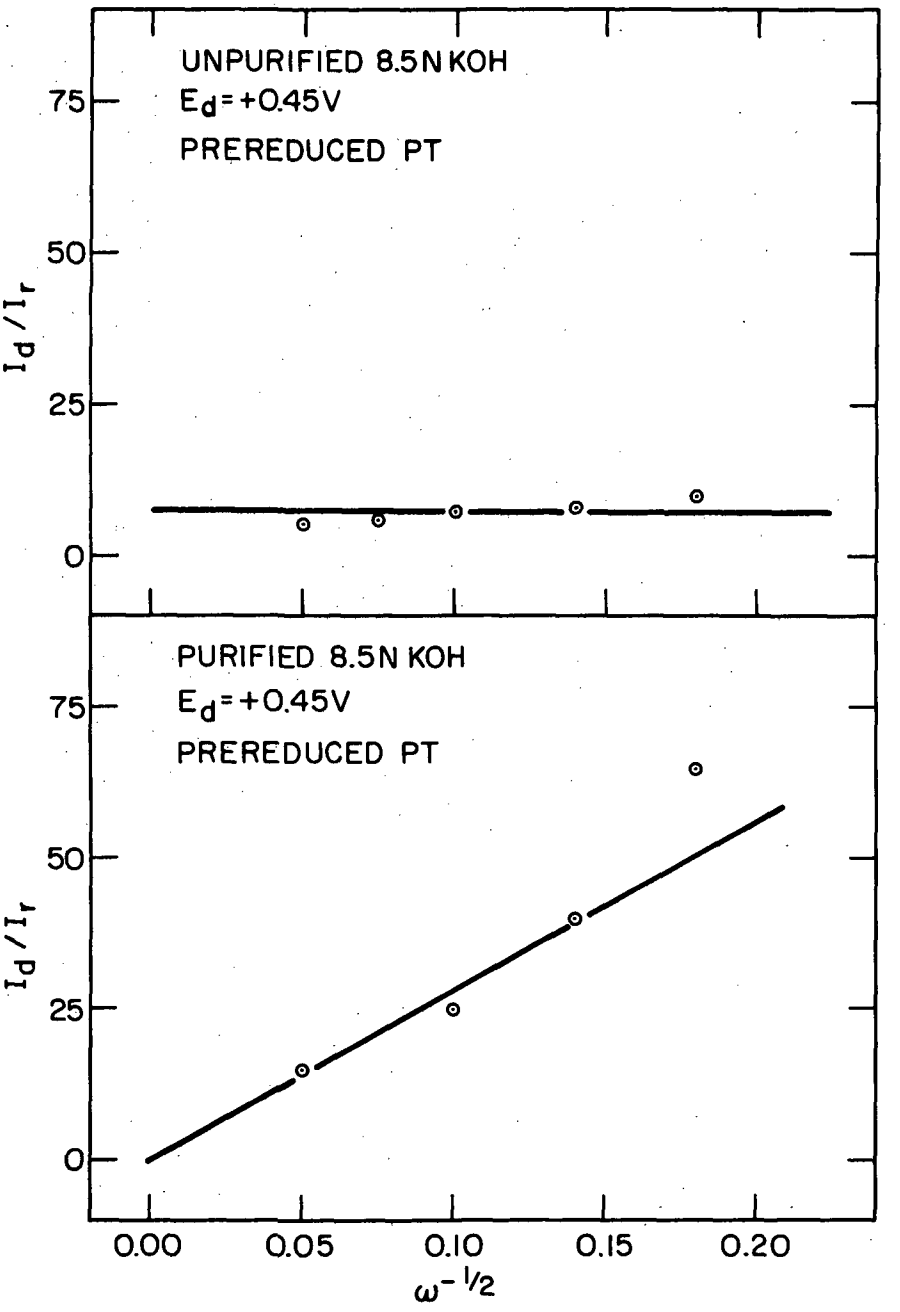

Fig. 43. I_d/I_r versus $\omega^{-1/2}$ plots for O_2 reduction at a prereduced smooth Pt disk electrode, E_d = +0.45 V, in unpurified and purified 8.5N KOH at 30 °C, with E_r = +1.2 V

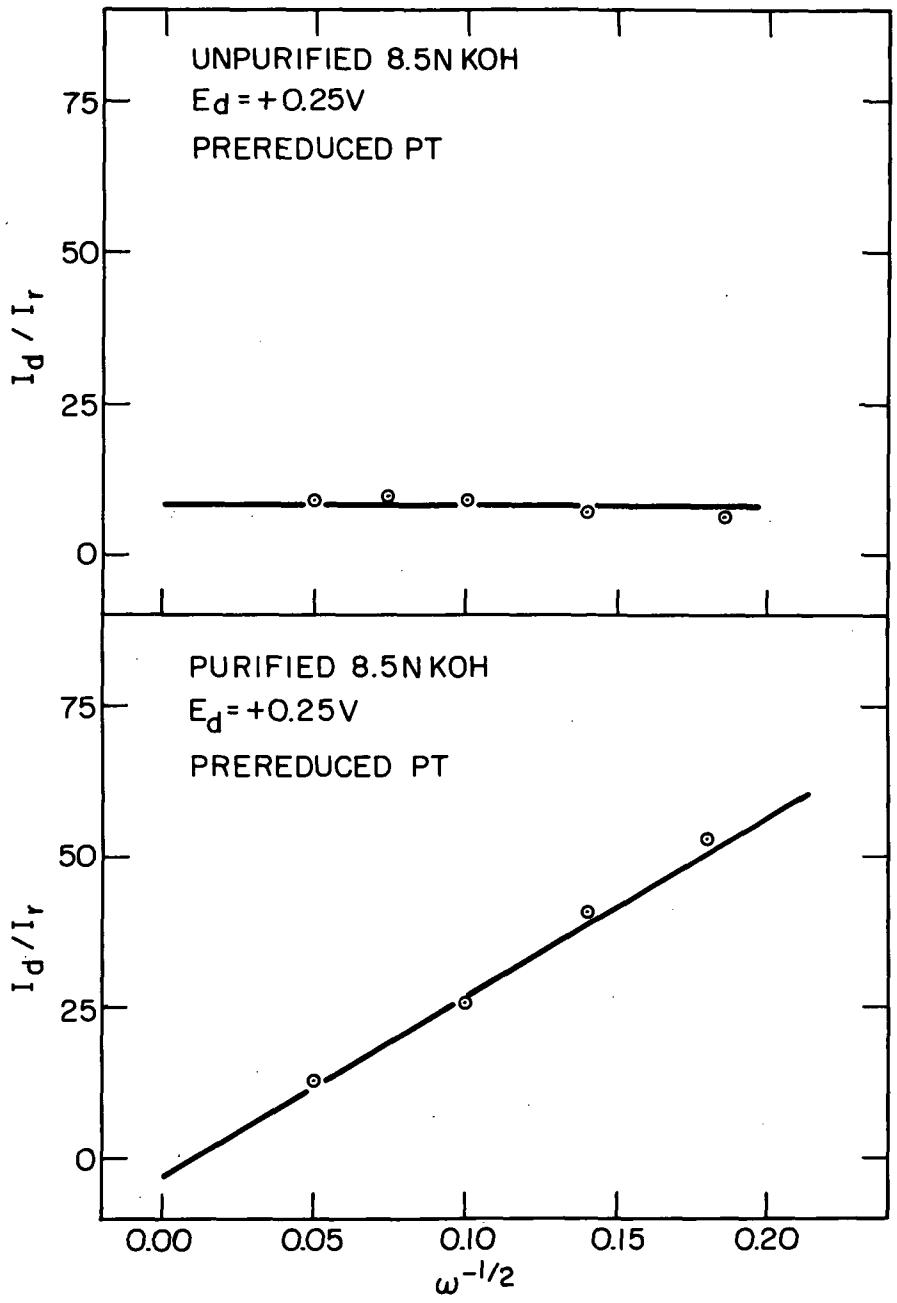

Fig. 44. I_d/I_r versus $\omega^{-1/2}$ plots for O_2 reduction at a prereduced smooth Pt disk electrode, E_d = +0.25 V, in unpurified and purified 8.5N KOH at 30 °C, with E_r = +1.2 V

is sufficient to give an I_d/I_r value which is independent of $\omega^{1/2}$ and greater than 1/N. It is not unlikely that k_3 and/or k_4 may be affected by $\omega^{1/2}$, especially in impure solution due to transport of impurities to the disk surface. Tables XVII and XVIII present two separate sets of I_d-I_r data for O_2 reduction on prereduced smooth Pt in purified 8.5 KOH. These data are plotted in Figs. 45 and 46. In Tables XIX and XX, we have compiled the least-square values of the intercepts and slopes of these plots.

The I_d/I_r intercepts of Tables XIX and XX average to a value of 3.1 ± 0.5 which is quite close to 1/N (~2.5) and therefore characteristic of an O_2 reduction mechanism wherein H_2O_2 is a reaction intermediate and can be reduced further to water. However, as mentioned earlier, this value is less than 2/N which is within the range of values which Breiter considers of insufficient accuracy to distinguish between the dual pathway and a single pathway.[46] From Eq. (29), we may speculate that, if the four-electron process is present, then $k_1/k_2 = 0.3$. This would seem to indicate that the stepwise two-electron reduction of O_2 is the preferred path in purified 8.5N KOH on prereduced electrodes.

From Tables XIX and XX, it can be seen that the slope values are relatively constant between +0.9 to 0.8 V. If $2k_1/k_2 << 1$, then the slope of the I_d/I_r versus $\omega^{-1/2}$ is a function of $2k_3 + k_4$ [see Eq. (39)]. Since k_3 should be potential dependent, this would be indicative of the presence of heterogeneous catalytic decomposition of H_2O_2 in the region of +0.9 to +0.8 V. At $E_d < +0.8$ V, k_3 very likely becomes the controlling factor (i.e., $2k_3 >> k_4$) and the slope increases correspondingly. Further treatment of the data after Bagotski, et al.,[42] does not seem feasible, however, because of the poor precision of these measurements.

In attempting to compare the O_2 reduction mechanism on preoxidized and prereduced smooth Pt, we noticed some anomalous behavior in I_d/I_r versus $\omega^{-1/2}$ plots for the preoxidized electrode surface. It was observed that the I_d/I_r versus $\omega^{-1/2}$ plots for the preoxidized electrode surface were nonlinear and show a marked curvature at the lower rotation rates. Figs. 47 and 48 examine this difference between preoxidized and prereduced electrodes in more detail by comparing I_d/I_r versus $\omega^{-1/2}$ and I_d versus $\omega^{1/2}$ plots for E_d = +0.45 V.

In Fig. 48, the I_d/I_r versus $\omega^{-1/2}$ plots are linear at $\omega^{-1/2} \leq 0.13$ and extrapolate to a value in the vicinity of 1/N for both preoxidized and prereduced electrode surfaces. At $\omega^{-1/2} \geq 0.13$ or less than 7 rps, the I_d/I_r versus $\omega^{-1/2}$ curve for the preoxidized electrode shows a marked upward curvature. While some deviation is also observed for the prereduced electrode, it is not believed to be too significant and is a reflection of the poor precision in measuring the low I_r values at these rotation rates. From Fig. 48, it can be seen that the I_d values for the preoxidized electrode surface are behaving anomolously since, at low rps, I_d is increasing with decreasing $\omega^{1/2}$ contrary to the normal type of behavior predicted for the Levich equation ($I_d \propto c\ \omega^{1/2}$) and exhibited by the prereduced surface.

This anomalous behavior appears to be traceable to an experimental problem associated with the pretreatment of the preoxidized electrode at +1.75 V where considerable oxygen is evolved. At low rotation speeds, it has been observed that gas bubbles tend to adhere to the

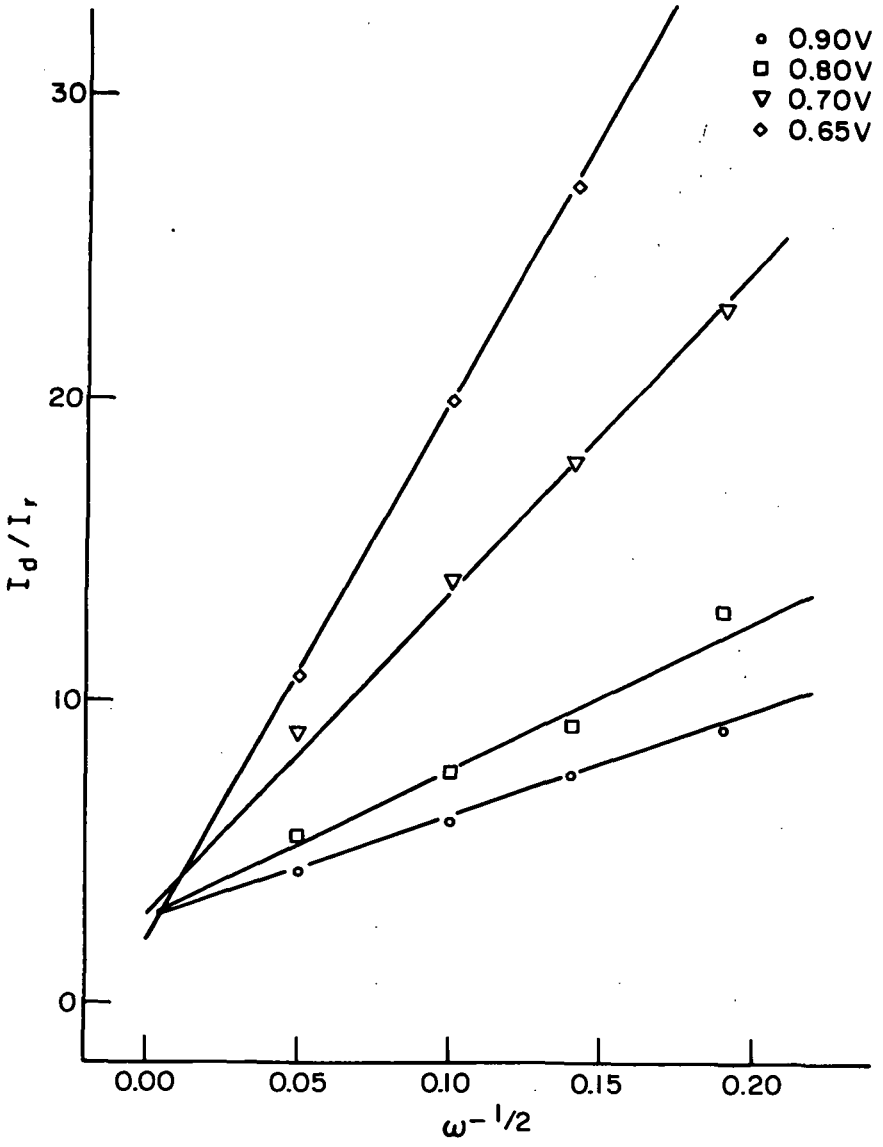

Fig. 45. I_d/I_r versus $\omega^{-1/2}$ plots for O_2 reduction at various disk potentials on prereduced smooth platinum in purified 8.5N KOH at 30°C (Data Set No. 1)

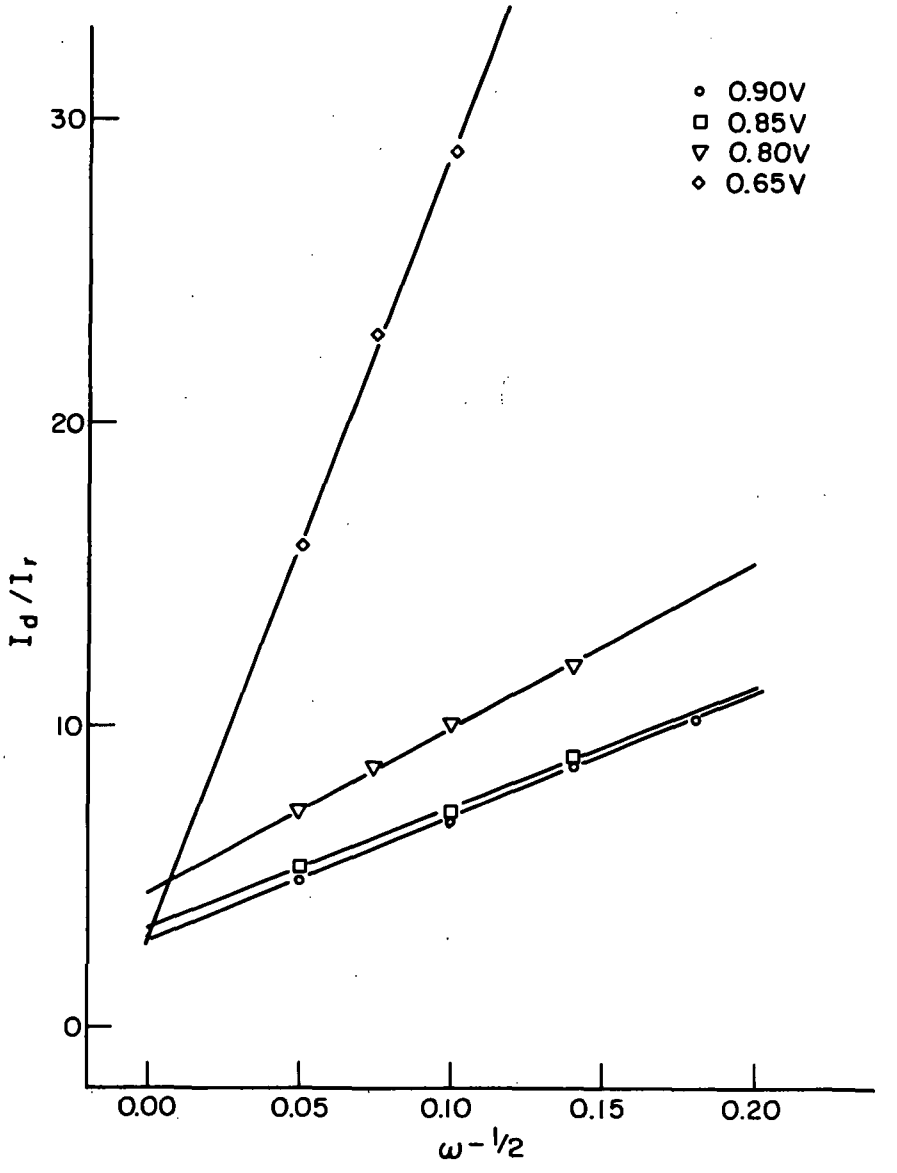

Fig. 46. I_d/I_r versus $\omega^{-1/2}$ plots for O_2 reduction at various disk potentials on prereduced smooth platinum in purified 8.5N KOH at 30 °C (Data Set No. 2)

Table XVII. Rotating Ring-Disk Electrode Data for O_2 Reduction on Prereduced Smooth Pt in Purified 8.5N KOH at 30 °C

E_d, volts	$\omega^{1/2}$ $(rad/sec)^{1/2}$	$\omega^{-1/2}$ $(rad/sec)^{-1/2}$	I_d, μA	I_r, μA	I_d/I_r
0.90	20	0.05	15.5	3.4	4.4
0.90	10	0.10	11.4	1.9	6.0
0.90	7.1	0.14	9.9	1.3	7.6
0.90	5.3	0.19	8.2	0.90	9.1
0.80	20	0.50	26.5	4.9	5.4
0.80	10	0.10	17.2	2.5	7.0
0.80	7.1	0.14	12.7	1.5	8.6
0.80	5.3	0.19	10.2	1.0	10.2
0.70	20	0.05	34.8	3.9	9.0
0.70	10	0.10	18.8	1.3	14
0.70	7.0	0.14	12.5	0.7	18
0.70	5.4	0.19	9.2	0.4	23
0.65	20.0	0.05	40.3	3.7	11.0
0.65	10.0	0.10	23.4	1.2	20.0
0.65	7.1	0.14	18.6	0.69	27.0
0.65	5.0	0.20	14.8	0.33	45.0

Table XVIII. Rotating Ring-Disk Electrode Data for Oxygen Reduction on Prereduced Smooth Pt in 8.5N KOH at 30 °C

E_d, volts	$\omega^{1/2}$ $(rad/sec)^{1/2}$	$\omega^{-1/2}$ $(rad\ sec)^{-1/2}$	I_d μA	I_r μA	I_d/I_r
0.90	20	0.05	30.6	6.2	4.9
0.90	10	0.10	18.7	2.7	6.9
0.90	7.3	0.14	14.8	1.7	8.7
0.90	5.8	0.18	12.2	1.2	10.2
0.85	20	0.05	36.0	6.8	5.3
0.85	10	0.10	21.0	2.9	7.2
0.85	7.3	0.14	17.0	1.9	8.9
0.80	20	0.05	39.0	5.4	7.2
0.80	13	0.08	28.4	3.3	8.6
0.80	10	0.10	23.0	2.3	10
0.80	7.3	0.14	17.5	1.5	12
0.65	20	0.05	46.7	3.0	16
0.65	13	0.08	34.0	1.5	23
0.65	10	0.10	27.2	0.95	29

Table XIX. Summary of Least-Squares Values of the Slope and Intercept of I_d/I_r Versus $\omega^{-1/2}$ Plots Using Data of Table XVII

E_d	Intercept	Slope
0.90	2.7	35
0.80	3.9	33
0.70	2.9	115
0.65	2.1	178

Table XX. Summary of Least-Squares Values of the Slope and Intercept of I_d/I_r Versus $\omega^{-1/2}$ Plots Using Data of Table XVIII

E_d	Intercept	Slope
0.90	2.8	42
0.85	3.3	40
0.80	4.4	55
0.65	2.8	265

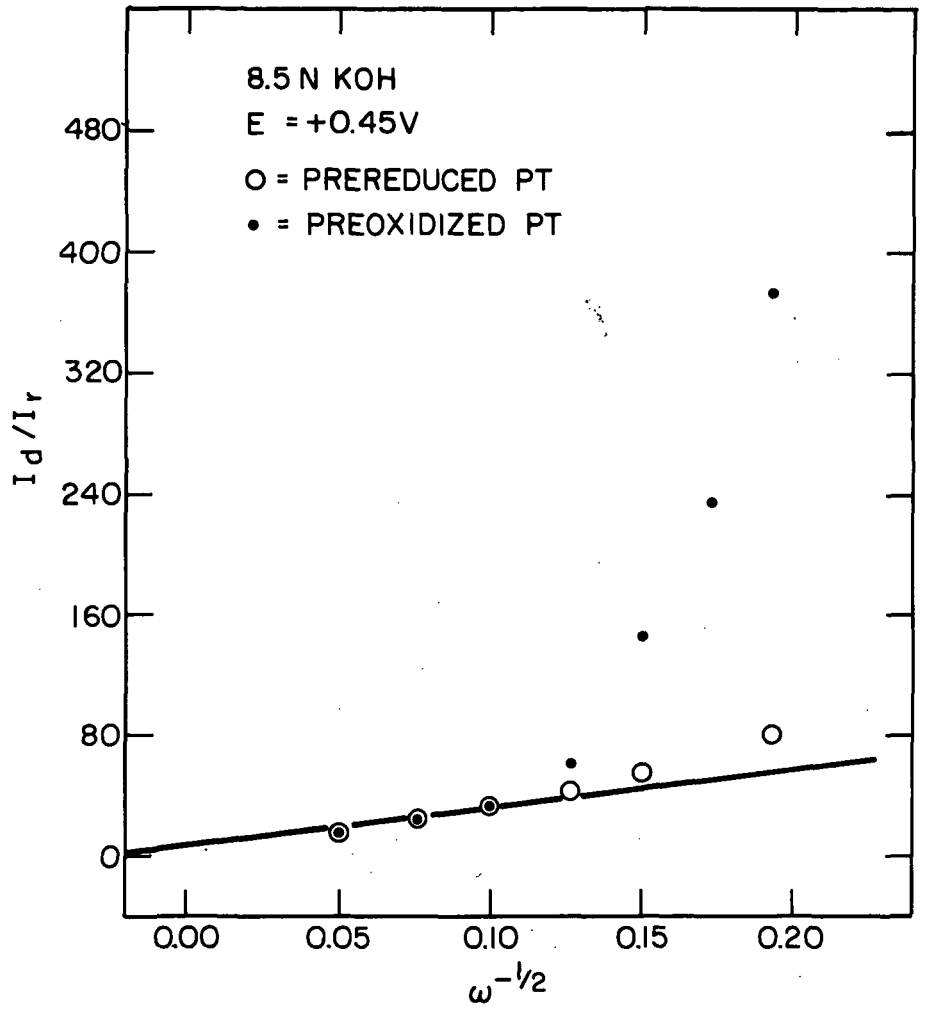

Fig. 47. I_d/I_r versus $\omega^{-1/2}$ plots for O_2 reduction at prereduced and preoxidized smooth Pt disk electrodes in purified 8.5N KOH at 30 °C for E_d = +0.45 V

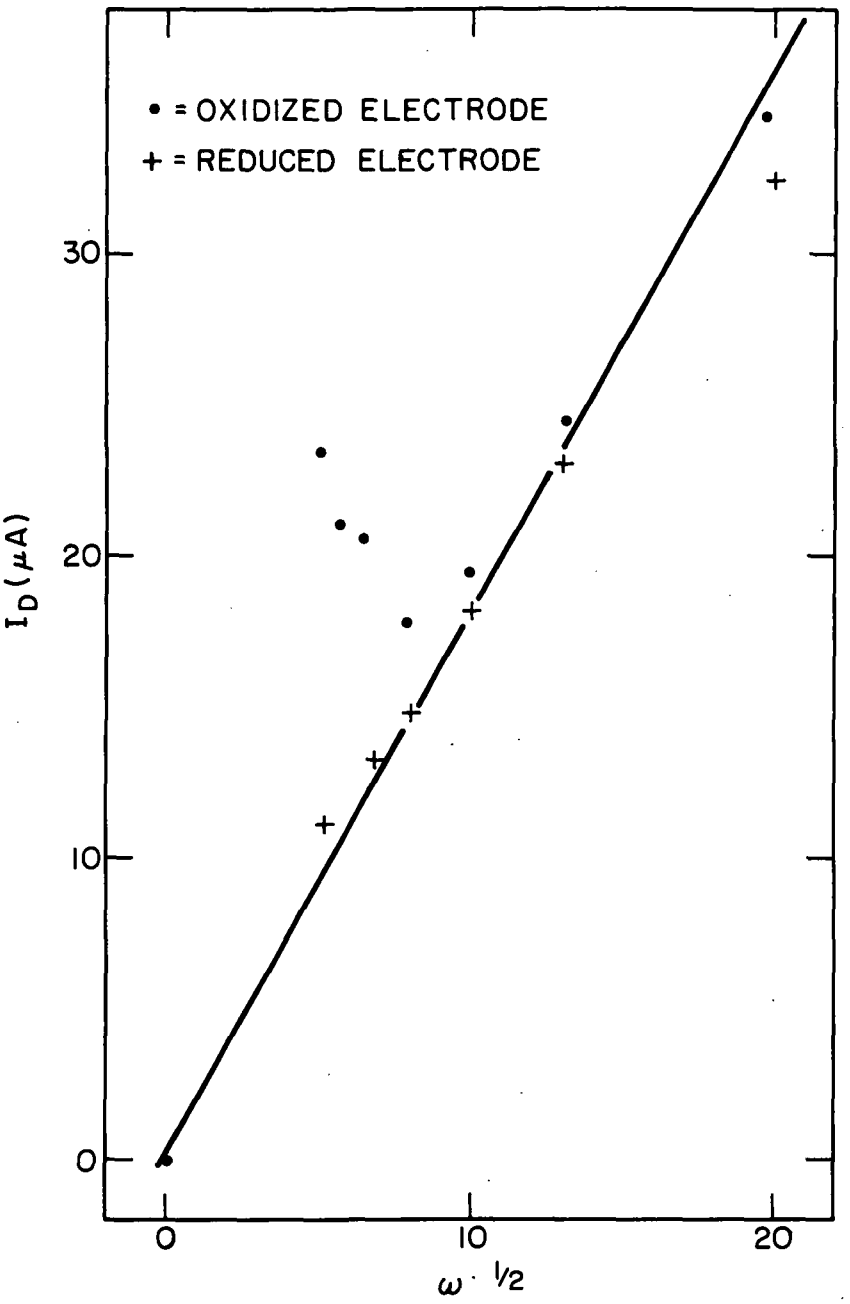

Fig. 48. I_d versus $\omega^{1/2}$ plots for O_2 reduction at prereduced and preoxidized smooth Pt disk electrodes in purified 8.5N KOH at 30 °C for E_d = +0.45 V

Teflon separation between disk and ring due to the hydrophobic character of the Teflon. This can result in a higher O_2 concentration at the edge of the disk due to the trapped O_2 bubbles. At the same time, these gas bubbles can prevent peroxide transport to the ring electrode. Therefore, I_d tends to increase while I_r may decrease with the net effect of an increase in I_d/I_r. For this reason we have not used I_d/I_r values obtained at $\omega^{-1/2} \geq 0.14$ in making any quantitative calculations.

Fig. 49 shows I_d/I_r verus $\omega^{-1/2}$ plots for a smooth Pt surface preoxidized at 1.75 V for 2 min for E_d = +0.9 V and E_d = +0.8 V. The observed intercepts are close to 1/N and therefore indicate no mechanism change between a preoxidized and a prereduced Pt surface. However, a change in slope is observed and is indicative of changes in k_3 and/or k_4 in this region. The observed difference in the kinetics of O_2 reduction on prereduced and preoxidized surfaces appears to be related to kinetics of peroxide formation. This idea is supported by the data of Fig. 50.

In Fig. 50, we have plotted 1/J versus $\omega^{-1/2}$ where J is the flux to the disk electrode given by:

$$J = I_d + I_r/N \qquad (40)$$

Such a plot enables one to correct for mass transfer effects and obtain Tafel data at high current densities by extrapolating plots of 1/J versus $\omega^{-1/2}$ to $\omega = \infty$.[52] The plots of Fig. 50 give corrected current values of 127 μA for the prereduced Pt surface and 26 μA for the preoxidized Pt surface at +0.85 V. This is consistent with other results which have indicated a higher activity for oxygen reduction on prereduced Pt surfaces.[53,54]

In purified 0.1N KOH, we have obtained plots of I_d/I_r versus $\omega^{-1/2}$ which are in disagreement with those of Damjanovic, et al.[38] Tables XXI and XXII present I_d/I_r data for O_2 reduction on prereduced and preoxidized smooth Pt in purified 0.1N KOH. These data are plotted in Fig. 51. In contrast to the range of I_d/I_r values of 15-80 reported by Damjanovic, et al., for prereduced smooth Pt, our I_d/I_r values are much higher (>100) indicating much less H_2O_2 formation. This disagreement is not surprising since we have already illustrated the effect of solution purity on H_2O_2 production in 0.1N KOH (Figs. 34-36).

It should also be mentioned here that Tarasevich, et al., also reported I_d/I_r data for O_2 reduction in 0.1N KOH which are in disagreement with those of Damjanovic, et al.[45] Our I_d/I_r values for the preoxidized surface at E_d = +0.80 V are comparable with those estimated from a paper of Tarasevich, et al., but at E_d = +0.65 V we are observing much less peroxide formation than reported by Tarasevich.

While these I_d/I_r versus $\omega^{-1/2}$ plots do show a positive slope, the very large I_d/I_r values observed are not amenable to further analysis. It seems justifiable to assume that an I_d/I_r value greater than 250 is indicative of insignificant H_2O_2 production since, under such conditions, further reduction of this amount of H_2O_2 would contribute at most 1% to the observed disk current. It should be recalled that Fig. 36 demonstrated that, at +0.9 V to

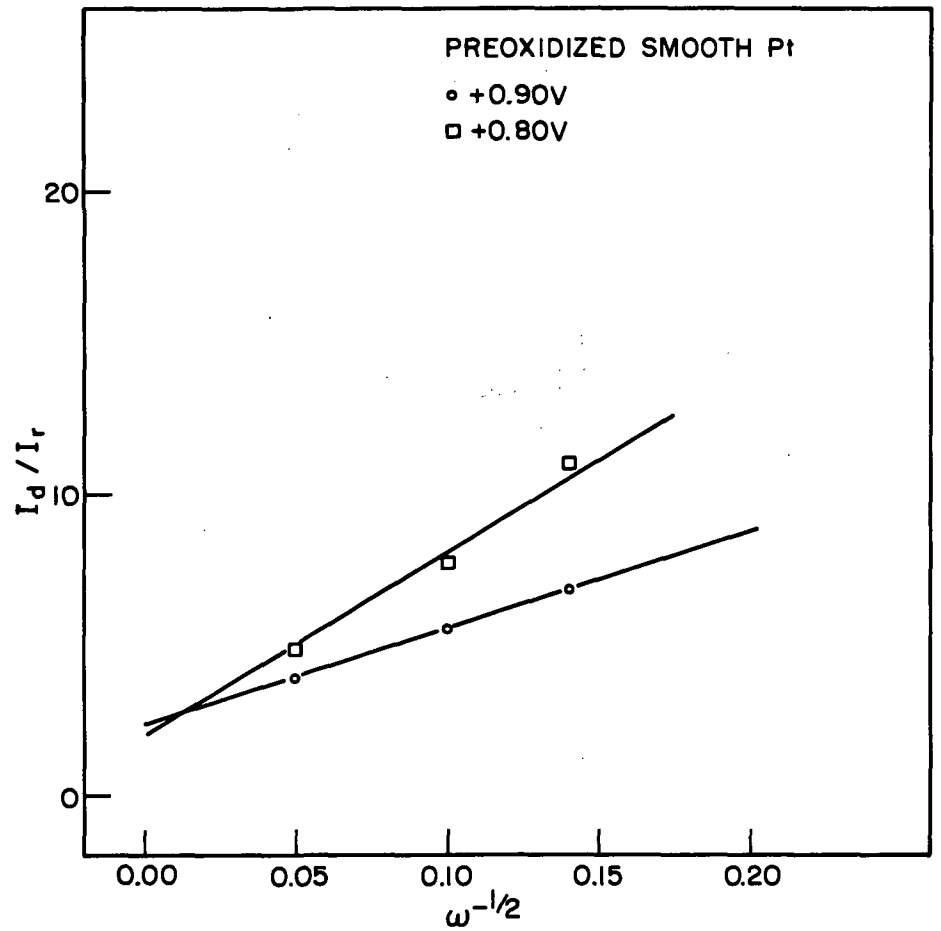

Fig. 49. I_d/I_r versus $\omega^{-1/2}$ plots for O_2 reduction at E_d = +0.90 V and E_d = +0.80 V on preoxidized smooth platinum in purified 8.5N KOH at 30 °C

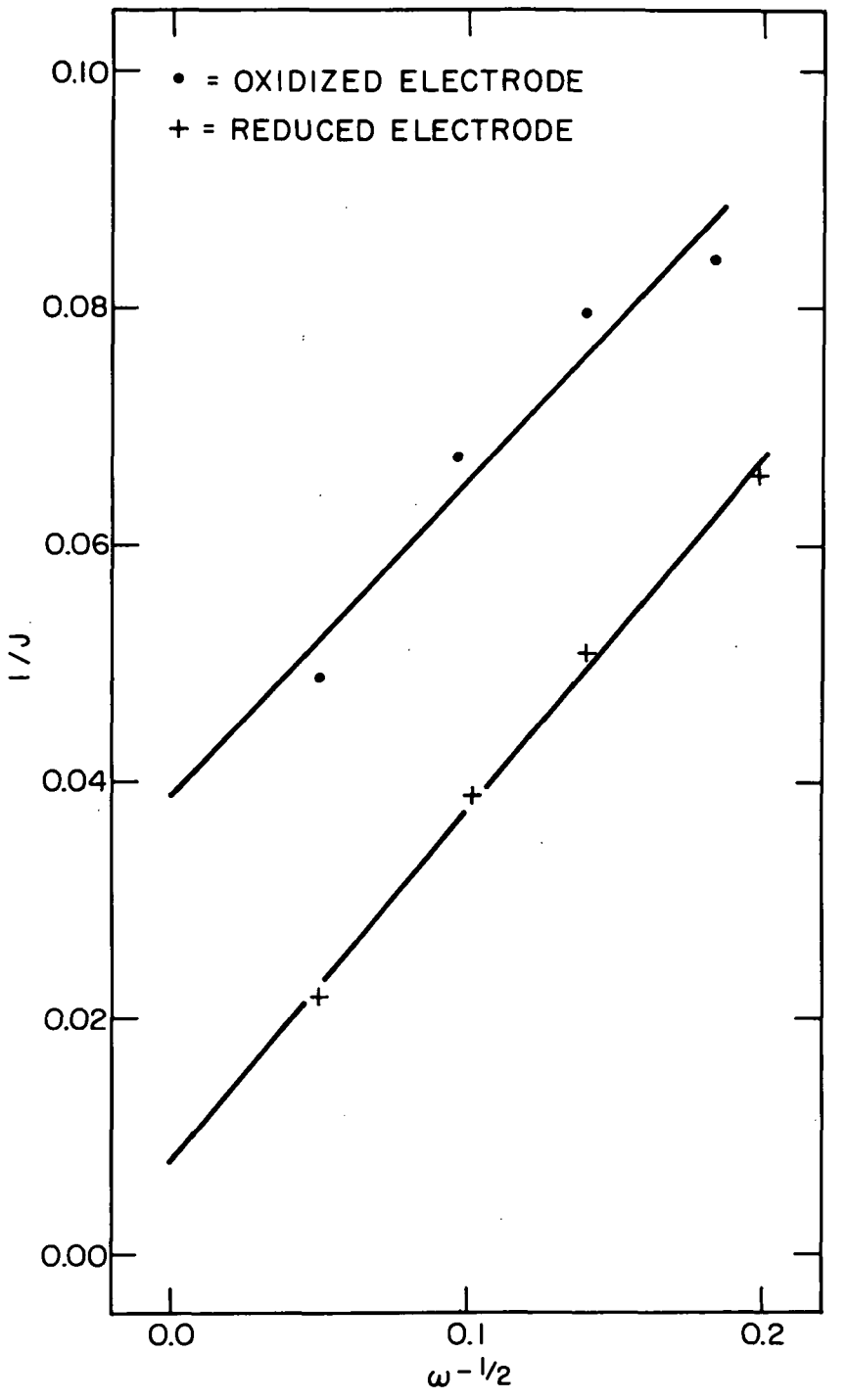

Fig. 50. Plot of the reciprocal of the corrected disk current, 1/J, versus $\omega^{-1/2}$ for prereduced and preoxidized smooth Pt disk electrodes in purified 8.5N KOH at 30 °C for E_d = +0.85 V

Table XXI. Rotating Ring-Disk Electrode Data for Oxygen Reduction on Prereduced Smooth Pt in Purified 0.1N KOH at 30 °C

E, volts	$\omega^{1/2}$ (rad/sec)$^{1/2}$	$\omega^{-1/2}$ (rad/sec)$^{-1/2}$	I_d, μA	I_r, μA	I_d/I_r
+0.80	20	0.05	137	3.3	42
+0.80	10	0.10	560	5.8	96
+0.80	7	0.14	500	3.5	144
+0.80	5.4	0.18	410	2.2	190
+0.65	20	0.05	1225	21.5	57
+0.65	10	0.10	800	4.4	181
+0.65	7	0.14	600	2.0	300
+0.65	5.4	0.18	475	1.0	475
+0.45	20	0.05	1540	10	154
+0.45	10	0.10	865	1.7	496
+0.45	7	0.14	620	0.75	825
+0.45	5.4	0.18	495	0.45	1100
+0.25	20	0.05	1625	25.2	64
+0.25	10	0.10	850	8.2	103
+0.25	7	0.14	625	4.0	156
+0.25	5.4	0.18	475	1.6	306

Table XXII. Rotating Ring-Disk Electrode Data for Oxygen Reduction on Preoxidized Smooth Pt in Purified 0.1N KOH at 30 °C

E, volts	$\omega^{1/2}$ (rad/sec)$^{1/2}$	$\omega^{-1/2}$ (rad/sec)$^{-1/2}$	I_d, μA	I_r, μA	I_d/I_r
+0.80	20	0.05	3.5	1.2	2.8
+0.80	10	0.10	345	14.2	24
+0.80	7	0.14	361	9.7	37
+0.80	5.4	0.18	320	6.8	47
+0.65	20	0.05	1175	21.5	55
+0.65	10	0.10	800	4.7	169
+0.65	7	0.14	600	2.0	300
+0.65	5.4	0.18	450	1.0	450
+0.45	20	0.05	1500	8.3	181
+0.45	10	0.10	850	1.6	530
+0.45	7	0.14	635	0.8	845
+0.45	5.4	0.18	485	0.3	1620
+0.25	20	0.05	1630	23	70
+0.25	10	0.10	860	6.2	139
+0.25	7	0.14	612	2.9	210
+0.25	5.4	0.18	500	1.5	328

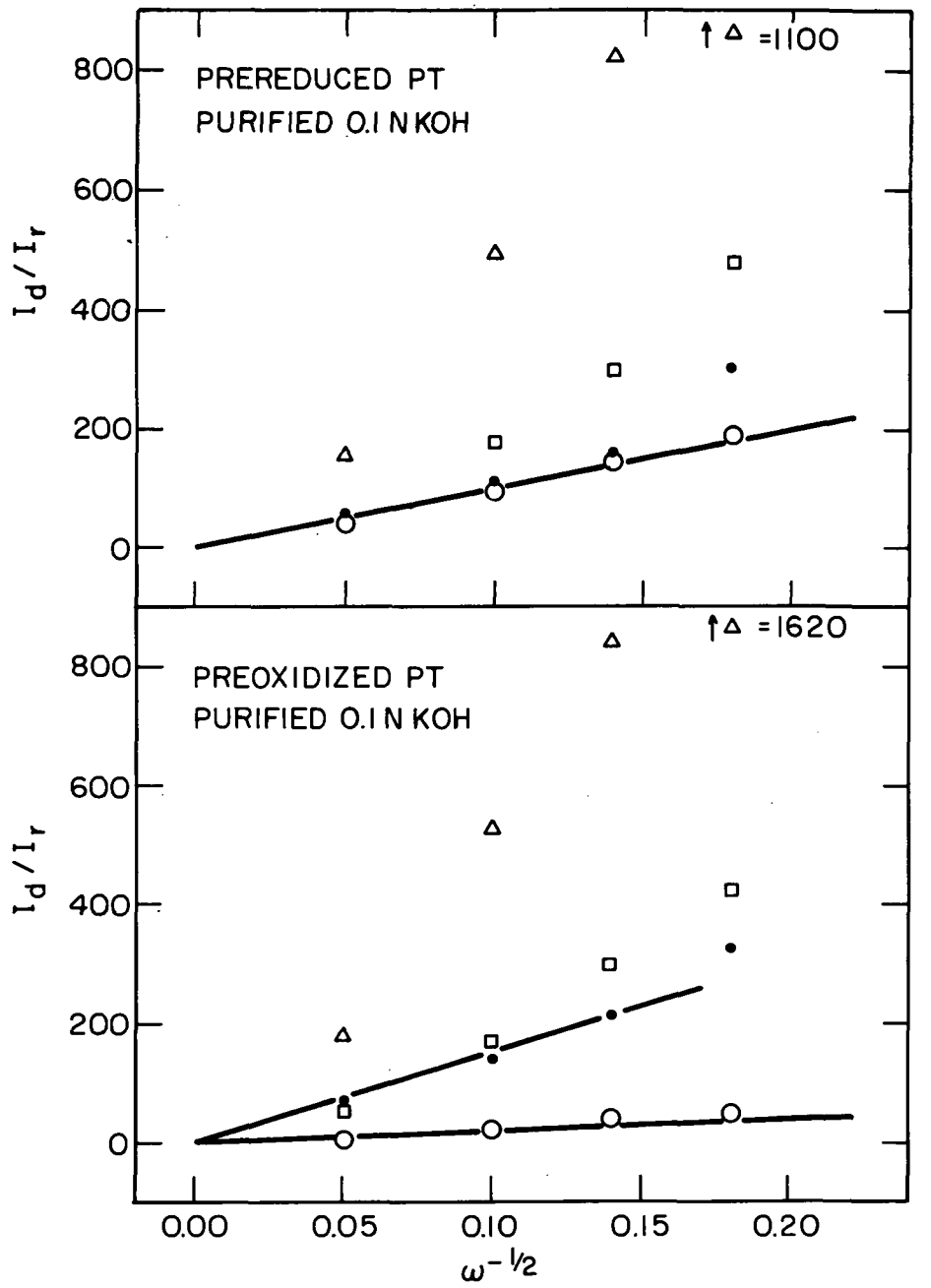

Fig. 51. I_d/I_r versus $\omega^{-1/2}$ plots for O_2 reduction at prereduced and preoxidized smooth Pt disk electrodes in purified 0.1N KOH at 30 °C with E_d: ○ = +0.80 V; □ = +0.65 V; △ = +0.45 V; and ● = +0.25 V

0.8 V, peroxide was observed even in a highly purified 0.1N KOH electrolyte as in 8.5N KOH.

We have also used the RRDE to study O_2 reduction on a platinized platinum disk electrode in purified 8.5N KOH. Fig. 52 shows a steady-state I-E curve obtained at 65 rps on a prereduced platinized platinum disk electrode in 8.5N KOH. Very little H_2O_2 is observed, although there is evidence of a maximum in I_r at +0.95 V, not unlike that observed for smooth Pt. Tables XXIII and XXIV present more data for platinized platinum on both prereduced and preoxidized surfaces. Very little H_2O_2 is observed for $E_d \leq +0.8$ V. There is some indication for less H_2O_2 production on the prereduced surface than on the preoxidized one.

2. O_2 reduction kinetics and path in 8.5N KOH containing various additives

In order to assess the effects of various soluble species which may be found in rechargeable H_2-O_2 fuel cells or metal-air batteries on O_2 reduction, we have carried out rotating ring-disk electrode studies of O_2 reduction in purified 8.5N KOH containing the following additions, identified as follows:

Electrolyte no.	
E-1	8.5N KOH
E-2	8.5N KOH saturated with CdO ($Cd^{2+} = 1.8 \times 10^{-4}$M)
E-3	8.5N KOH saturated with ZnO ($Zn(OH)_4^{2-} = 5.4 \times 10^{-1}$M)
E-4	6.5N KOH with added 1M K_2CO_3
E-5	8.5N KOH with added 0.02M K Cl
E-6	8.5N KOH with added 0.02M K_2SO_4
E-7	8.5N KOH saturated with Johns-Manville "Fuel Cell Asbestos"
E-8	8.5N KOH with 100 ppm Fe^{3+}

We have also studied O_2 reduction in 0.1N KOH containing various amounts of soluble cadmate species. The influence of soluble cadmium species was of particular interest in these studies since Wagner had reported poisoning of the air electrode in cadmium-air cells by soluble cadmate species.[4]

I_d/I_r data appear in Tables XXV through XXXVIII for each of these eight electrolytes for both prereduced and preoxidized smooth Pt electrodes. Corresponding I_d/I_r versus $\omega^{-1/2}$ plots are presented in Figs. 53 through 60. In these plots we have drawn least-squares straight lines calculated on the basis of $\omega^{-1/2} = 0.05$, 0.10, and 0.14. We have not included I_d/I_r values at $\omega^{-1/2} = 0.18$, i.e., the lowest rotation rate, since we feel that these values are suspect due to the experimental difficulty in working with the preoxidized electrode surface mentioned earlier. Tables XXXIX through XLII give the calculated least-squares intercepts and slopes for these seven electrolytes (Electrolytes E-2 through E-8) and 8.5N KOH (Electrolyte E-1).

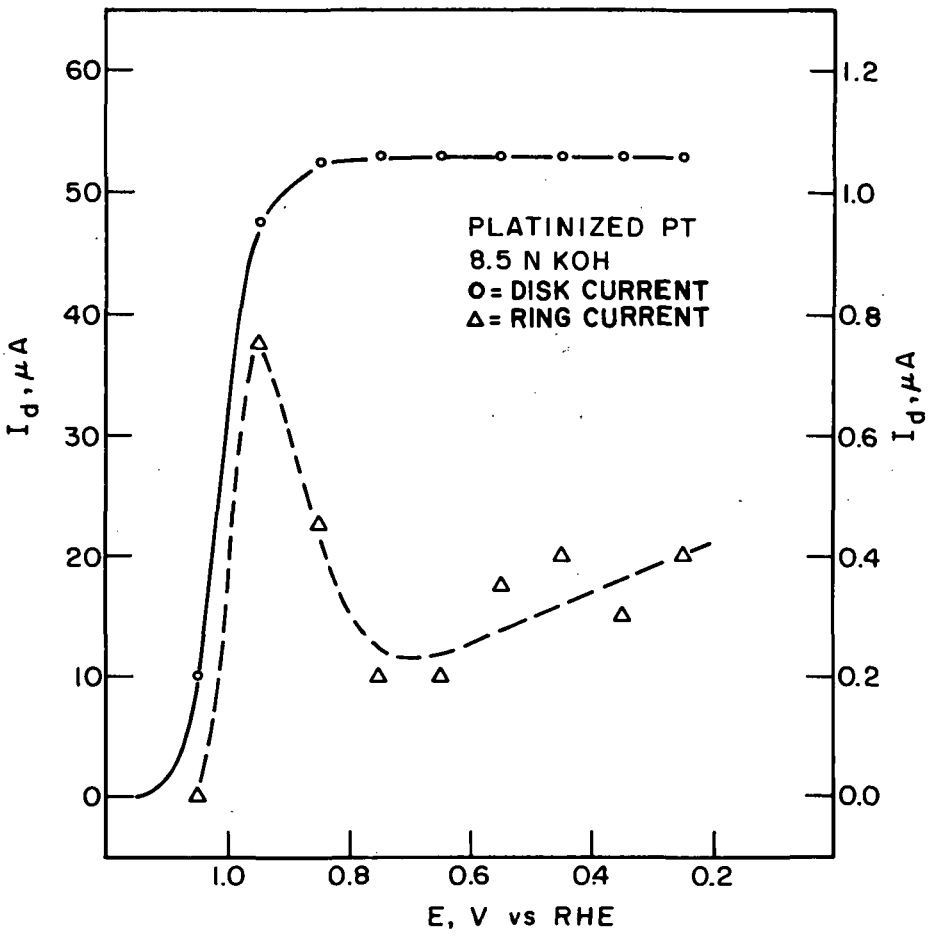

Fig. 52. Steady-state I_d/I_r versus E_d curves for O_2 reduction on a pre-reduced platinized platinum disk electrode at 65 rps in purified 8.5N KOH at 30 °C

Table XXIII. Rotating Ring-Disk Electrode Data for O_2 Reduction on Prereduced Platinized Platinum in Purified 8.5N KOH at 30°C

E_d, V	$\omega^{-1/2}$	I_d, μA	I_r, μA	I_d/I_r
+0.25	0.05	60.0	0.21	285
	0.10	30.0	0.03	>1000
	0.14	21.0	<0.01	>1000
	0.18	17.2	<0.01	>1000
+0.45	0.05	60.0	0.20	300
	0.10	30.0	0.04	750
	0.14	22.0	<0.01	>1000
	0.18	17.0	<0.01	>1000
+0.65	0.05	60.0	0.21	285
	0.10	31.0	0.08	390
	0.14	23.2	0.07	330
	0.18	17.7	0.06	295
+0.85	0.05	57.5	0.88	65
	0.10	30.0	0.27	111
	0.14	22.0	0.14	157
	0.18	16.5	0.12	148

Table XXIV. Rotating Ring-Disk Electrode Data for O_2 Reduction on Preoxidized Platinized Platinum in Purified 8.5N KOH at 30 °C

E_d, V	$\omega^{-1/2}$	I_d, μA	I_r, μA	I_d/I_r
+0.85	0.05	47.5	1.85	26
	0.10	27.0	0.45	63
	0.14	19.7	0.27	73
	0.16	16.5	0.17	97
+0.65	0.05	55.6	0.25	220
	0.10	29.0	0.04	720
	0.13	22.0	0.01	>1000
+0.45	0.05	59.0	0.10	590
	0.10	32.0	0.03	>1000
	0.14	22.0	0.02	>1000
+0.25	0.05	59.0	0.26	230
	0.10	31.0	0.05	620
	0.14	22.0	0.03	730

Table XXV. Rotating Ring-Disk Electrode Data for Oxygen Reduction on Prereduced Smooth Pt in 8.5N KOH Saturated with CdO at 30 °C

E, volts	$\omega^{1/2}$ (rad/sec)$^{1/2}$	$\omega^{-1/2}$ (rad/sec)$^{-1/2}$	I_d, μA	I_r, μA	I_d/I_r
0.85	20.0	0.05	30.8	5.6	5.5
0.85	10.0	0.10	18.8	2.7	7.0
0.85	7.1	0.14	15.9	1.7	9.4
0.85	5.3	0.19	13.5	0.96	14.0
0.65	20.0	0.05	43.0	6.4	6.7
0.65	10.0	0.10	26.0	0.74	35.0
0.65	7.1	0.14	20.7	0.40	52.0
0.65	5.3	0.19	17.5	0.19	92.0
0.45	20.0	0.05	48.1	1.1	43.0
0.45	10.0	0.10	26.7	0.29	92.0
0.45	7.3	0.14	20.8	0.18	116.0
0.45	5.1	0.20	17.0	0.07	243.0
0.25	20.0	0.05	49.8	0.56	89.0
0.25	10.0	0.10	27.0	0.15	180.0
0.25	7.3	0.14	21.6	0.10	216.0
0.25	5.1	0.20	17.8	0.04	445.0

Table XXVI. Rotating Ring-Disk Electrode Data for Oxygen Reduction on Preoxidized Smooth Pt in 8.5N KOH Saturated with CdO at 30 °C

E, volts	$\omega^{1/2}$ (rad/sec)$^{1/2}$	$\omega^{-1/2}$ (rad/sec)$^{-1/2}$	I_d, μA	I_r, μA	I_d/I_r
0.85	20.0	0.05	10.8	2.1	5.2
0.85	10.0	0.10	9.8	1.9	5.1
0.85	7.4	0.14	9.1	1.4	6.4
0.85	5.1	0.20	8.1	0.84	9.7
0.65	20.0	0.05	58.0	2.6	22.0
0.65	10.0	0.10	29.5	0.78	38.0
0.65	7.4	0.14	23.3	0.42	55.0
0.65	5.1	0.20	18.5	0.14	128.0
0.45	20.0	0.05	51.0	1.4	36.0
0.45	10.0	0.10	27.4	0.40	68.0
0.45	7.3	0.14	21.3	0.17	125.0
0.45	5.2	0.19	18.3	0.10	183.0
0.25	20.0	0.05	52.4	0.64	82.0
0.25	10.0	0.10	27.5	0.23	120.0
0.25	7.3	0.14	21.3	0.11	192.0
0.25	5.2	0.19	18.2	<0.01	>1000.0

Table XXVII. Rotating Ring-Disk Electrode Data for Oxygen Reduction on Prereduced Smooth Pt in 8.5N KOH Saturated with ZnO at 30 °C

E, volts	$\omega^{1/2}$ (rad/sec)$^{1/2}$	$\omega^{-1/2}$ (rad/sec)$^{-1/2}$	I_d, μA	I_r, μA	I_d/I_r
0.85	20.0	0.05	56.0	9.7	5.8
0.85	10.0	0.10	34.4	5.6	6.2
0.85	7.2	0.14	28.6	4.0	7.1
0.85	5.4	0.19	24.4	2.9	8.5
0.65	20.0	0.05	88.3	9.1	9.2
0.65	10.0	0.10	49.5	3.8	13.0
0.65	7.2	0.14	39.0	2.4	16.0
0.65	5.4	0.19	32.2	1.6	20.0
0.45	20.0	0.05	92.4	6.6	14.0
0.45	10.0	0.10	51.0	2.8	18.0
0.45	7.2	0.14	38.6	1.8	22.0
0.45	5.0	0.20	29.0	1.2	24.0
0.25	20.0	0.05	102.0	3.9	26.0
0.25	10.0	0.10	56.0	1.8	31.0
0.25	7.2	0.14	40.5	1.3	31.0
0.25	5.0	0.20	30.5	1.3	24.0

Table XXVIII. Rotating Ring-Disk Electrode Data for Oxygen Reduction on Prereduced Smooth Pt in 8.5N KOH Saturated with ZnO at 30°C

E, volts	$\omega^{1/2}$ (rad/sec)$^{1/2}$	$\omega^{-1/2}$ (rad.sec)$^{-1/2}$	I_d, μA	I_r, μA	I_d/I_r
0.85	20.0	0.05	31.8	5.8	5.5
0.85	10.0	0.10	19.6	2.5	7.7
0.85	7.1	0.14	15.6	1.7	9.2
0.85	5.0	0.20	12.7	0.98	13.0
0.65	20.0	0.05	40.3	3.7	11.0
0.65	10.0	0.10	23.4	1.2	20.0
0.65	7.1	0.14	18.6	0.69	27.0
0.65	5.0	0.20	14.8	0.33	45.0
0.45	20.0	0.05	41.5	2.8	15.0
0.45	10.0	0.10	23.5	0.94	25.0
0.45	7.0	0.14	17.5	0.44	40.0
0.45	5.5	0.18	13.6	0.21	65.0
0.25	20.0	0.05	41.5	3.2	13.0
0.25	10.0	0.10	23.8	0.92	26.0
0.25	7.0	0.14	17.5	0.43	41.0
0.25	5.5	0.18	13.8	0.26	53.0

Table XXIX. Rotating Ring-Disk Electrode Data for Oxygen Reduction on Prereduced Smooth Pt in 6.5N KOH with 1M K_2CO_3 Added at 30 °C

E, volts	$\omega^{1/2}$(rad/sec)$^{1/2}$	$\omega^{-1/2}$(rad/sec)$^{-1/2}$	I_d, μA	I_r, μA	I_d/I_r
0.85	20	0.05	33.4	4.9	6.8
0.85	10	0.10	20.8	1.9	11
0.85	7.1	0.14	18.0	1.1	17
0.85	5.1	0.20	18.2	0.25	73
0.65	20	0.05	37.3	3.4	11
0.65	10	0.10	22.7	1.1	21
0.65	7.1	0.14	19.2	0.52	37
0.65	5.1	0.20	18.4	0.16	116
0.45	20	0.05	32.6	1.9	17
0.45	10	0.10	18.2	0.76	24
0.45	7.2	0.14	14.3	0.38	38
0.45	5.0	0.20	12.0	0.18	67
0.25	20	0.05	34.2	1.5	23
0.25	10	0.10	18.9	0.57	33
0.25	7.2	0.14	14.5	0.27	54
0.25	5.0	0.20	12.5	0.12	106

Table XXX. Rotating Ring-Disk Electrode Data for Oxygen Reduction on Preoxidized Smooth Pt in 6.5N KOH with 1M K_2CO_3 Added at 30 °C

E, volts	$\omega^{1/2}$(rad/sec)$^{1/2}$	$\omega^{-1/2}$(rad/sec)$^{-1/2}$	I_d, μA	I_r, μA	I_d/I_r
0.85	20	0.05	28.5	5.4	5.3
0.85	10	0.10	18.2	2.8	6.4
0.85	7.1	0.14	15.4	1.7	9.0
0.85	5.0	0.20	14.1	0.79	18
0.65	20	0.05	40.9	4.9	8.3
0.65	10	0.10	23.2	1.7	14
0.65	7.1	0.14	19.8	0.86	23
0.65	5.0	0.20	17.5	0.37	47
0.45	20	0.05	35.7	2.4	15
0.45	10	0.10	19.7	0.76	26
0.45	7.1	0.14	15.5	0.42	37
0.45	5.3	0.19	14.6	0.17	86
0.25	20	0.05	36.3	1.9	19
0.25	10	0.10	20.2	0.60	34
0.25	7.1	0.14	16.2	0.30	49
0.25	5.3	0.19	17.6	0.10	176

Table XXXI. Rotating Ring-Disk Electrode Data for Oxygen Reduction on Prereduced Smooth Pt in 8.5N KOH with 0.02M KCl Added at 30 °C

E, volts	$\omega^{1/2}$ (rad/sec)$^{1/2}$	$\omega^{-1/2}$ (rad/sec)$^{-1/2}$	I_d, μA	I_r, μA	I_d/I_r
0.85	20	0.05	34.0	5.3	6.4
0.85	10	0.10	21.8	2.3	9.4
0.85	7.2	0.14	17.2	1.4	12
0.85	5.5	0.18	15.0	0.88	17
0.65	20	0.05	50.5	2.5	20
0.65	10	0.10	28.0	0.88	32
0.65	7.2	0.14	21.4	0.50	43
0.65	5.5	0.18	16.8	0.28	61
0.45	20	0.05	59.6	1.7	36
0.45	10	0.10	28.0	0.48	58
0.45	7.1	0.14	20.4	0.24	86
0.45	5.5	0.18	17.5	0.14	125
0.25	20	0.05	43.8	1.8	25
0.25	10	0.10	23.5	0.59	40
0.25	6.9	0.14	19.1	0.27	71
0.25	5.0	0.20	21.0	0.11	195

Table XXXII. Rotating Ring-Disk Electrode Data for Oxygen Reduction on Preoxidized Smooth Pt in 8.5N KOH with 0.02M KCl Added at 30 °C

E, volts	$\omega^{1/2}$ (rad/sec)$^{1/2}$	$\omega^{-1/2}$ (rad/sec)$^{-1/2}$	I_d, μA	I_r, μA	I_d/I_r
0.85	20	0.05	14.5	2.9	5.0
0.85	9.9	0.10	12.9	2.0	6.6
0.85	6.9	0.14	12.4	0.96	13
0.85	5.4	0.19	12.6	0.47	27
0.65	20	0.05	46.0	3.5	13
0.65	9.8	0.10	28.0	0.94	30
0.65	6.9	0.14	25.2	0.29	86
0.65	5.4	0.19	23.0	0.13	181
0.45	20	0.05	52.5	1.5	34
0.45	9.0	0.11	29.5	0.42	70
0.45	7.1	0.14	28.0	0.13	210
0.45	5.4	0.19	31.8	0.08	386
0.25	20	0.05	48.8	1.9	25
0.25	10	0.10	27.5	0.63	44
0.25	6.9	0.14	32.3	0.18	181
0.25	5.5	0.18	41.2	0.08	516

Table XXXIII. Rotating Ring-Disk Electrode Data for Oxygen Reduction on Prereduced Smooth Pt in 8.5N KOH with 0.02M K_2SO_4 Added at 30 °C

E, volts	$\omega^{1/2}$ (rad/sec)$^{1/2}$	$\omega^{-1/2}$ (rad/sec)$^{-1/2}$	I_d, μA	I_r, μA	I_d/I_r
0.85	20	0.05	33.5	5.6	6.0
0.85	10	0.10	19.5	2.5	7.9
0.85	6.9	0.14	16.0	1.6	9.9
0.85	5.1	0.20	13.6	0.97	14
0.65	20	0.05	42.8	3.6	12
0.65	10	0.10	23.8	1.1	21
0.65	6.9	0.14	19.1	0.55	35
0.65	5.1	0.20	16.8	0.24	70
0.45	20	0.05	41.0	2.3	18
0.45	10	0.10	22.2	0.57	39
0.45	6.9	0.14	18.2	0.23	79
0.45	4.8	0.21	18.8	0.04	520
0.25	20	0.05	40.0	2.7	15
0.25	10	0.10	23.0	0.66	35
0.25	6.9	0.14	16.6	0.26	64
0.25	4.8	0.21	26.2	0.07	360

Table XXXIV. Rotating Ring-Disk Electrode Data for Oxygen Reduction on Preoxidized Smooth Pt in 8.5N KOH with 0.02M K_2SO_4 Added at 30 °C

E, volts	$\omega^{1/2}$ (rad/sec)$^{1/2}$	$\omega^{-1/2}$ (rad/sec)$^{-1/2}$	I_d, μA	I_r, μA	I_d/I_r
0.85	20	0.05	17.9	3.8	4.7
0.85	10	0.10	14.3	0.75	19
0.85	7.2	0.14	13.1	0.87	15
0.85	5.3	0.19	11.8	0.54	22
0.65	20	0.05	47.2	3.4	14
0.65	10	0.10	26.8	0.32	85
0.65	7.2	0.14	22.0	0.21	107
0.65	5.3	0.19	21.0	0.27	78
0.45	20	0.05	44.2	2.8	16
0.45	10	0.10	26.5	0.54	49
0.45	6.9	0.14	24.5	0.22	112
0.45	4.1	0.24	24.5	<0.01	>1000
0.25	20	0.05	45.8	2.5	18
0.25	10	0.10	26.4	0.74	36
0.25	6.9	0.14	25.1	0.38	66
0.25	4.1	0.24	19.1	0.05	385

Table XXXV. Rotating Ring-Disk Electrode Data for Oxygen Reduction on Preoxidized Smooth Pt in Purified 8.5N KOH Saturated with Johns-Manville "Fuel Cell Asbestos" at 30 °C

E, volts	$\omega^{1/2}$ (rad/sec)$^{1/2}$	$\omega^{-1/2}$ (rad/sec)$^{-1/2}$	I_d, μA	I_r, μA	I_d/I_r
+0.85	20	0.05	30.7	4.5	6.8
+0.85	10	0.10	19.5	1.9	10
+0.85	8.4	0.12	16.8	1.3	13
+0.85	7.2	0.14	17.7	0.98	18
+0.65	20	0.05	43.1	2.5	17
+0.65	10	0.10	25.6	0.45	57
+0.65	8.4	0.12	22.0	0.30	74
+0.65	7.2	0.14	20.5	0.24	85
+0.45	20	0.05	36.5	2.43	15
+0.45	10	0.10	21.0	0.84	25
+0.45	8.1	0.12	16.5	0.55	30
+0.25	20	0.05	37.0	2.31	16
+0.25	10	0.10	21.1	0.96	22
+0.25	8.1	0.12	17.7	0.74	24

Table XXXVI. Rotating Ring-Disk Electrode Data for Oxygen Reduction on Preoxidized Smooth Pt in Purified 8.5N KOH Saturated with Johns-Manville "Fuel Cell Asbestos" at 30 °C

E, volts	$\omega^{1/2}$ (rad/sec)$^{1/2}$	$\omega^{-1/2}$ (rad/sec)$^{-1/2}$	I_d, μA	I_r, μA	I_d/I_r
+0.85	20	0.05	14.0	2.5	5.5
+0.85	11	0.09	9.3	1.7	5.4
+0.85	8.7	0.11	9.1	1.4	6.3
+0.85	8.3	0.13	8.6	1.0	8.4
+0.65	20	0.05	45.8	2.5	18
+0.65	11	0.09	28.0	0.65	43
+0.65	8.7	0.11	23.8	0.34	69
+0.65	8.3	0.13	20.5	0.23	90
+0.45	20	0.05	40.5	2.7	15
+0.45	10	0.09	24.2	0.69	35
+0.45	8.4	0.12	19.0	0.59	32
+0.45	4.9	0.20	16.2	0.25	65
+0.25	20	0.05	41.0	2.7	15
+0.25	10	0.09	25.5	0.98	26
+0.25	8.4	0.12	10.0	0.45	22
+0.25	4.8	0.20	14.5	0.34	42

Table XXXVII. Rotating Ring-Disk Electrode Data for Oxygen Reduction on Prereduced Smooth Pt in Purified 8.5N KOH Containing 100 ppm Fe^{3+}

E, volts	$\omega^{1/2}$ (rad/sec)$^{1/2}$	$\omega^{-1/2}$ (rad/sec)$^{-1/2}$	I_d, μA	I_r, μA	I_d/I_r
+0.85	20	0.05	40.5	6.5	6.2
+0.85	10	0.10	22.7	3.2	7.2
+0.85	7.4	0.13	16.2	2.2	7.5
+0.85	5.4	0.18	13.3	1.3	10
+0.65	20	0.05	50.2	4.6	11
+0.65	10	0.10	26.5	1.8	15
+0.65	7.4	0.13	19.7	1.2	17
+0.65	5.4	0.18	15.5	0.62	25
+0.45	20	0.05	49.0	3.8	13
+0.45	10	0.10	27.0	1.3	21
+0.45	7.2	0.14	20.5	0.51	40
+0.45	5.5	0.18	22.5	0.28	80
+0.25	20	0.05	56.7	1.7	34
+0.25	10	0.10	30.2	0.50	61
+0.25	7.2	0.14	24.0	0.21	112
+0.25	5.5	0.18	25.2	0.10	245

Table XXXVIII. Rotating Ring-Disk Electrode Data for Oxygen Reduction on Preoxidized Smooth Pt in Purified 8.5N KOH Containing 100 ppm Fe^{3+}

E, volts	$\omega^{1/2}$ (rad/sec)$^{1/2}$	$\omega^{-1/2}$ (rad/sec)$^{-1/2}$	I_d, μA	I_r, μA	I_d/I_r
+0.85	20	0.05	19.8	5.2	3.8
+0.85	10	0.10	15.5	3.9	4.0
+0.85	7.2	0.14	11.8	2.8	4.2
+0.85	5.4	0.18	15.7	1.6	10
+0.65	20	0.05	46.2	5.1	9.1
+0.65	10	0.10	29.0	2.1	14
+0.65	7.2	0.14	20.0	1.2	16
+0.65	5.4	0.18	19.0	0.46	41
+0.45	20	0.05	53.5	3.8	14
+0.45	10	0.10	29.0	1.4	20
+0.45	7.2	0.14	21.5	0.74	29
+0.45	5.7	0.18	22.2	0.41	54
+0.25	20	0.05	61.0	1.6	38
+0.25	10	0.10	31.3	0.50	63
+0.25	7.2	0.14	22.5	0.24	93
+0.25	5.7	0.17	20.0	0.17	120

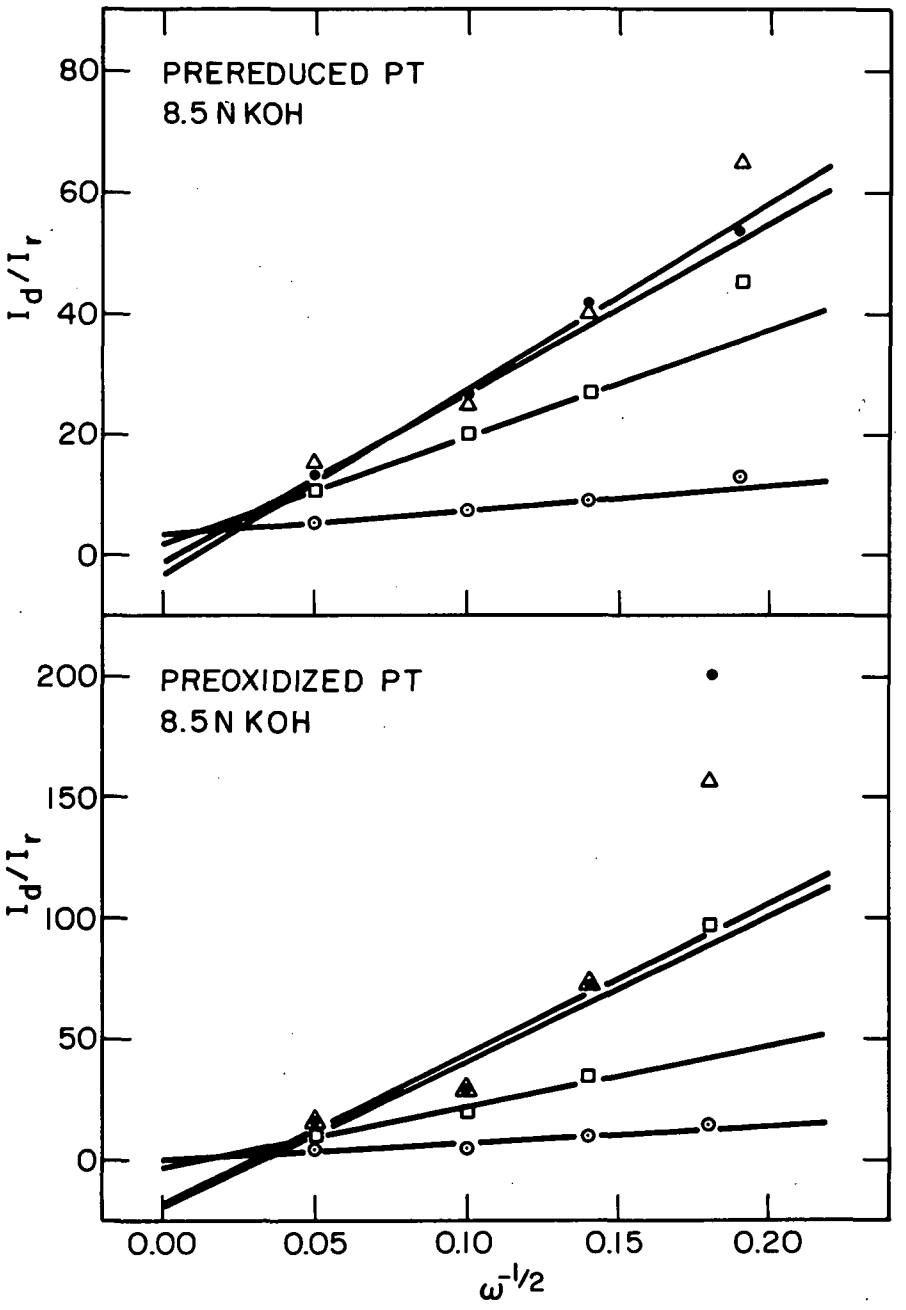

Fig. 53. I_d/I_r versus $\omega^{-1/2}$ plots for O_2 reduction at prereduced and preoxidized smooth Pt disk electrodes in purified 8.5N KOH at 30 °C with E_d: ○ = +0.85 V; □ = +0.65 V; △ = +0.45 V; and ● = +0.25 V

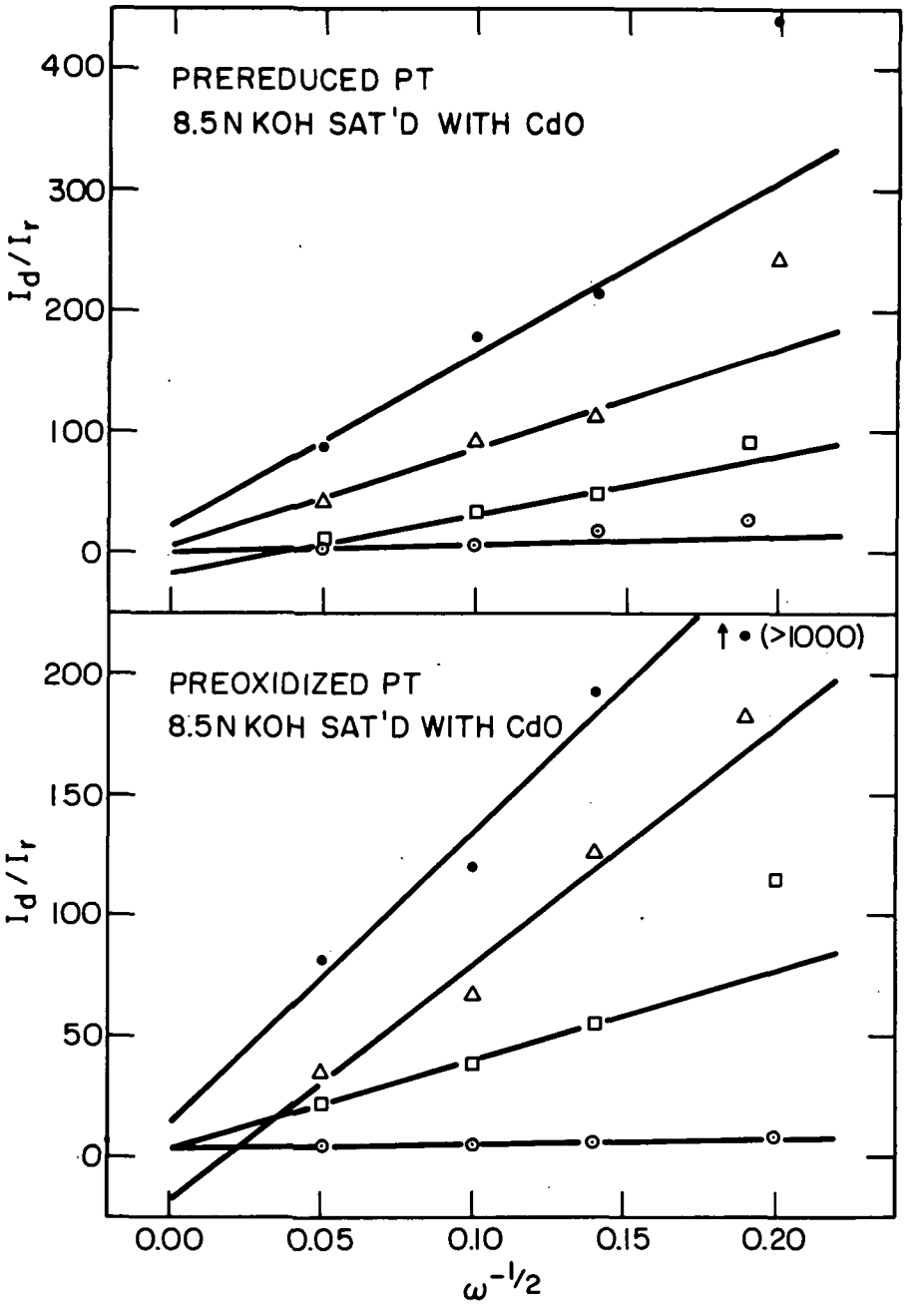

Fig. 54. I_d/I_r versus $\omega^{-1/2}$ plots for O_2 reduction at prereduced and preoxidized smooth Pt disk electrodes in purified 8.5N KOH saturated with CdO at 30 °C for E_d: ○ = +0.85 V; □ = +0.65 V; △ = +0.45 V; and ● = +0.25 V

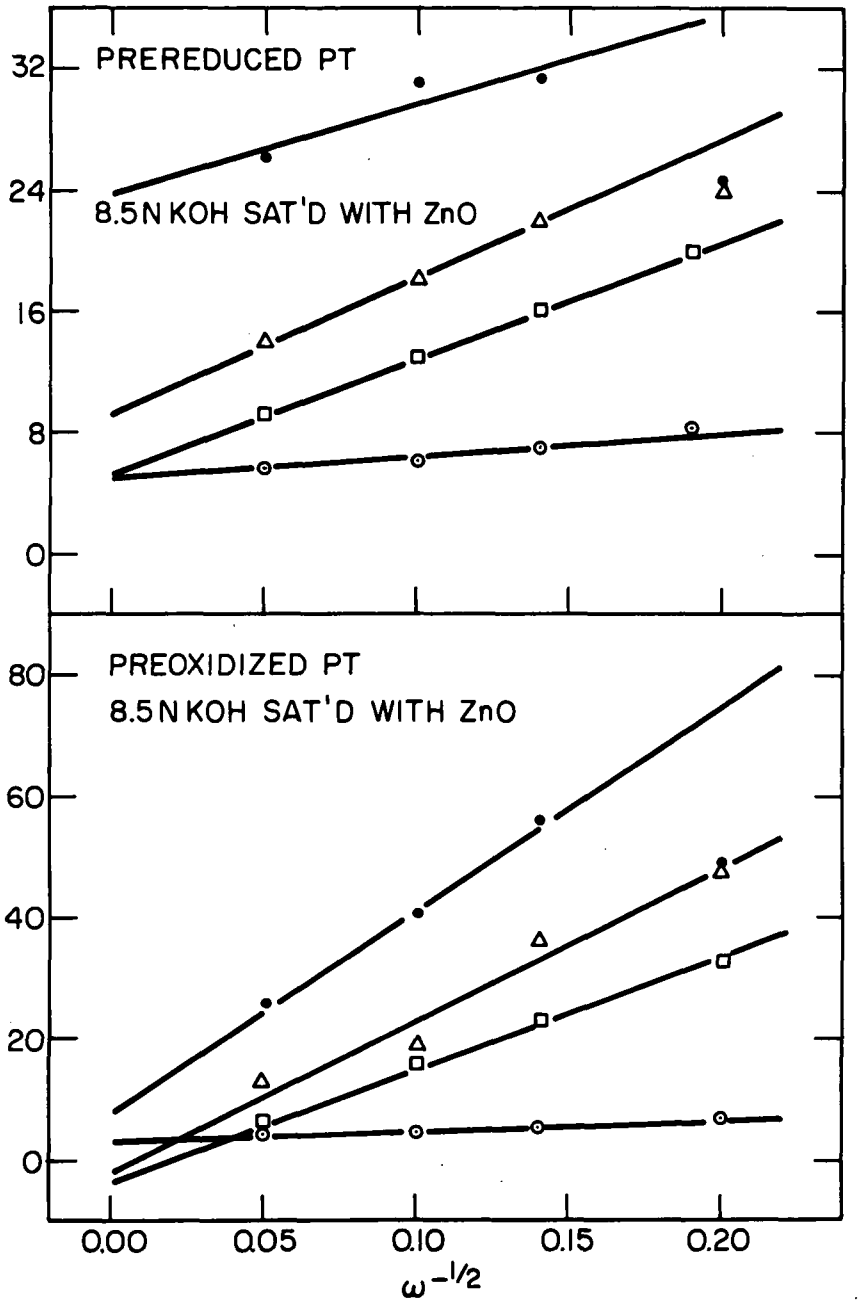

Fig. 55. I_d/I_r versus $\omega^{-1/2}$ plots for O_2 reduction at prereduced and preoxidized smooth Pt disk electrodes in purified 8.5N KOH saturated with ZnO at 30 °C for E_d: ○ = +0.85 V; □ = +0.65 V; △ = +0.45 V; and ● = +0.25 V

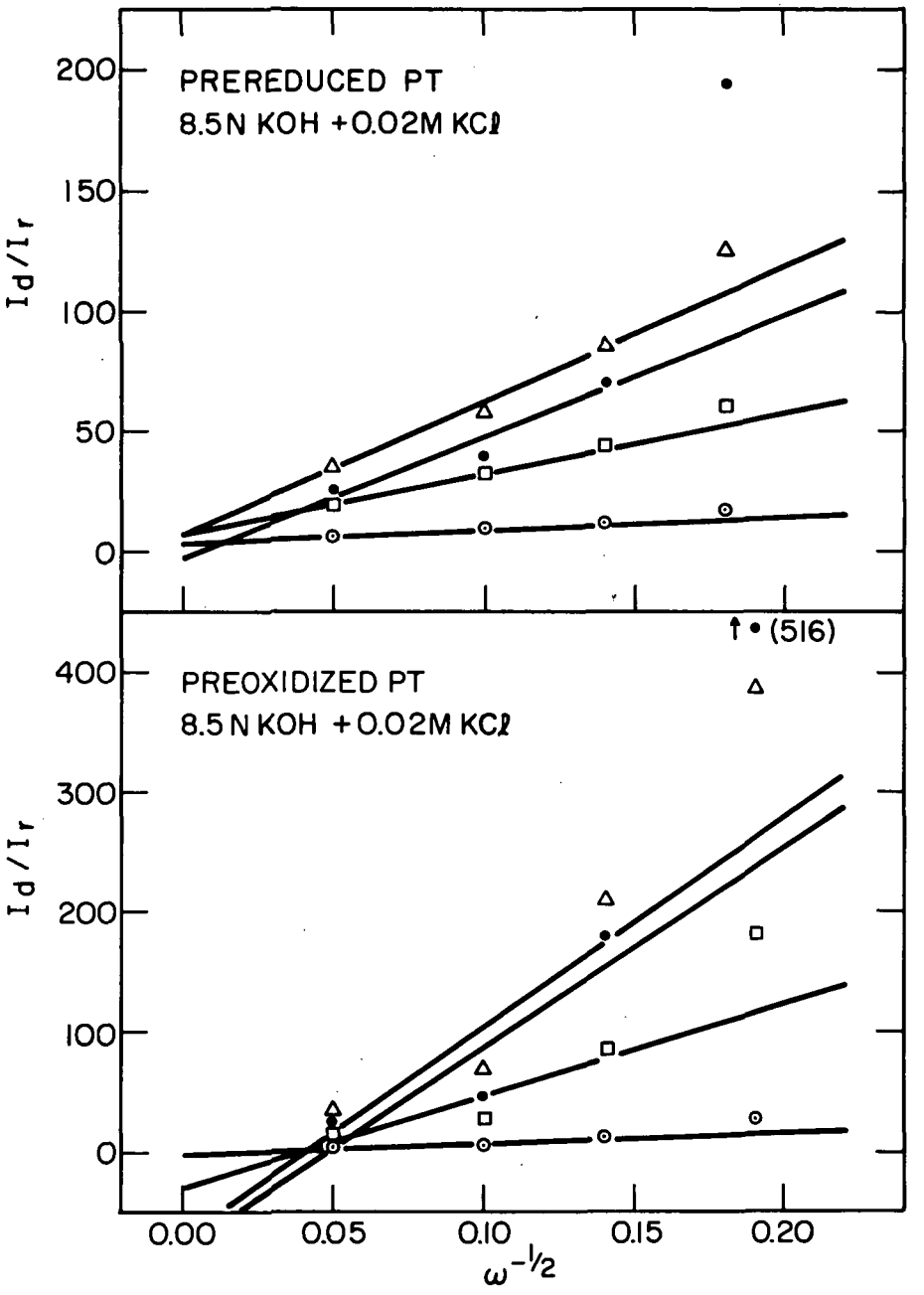

Fig. 56. I_d/I_r versus $\omega^{-1/2}$ plots for O_2 reduction at prereduced and preoxidized smooth Pt disk electrodes in purified 8.5N KOH +0.02M KCl at 30 °C for E_d: ○ = +0.85 V; □ = +0.65 V; △ = +0.45 V; and ● = +0.25 V

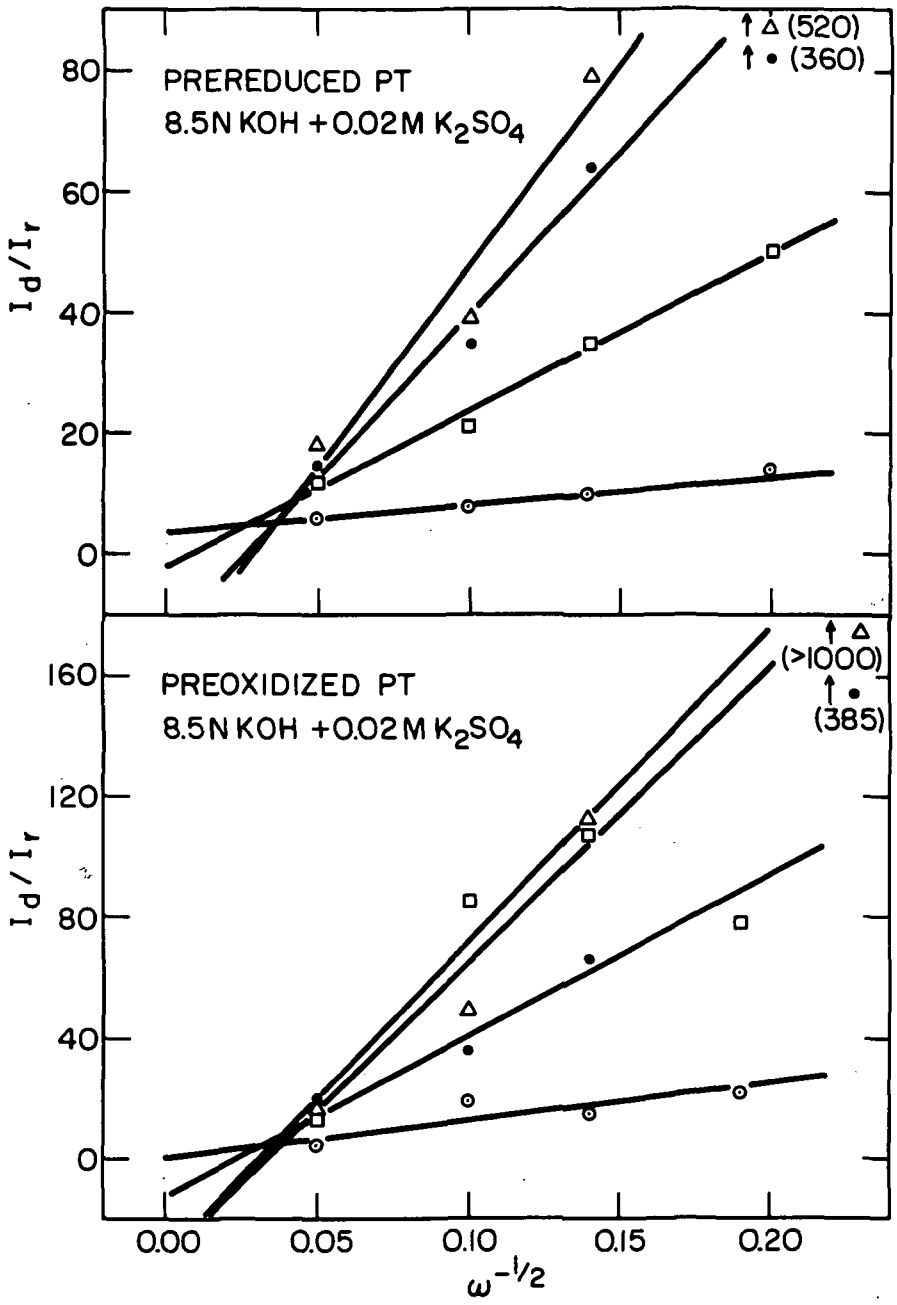

Fig. 57. I_d/I_r versus $\omega^{-1/2}$ plots for O_2 reduction at prereduced and preoxidized smooth Pt disk electrodes in purified 8.5N KOH + 0.02M K_2SO_4 at 30 °C for E_d: ⊙ = +0.85 V; □ = +0.65 V; △ = +0.45 V; and ● = +0.25 V

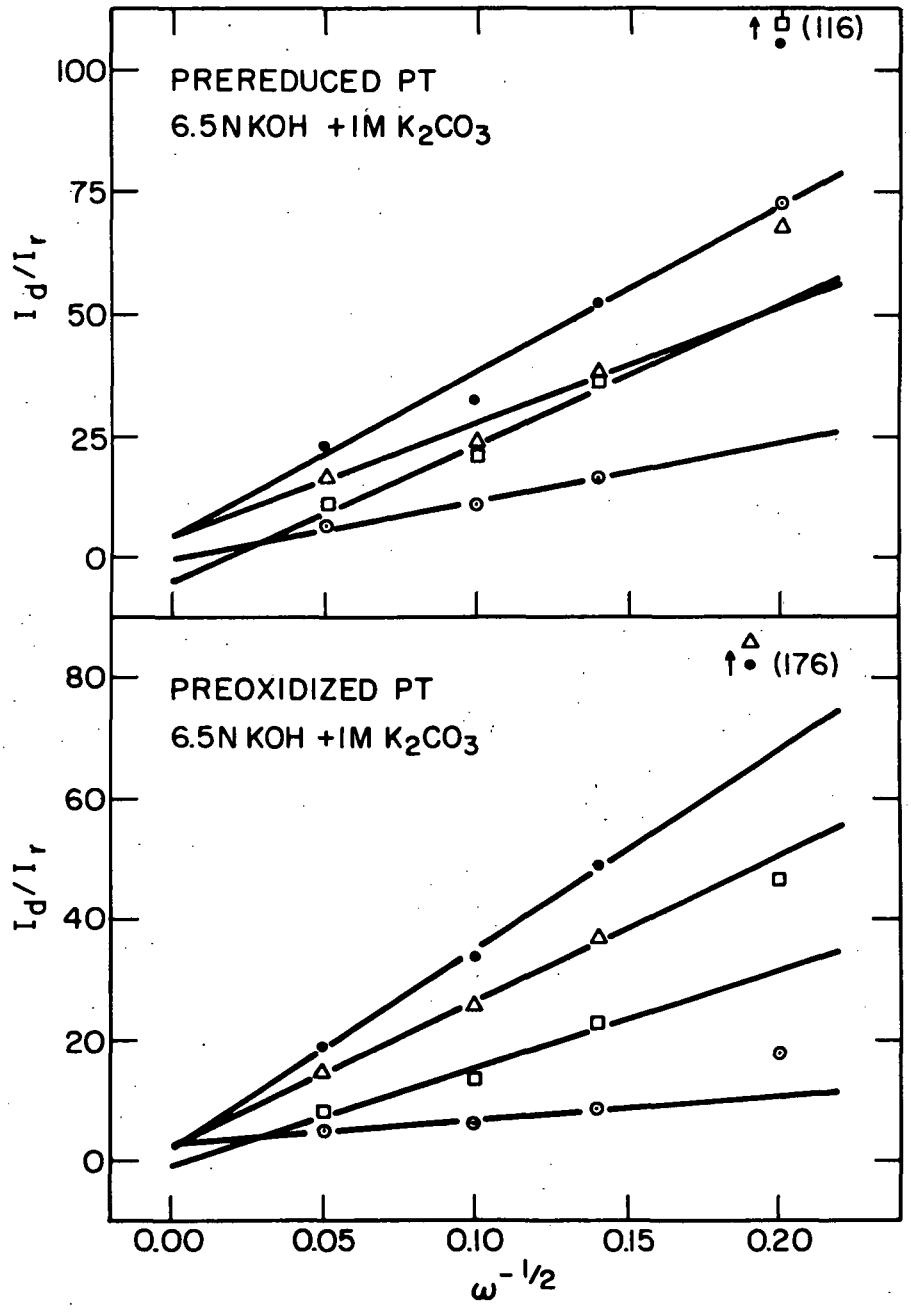

Fig. 58. I_d/I_r versus $\omega^{-1/2}$ plots for O_2 reduction at prereduced and preoxidized smooth Pt disk electrodes in purified 6.5N KOH + $1M K_2CO_3$ at 30 °C for E_d: ⊙ = +0.85 V; ⊡ = +0.65 V; △ = +0.45 V; and ● = +0.25 V

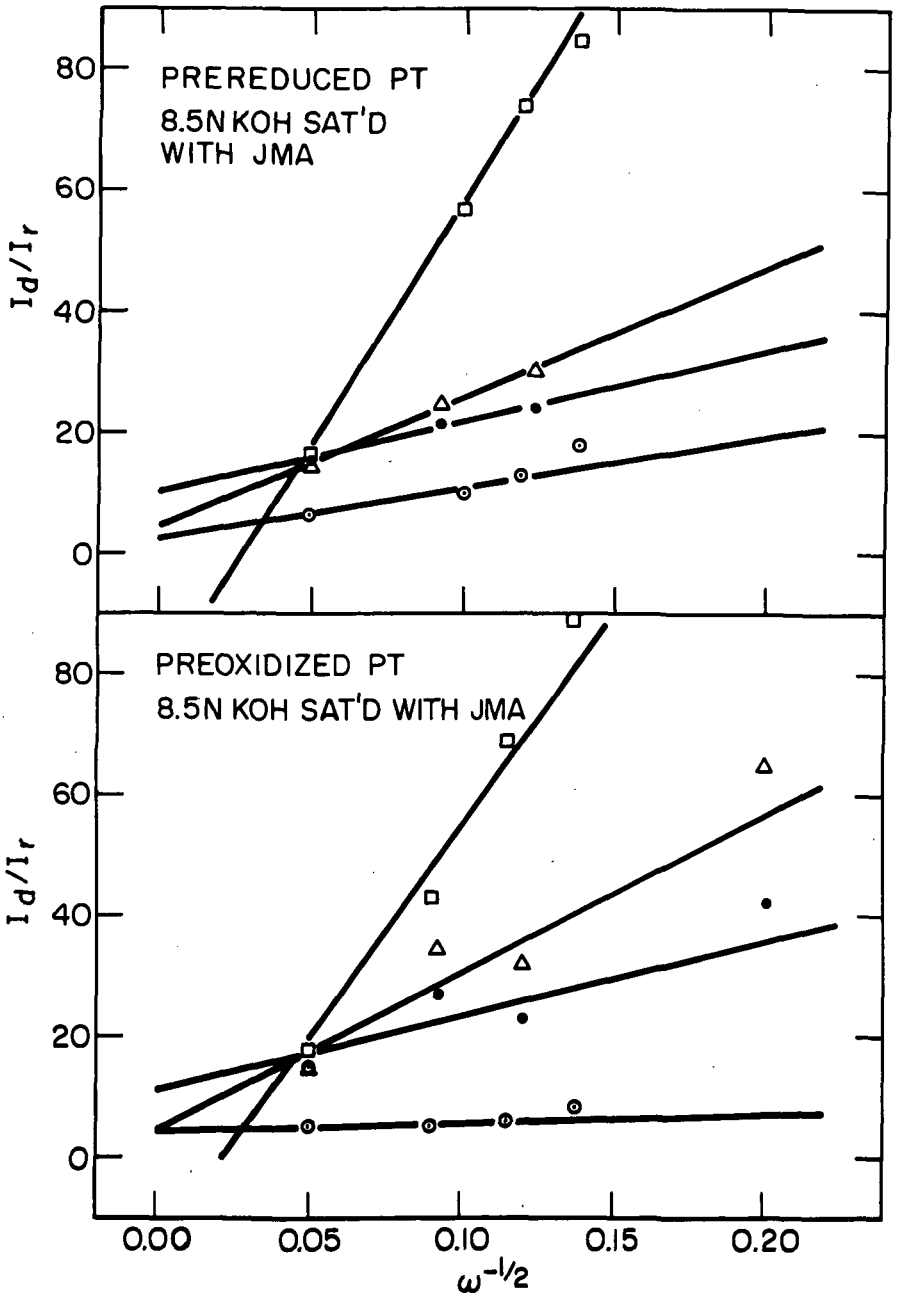

Fig. 59. I_d/I_r versus $\omega^{-1/2}$ plots for O_2 reduction at prereduced and preoxidized smooth Pt disk electrodes in purified 8.5N KOH saturated with Johns-Manville Fuel Cell Asbestos at 30 °C for E_d: ⊙ = +0.85 V; ⊡ = +0.65 V; △ = +0.45 V; and ● = +0.25 V

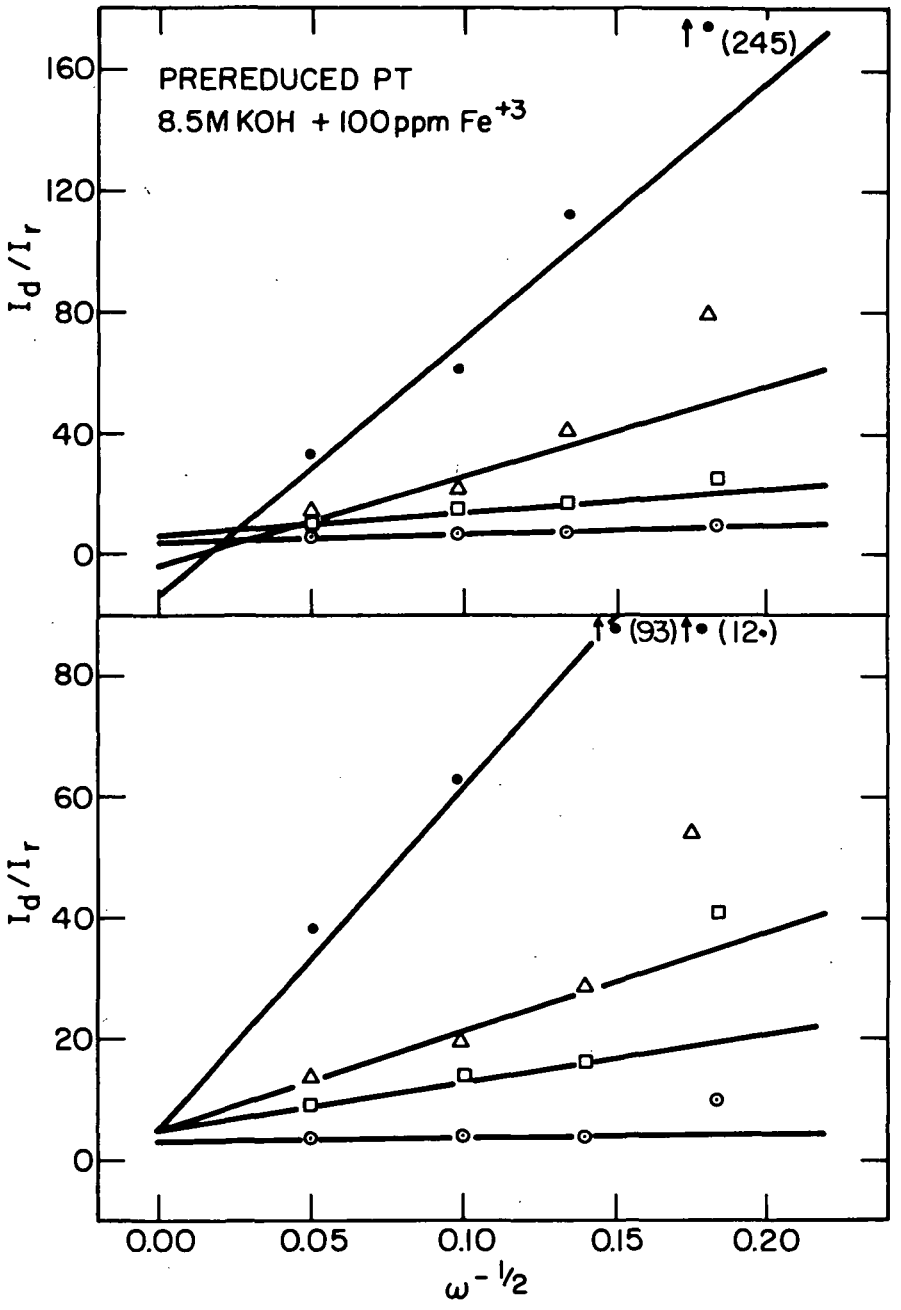

Fig. 60. I_d/I_r versus $\omega^{-1/2}$ plots for O_2 reduction at prereduced and preoxidized smooth Pt disk electrodes in purified 8.5N KOH + 100 ppm Fe^{3+} at 30 °C for E_d: ○ = +0.85 V; ⊡ = +0.65 V; △ = +0.45 V; and ● = +0.25 V

Table XXXIX. Least-Squares Calculated Intercepts of I_d / I_r versus $\omega^{-1/2}$ Plots in Electrolytes E-1 Through E-8 on Prereduced Smooth Pt

Electrolyte	INTERCEPT E_d = +0.85	+0.65	+0.45	+0.25
E-1	3.5	2.1	0.1	-3.2
E-2	3.2	-19	4.6	24
E-3	5.0	5.4	9.4	24
E-4	0.8	-4.6	4.1	3.9
E-5	3.3	7.0	6.8	-3.2
E-6	3.8	-1.7	-19	-14
E-7	2.4	-24	4.6	11
E-8	5.4	7.3	-3.8	-14

Table XL. Least-Squares Calculated Intercepts of I_d / I_r versus $\omega^{-1/2}$ Plots in Electrolyte E-1 Through E-8 on Preoxidized Smooth Pt

Electrolyte	INTERCEPT E_d = +0.85	+0.65	+0.45	+0.25
E-1	1.1	-3.4	-22	-20
E-2	4.3	3.1	-18	15
E-3	3.6	-3.0	-1.5	8.7
E-4	3.0	-0.5	2.5	1.9
E-5	-17	-34	-72	-79
E-6	1.2	-33	-42	-11
E-7	4.8	-25	5.1	12
E-8	3.6	5.5	5.1	6.0

Table XLI. Least-Squares Calculated Slopes of I_d/I_r versus $\omega^{-1/2}$ Plots in Electrolyte E-1 Through E-8 on Prereduced Smooth Pt

Electrolyte	SLOPE			
	E_d = +0.85 V	+0.65 V	+0.45 V	+0.25 V
E-1	41	178	275	309
E-2	43	506	818	1430
E-3	14	76	88	57
E-4	112	285	230	338
E-5	62	255	551	502
E-6	43	252	667	538
E-7	84	812	216	116
E-8	17	76	294	853

Table XLII. Least-Squares Calculated Slopes of I_d/I_r versus $\omega^{-1/2}$ Plots in Electrolytes E-1 Through E-8 on Preoxidized Smooth Pt

Electrolyte	SLOPE			
	E_d = +0.85 V	+0.65 V	+0.45 V	+0.25 V
E-1	58	263	630	620
E-2	13	365	975	1200
E-3	13	187	250	331
E-4	40	161	243	332
E-5	87	792	1760	1680
E-6	121	1050	1050	526
E-7	11	818	257	109
E-8	4.4	78	165	606

In Tables XXXIX and XL and Figs. 53 through 60, it can be seen that negative I_d/I_r values or I_d/I_r values $<1/N$ were obtained in 30 out of 64 cases. These negative values of the I_d/I_r intercepts are presumably a reflection of the poor precision in the I_d/I_r determination arising from measurement of low I_r values. Disregarding these negative values and also I_d/I_r intercepts $<1/N$ (2.5), we calculate an average I_d/I_r intercept of 7 ± 4 for the prereduced Pt surface and 6 ± 3 for preoxidized Pt surface. These average values are in the vicinity of $1/N$ and thus would be in agreement with our earlier postulation of a two-step reduction of O_2 to H_2O involving H_2O_2 as a reaction intermediate. Thus, the effect of these additives on the O_2 reduction pathway appears to be minimal. A more marked difference can be seen, however, in the calculated least-squares slopes, which are a direct indication of changes in the rate constants for H_2O_2 decomposition.

In Figs. 61-64, we present the potential dependence of the calculated least-squares slopes of the I_d/I_r versus $\omega^{-1/2}$ plots. The slope of such a plot is proportional to the rate constant for H_2O_2 [see Eq. (20)]. The effects of metal-ion additions are compared in Figs. 61 and 62 for prereduced and preoxidized smooth platinum while Figs. 63 and 64 deal with anionic additives (we have arbitrarily classified impurities leached from Johns-Manville Fuel Cell Asbestos as being anionic in nature).

In Figs. 61 and 62, there is a general trend to an increase in the H_2O_2 decomposition rate as the electrode potential decreases. Soluble cadmium species appear to accelerate H_2O_2 decomposition, while $Zn(OH)_4^{2-}$ and Fe^{3+} tend to inhibit peroxide decomposition, the effect of Fe^{3+} being more pronounced on the prereduced surface.

Anionic impurities, as can be seen from Figs. 63 and 64, have less marked influence regarding H_2O_2 decomposition on a prereduced surface than on a preoxidized surface. Generally the anions seem to accelerate H_2O_2 decomposition with the exception of carbonate and "asbestos" which lead to more H_2O_2 production. Impurities leached from Johns-Manville Asbestos appear to undergo a strongly potential-dependent adsorption process since there is an apparent maximum in the rate of peroxide decomposition at +0.65 V.

We have also investigated the influence of $Zn(OH)_4^{2-}$, $Cd(OH)_4^{2-}$ and Fe^{3+} on O_2 reduction on preoxidized and prereduced platinized platinum. The I_d/I_r results are given in Tables XLIII through XLVIII. While the I_d/I_r values obtained are quite high, there seems to be a tendency for more H_2O_2 formation in the presence of these metal ions.

It was interesting to note that we did not observe severe poisoning of O_2 reduction by soluble cadmium species in 8.5N KOH, either with smooth or platinized platinum electrodes. We therefore made some further studies of the effects of cadmate species on O_2 reduction in 0.1N KOH.

Our first experiments were carried out in purified 0.1N KOH (100 ml) to which 1 ml of a 10^{-1}M $Cd(NO_3)_2$ solution was added. This addition led to the formation of a precipitate, presumably CdO, since the solubility of CdO in 0.1N KOH is on the order of 10^{-6}M (based on a solubility of 1.3×10^{-6}M in 0.1N NaOH taken from Linke).[55]

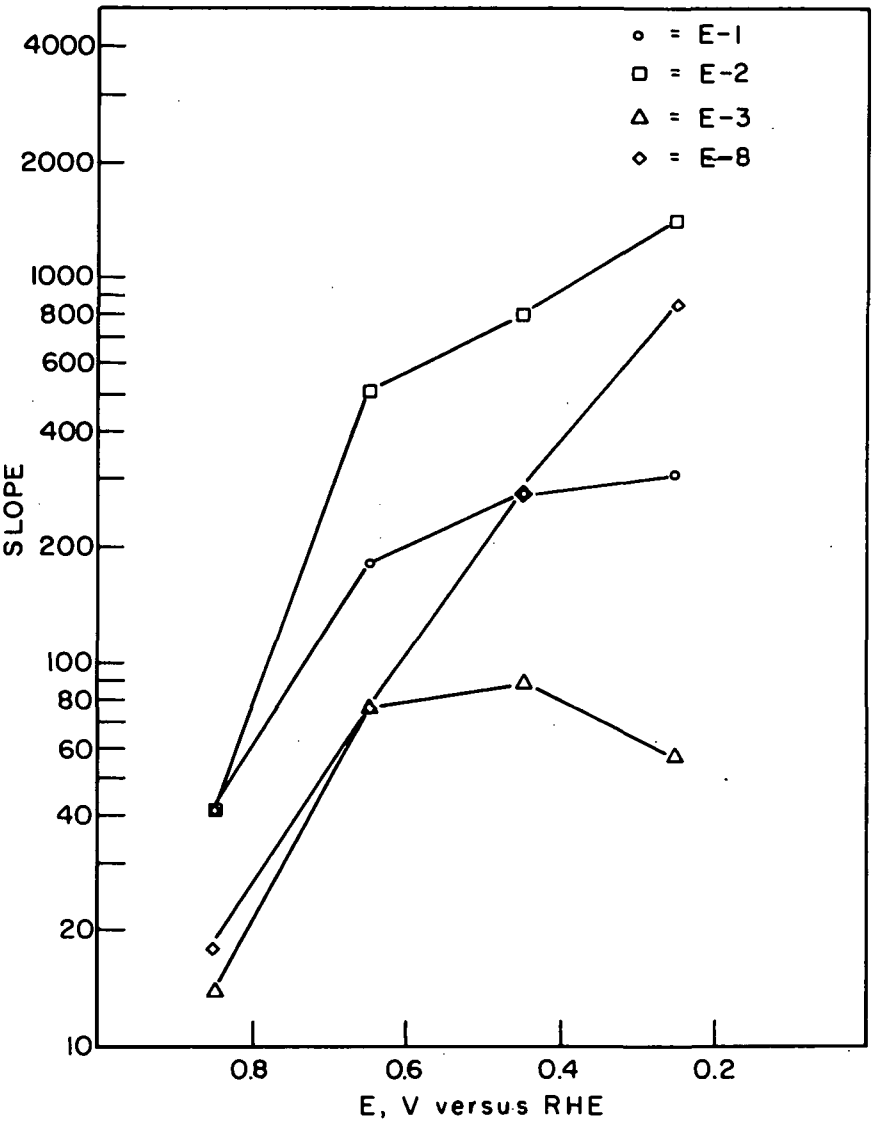

Fig. 61. Effects of cationic species on the rate constant for H_2O_2 reduction on prereduced smooth platinum as reflected in the slopes of I_d/I_r versus $\omega^{-1/2}$ plots for O_2 reduction in KOH electrolytes at 30 °C

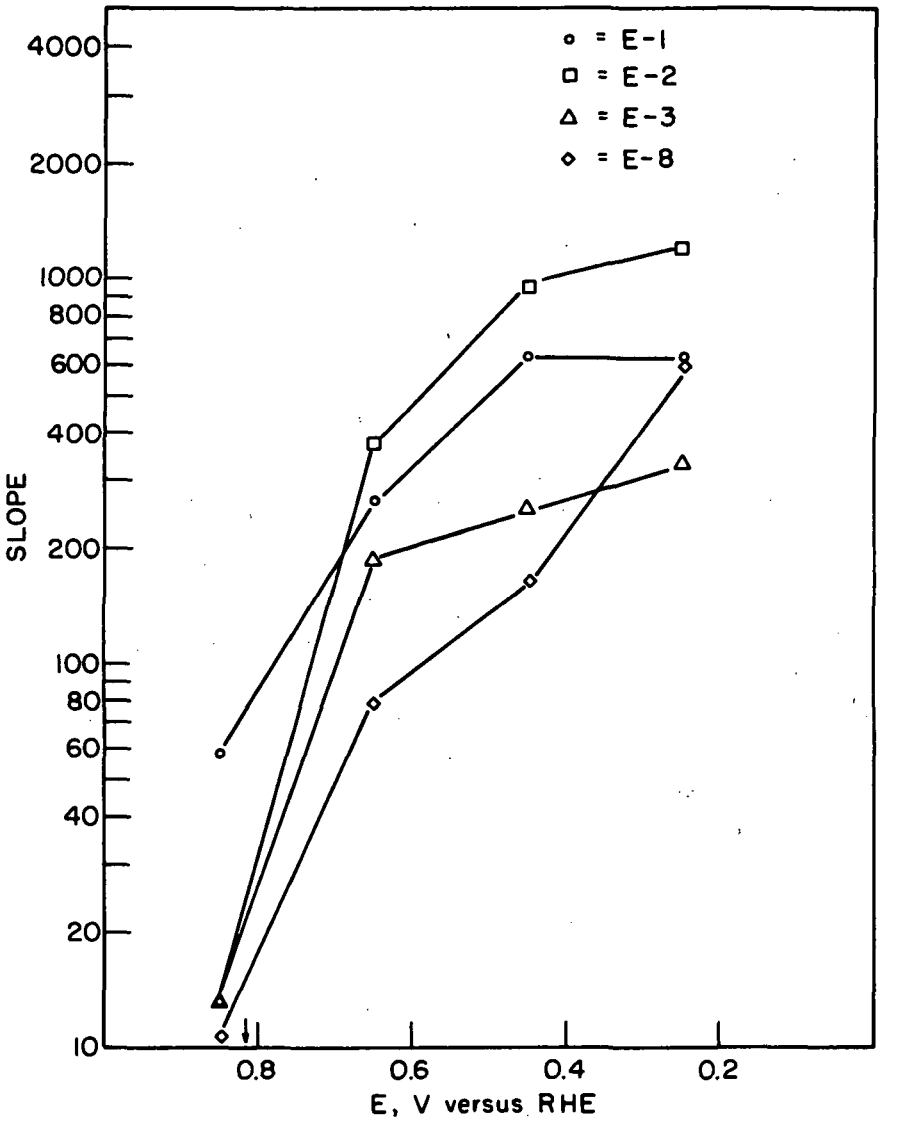

Fig. 62. Effects of cationic species on the rate constant for H_2O_2 reduction on preoxidized smooth platinum as reflected in the slopes of I_d/I_r versus $\omega^{-1/2}$ plots for O_2 reduction in KOH electrolytes at 30 °C

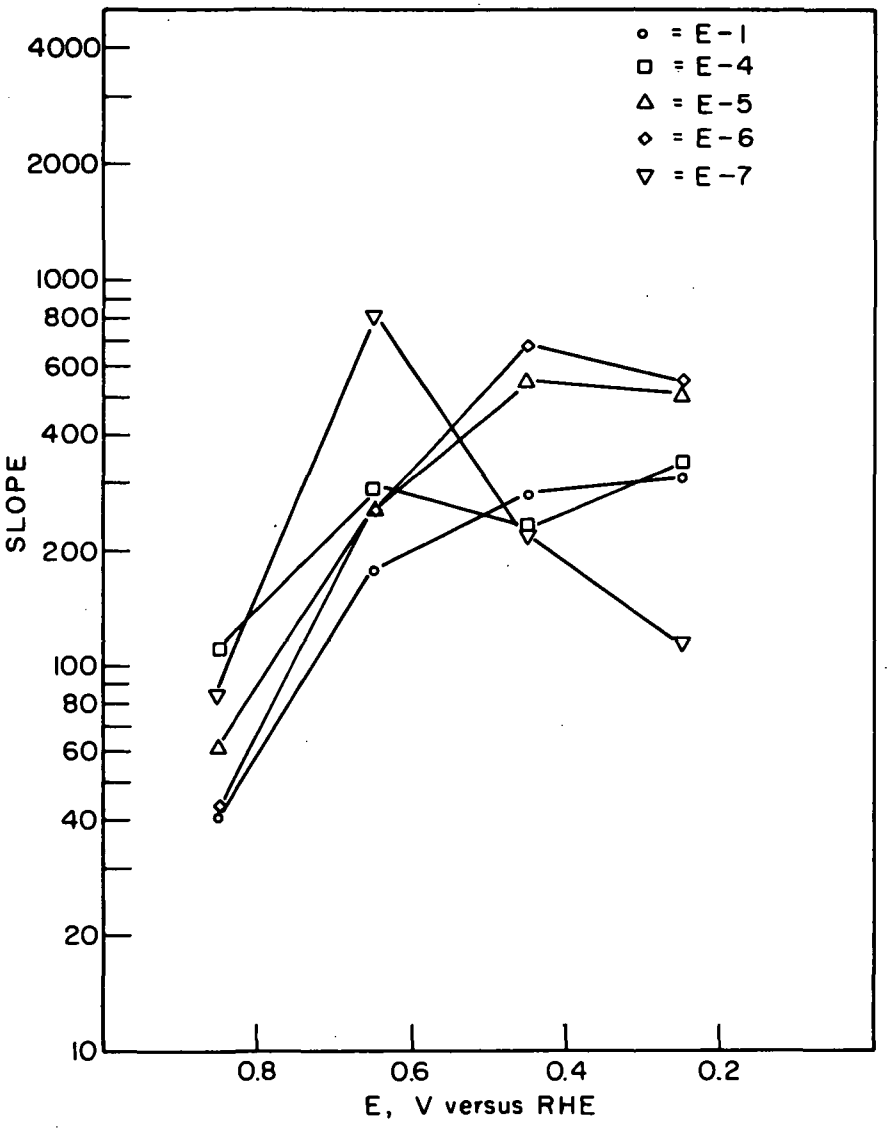

Fig. 63. Effects of anionic species on the rate constant for H_2O_2 reduction on prereduced smooth platinum as reflected in the slopes of I_d/I_r versus $\omega^{-1/2}$ plots for O_2 reduction in KOH electrolytes at 30 °C

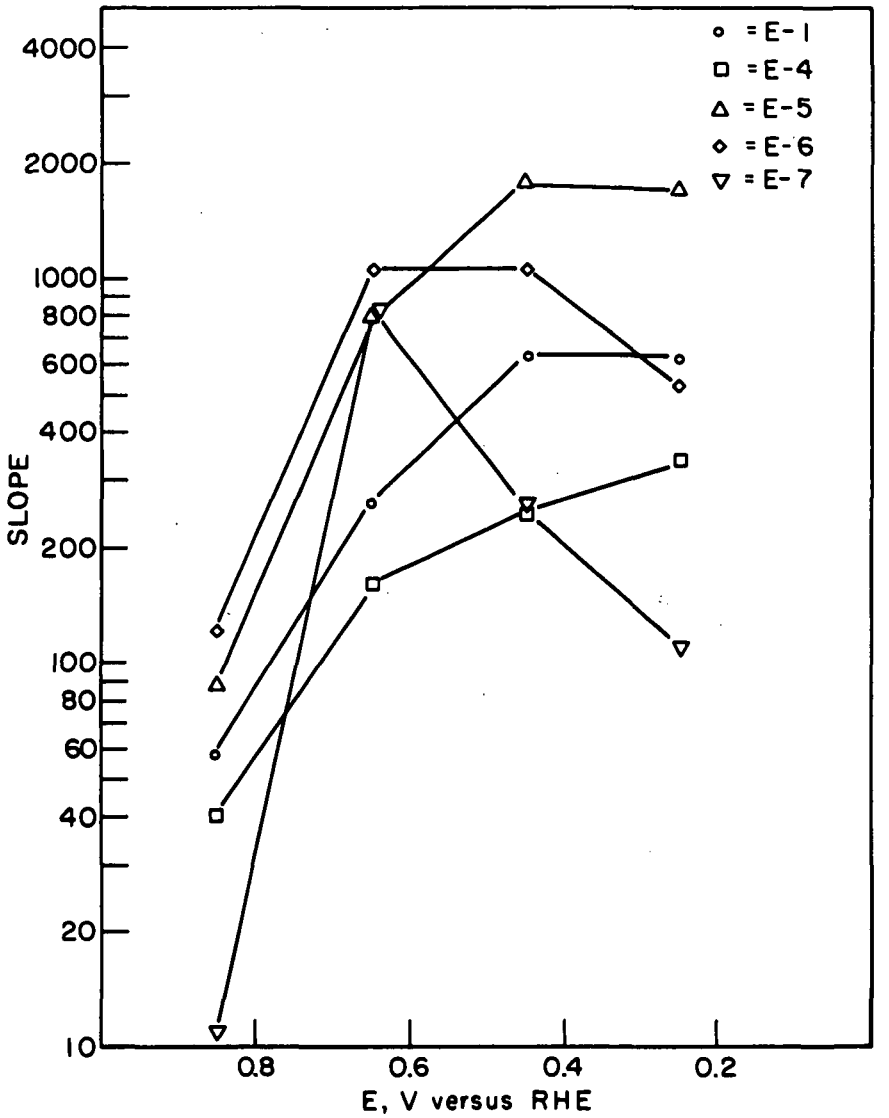

Fig. 64. Effects of anionic species on the rate constant for H_2O_2 reduction on preoxidized smooth platinum as reflected in the slopes of I_d/I_r versus $\omega^{-1/2}$ plots for O_2 reduction in KOH electrolytes at 30 °C

Table XLIII. Rotating Ring-Disk Electrode Data for O_2 Reduction on Prereduced Platinized Platinum in Purified 8.5N KOH Saturated With CdO at 30 °C

E_d, volts	$\omega^{1/2}$ (rad/sec)$^{1/2}$	$\omega^{-1/2}$ (rad/sec)$^{-1/2}$	I_d, μA	I_r, μA	I_d/I_r
0.85	20	0.05	50.5	1.3	37
0.85	10	0.10	27.0	0.40	68
0.85	7.3	0.14	20.0	0.25	80
0.85	5.7	0.18	15.0	0.15	100
0.65	20	0.05	56.4	0.65	87
0.65	10	0.10	30.0	0.12	240
0.65	7.2	0.14	21.0	<0.02	>1000
0.45	20	0.05	56.5	0.25	225
0.45	10	0.10	31.0	0.18	170
0.45	23	0.14	23.0	0.05	460
0.25	20	0.05	57.0	0.25	230
0.25	10	0.10	31.0	0.12	260

Table XLIV. Rotating Ring-Disk Electrode Data for O_2 Reduction on Preoxidized Platinized Platinum in Purified 8.5N KOH Saturated With CdO at 30 °C

E_d, volts	$\omega^{1/2}$ (rad/sec)$^{1/2}$	$\omega^{-1/2}$ (rad/sec)$^{-1/2}$	I_d, μA	I_r, μA	I_d/I_r
0.85	20	0.05	43.0	4.0	11
0.85	10	0.10	25.0	1.5	17
0.85	7.1	0.14	18.7	0.85	22
0.85	5.8	0.18	16.5	0.60	28
0.65	20	0.05	60.0	0.53	113
0.65	10	0.10	31.0	0.11	280
0.65	7.3	0.14	23.0	0.10	230
0.45	20	0.05	61.0	0.32	190
0.45	10	0.10	29.7	0.10	297
0.45	7.3	0.14	21.0	0.05	420
0.25	20	0.05	58.0	0.35	165
0.25	10	0.10	31.0	0.18	170
0.25	7.3	0.14	23.0	0.12	190

Table XLV. Rotating Ring-Disk Electrode Data for O_2 Reduction on Prereduced Platinized Platinum in Purified 8.5N KOH Saturated With ZnO at 30 °C

E_d, volts	$\omega^{1/2}$ (rad/sec)$^{1/2}$	$\omega^{-1/2}$ (rad/sec)$^{-1/2}$	I_d, μA	I_r, μA	I_d/I_r
0.85	20	0.05	49.0	0.95	52
0.85	10	0.10	26.5	0.28	95
0.85	7.2	0.14	19.0	0.18	105
0.65	20	0.05	51.0	0.23	222
0.65	10	0.10	25.7	0.03	860
0.45	20	0.05	51.0	0.52	98
0.45	10	0.10	26.5	0.14	186
0.25	20	6.05	52.0	0.48	108
0.25	10	0.10	27.0	0.15	180
0.25	7.3	0.14	19.3	0.12	161

Table XLVI. Rotating Ring-Disk Electrode Data for O_2 Reduction on Preoxidized Platinized Platinum in Purified 8.5N KOH Saturated With ZnO at 30 °C

E_d, volts	$\omega^{1/2}$ (rad/sec)$^{1/2}$	$\omega^{-1/2}$ (rad/sec)$^{-1/2}$	I_d, μA	I_r, μA	I_d/I_r
0.85	20	0.05	50.5	0.30	170
0.85	10	0.10	20.0	0.11	182
0.65	20	0.05	51.0	0.17	300
0.65	10	0.10	26.0	0.05	520
0.45	20	0.05	51.0	0.43	118
0.45	10	0.10	26.8	0.16	170
0.25	20	0.05	51.0	0.37	138
0.25	10	0.10	26.7	0.14	191
0.25	7.4	0.14	20.0	0.12	167

Table XLVII. Rotating Ring-Disk Electrode Data for O_2 Reduction on Prereduced Platinized Platinum in Purified 8.5N KOH Containing Fe^{3+} (100 ppm) at 30 °C

E_d, volts	$\omega^{1/2}$ (rad/sec)$^{1/2}$	$\omega^{-1/2}$ (rad/sec)$^{-1/2}$	I_d, μA	I_r, μA	I_d/I_r
0.85	20	0.05	45.8	2.6	18
0.85	10	0.10	25.2	0.87	29
0.85	7.4	0.14	18.5	0.45	41
0.85	5.8	0.18	14.0	0.27	52
0.65	20	0.05	53.0	0.75	71
0.65	10	0.10	25.6	0.15	171
0.65	7.2	0.14	17.5	0.08	219
0.45	20	0.05	57.0	1.0	57
0.45	10	0.10	28.5	0.25	114
0.45	7.2	0.14	18.5	0.18	103
0.25	20	0.05	59.0	0.58	102
0.25	10	0.10	30.5	0.14	218
0.25	7.2	0.14	22.5	0.08	281

Table XLVIII. Rotating Ring-Disk Electrode Data for O_2 Reduction on Preoxidized Platinized Platinum in Purified 8.5N KOH Containing Fe^{3+} (100 ppm) at 30 °C

E_d, volts	$\omega^{1/2}$ (rad/sec)$^{1/2}$	$\omega^{-1/2}$ (rad/sec)$^{-1/2}$	I_d, μA	I_r, μA	I_d/I_r
0.85	20	0.05	44.2	3.6	12
0.85	10	0.10	24.0	1.3	18
0.85	7.2	0.14	18.2	0.80	23
0.85	5.6	0.18	15.5	0.58	27
0.65	20	0.05	54.2	1.0	54
0.65	10	0.10	26.0	0.30	87
0.65	7.4	0.14	18.2	0.17	107
0.65	6.0	0.17	15.0	0.09	167
0.45	20	0.05	56.0	1.0	56
0.45	10	0.10	28.5	0.35	81
0.45	7.3	0.14	20.5	0.16	128
0.45	5.8	0.17	16.5	0.10	165
0.25	20	0.05	58.5	0.55	106
0.25	10	0.10	30.0	0.18	167
0.25	7.2	0.14	21.4	0.12	178

We observed that the oxygen reduction process was almost completely inhibited. We feel that this was due to the precipitation of species on the disk surface since excess solid phase was present in the electrolyte.

In a more controlled experiment, we compared composite I_d-I_r versus E_d curves for O_2 reduction on smooth Pt in unpurified 0.1N KOH and 0.1N KOH which had been saturated with CdO, but with removal of the solid phase after equilibrium. Fig. 65 shows a typical I_d-I_r versus E curve in the CdO-saturated, unpurified 0.1N KOH. (For references to similar curves in unpurified 0.1N KOH, see Fig. 34.) The addition of CdO does seem to lead to more H_2O_2 production, especially on the reverse sweep at E_d>+0.6 V, where a peak is seen at ~+0.7 V. However, no severe poisoning of the O_2 reduction process was observed.

In purified 0.1N KOH to which 1 ml of a 0.1N KOH electrolyte saturated with CdO had been added, we did not observe any effects of the soluble cadmium species, which would be present at a concentration of $\sim 10^{-8}$M. In purified 0.1N KOH to which we added 0.5 ml of 8.5N KOH saturated with CdO [$(Cd^{2+}) = 1.4 \times 10^{-4}$M] to give a $(Cd^{2+}) = 6 \times 10^{-7}$M, we observed a distinct plateau in the forward sweep at +0.8 - +0.7 V, accompanied by a general increase in peroxide formation. Further addition (0.5 ml) of the 8.5N KOH/CdO led to I_d-I_r curves similar to those of Fig. 65, in which a peak in the I_r versus E_d curves appears on the anodic (or reverse) sweep, along with a further increase in H_2O_2 production. The similarity between these results and those obtained in impure 0.1N KOH saturated with CdO is not surprising since the soluble cadmium concentration should be the same $\sim 1 \times 10^{-6}$M. Therefore, there does not appear to be any poisoning of smooth Pt for O_2 reduction in 0.1N KOH containing soluble cadmium ionic species up to $\sim 1 \times 10^{-6}$M, which is probably just below the solubility limit. Some increase in H_2O_2 accumulation can be observed, however.

It is curious why soluble cadmiate species poison air electrodes in cadmium-air cells but no marked effects are observed on smooth or platinized electrodes other than a tendency for increased peroxide formation. It seems possible that, in the porous O_2 electrode, insoluble CdO or $Cd(OH)_2$ may precipitate due to a decrease in pH. This explanation also is supported by Wagner's findings that, if sufficient carbonate is present, cadmiate poisoning does not occur, since carbonate increased cadmium solubility.

3. Effects of cycle regime I on O_2 reduction and evolution on smooth and platinized Pt

We have also made an investigation of the effects of cycling smooth Pt under regime I (+1.75 V/10 min, +0.85 V/5 min) by continuously monitoring I_d and I_r for a sufficient number of cycles so that I_d undergoes no further change with cycle number. Figs. 66 through 73 show the I_d values as measured at the end of each cycle at +0.85 and +1.75 V for all six electrolytes studied.

All the electrolytes show a decrease in both oxygen reduction current at +0.85 V and oxygen evolution current at +1.75 V with cycle number to a limiting value after ~15 cycles.

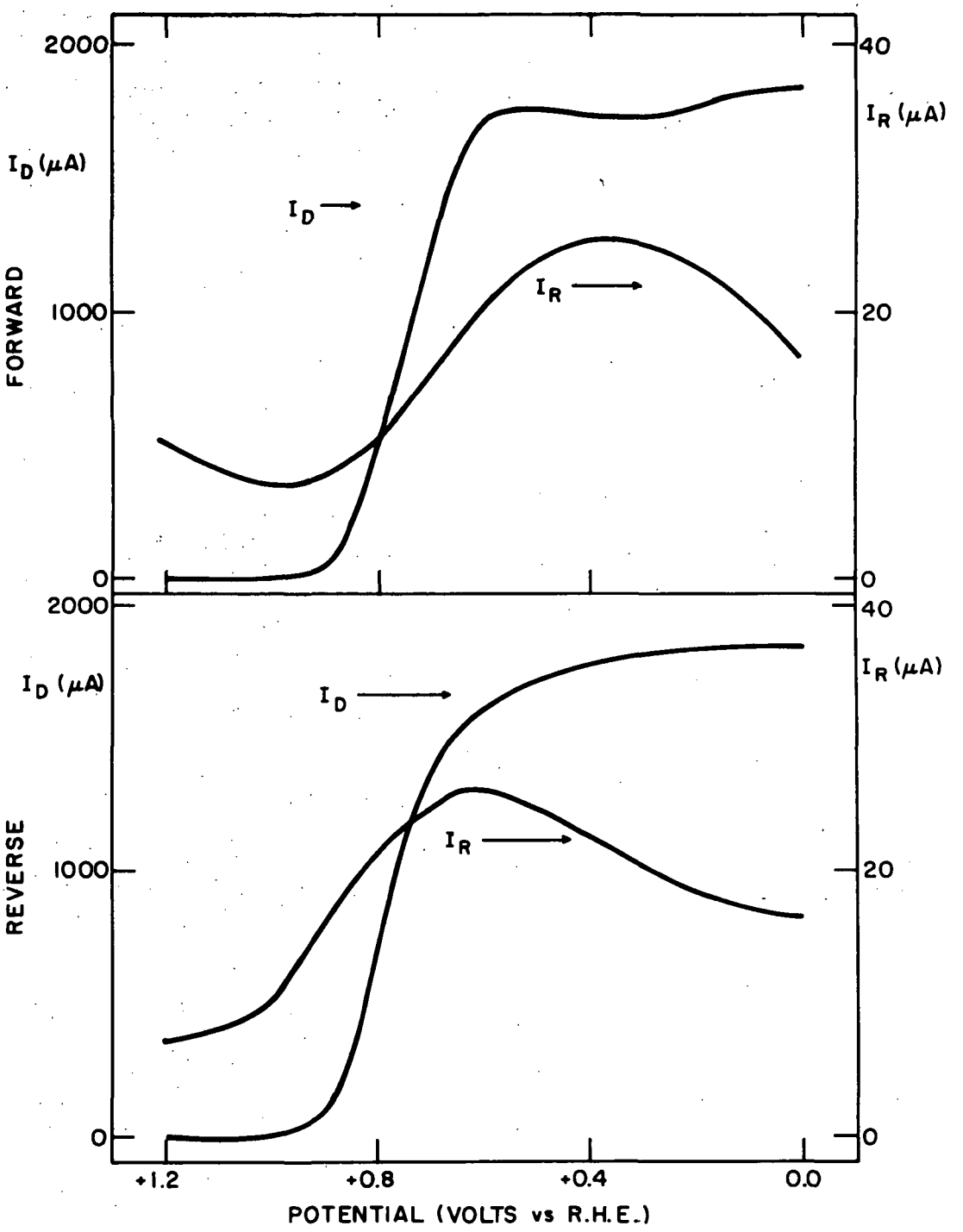

Fig. 65. Composite I_d/I_r versus E_d curves obtained by sweeping from +1.2 V to 0.0 V (forward), then 0.0 V to +1.2 V (reverse) at 100 mV/min on a smooth Pt disk electrode (66 rps) at 30 °C in O_2-saturated unpurified 0.1N KOH which has been saturated with CdO. E_r was held at +1.2 V

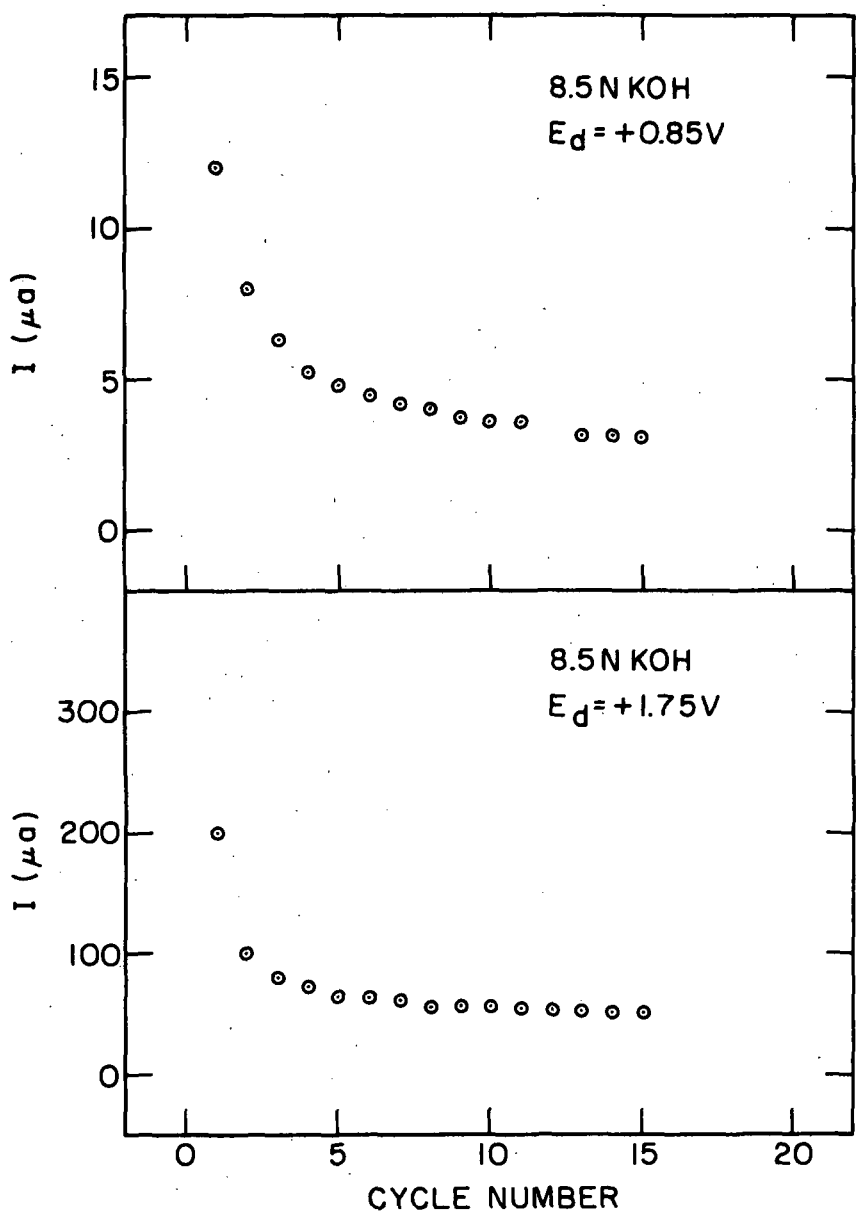

Fig. 66. Variation in I_d with cycle number for a smooth Pt disk electrode under Regime I (+1.75 V/10 min, +0.85 V/5 min) in purified 8.5N KOH at 30 °C

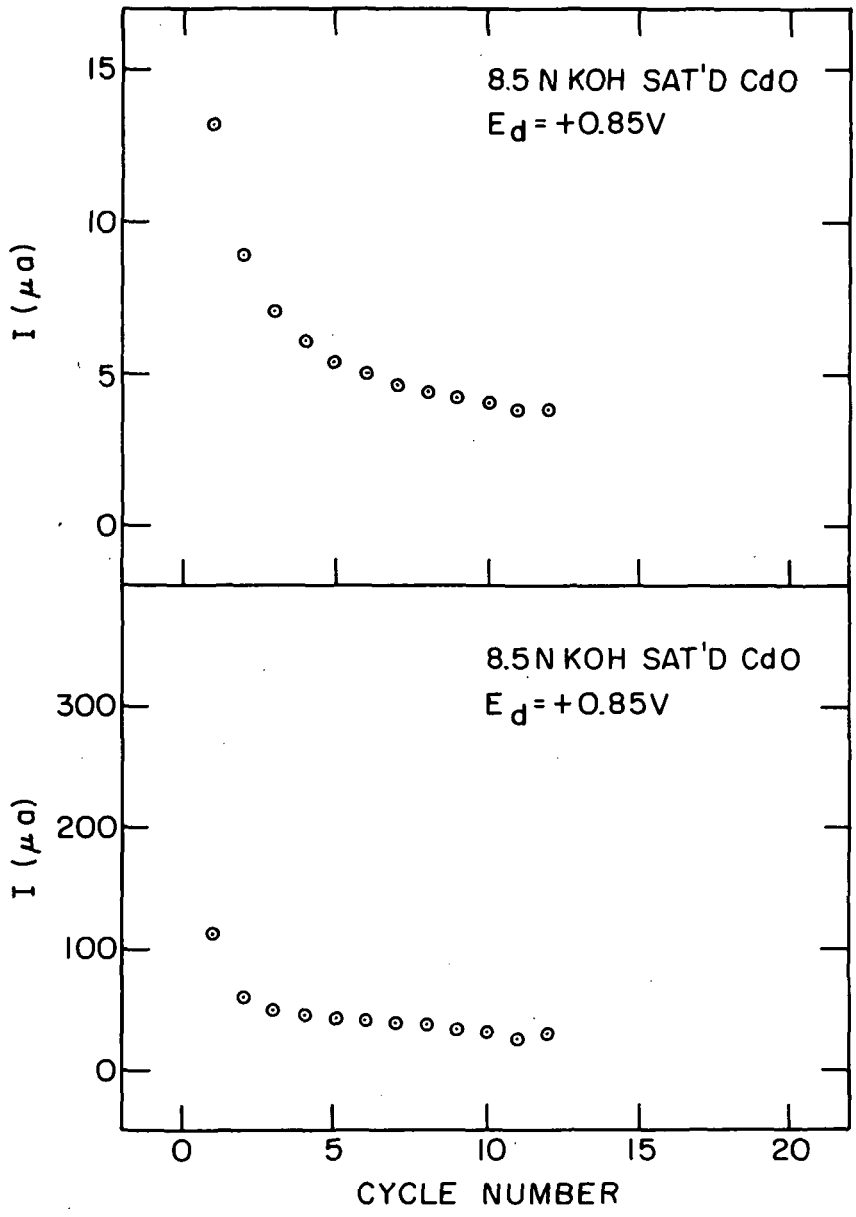

Fig. 67. Variation in I_d with cycle number for a smooth Pt disk electrode under Regime I (+1.75 V/10 min, +0.85 V/5 min) in purified 8.5N KOH saturated with CdO at 30 °C

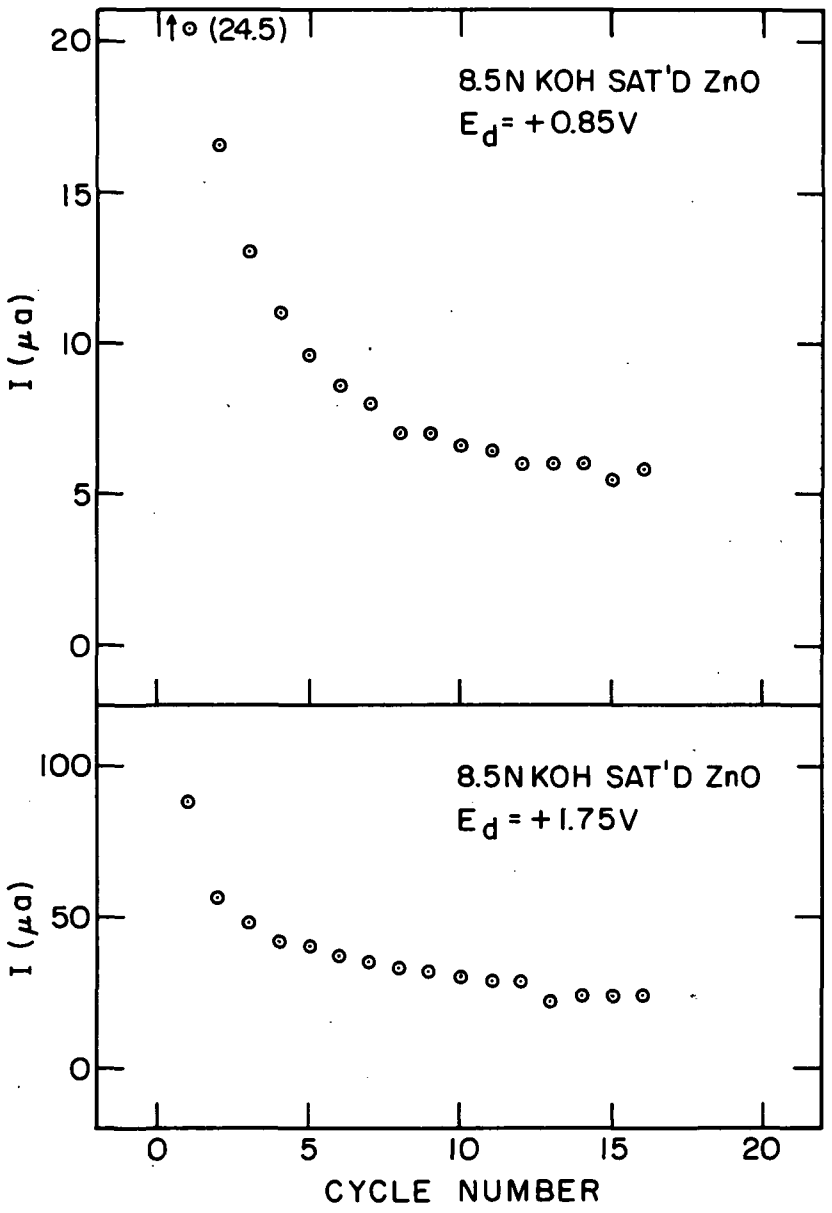

Fig. 68. Variation in I_d with cycle number for a smooth Pt disk electrode under Regime I (+1.75 V/10 min, +0.85 V/5 min) in purified 8.5N KOH saturated with ZnO at 30 °C

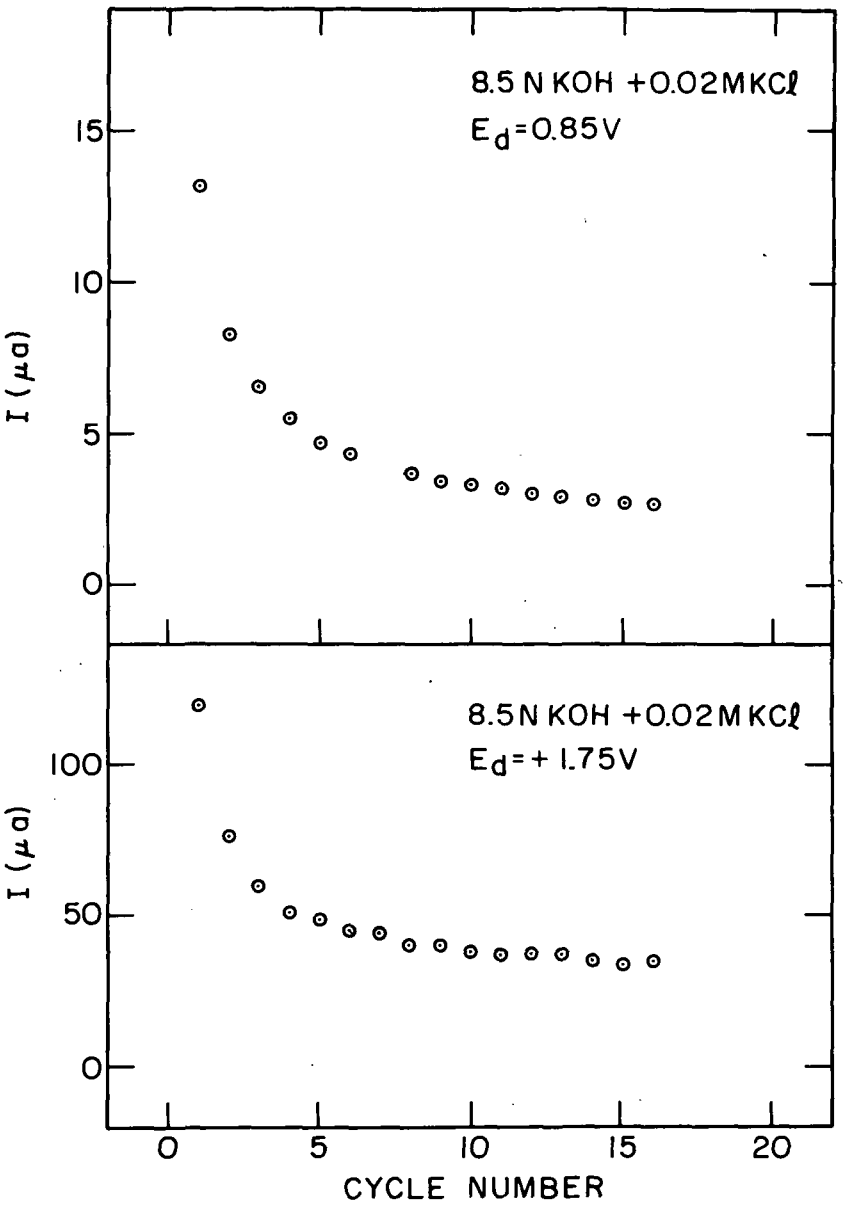

Fig. 69. Variation in I_d with cycle number for a smooth Pt disk electrode under Regime I (+1.75 V/10 min, +0.85 V/5 min) in purified 8.5N KOH +0.02M KCl at 30 °C

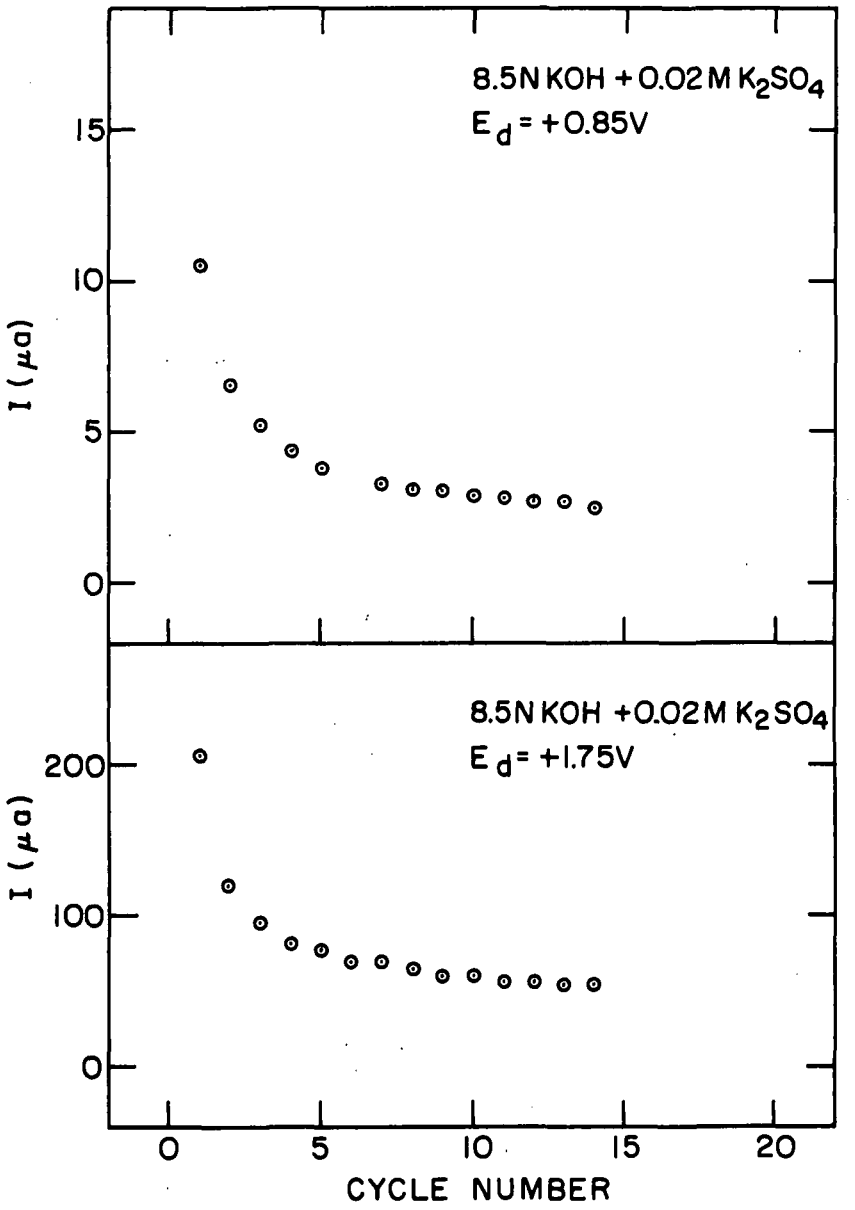

Fig. 70. Variation in I_d with cycle number for a smooth Pt disk electrode under Regime I (+1.75 V/10 min, +0.85 V/5 min) in purified 8.5N KOH +0.02M K_2SO_4 at 30 °C

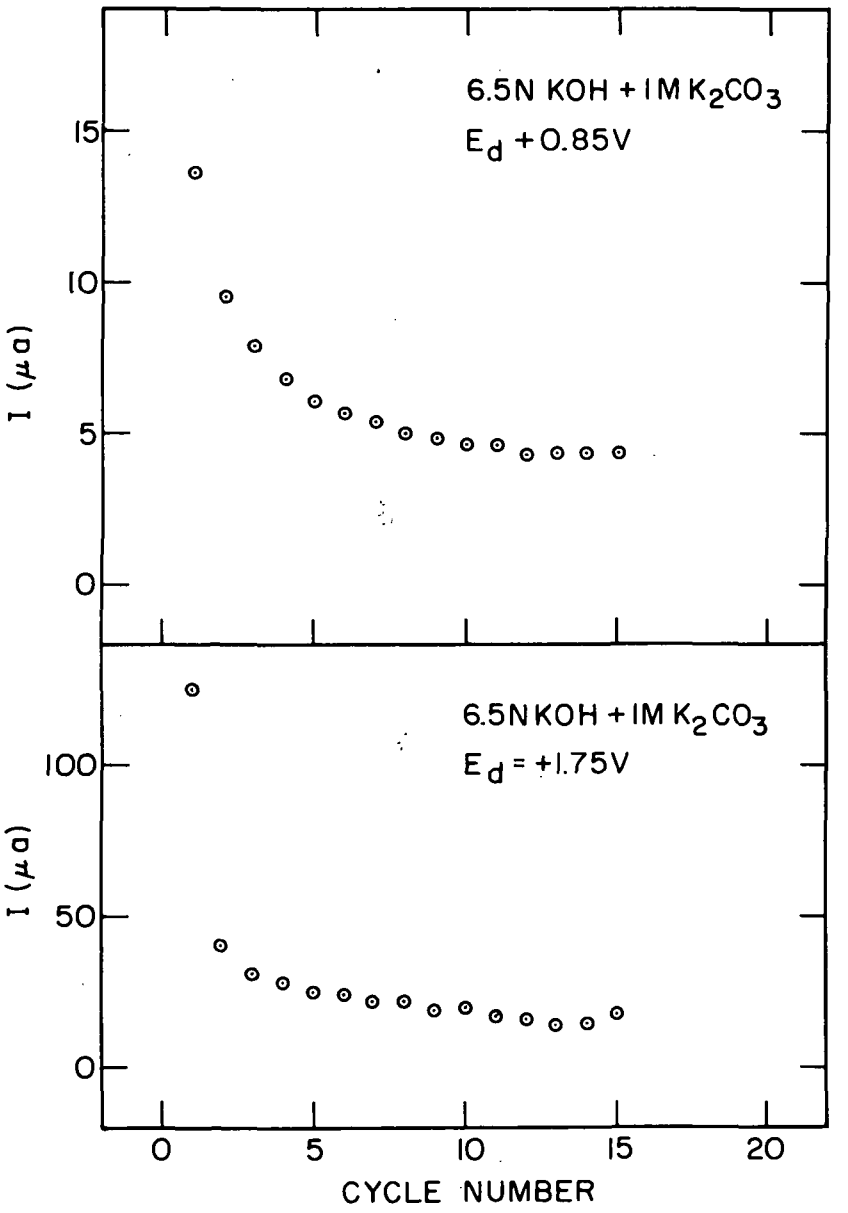

Fig. 71. Variation in I_d with cycle number for a smooth Pt disk electrode under Regime I (+1.75 V/10 min, +0.85 V/5 min) in purified 6.5N KOH + 1M K_2CO_3 at 30 °C

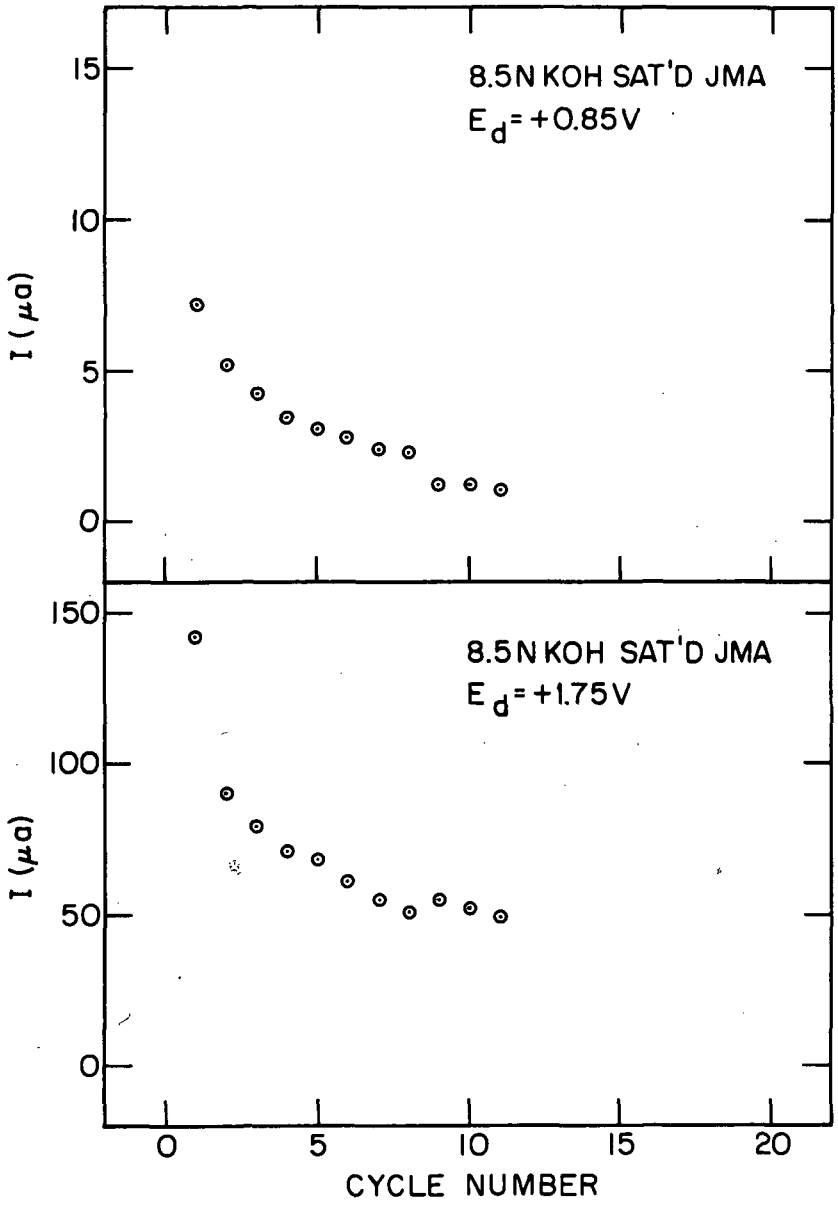

Fig. 72. Variation in I_d with cycle number for a smooth Pt disk electrode under Regime I (+1.75 V/10 min, +0.85 V/5 min) in purified 8.5N KOH saturated with Johns-Manville Fuel Cell Asbestos at 30 °C

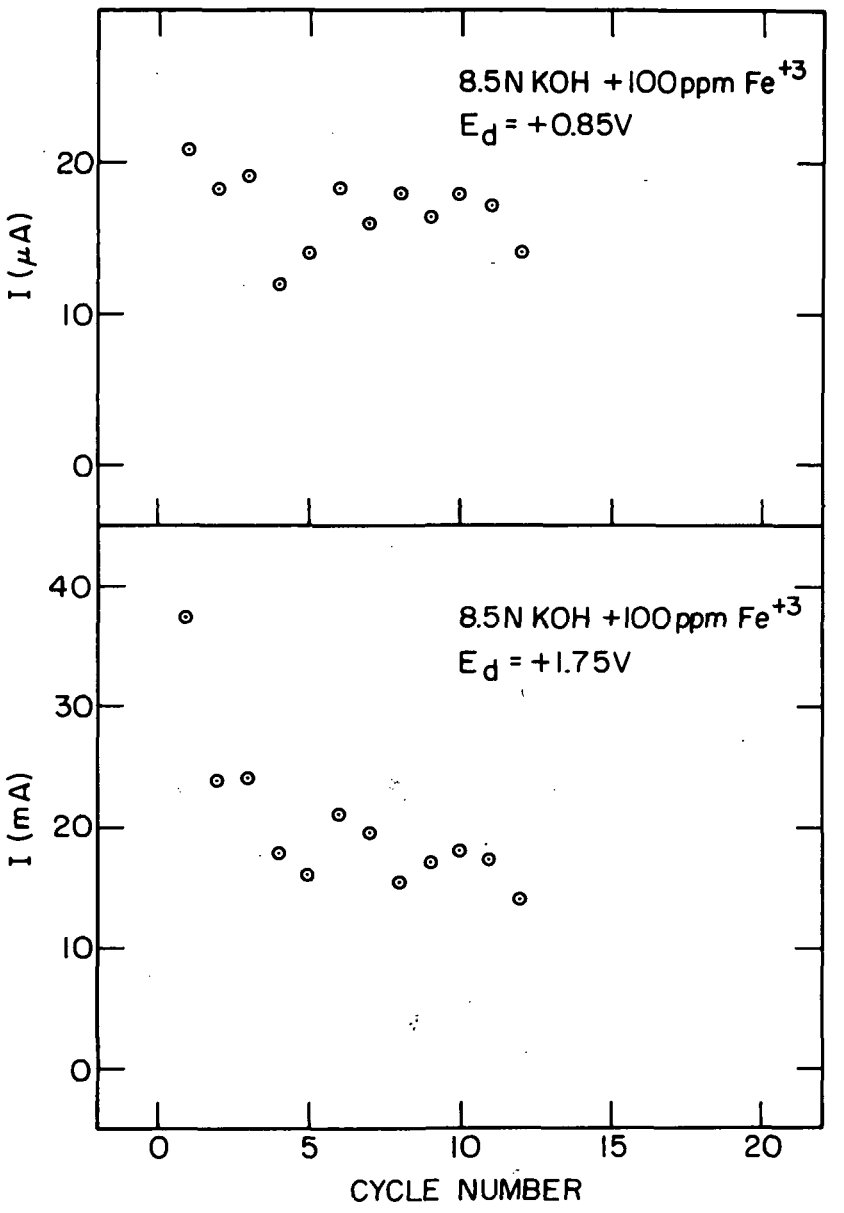

Fig. 73. Variation in I_d with cycle number for a smooth Pt disk electrode under Regime I (+1.75 V/10 min, +0.85 V/5 min) in purified 8.5N KOH containing 100 ppm Fe^{3+} at 30 °C

For example, there is a decrease in oxygen reduction current from 12 μA after cycle 1 in 8.5N KOH to 3.1 μA after 15 cycles or a 75% decrease. The oxygen evolution current at +1.75 V has also decreased by 75%. Table XLIX summarizes the observed changes in I_d.

Table XLIX. Percentage Change in Oxygen Reduction Current at +0.85 V and Oxygen Evolution Current at +1.75 V After ~ 15 Cycles Under Cycle Regime I at 30 °C for Various Electrolytes

Electrolyte	% Decrease in I_d, +0.85 V	% Decrease in I_d, +1.75 V
8.5N KOH	74	75
8.5N KOH saturated with CdO	77	64
8.5N KOH saturated with ZnO	76	73
8.5N KOH + 0.02M KCl	80	71
8.5N KOH + 0.02M K_2SO_4	76	76
6.5N KOH + 1M K_2CO_3	67	86
8.5N KOH saturated with "Fuel Cell Asbestos"	83	66
8.5N KOH + 100 ppm Fe^{3+}	6	63

In the 8.5N KOH containing 100 ppm Fe^{3+}, very little change in I_d at +0.85 V is observed. This current may not be due to oxygen reduction since the O_2 evolution currents observed at +1.75 V are an order of magnitude too high (1 mA - 4 mA versus 100 μA) when compared to the other electrolytes. Gradual reduction of Fe^{3+} to Fe^{2+} during the O_2 reduction experiments run previously in this electrolyte could yield these high currents due to Fe^{2+} oxidation at +1.75 V. Also Fe_3O_4 precipitated on the electrode may be a catalyst for O_2 reduction. Aside from 8.5N KOH containing 100 ppm Fe^{3+}, the nature of the electrolyte seems to have little bearing on the behavior of smooth Pt when cycled according to Regime I. There is no question, however, that cycling smooth Pt under this regime has a deleterious effect on both O_2 reduction and evolution.

It was suspected that this decrease in oxygen reduction activity was due to the buildup of a refractory anodic layer on cycling under Regime I. Although our studies in Section IV had failed to detect such a layer on smooth platinum electrodes, a difficult to reduce anodic layer could be readily observed on platinized platinum (see Fig. 23, Section IV). We then made some further studies of the influence of cycle Regime I on oxygen reduction and evolution using a platinized platinum disk electrode in 8.5N KOH.

Fig. 74 shows the behavior of I_d at E_d = +0.85 V and +1.75 V after cycling at +1.75 V/10 min, then +0.85 V/5 min. Fig. 75 shows the corresponding I_d/I_r values as a function of cycle number. The disk current at +0.85 V has decreased to 50% of its original value after 8 cycles, while I_d at +1.75 V has decreased to 16% of its original value of 2.2 mA. After the eighth cycle, the electrode was pulsed to +0.65 V for 30 sec, then returned to +0.85 V. The current after 5 min at +0.85 V had a value of 61 μA after this treatment, thus the O_2 reduction activity was restored by this method. In another experiment, the electrode was again cycled eight times under regime I, then pulsed to +0.45 V for 30 sec. This treatment also restored the electrode activity for O_2 reduction at +0.85 V.

The rejuvenation of O_2 reduction activity by imposing a potential sufficient to reduce the anodic surface layer is consistent with the degradation in performance being the result of the buildup of an anodic layer on cycling under regime I. The I_d/I_r values of Fig. 75 show that peroxide formation increased with cycling. However, it does not appear that the decrease in I_d is due solely to inefficient peroxide reduction as Fig. 76 demonstrates.

Fig. 76 replots I_d at +0.85 V from Fig. 75 and the disk current value, I_d^c, corrected for the peroxide detected at the ring, i.e.,

$$I_d^c = I_d + I_r/N$$

There is still a decrease in I_d^c at +0.85 V to 56% of its value after cycle one.

Fig. 77 shows the effects of using a modified cycle regime I, where we have inserted a 30-sec step to +0.60 V, viz.,

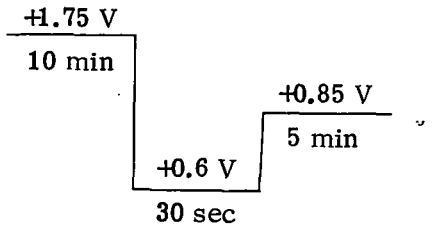

As Fig. 72 shows there is little or no change in I_d at +0.85 V under this cycling regime. There is an initial decrease in I_d at +1.75 V but it levels out at a value which is 80% of the original value.

Some caution should be exercised when extending these results, relating to a relatively small number of cycles, to more extended periods of cycling. The nature of the anodic layer formed after 250 cycles may be considerably different and thus its reduction or removal may require a different regeneration sequence due to different kinetic parameters.

D. Conclusions

Studies of oxygen reduction kinetics and path on preoxidized and prereduced smooth platinum electrodes using the rotating ring-disk electrode technique have been carried out in: (1) 8.5N KOH, (2) 0.1N KOH, (3) 8.5N KOH saturated with CdO, (4) 0.1N KOH saturated with CdO, (5) 8.5N KOH saturated with ZnO, (6) 6.5N KOH containing 1M K_2CO_3, (7) 8.5N KOH containing 0.02M KCl, (8) 8.5N KOH containing 0.02M K_2SO_4, (9) 8.5N KOH saturated with

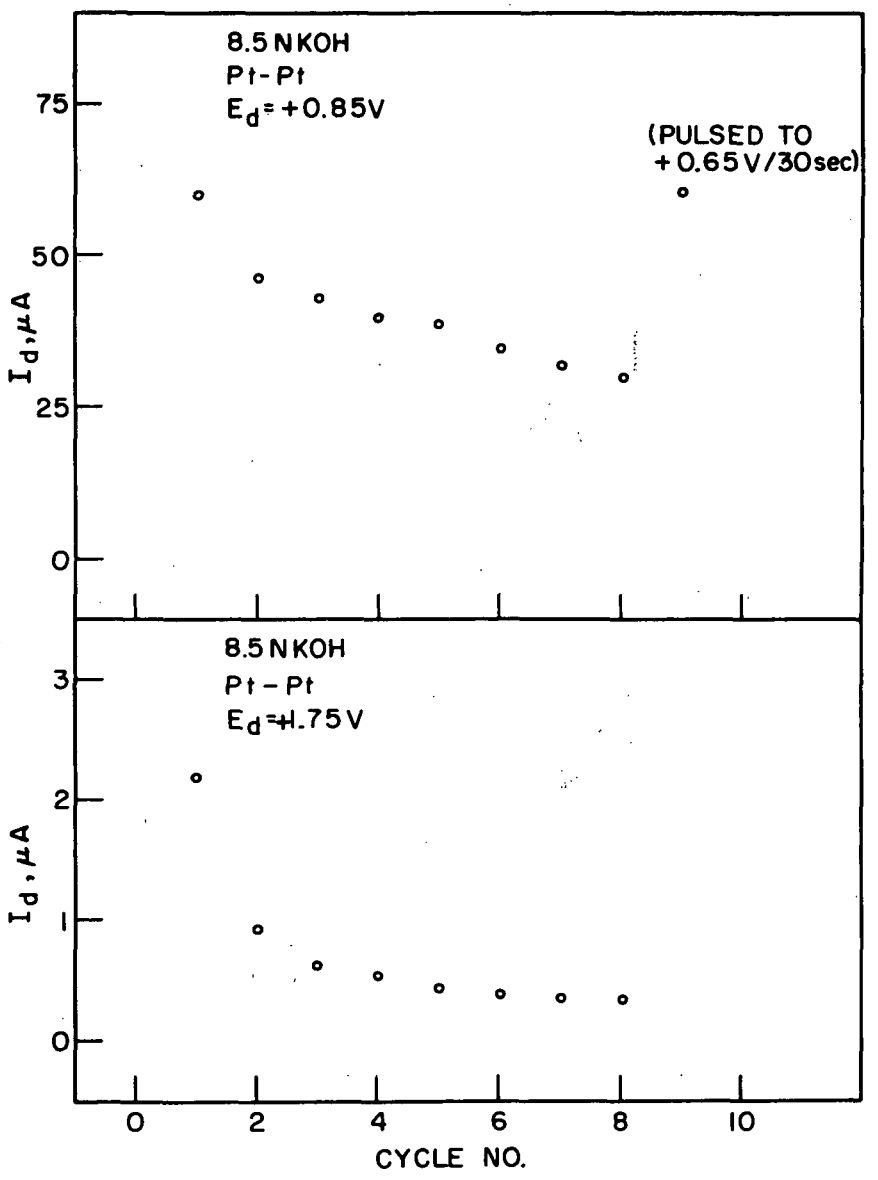

Fig. 74. Variation in I_d during cycling of a platinized platinum disk electrode under regime I (+1.75 V/10min, +0.85 V/5 min) in O_2-saturated 8.5N KOH at 30 °C

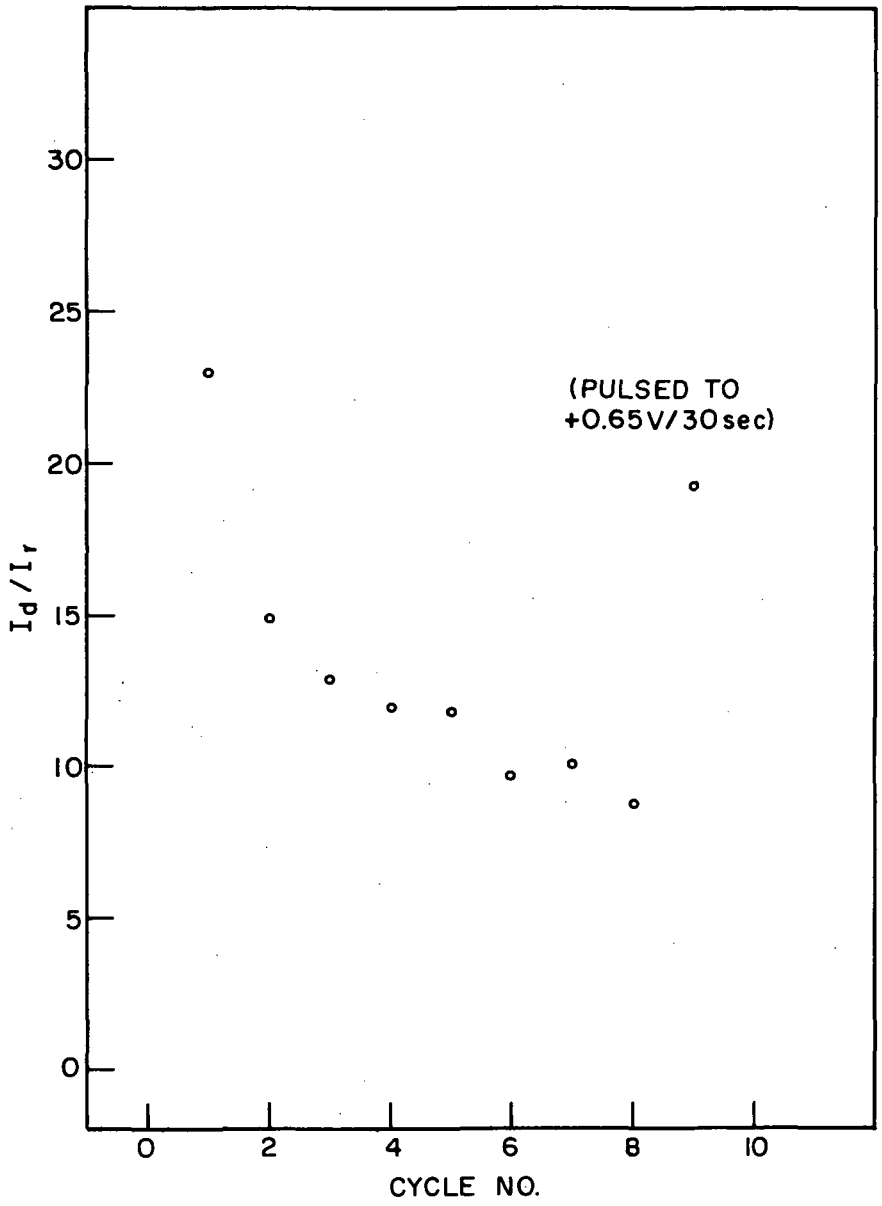

Fig. 75. Variation in I_d/I_r during cycling of a platinized platinum disk electrode under regime I (+1.75 V, 10 min, +0.85 V/5 min) in O_2-saturated 8.5N KOH at 30 °C

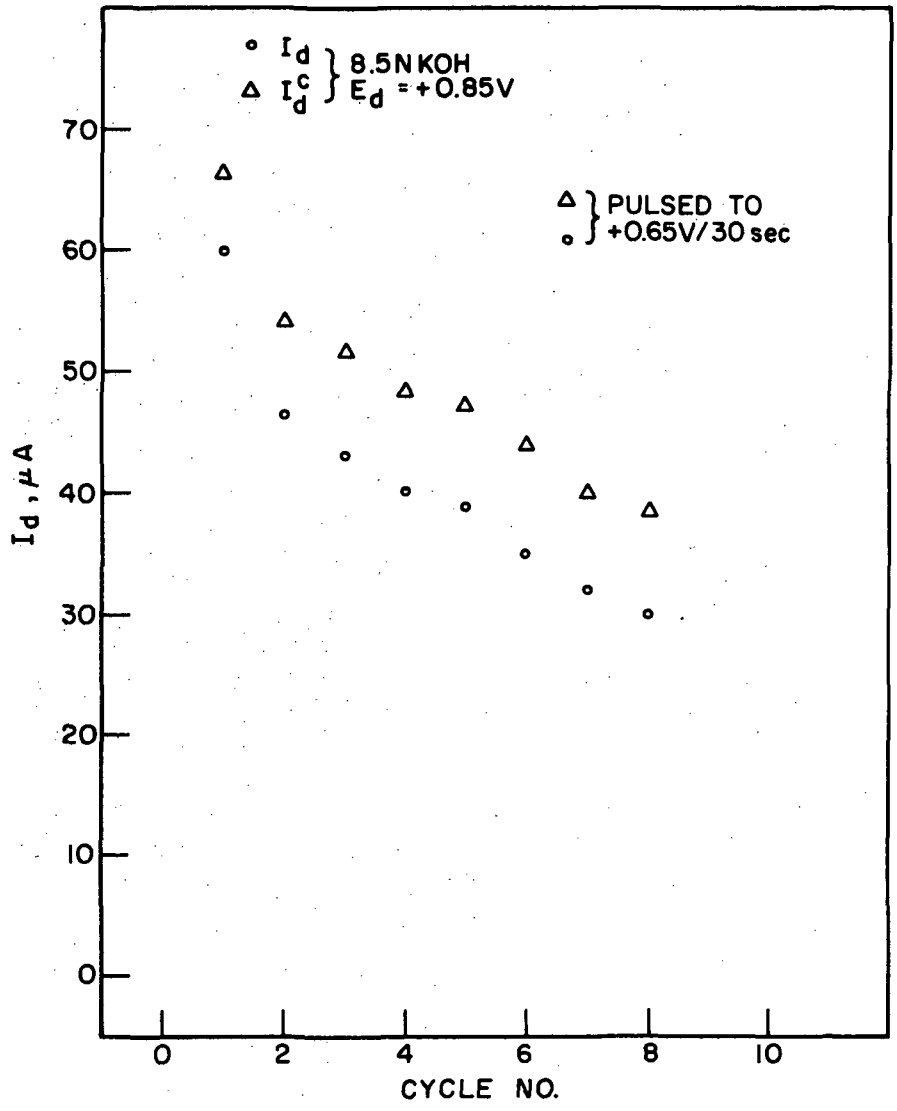

Fig. 76. Variation in I_d and I_d^c (the current corrected for H_2O_2 production, $I_d^c = I_d + I_r/N$) during cycling of a platinized platinum-disk electrode under regime I (+1.75 V/10 min, +0.85 V/5 min) in O_2-saturated 8.5N KOH at 30 °C

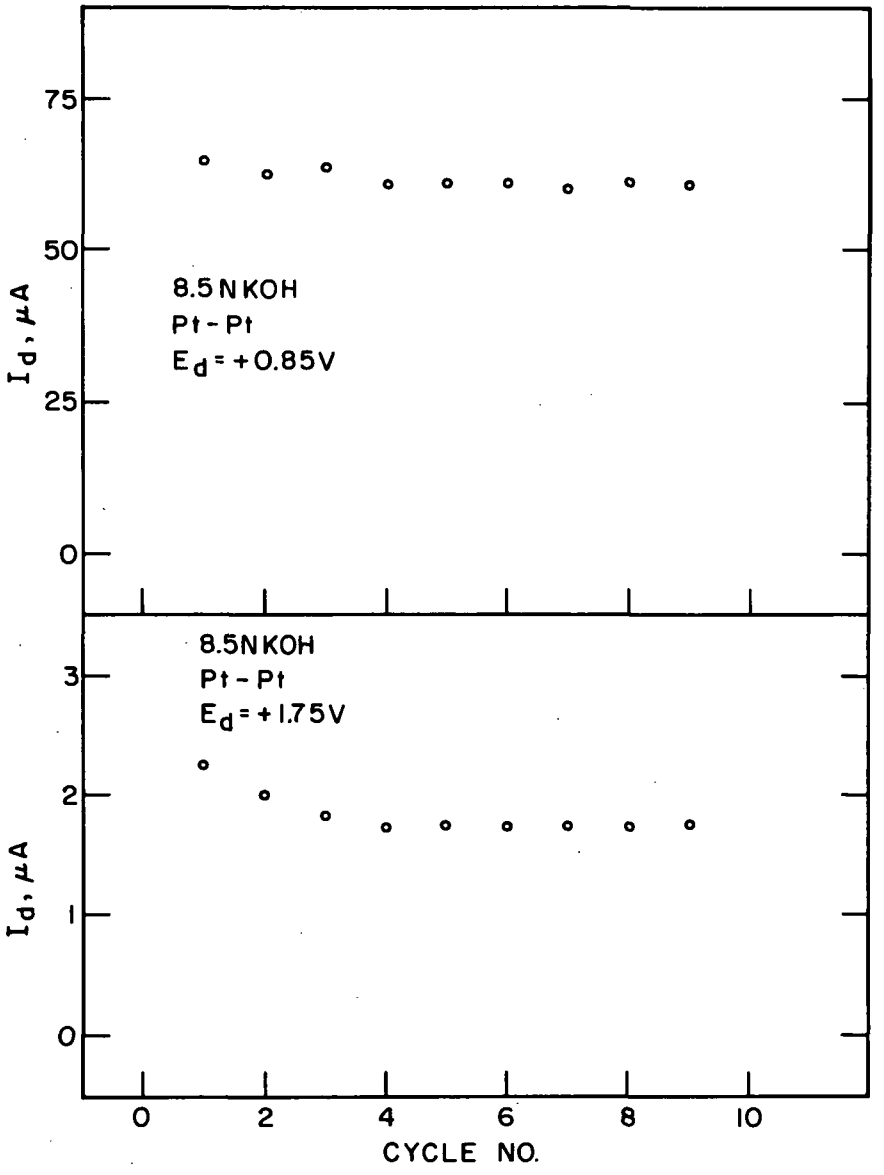

Fig. 77. Variation in I_d during cycling of a platinized platinum disk electrode under a modified cycle regime I wherein a 30 sec pulse to +0.65 V is inserted between the +1.75 V and +0.85 V protions of the cycle

Johns-Manville Fuel Cell Asbestos, and (10) 8.5N KOH containing 100 ppm Fe^{3+}.

The reduction of oxygen on platinum electrodes in the pure KOH electrolytes appears to proceed mainly via hydrogen peroxide as a reactive intermediate. At potentials less than +0.8 V, the observation of hydrogen peroxide is related to the impurity content of the electrolyte. The effect of impurities appears to be on the rate of reduction of H_2O_2. Above +0.8 V, even under conditions of high purity and/or high surface area platinized platinum electrodes, H_2O_2 can be observed, presumably due to insufficient overpotential for further H_2O_2 reduction. No conclusive evidence for the presence of a parallel path of oxygen reduction, i.e., the direct four-electron reduction to water, has been obtained, although the presence of the heterogeneous catalytic decomposition of H_2O_2 may be inferred.

The influence of various ionic additives is reflected primarily in terms of hydrogen peroxide accumulation, i.e., peroxide decomposition kinetics, with no mechanistic changes apparent. Cadmium species tend to inhibit H_2O_2 accumulation while $Zn(OH)_4^{2-}$ and Fe^{3+} apparently lead to H_2O_2 accumulation in 8.5N KOH. Anionic species such as chloride and sulfate enhance H_2O_2 decomposition whereas carbonate and impurities leached from Johns-Manville Fuel Cell Asbestos tend to inhibit H_2O_2 decomposition. It was observed that soluble cadmiate species do not intrinsically poison oxygen reduction on smooth or platinized platinum. Thus cadmium poisoning of air cathodes in metal-air cells appears to be related to precipitation of insoluble cadmium species.

It has been shown that cycling platinum electrodes under cycle regime I, which is typical of rechargeable oxygen electrodes, leads to marked decreases in oxygen reduction and evolution activity. Since it has been pointed out that preoxidized electrodes have lower O_2 reduction activity than prereduced electrodes, the effects of anodic pretreatment on O_2 reduction are not surprising. However, it is possible by a relatively short time cathodic pulse to restore or maintain oxygen electrode activity. Further work is still needed on the practical implications of this technique over extended periods of cycling.

VI. OXYGEN EVOLUTION KINETIC STUDIES

A. Background

As Milner pointed out, there are many possible reaction paths for the anodic evolution of oxygen.[56] Tafel parameters alone cannot unambiguously identify the complete mechanism. There seems to be general agreement that the discharge of OH^- (in alkaline solution) to form radicals on the surface is the most likely rate limiting step.[17] The usual anodic Tafel slope of RT/F would be consistent with a rate limiting electron transfer step.

However, in a recent paper, Damjanovic, Dey, and Bockris reported a Tafel slope of RT/F at low current density but also found a Tafel slope of 2RT/F at higher current densities for oxygen evolution in 1N KOH.[54] This change in slope was interpreted as due to a mechanism change. At low anodic overvoltages a rate controlling chemical step was postulated to follow a fast OH^- discharge. At high anodic η, the mechanism changes and, for the same path, the primary discharge of OH^- becomes rate-determining.

In this section, we present a series of measurements of the kinetics of the anodic evolution of oxygen on smooth platinum and platinized platinum, our primary concern being the effect of ionic additions rather than a mechanistic effort.

B. Experimental

Current-potential curves were obtained potentiostatically on rotating disk electrodes at 60 rps. The primary purpose of electrode rotation was to prevent oxygen bubbles from adhering to the electrode surface. Surface areas of both smooth and platinized electrodes were measured by cathodic hydrogen deposition. All measurements were made in O_2-saturated electrolyte at 30 °C.

C. Results and Discussion

Our original intention was to compare O_2 evolution on prereduced and preoxidized electrodes. However, initial experiments showed that steady-state reproducible current values were not obtained on prereduced electrodes even at times of up to 1 hr. We found that steady-state reproducible current values could be obtained after prolonged (30 min) anodic pretreatment at +2.00 V, then stepping cathodically in 25 mV or 50 mV increments.

Fig. 78 shows a typical Tafel plot on smooth Pt in purified 8.5N KOH at 30 °C. Below +1.8 V, the Tafel plot begins to deviate and the presence of a mass transfer controlled process

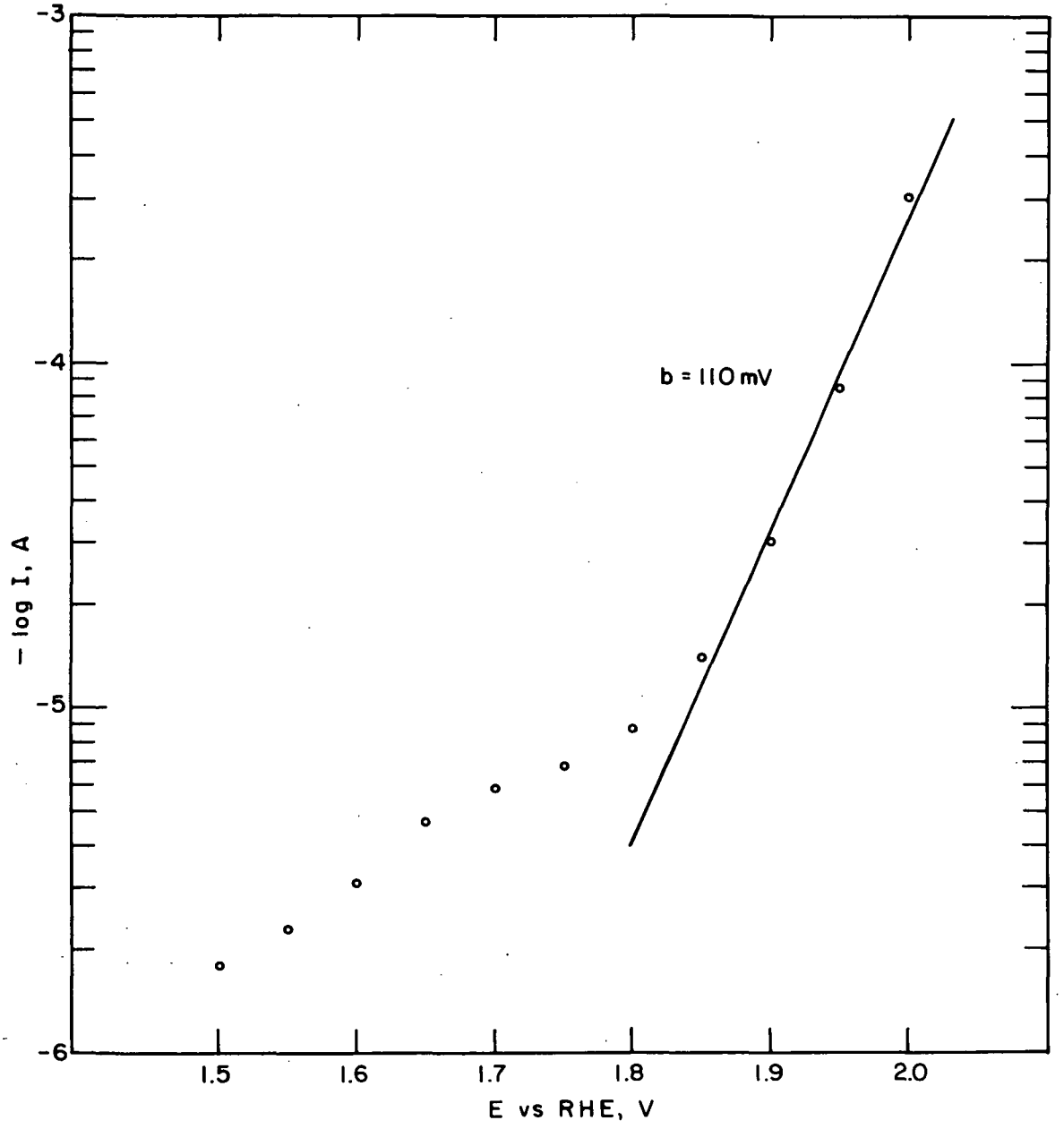

Fig. 78. Tafel plot for oxygen evolution on a smooth platinum disk electrode in purified 8.5N KOH at 30 °C (N = 60 rps)

could be confirmed by the proportionality between current and $\omega^{1/2}$. A likely candidate for this oxidizable species, which appears to be present at a concentration of $\sim 10^{-6}$M, would be hydrogen peroxide. Therefore, we have restricted our measurement to the region of +1.8 - 2.0 V.

Table L summarizes the Tafel data obtained on a smooth Pt disk electrode (geometric area = 0.2 cm, real area = 0.7 cm) in the nine electrolytes studied. The measured exchange current varied from $2.0 \pm 0.4 \times 10^{-12}$ A/cm^2 for pure 8.5N KOH to $1.3 \pm 0.5 \times 10^{-10}$ A/cm^2 for 8.5N KOH saturated with Johns-Manville Fuel Cell Asbestos. The Tafel slopes are somewhat less than a value of 2RT/F (120 mV) ranging from 84 ± 3 mV for 8.5N KOH to 114 ± 3 mV for 6.5N KOH/1M K_2CO_3. Measurements could not be made in 8.5N KOH saturated with ZnO because of a diffusion-controlled anodic limiting current of the order of 10^{-3} A/cm^2. The value of $5 \pm 1 \times 10^{-11}$ A/cm^2 for I^0 in 0.1N KOH compares well with that of 1×10^{-11} A/cm^2 reported by Damjanovic, Dey, and Bockris, who also reported a Tafel slope of 110 mV ± 10 compared to our value of 112 ± 4 mV. In 8.5N KOH, our exchange current density is a factor of 25 smaller than in 0.1N KOH, and a lower Tafel slope is observed (84 ± 1 mV).

Table L. Summary of Tafel Data for O_2 Evolution on Smooth Pt in Various Electrolytes

	I^0 A/cm^2) $\times 10^{11}$	b, mV	No. of Determinations
8.5N KOH	0.2 ± 0.04	84 ± 1	4
8.5N KOH/CdO	3 ± 2	93 ± 3	2
8.5N KOH/KCl	0.7 ± 0.2	92 ± 2	2
8.5N KOH/K_2SO_4	2 ± 1	88 ± 3	3
6.5N KOH/K_2CO_3	4 ± 2	114 ± 3	3
8.5N KOH/JMA	13 ± 3	113 ± 4	3
8.5N KOH/Fe^{3+}	1.8 ± 0.4	98 ± 2	2
0.1N KOH	5 ± 1	112 ± 2	4
0.1N KOH/CdO	3 ± 1	110 ± 3	4

Various additions to the purified 8.5N KOH electrolyte do not appear to cause any distinct mechanism change since the Tafel slopes show no significant variation. The somewhat higher I^0 value in 8.5N KOH saturated with Johns-Manville Fuel Cell Asbestos may very well be attributed to oxidation of impurities present in the asbestos. This same reason may very well apply to the lower exchange currents observed in the pure 8.5N KOH when compared to pure 8.5N KOH containing the various additives.

On platinized platinum, we obtained the data shown in Table LI. I^0 values are given in terms of real surface areas and compare well with those determined for smooth platinum.

D. Conclusions

There does not appear to be any significant effects of the various ionic additives studied on O_2 evolution in 8.5N KOH. I° values are on the order of 10^{-11} A/cm^2 with Tafel slopes of approximately 100 mV (~2 RT/F).

Table LI. Tafel Parameters for Oxygen Evolution on Platinized Platinum in 8.5N KOH Containing Various Additives at 30 °C

Electrolyte	I^0 (A/cm^2) $\times 10^{11}$	b, mV	No. of Determinations
8.5N KOH	3 ± 1	100 ± 2	4
8.5N KOH/ZnO	20	120	1
8.5N KOH/K_2SO_4	10 ± 10	106 ± 5	3

VII. PLATINUM DISSOLUTION STUDIES

A. Background

The anodic dissolution of platinum is of concern in the operation of rechargeable oxygen electrodes since loss of platinum can: (1) lead to decreases in electrode activity, and (2) result in interelectrode shorts due to the growth of platinum dendrites in the separator. Furthermore, in zinc-air cells, platinum dissolution is extremely deleterious since it decreases the hydrogen overvoltage on the zinc anode.[5] One may expect such dissolution to occur at rechargeable O_2 electrodes, because of the high anodic potentials observed during the charging process. Although the corrosion of platinum in chloride solution has long been recognized, its dissolution in non-chloride containing electrolytes has been little studied.

Vetter and Berndt originally reported the corrosion rate of smooth platinum in 0.5M H_2SO_4 at 25 °C to be smaller than 0.2 μ A/cm^2.[57] Grunenberg reported that platinum contamination of a gold electrode gave rise to hydrogen oxidation activity not observed on a pure gold surface.[58] Platinum contamination of the gold electrode was caused either by dissolution of the platinum counterelectrode or by the previous use of a platinum electrode in the same system (1N H_2SO_4). Brummer also reported on platinum contamination of gold working electrodes by the use of platinum counterelectrodes in 1N $HClO_4$.[59] Malachesky, et al., in a study of the preelectrolysis of caustic electrolytes, found that the normal preelectrolysis procedure wherein platinum electrodes can reach oxygen evolution potentials resulted in platinum contamination of 2N KOH.[60] The reduction of oxygen on oxidized cadmium and the displacement of the hydrogen evolution potential on gold were used to detect traces of Pt. Giner reported similar results for 1N H_2SO_4 and also reported that platinum dissolution occurred at potentials as low as +0.8 - +0.9 V.[61] Biegler reported that, in some instances, dissolved platinum could be detected after smooth platinum electrodes had been extensively cycled in 1N H_2SO_4 under conditions which led to surface roughening or smoothing.[31]

Chemadanov, et al., used a radiochemical method to study the dissolution of platinum in acidic electrolytes.[62] Smooth platinum foils were neutron-irradiated, thus allowing determination of very small amounts of dissolved platinum by γ-ray scintillation counting. Studies were carried out in normal solutions of sulfuric, perchloric, and nitric acids. The rate of platinum dissolution in 1N H_2SO_4 was independent of potential in the region of +1.2 to +1.8 V and was on

the order of 10^{-8} - 10^{-9} A/cm^2. At potentials greater than +1.8 V, the dissolution process increased with increasing potential. A limiting dissolution current could be observed between +2.2 and +2.8 V, followed by further dissolution. Platinum corrosion was also found if reduction of the surface oxygen layer was allowed to occur.

Johnson, Napp, and Bruckenstein used the RRDE to collect soluble electroactive species formed during potential cycling of smooth platinum electrodes in 2N H_2SO_4 and 0.1N HCl O_4.[63] It was proposed that cathodic reduction of anodically-formed PtO_2 led to soluble Pt(II) via the reaction:

$$PtO_2 + 4H^+ + 2e \rightarrow Pt(II) + 2\ H_2O$$

Both oxidation and reduction of Pt(II) could be observed. As the disk electrode was scanned anodically, at +0.8 V versus SCE ($\sim$ + 1.0 V versus RHE), an unidentifiable reducible species was formed. It was deduced that this species underwent a first-order homogeneous decomposition reaction.

We have used a variety of techniques, including the RRDE, in an effort to study the dissolution of smooth platinum electrodes in 8.5N KOH at 30°C.

B. Experimental

Two techniques have been used here for the determination of platinum: (1) the catalysis of the hydrogen oxidation reaction on gold by trace amounts of platinum, and (2) the spectrophotometric determination of platinum using the stannous chloride method.

The detection of platinum in solution using a gold detecting electrode relies on the lack of catalytic activity for hydrogen oxidation on pure gold as Grunenberg demonstrated.[58] It was also shown that the decrease in the hydrogen evolution potential could be used for detection of dissolved platinum in alkaline solution.[60] A number of different experimental arrangements have been used in this work, based on the hydrogen oxidation reaction. These will be described, as needed, in the next section.

The spectrophotometric method is based on the formation of a colored complex between Pt(IV) and stannous chloride in acidic solutions as described in detail by Sandell.[64] The procedure, as typically used by us for the determination of platinum in 8.5N KOH, first involves neutralization with glacial acetic acid (acetic acid is used since the solubility of potassium acetate is much greater than potassium chloride, sulfate, or perchlorate). After neutralization, bromine water is added to oxidize any Pt(II) to Pt(IV) and excess bromine removed by heating. Excess stannous chloride in 3.5M HCl is then added to form the colored complex. Solutions were run in 5 cm cells versus a similarly treated unused 8.5N KOH sample on a Perkin-Elmer Model 450 UV-Vs-NIR Spectrophotometer. Fig. 79 shows a calibration curve of absorbance versus Pt(IV) concentration at a wavelength of 394 mμ. The plot is linear up to at least 10 μM, although above 20 μM some deviation from linearity has been observed. Based on a minimum decrease in transmittance of 1% (i.e., T = 99.0%), our limit of detection is 0.2 μM [Pt(IV)]. However, our practical detection limit using a dilution factor of 12.5 is 2.5 μM.

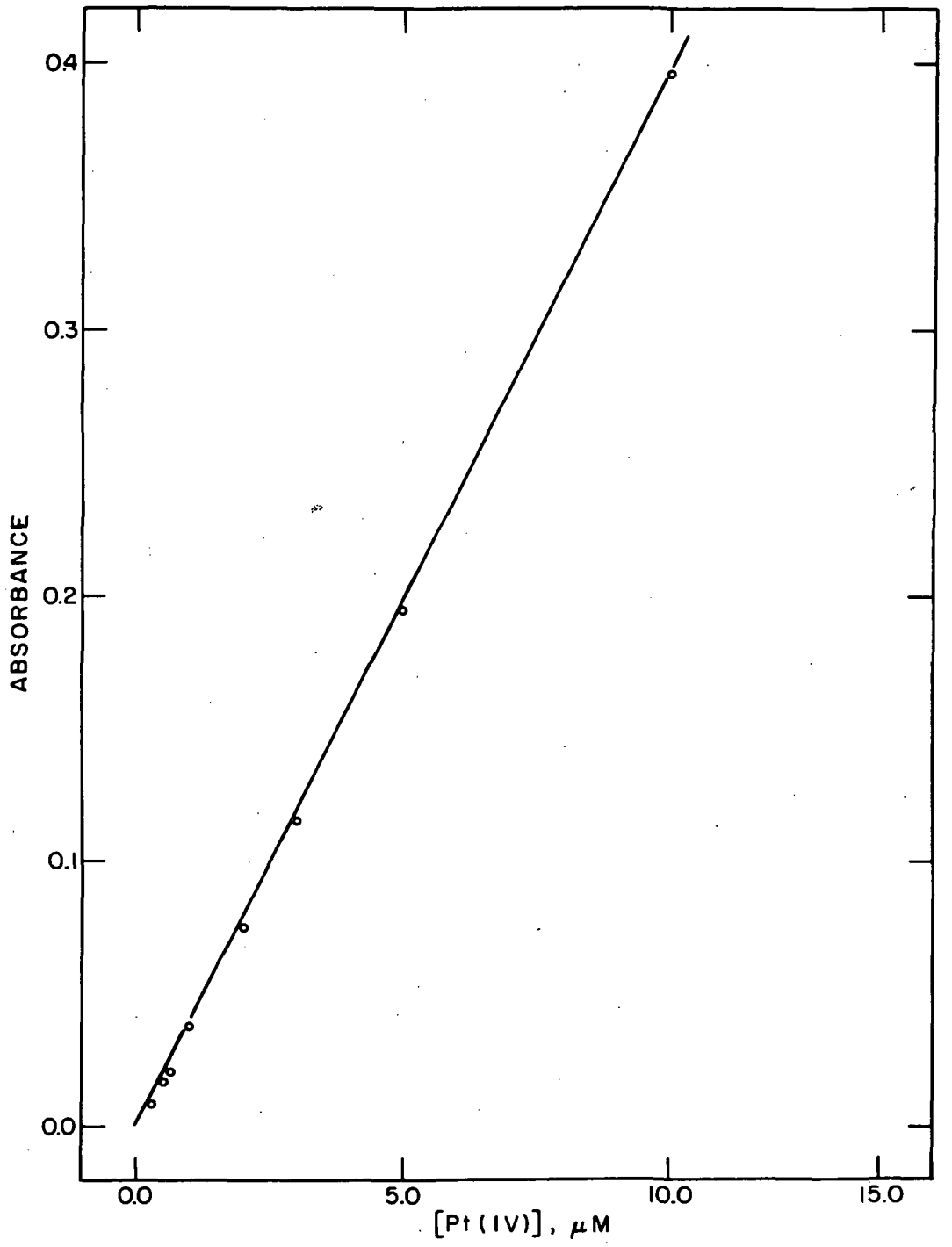

Fig. 79. Calibration curve of optical absorbance at 394 mμ versus concentration of Pt (IV) using the Stannous chloride method

C. Results and Discussion

Our initial experiments on platinum dissolution involved the use of the RRDE in 8.5N KOH. For these experiments, we used a smooth platinum disk with a gold ring. Fig. 80 shows the I_r versus E_d curves observed in H_2-saturated 8.5N KOH, as the disk is swept from -0.25 V to +1.10 V versus RHE at a sweep rate of 250 mV/min. The gold ring was held at +0.30 V.

At $E_d \sim +0.6$ V, there is an increase in the anodic current to a limiting value. As the sweep is reversed, the current decreases at $E_d \sim +0.7$ V to its original level. Our initial interpretation of these results was that the increase in ring current was due to dissolution of platinum as the disk was made more anodic. Platinum which had dissolved could be deposited in the Au ring, therefore increasing the H_2-oxidation current at the ring. However, the reversibility of this behavior seemed contrary to this interpretation. It was then suspected that the observed increases in the ring current were due to a shielding effect.

The shielding efficiency, S, of an RRDE is the ratio of the ring current observed when the disk electrode is at a potential corresponding to the limiting current for the ring electrode reaction to the ring current observed when the disk is at open circuit. The shielding efficiency is a function of electrode geometry only and is given by:

$$S = (1 - N/\beta^{2/3})$$

where

$$\beta = (R_3/R_1)^3 - (R_2/R_1)^3$$

For our electrode N = 0.41 and β =1.504, giving a shielding efficiency of 0.71. From the I_r values in Fig. 80, we calculate the ratio of the ring currents to be 2.70/3.45 or 0.78. This seems to support the hypothesis of a shielding effect in this case. The observed ring currents in Fig. 80 are consistent then, with a Pt-contaminated Au ring which shows a simple shielding effect as E_d becomes greater than +0.6 V because of the well-known decrease in hydrogen oxidation limiting currents at these potentials. The reversibility observed here would also be consistent with this effect.

Further experiments conducted with the Au-ring, Pt-disk electrode revealed that it was not feasible to use this configuration to measure Pt dissolution via the Pt-catalyzed H_2-oxidation on Au. This was a result of the difficulty in preventing Pt-contamination of the Au ring during polishing procedures. Polishing was necessary in order to prepare an uncontaminated (by Pt) gold surface. Other arrangements were then tried.

The first arrangement used consisted of a "sandwich" configuration. A perforated Au foil "sandwiched" between a smooth Pt foil working electrode and an Au counterelectrode served as the detection electrode and was kept at +0.1 V. While this configuration did show some promise, preparing an uncontaminated detection electrode was difficult since the three-electrode package was an integral system and cleaning via aqua regia led to Pt-contamination.

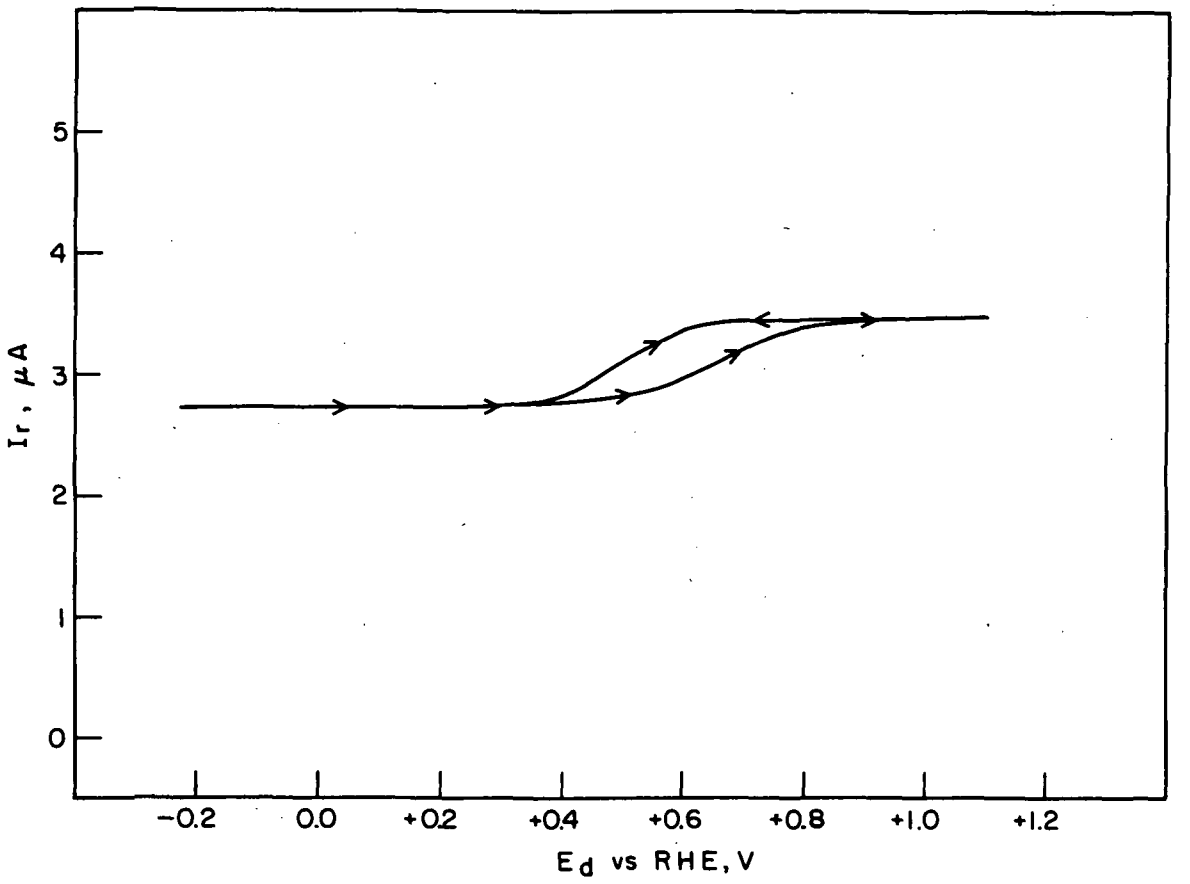

Fig. 80. Ring current-disk potential curves for a gold ring-platinum disk electrode at 30 rps in H_2-saturated 8.5N KOH at 30 °C (dE/dt = 250 mV/min), E_r = +0.2 V

An experimental cell design which circumvented this difficulty is depicted in Fig. 81. A gold electrode is in close proximity to a smooth Pt foil electrode and can be removed from this cell and transferred to another vessel containing H_2SO_4 where it can be tested for its H_2 oxidation activity. Initially, a gold mesh electrode was used but it failed to withstand the aqua regia treatment necessary to remove platinum contamination. A gold wire shaped into a flat coil was then used as the detection electrode. The use of the irregular geometry of the coiled electrode led to irreproducible behavior when running I-E curves in the H_2-saturated 1N H_2SO_4. To alleviate this problem, we then used a rotating gold disk electrode (Beckmann) which was rotated at 10 rps in order to obtain reproducible mass transport conditions.

With this arrangement, consistent, reproducible results were not obtained, although there were definite indications of platinum dissolution. It was then decided to investigate the platinum contamination of an Au electrode as a technique for analysis of solutions in which large area smooth Pt foils were anodized in order to improve the detection limit of the spectrophotometric method.

It was assumed that there would be a relationship between the observed H_2-oxidation limiting current at a Pt-contaminated Au disk electrode and the amount of Pt deposited on the Au disk electrode. A 1N H_2SO_4 solution was prepared containing 10^{-7} M Pt(IV). Pt was deposited at 0.0 V on an Au disk electrode for various times in this electrolyte, then transferred to another cell where I-E curves were recorded in H_2-saturated 1N H_2SO_4. However, there was no correlation between the observed H_2-limiting currents and the time of deposition. This leads us to suspect that the catalytic activity of the platinum deposit on gold electrode is strongly dependent on experimental conditions, especially the surface condition of the Au substrate. Thus, while the use of this technique originally appeared to be the ideal approach to the problem, there appears to be extensive complications which could not be studied in detail and eliminated in the available time. It was then decided to focus our efforts on the better developed spectrophotometric technique used in conjunction with dissolution experiments on large area smooth Pt foil electrodes.

Dissolution experiments were carried out on large area, smooth platinum foil electrodes in quartz H-type cells which allowed electrode area to solution volume ratios of 1 to 2. A sintered quartz frit (15-40 μ) served to separate the Au counterelectrode compartment from the working electrode compartment. A modified dynamic hydrogen electrode was used wherein the usual DHE platinum counterelectrode which evolves oxygen is replaced by gold. The DHE reference electrode was placed in the counterelectrode compartment to minimize its contribution to the observed soluble platinum in the working electrode compartment. Several spectrophotometric analyses for dissolved platinum in the counterelectrode-reference electrode compartment did not detect platinum under a wide variety of experimental conditions.

Experiments were performed on the dissolution of smooth Pt foils anodized at +0.85 V, +1.20 V, and +1.75 V versus RHE for 65 hr periods. In general, detectable amounts of platinum were found in the working electrode compartment at all potentials, on the order of 2.5 to 6.0 μM. This would correspond to a corrosion rate of $\sim 10^{-8}$ A/cm^2. Some experiments, however,

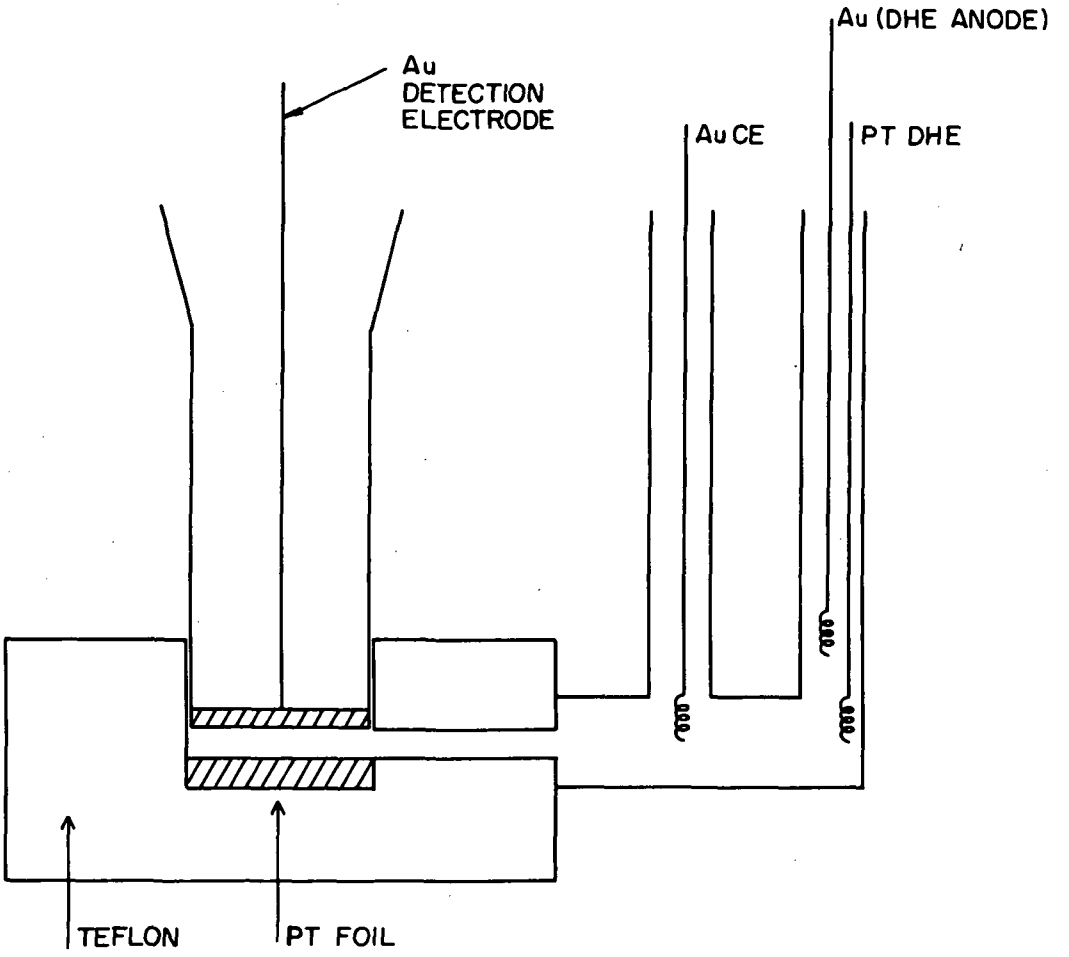

Fig. 81. Experimental configuration for platinum dissolution studies in 8.5N KOH

carried out under identical conditions showed no detectable platinum ([Pt] $\leq$ 2 μM). From the experiments of Chemadanov, et al., and Johnson, et al., the reduction of the "oxide" layer seemed important in the dissolution process, especially from the viewpoint of an operating rechargeable oxygen electrode where some surface reduction may occur during cycling. Therefore, it was decided to investigate the effects of various cycling regimes on the platinum dissolution rate.

These three cycling regimes were studied:

Regime A: 10 min at +1.75 V, followed by 5 min at +0.85 V
Regime B: 10 min at +1.75 V, followed by 5 min at +0.40 V
Regime C: 10 min at +2.00 V, followed by 5 min at +0.40 V

The results of three sets of experiments using these three regimes is shown in Table LII. Regime C seems to result in markedly more platinum dissolution. It appears that the more anodic potential of +2.00 V results in greater Pt dissolution than if the anodic limit were +1.75 V. If the primary mode of platinum dissolution is via the reduction of the oxide, PtO_2, as postulated by Johnson, et al., this result may be interpreted as indicating the formation of larger amounts of PtO_2 at these more anodic potentials in contrast to +1.75 V where all indications seem to support the presence of a chemisorbed oxygen layer. A comparison of regimes A and B which should indicate effects of the cathodic potential limit does not reveal any striking difference. Roughly the same amount of dissolved platinum is found in each.

Table LII. Results of Dissolution Studies on Smooth Platinum Foil Electrodes in 8.5N KOH for Various Cycle Regimes

	[Pt] μM		
Experiment No.	Regime A	Regime B	Regime C
1	4	—	23
2	4	—	24
3	11	6	34

Since platinum dissolution in acidic, chloride-containing electrolytes is quite marked, it was of interest to investigate the effects of chloride ion (0.02M) on platinum dissolution in 8.5N KOH. Cycle A was used in these studies and also a 48 hr period at +1.75 V. After 84 hr of regime A, 4 μM Pt was detected which is the equivalent of that obtained in 8.5N KOH, in the absence of chloride ion. After 48 hr at +1.75 V, 3 μM Pt was detected, again not significantly different than that observed in 8.5N KOH without chloride ion.

Some attempts were made to conduct similar experiments as reported by Johnson, et al., but in 8.5N KOH by means of the RRDE. A platinum disk with a gold ring was used in these studies. The ring potential was kept at +0.2 V versus RHE and ring current-disk potential curves were obtained at 60 rps using a potential sweep of 100 mV/min. The ring background current was found to be quite high, but allowed some interesting observations to be made concerning the unidentifiable species described by Johnson, et al.

The disk was pretreated at +1.4 V for 1 min before pulsing to -0.20 V where the sweep was begun. It was found that the time at -0.20 V had a marked effect on the observed I_r versus E_d curves. Fig. 82 shows the I_r versus E_d curves obtained after 10 sec, 15 min, and 30 min at -0.200 V. There is an increase in the current at +0.9 V after 15 min at -0.20 V while after 30 min at -0.20 V, there are definite indications of a current peak at +0.90 V. There is also a sharp anodic current peak at +0.1 V on the forward sweep which also increases with time at -0.20 V. The ring current peak at E_d = +0.90 V is quite similar to that reported by Johnson, et al., for Pt in 1M H_2SO_4. The observed dependence of the magnitude of this peak on the time at -0.20 V would seem to indicate that it could be due to the dissolution of a metallic impurity deposited on the Pt disk at -0.20 V rather than a platinum species arising from dissolution of the platinum disk itself. Fig. 83 shows the very marked I_r peak observed after 2 hr at E_d = -0.20 V which also speaks for a metal deposition process. Further evidence for a metal deposition process can be found in the observations of Johnson, et al., that the reduction of this species is a surface controlled reaction. Their finding that the height of this peak increased with increasing rotation rate also points to an increasing amount of metallic species on the disk as the rotation rate increases, leading to large ring currents as it dissolves. The nature of the anodic current peak at +0.1 V is not clear.

D. Conclusions

We conclude that, under constant potential conditions in the region of +0.85 V to +1.75 V, the corrosion current of smooth Pt electrodes in 8.5N KOH is on the order of 10^{-8} A/cm^2. Potential cycling regimes lead to more dissolution than static potential treatment, especially with a regime of +2.0 V/10 min followed by +0.4 V/5 min. Dissolution seems to be favored by cycling regimes which allow reduction of the Pt-O layer to occur.

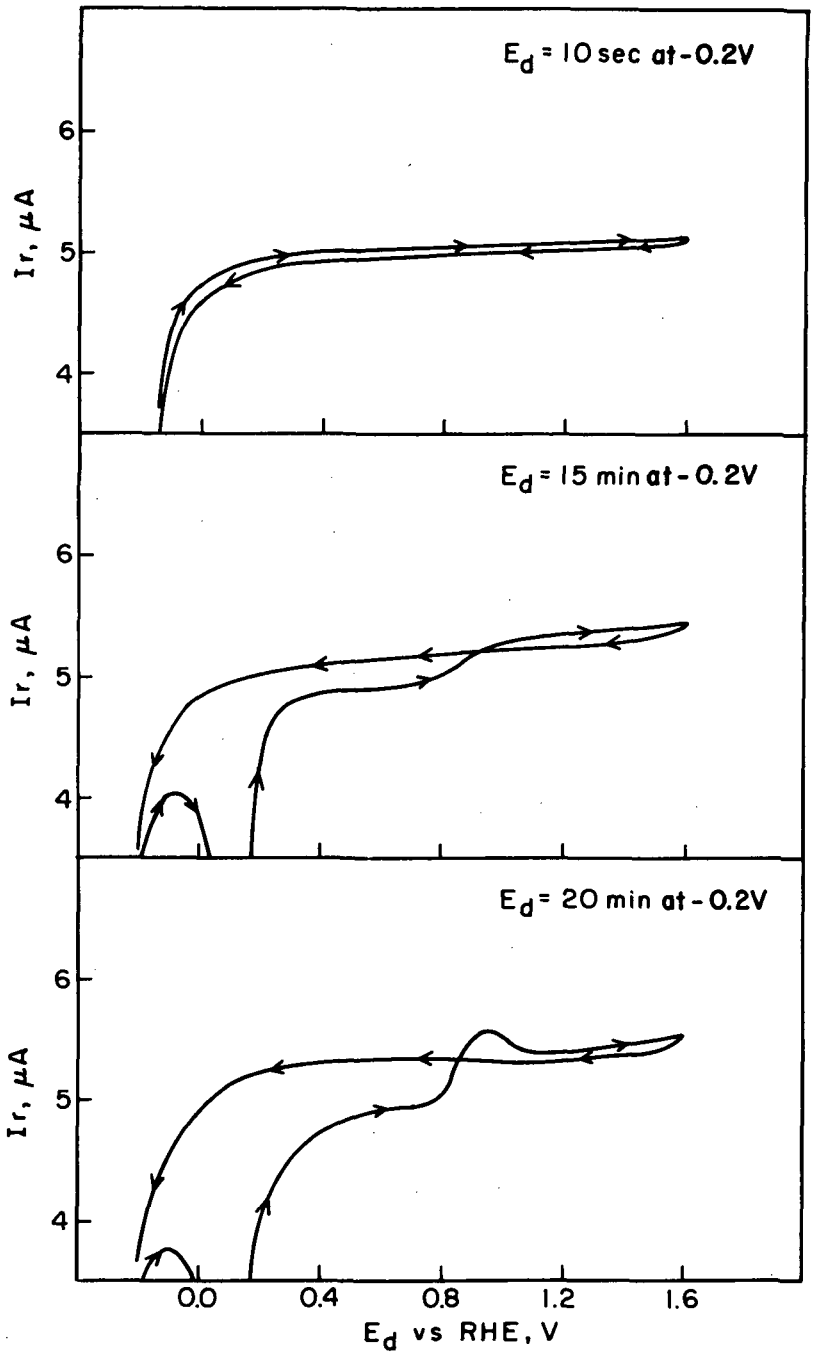

Fig. 82. Ring current-disk potential curves for a gold ring-platinum disk electrode at 60 rps in argon-saturated 8.5N KOH after varying times at -0.2 V

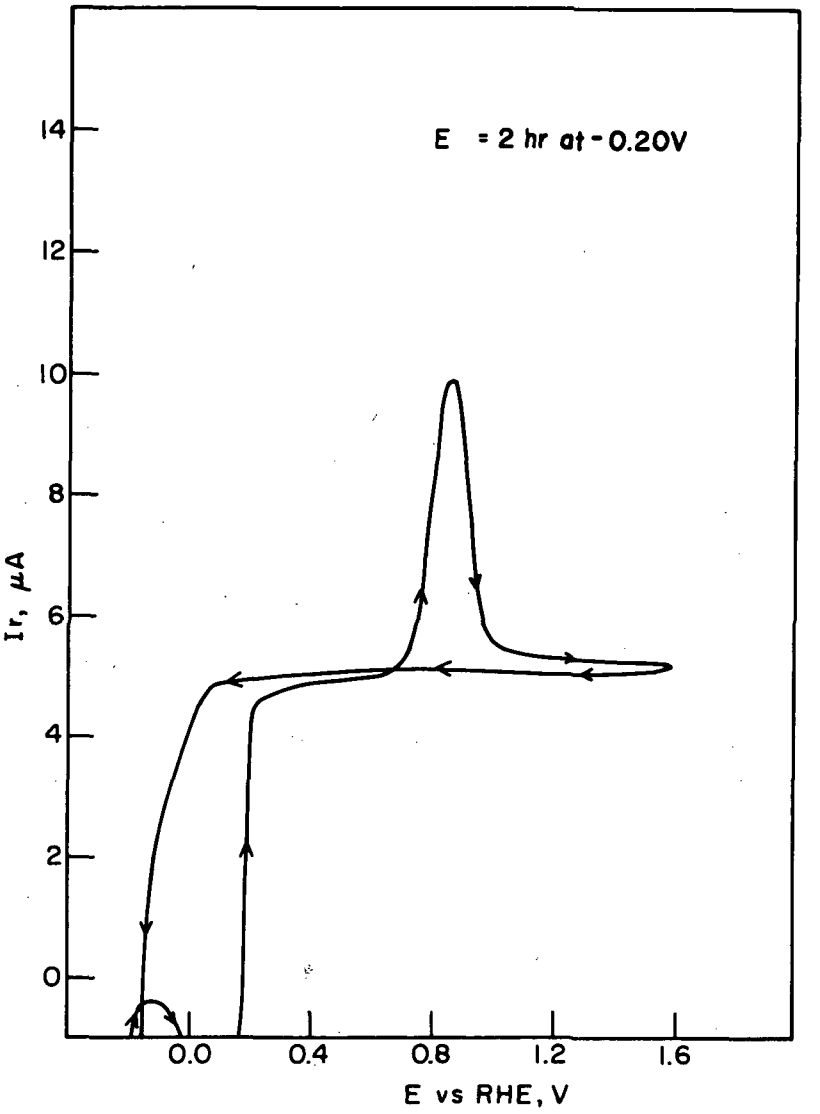

Fig. 83. Ring current-disk potential curve for a gold-ring platinum disk electrode at 60 rps in argon-saturated 8.5N KOH after 2 hr at -0.2 V

VIII. TEFLON-BONDED ELECTRODES

A. Background

This section is concerned with the physical and electrochemical characterization of Teflon-bonded platinum electrodes operating in a typical rechargeable oxygen electrode regime involving a 60 min charge period at 25 mA/cm^2 followed by a 30 min discharge period at 50 mA/cm^2. While the "floating electrode" configuration[66] appeared to be ideally suited to studies of such electrochemical parameters as the state of surface oxidation, electrochemically active surface area, hydrogen peroxide production, etc., it appeared necessary to carry out some studies in an actual fuel cell configuration for a number of reasons. First, it was anticipated that, under "floating electrode" conditions, the failure mechanism of the oxygen electrode might be different than under fuel cell conditions. In the "floating electrode," no appreciable pressure differential can be applied to the back side (gas side) to prevent the frequently observed "weeping" of oxygen electrodes which could result in flooding of the electrode. Secondly, the larger size electrodes of a fuel cell (~50 cm^2) were more appropriate for measurements of the BET surface area and pore size distribution. Also, the relatively large ratio of electrolyte volume to electrode area (~50 cc/cm^2) in the floating electrode configuration as opposed to actual fuel cell conditions could be a consideration in the interpretation of results.

We therefore have carried out experiments in both the "floating electrode" configuration and in an actual rechargeable fuel cell configuration. Five "floating electrode" cells were operated. Cells No. 1 and 5 contained 8.5N KOH, Cell No. 2 contained 8.5N KOH saturated with Johns-Manville Fuel Cell asbestos, Cell No. 3 contained 8.5N KOH saturated with Fe_2O_3 while Cell No. 4 contained 6.5N KOH/1M K_2CO_3. Four full fuel cells were also operated, two containing 8.5N KOH (Cells No. 12 and 15) while the others contained 8.5N KOH saturated with Fe_2O_3 (Cell No. 18) and 6.5N KOH/1M K_2CO_3 (Cell No. 21). In order to eliminate any complications arising from the screen substrate, we have used Teflon-bonded platinum black electrodes prepared on pure platinum screen.

More than 500 test cycles were conducted on these cells. The following parameters were measured on the "floating electrode" after approximately 5, 50, 100, and 500 cycles: (1) surface oxidation state, (2) electrochemical surface area, (3) polarization behavior (both anodic and cathodic), and (4) dissolved platinum and hydrogen peroxide. With the full fuel cells, electrodes were characterized after 100 and 500 cycles by measurements of: (1) BET

surface area, (2) pore size distribution, (3) average particle size, and (4) internal structure (scanning electron microscopy).

B. Experimental

1. Teflon-bonded platinum black electrode manufacture

Our aim in electrode fabrication was a Teflon-bonded platinum black electrode of ~400 cm^2 with a nominal loading of 9 mg Pt/cm^2 and 30% Teflon on a platinum screen substrate. The basic procedure involved backing the platinum screen with aluminum foil then spraying it with a suspension of platinum black and Teflon. After vacuum drying, the electrode was sintered in an inert atmosphere and the aluminum foil removed by dissolution in caustic solution. The final procedure developed is detailed below.

Three 3 in. by 3 in. pieces of thin aluminum foil were positioned on a flat aluminum plate. They were then covered with the platinum screen (417 cm^2, 52 mesh, 4 mil wire, obtained from Englehard Ind.) and pressed at a total pressure of 50 tons. This procedure formed a weak bond between the screen and the foil. The required amounts of platinum and Teflon (5.45g Pt black, 2.34 g Pt black, 2.34 g Teflon) were then calculated, assuming a 2 cm wide circumferential strip in order to compensate for spraying losses. Two equal batches of the suspension were prepared from fuel cell platinum black (Englehard Ind. Lot 17403) and Teflon suspension (Teflon 30, Dupont) in ~20 ml of water. Spraying was carried out with a Pashe Air Brush small point sprayer. During spraying the air temperature above the screen was kept at 60 - 70 °C. The platinum black - Teflon suspension had a tendency to coagulate. Therefore, it was necessary to prepare an additional suspension of Pt black and Teflon to compensate for losses.

After spraying, the electrode was covered with perforated aluminum foil and pressed again. The electrode was then vacuum dried overnight at 40 °C. Sintering was carried out under argon at 275 - 280 °C for 15 min. In order to avoid separation of the electrode material from the screen, a slight physical pressure was maintained throughout the sintering process. After cooling, the aluminum foil was dissolved with dilute KOH. After several washings with dilute KOH and then triply-distilled water, the electrode was dried. The nominal platinum loading was determined to be 11 mg/cm^2.

2. Floating electrode cell

The cell arrangement for the "floating electrode" configuration is depicted in Fig. 84. The cell body itself was constructed of quartz while the cell top was made of Teflon. The cell was made gas tight by sealing with Kel-F wax where required. Fig. 85 shows the experimental arrangment, including the thermostating bath.

The floating electrodes had geometric areas of 1.14 cm^2. A dynamic hydrogen electrode (DHE) served as the reference, with a smooth platinum wire spiral as the counterelectrode. A rubber septum arrangement allowed the removal of electrolyte samples for platinum and hydrogen peroxide analysis and also addition of electrolyte to maintain the solution level.

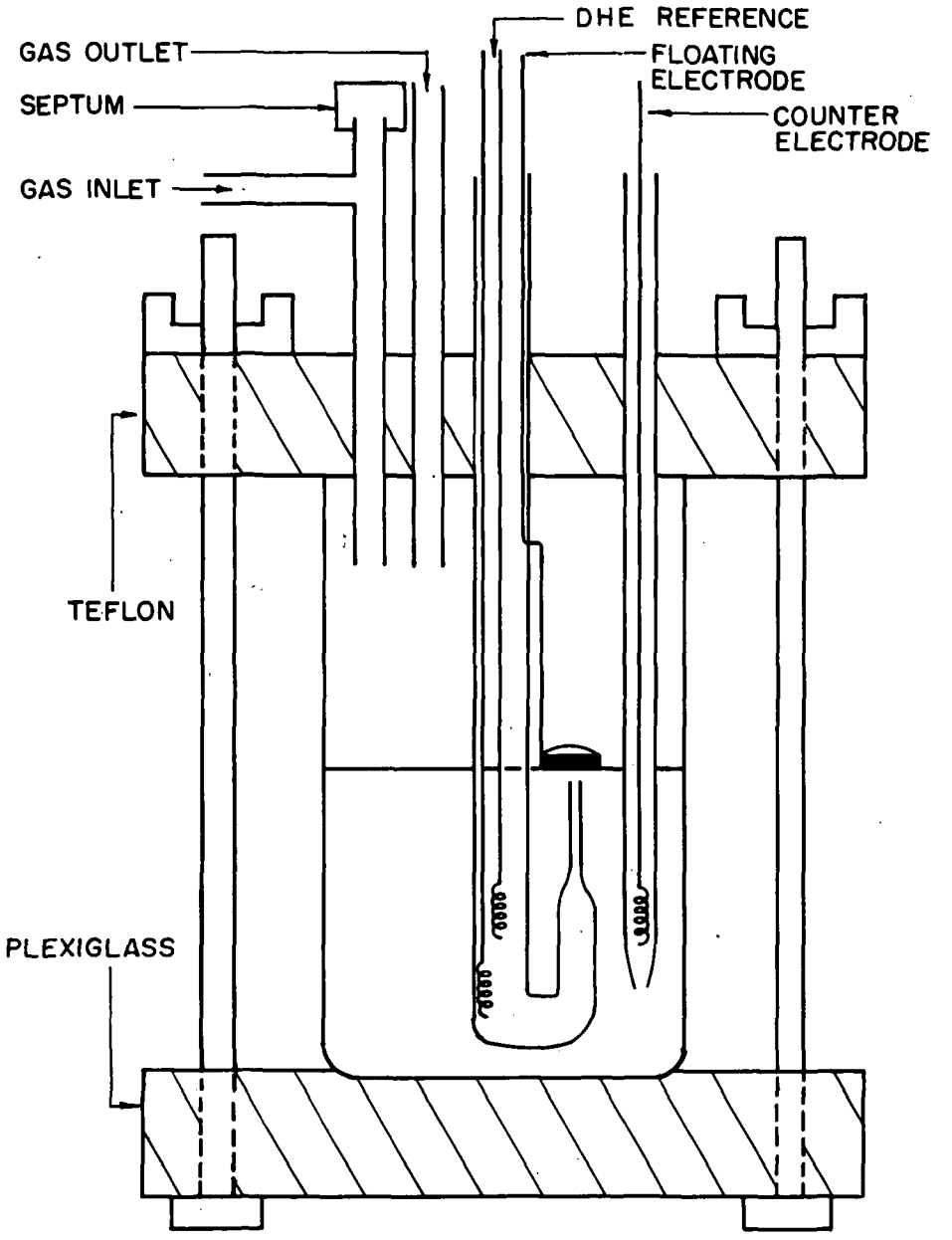

Fig. 84. Floating electrode test cell

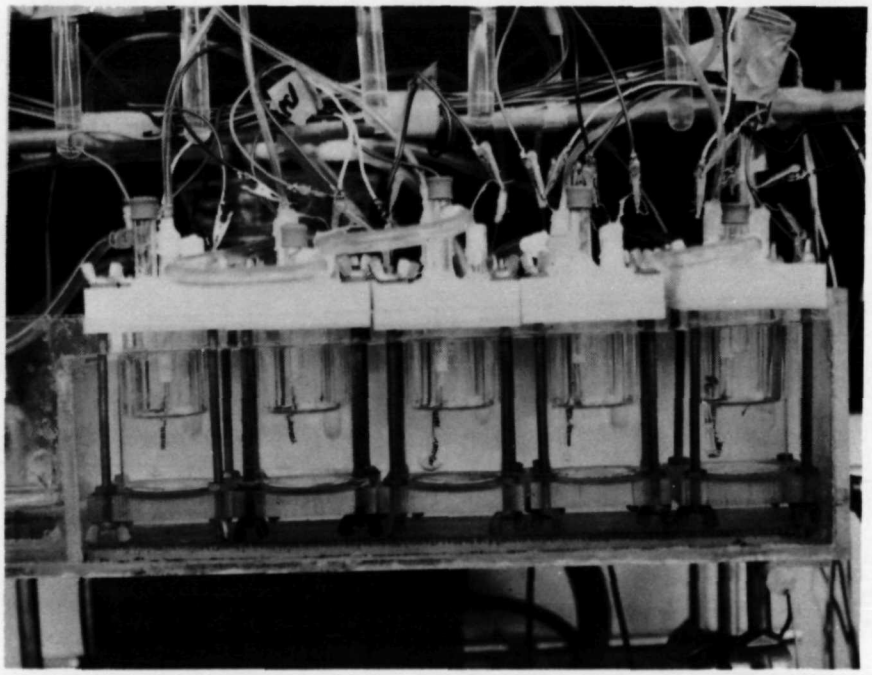

Fig. 85. Floating electrode test cell apparatus

The temperature of the gas presaturator was maintained at ~18 °C to minimize water loss and electrolyte concentration changes.

The five cells were connected in series with a Wenking potentiostat operating in the galvanostatic mode. The reference input of the potentiostat was switched with a mechanical timing arrangement to achieve the necessary charge and discharge cycles. The potentials of the working electrodes were recorded on a Esterline Angus Multipoint Recorder. A simple switching arrangement allowed each cell to be removed from the cycling circuit in order to carry out the necessary electrochemical measurements when desired.

3. Full fuel cells

The individual test cell arrangment has been described in detail elsewhere.[67] We have used American Cyanamid AB-40 fuel cell electrode material for the hydrogen electrode with Pt-black on Pt screen cathodes prepared as just described. Under these conditions, cell performance should be limited by the oxygen electrode since, at the current density used, very little polarization would result from the anode. Johns-Manville Fuel Cell Asbestos (40 mil) served as the separator.

It should be recognized that these cells are being run open ended and do not depend for discharge on the O_2 evolved during charge. The main purpose of running these cells is to observe changes in the physical structure of the oxygen electrodes with cycling for which large electrode areas must be used.

The cells were discharged at constant current, with cell voltages also recorded on the Esterline Angus Multipoint Recorder. The test rig arrangement is given in Fig. 86.

4. Electrode characterization techniques

We have used three techniques to study changes occurring in the structure of Teflon-bonded platinum black oxygen electrodes with cycling. These are: (1) BET gas absorption (used for both surface area and pore size distribution measurements), (2) X-ray diffraction (average particle size estimation), and (3) scanning electron microscopy (morphology).

Surface area and pore size distribution measurements were carried out on a Engelhard Isorpta Analyzer using analysis of the complete adsorption isotherm. As the relative pressure is increased, capillary condensation occurs in the internal pores, permitting an estimate of pore size distribution to be made based on the Kelvin equation[68] as applied by Cranston and Inkley. Since the calculations involved are quite tedious, we have made use of a recently published computer program to evaluate these data.[69] Electrode areas of ~50 cm^2 were used in the in these determinations on uncycled electrode material and electrodes cycled 100 and 500 times in the fuel cell configuration.

We have used X-ray line broadening to obtain the average particle size, based on the following equation:[70]

$$\epsilon_{hkl} = \frac{K \lambda}{B \cdot \cos \Theta}$$

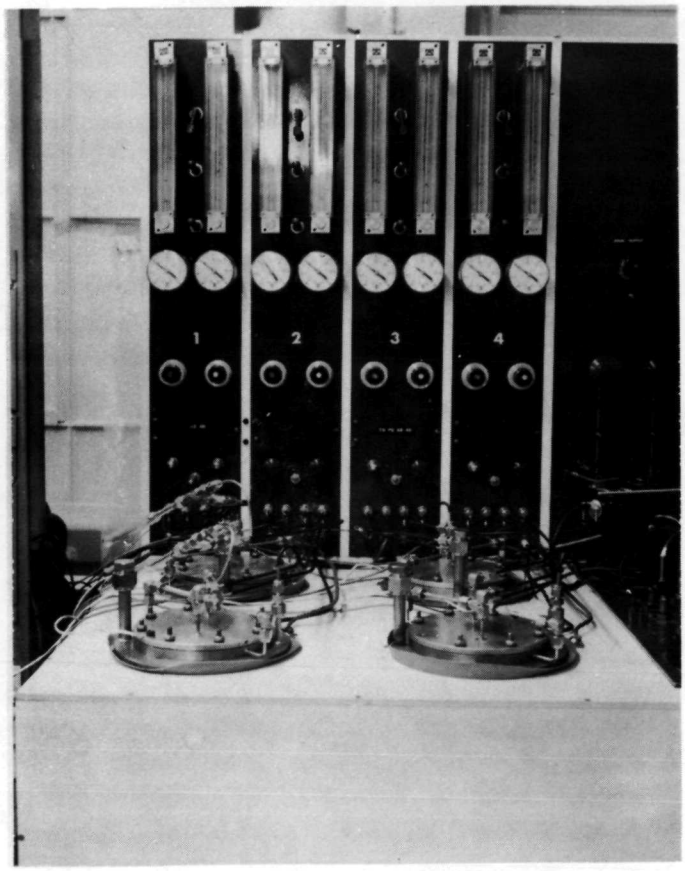

Fig. 86. Testing rig for full fuel cells

where ϵ_{hkl} is the mean apparent crystallite size normal to the reflecting plane, K is the Scherrer constant (taken here as 0.9), B is the diffraction broadening (the experimentally obtained width of the diffraction peak measured in radians at half-height), cos Θ is the cosine of the Bragg angle of reflection, and λ is the wavelength of the incident radiation.

Scanning electron microscope photos of uncycled and cycled electrodes were obtained using the facilities of Photometrics, Inc., Lexington, Massachusetts.

5. Dissolved platinum and H_2O_2 analysis

We have used the spectrophotometric technique as described in Section VII for the determination of dissolved platinum in the floating electrode test cells. The hydrogen peroxide concentrations were determined using the Ti (IV) reaction with H_2O_2 to form a yellow complex ion as discussed in Sandell.[71]

C. Results and Discussion

1. State of surface oxidation of Teflon-bonded platinum black electrodes

It was of interest to compare state of surface oxidation data for a Teflon-bonded electrode with similar data acquired for smooth and platinized platinum. Fig. 87 plots the charge required to reduce the oxygen layer, Q_{ox}, and Q_H, the charge required to deposit a layer of chemisorbed hydrogen, as a function of the potential of formation. A galvanostatic pulse of 50 mA (44 mA/geom. cm^2) was used after 1 min at the potential of interest. The amount of charge required to reduce the oxygen layer was determined to be independent of the time of formation in the range of 1-6 min.

In the region of +1.0 V to +1.7 V, there is an almost linear increase of Q_{ox} with potential. Q_H has a tendency to increase at potentials greater than +1.0 V. This increase may be due to a carry over of oxygen layer reduction into the hydrogen region. In Fig. 88, we have plotted $Q_{ox}/2Q_H$ versus E in order to estimate the state of surface oxidation. For Q_H, a value of 234 mcoul/geom. cm^2 was used which is the average Q_H value for $E < +1.0$ V.

At +1.7 V, the ratio $Q_{ox}/2Q_H$ reaches 1.3 which is somewhat higher than the ratio of ~1.0 obtained for both smooth and platinized Pt at +1.7 V. The higher value for the Teflon-bonded electrode may be due to bulk oxide formation and/or oxygen dissolution into the lattice as opposed to simple chemisorption of oxygen. The value of Q_H used here may also be suspect since Giner, et al., have discussed the difficulties associated with measurement of the extent of hydrogen chemisorption (Q_H) with floating electrodes due to premature hydrogen evolution.[72] This occurs because the hydrophobic electrode structure permits very rapid diffusion of hydrogen away from the surface so that the equilibrium partial pressure of hydrogen corresponding to the electrode potential is never attained. Thus, Q_H as measured may not reflect full coverage with adsorbed hydrogen, making the $Q_{ox}/2Q_H$ ratio too large. One can measure Q_H unambiguously by making similar measurements on a flooded electrode, since only small quantities of dissolved hydrogen are needed to satisfy the thermodynamic requirement at potentials above the reversible hydrogen electrode.

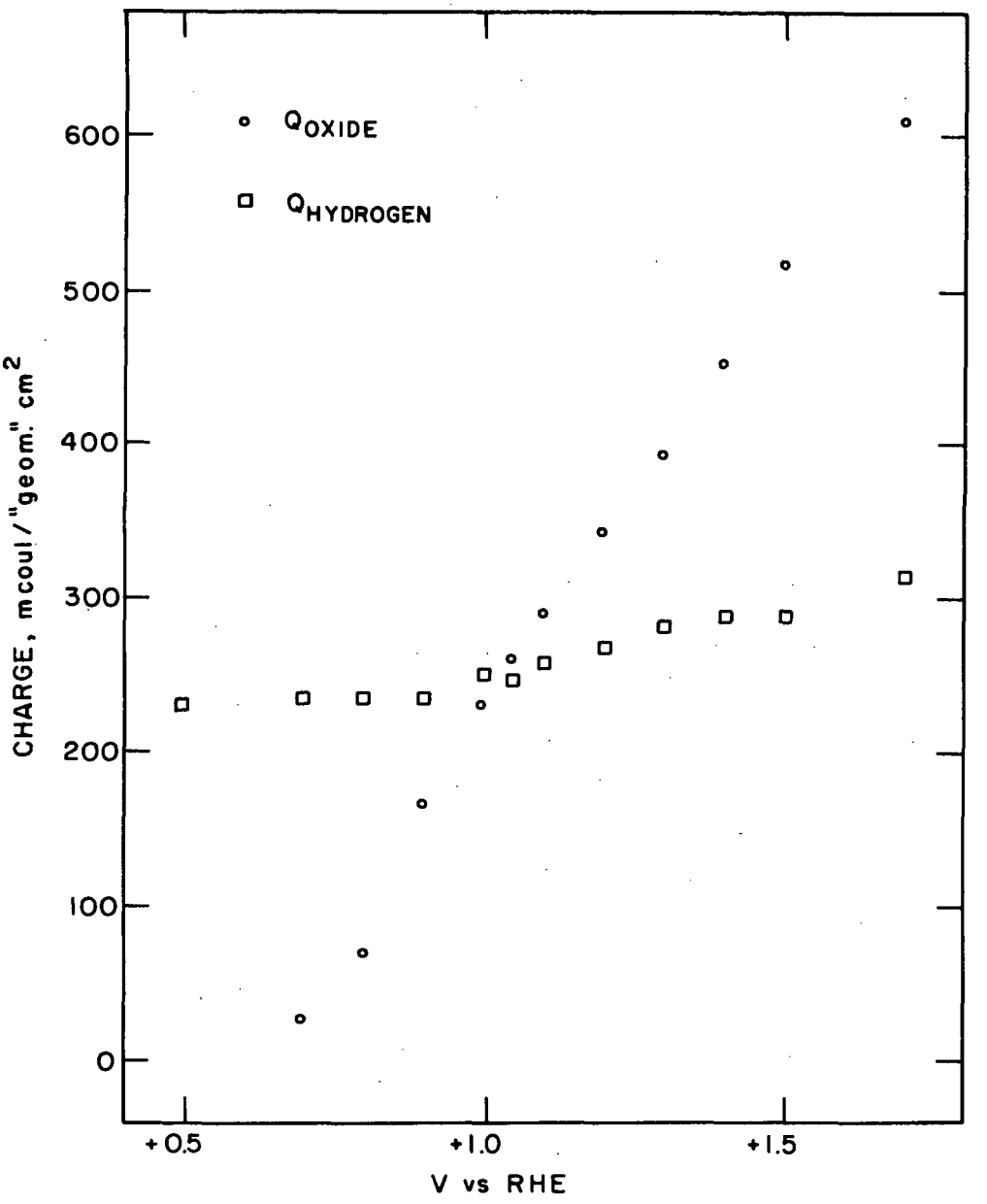

Fig. 87. Dependence of Q_{ox} and Q_H on potential for a Teflon-bonded platinum black electrode in the floating electrode configuration in 8.5N KOH at 30 °C (data obtained glavanostatically at 44 mA/geom cm^2 after 1 min at each potential)

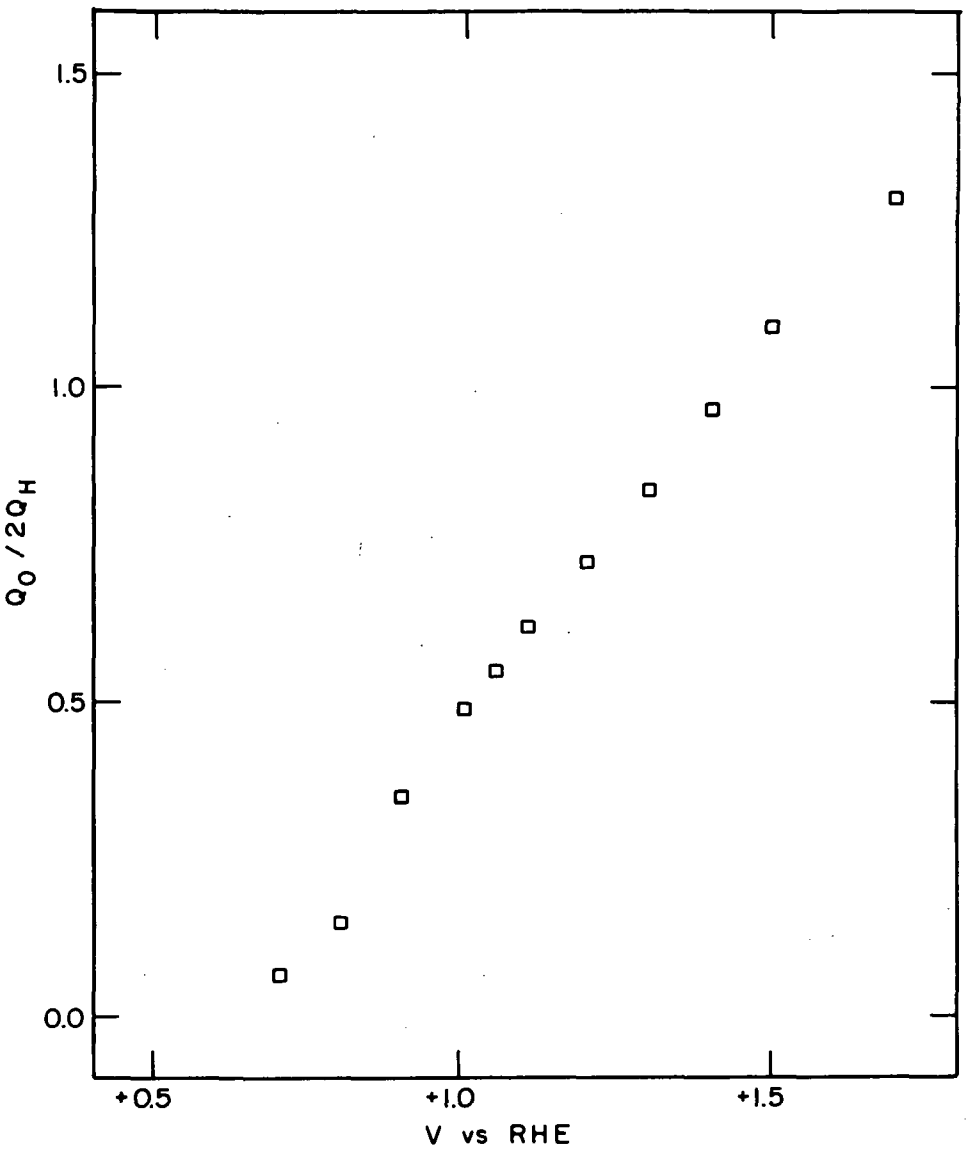

Fig. 88. $Q_{ox}/2Q_H$ as a function of potential for a Teflon-bonded platinum black electrode in the floating electrode configuration in 8.5N KOH at 30 °C

We have compared Q_H measurements on both floating and submerged electrodes and no serious discrepancies have been observed. Table LIII shows Q_{ox} and Q_H as measured from E = +1.05 V for various times for the same electrode floating and submerged. This lack of difference in Q_H values as measured for floating and submerged electrodes is contrary to the findings of Giner, et al., for Teflon-bonded electrodes in 85% H_3PO_4 at 150 °C.[72] This difference may be attributed to the much higher exchange current for the hydrogen reaction in acid solution and at a much higher temperature when compared to 8.5N KOH at 30 °C. Differences in hydrogen solubility may also play a role.

Table LIII. Comparison of Q_{ox} and Q_H After Various Times at +1.05 V for Submerged and Floating Teflon-Bonded Platinum Black Electrodes in 8.5N KOH at 30 °C

	Floating		Submerged	
Time at +1.05 V	Q_{ox}*	Q_H	Q_{ox}	Q_H
30	248	248	250	248
60	252	253	253	248
120	256	257	253	248
300	258	258	257	251

*All Q's in mcoul/geom. cm^2.

For our studies of the cycling of floating electrodes, it was necessary to develop routine procedures for measurement of the state of surface oxidation and surface area after the specified number of cycles. Measurements of the state of surface oxidation are made after a charging cycle. To eliminate any effects of residual dissolved oxygen, a waiting time at a lower potential, during which oxygen is purged from the system, must be introduced. Table LIV shows the effect of time at +1.2 V after forming the anodic layer at +1.70 V for 1 min. After 3 min, there is relatively little effect on Q_{ox} or Q_H. Therefore, we adopted a waiting period of 5 min at +1.2 V before measuring the state of surface oxidation after the appropriate charging cycle. After the measurement of the state of surface oxidation, the electrode was then pretreated at +1.35 V for 2 min then +0.05 V for 1 min before potentiostating at +1.05 V for 3 min. The electrochemical surface area was then measured using a galvanostatic pulse of 50 mA using either Q_{ox} or Q_H.

2. Floating electrode cells

The five floating electrode cells were cycled for a total of 650 cycles. Contrary to our original expectations, no gross failure due to flooding was observed in any of these cells.

This is presumably due to the charging process which may result in "drying" of the electrode during anodic oxygen evolution which cannot occur during static discharge operation.

Table LIV. Effect of Holding Time at +1.2 V on Measurement of State of Surface Oxidation of a Teflon-Bonded Platinum Black Electrode after 1 Min at +1.70 V

Time, sec	Q_{ox}*	Q_H	Q_T
60	472	341	813
180	497	307	804
360	502	322	824

*All Q's in mcoul/geom. cm^2.

Figs. 89 through 93 show the observed end-of-charge and discharge potentials. The numbered arrows indicate the points and cycles at which cycling was interrupted and the appropriate measurements made. It should be mentioned here that, while we performed the appropriate measurements after approximately 5, 50, 100 and 500 cumulative cycles, the actual cycle lengths used were 5, 45, 50 and 400 cycles since the electrochemical techniques used to measure surface oxide and surface area destroy any accumulated anodic layer.

After a cumulative total of ~ 175 cycles, the observed end-of-discharge potentials are in the vicinity of +0.8 V versus RHE varying little from electrolyte to electrolyte. The end-of-discharge potentials then begin to decrease, and a value in the vicinity of +0.60 - +0.65 V is reached after 225-250 cycles where it remains constant. The end-of-charge potentials are subject to much smaller variation, staying relatively constant at ~ 1.80 V. Cell 4, containing 6.5N KOH/1M K_2CO_3, does not seem to decrease in potential as much as the other cells, reaching +0.70 V after ~ 500 cycles, but maintaining an end-of-discharge potential of ~ +0.90 V for 360 cycles. While these results with regard to the effect of carbonate are interesting, indicating no deleterious effects, more experimental work is indicated in this area.

In Figs. 94 and 95 we show the observed potential-time curves during charge and discharge for two of the cells containing 8.5N KOH and 6.5N KOH/1M K_2CO_3. Initially the discharge potential versus time curves are quite flat. As cycling progresses, it can be seen that the potential-time behavior becomes quite erratic. The rather sharp increase in potential as exhibited by both cells after 151 and 300 cycles are not atypical and occurred in all cells. While a gradual increase in potential could be attributed to a wetting phenomenon or to the gradual removal of an inhibiting layer, this sudden potential rise of 100-200 mV in less than 1 min is not compatible with such processes and remains open to question. In contrast to the varied

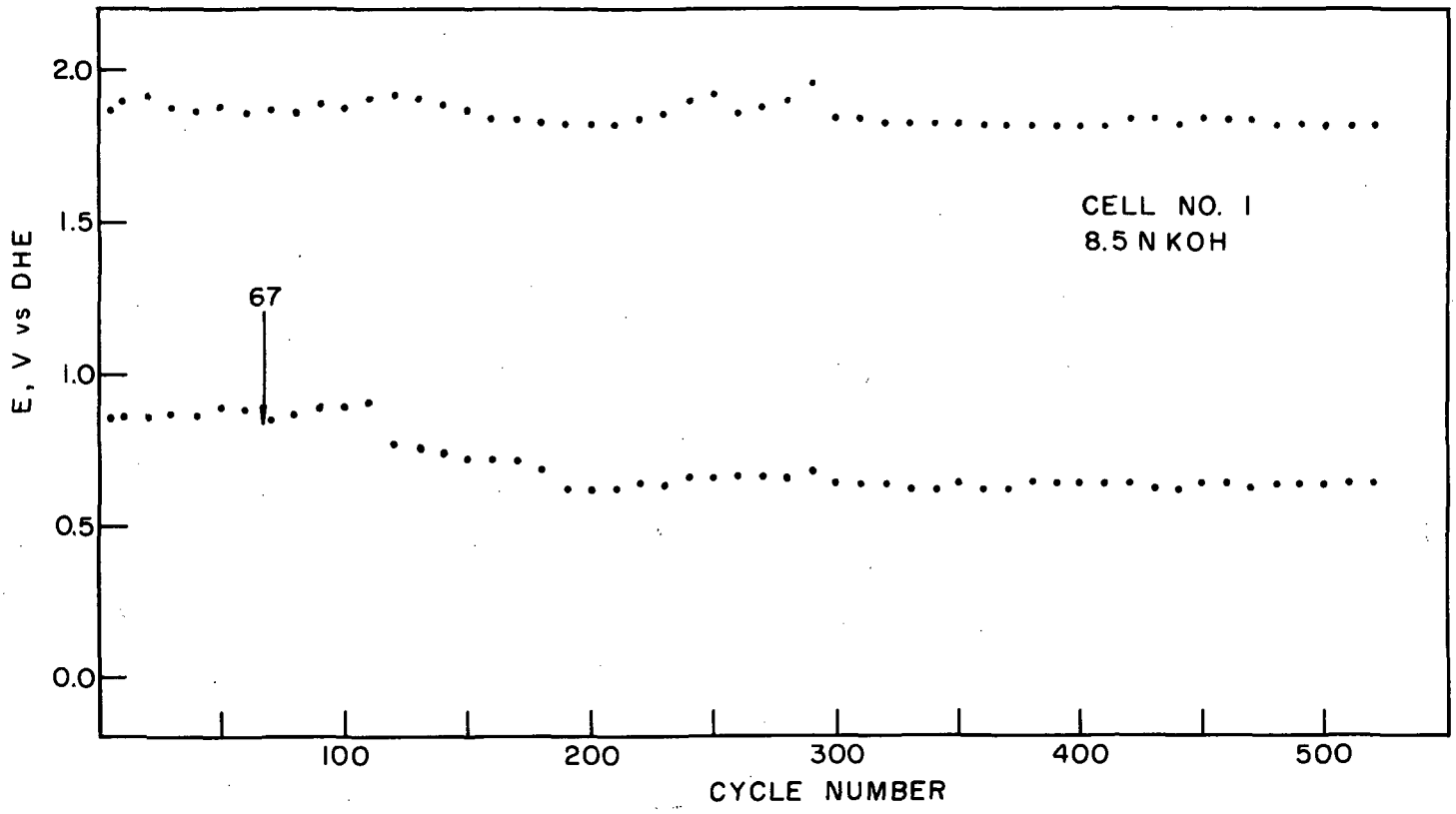

Fig. 89. Oxygen electrode potential during cycling (60 min charge at 25 mA/cm^2, 30 min discharge at 50 mA/cm^2) of a Teflon-bonded platinum black electrode in the floating electrode configuration in 8.5N KOH (cell no. 1) at 30 °C

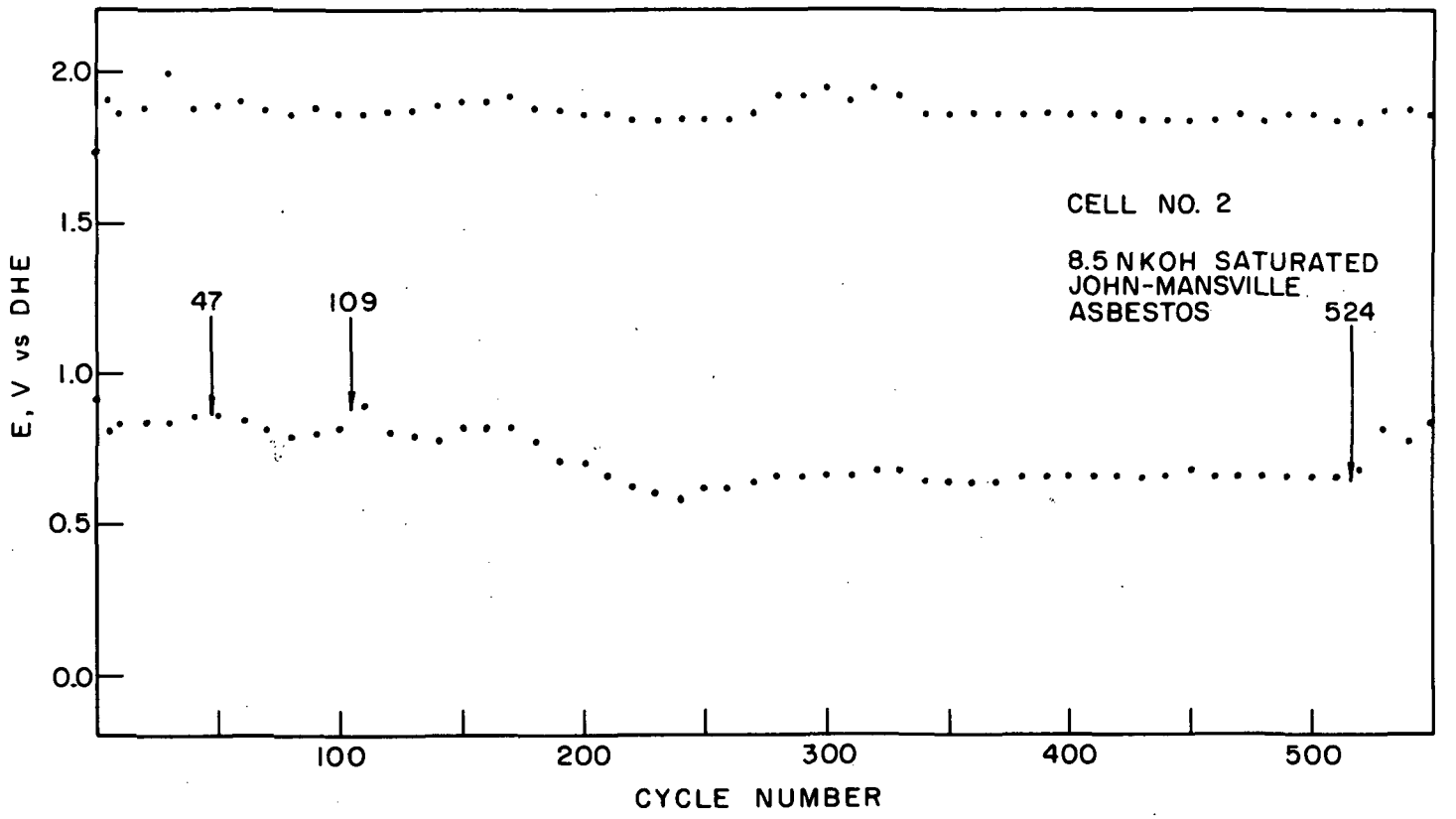

Fig. 90. Oxygen electrode potential during cycling (60 min charge at 25 mA/cm^2, 30 min discharge at 50 mA/cm^2) of a Teflon-bonded platinum black electrode in the floating electrode configuration in 8.5N KOH saturated with Johns-Manville Fuel Cell Asbestos (cell no. 2) at 30 °C

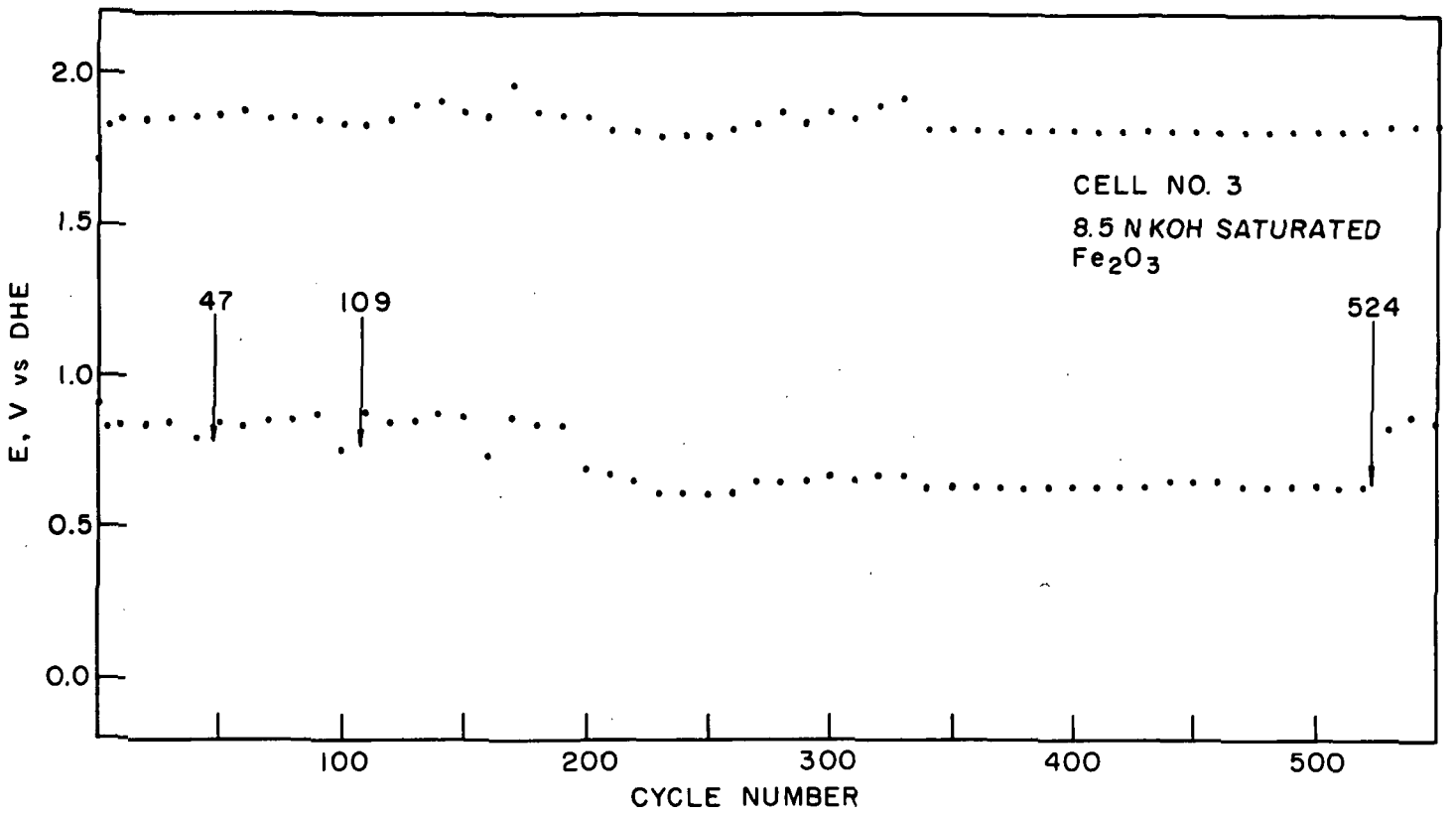

Fig. 91. Oxygen electrode potential during cycling (60 min charge at 25 mA/cm^2, 30 min discharge at 50 mA/cm^2) of a Teflon-bonded platinum black electrode in the floating electrode configuration in 8.5N KOH saturated with Fe_2O_3 (cell no. 3) at 30 °C

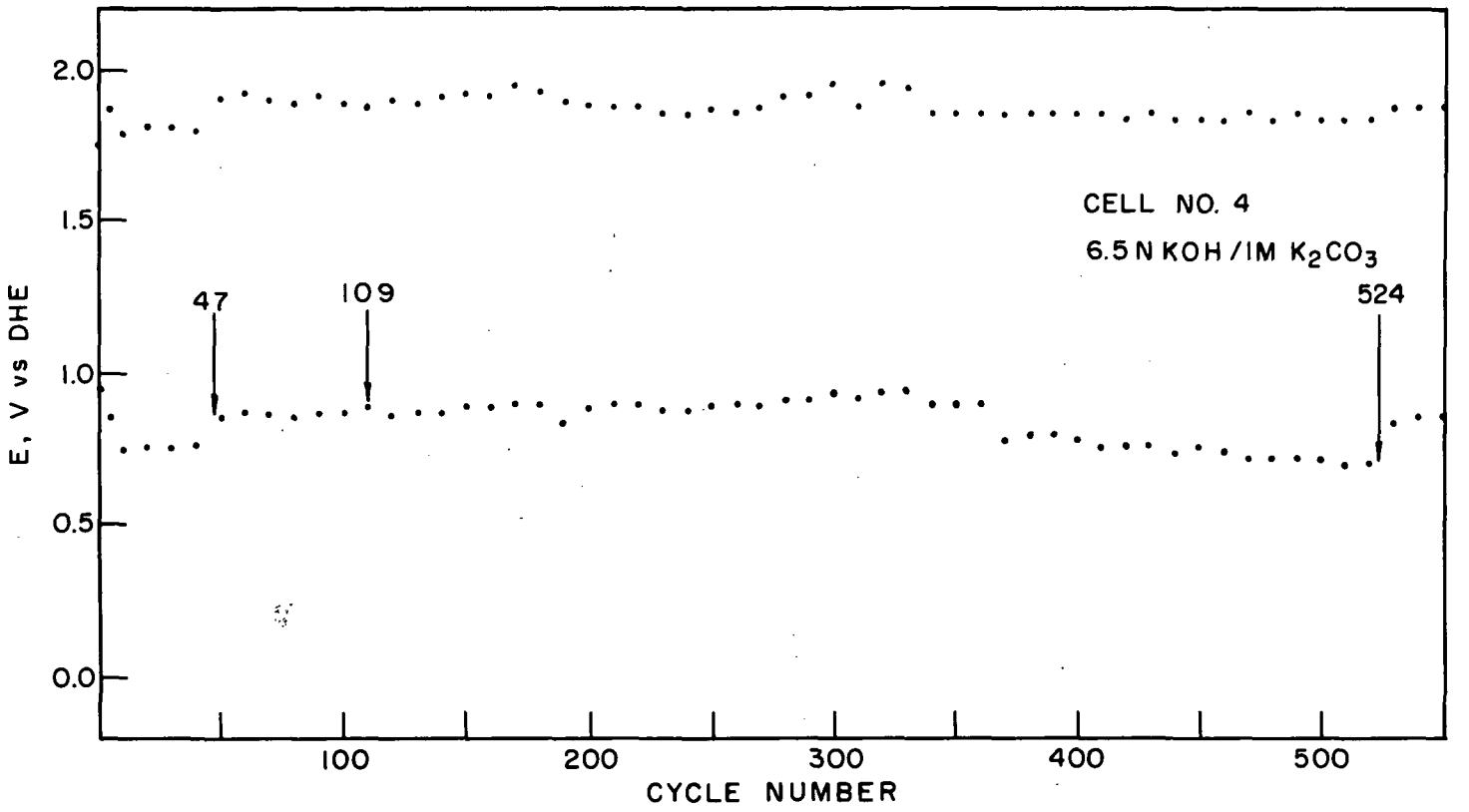

Fig. 92. Oxygen electrode potential during cycling (60 min charge at 25 mA/cm^2, 30 min discharge at 50 mA/cm^2) of a Teflon-bonded platinum black electrode in the floating electrode configuration in 6.5N KOH/1M K_2CO_3 (cell no. 4) at 30 °C

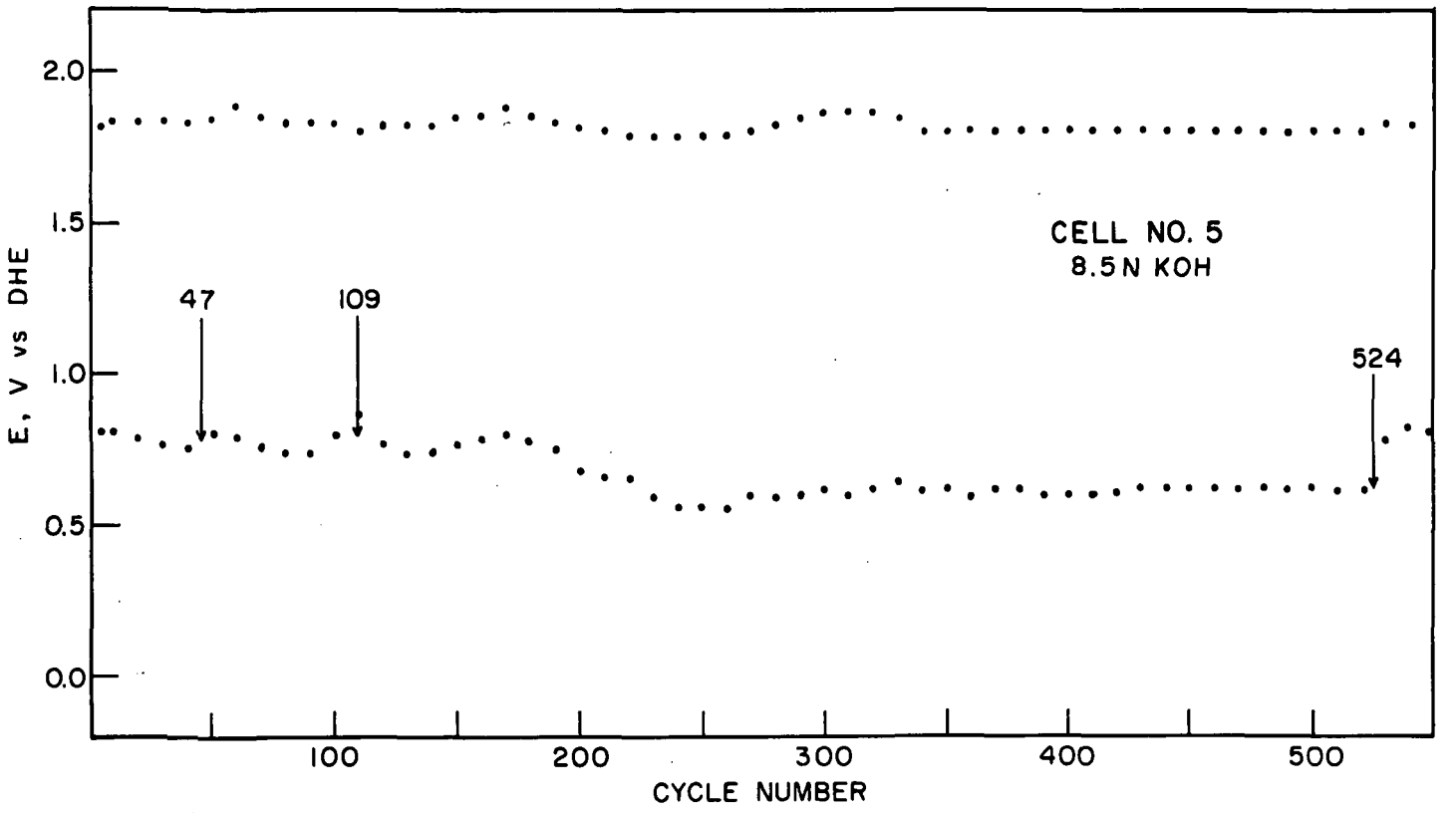

Fig. 93. Oxygen electrode potential during cycling (60 min charge at 25 mA/cm^2, 30 min discharge at 50 mA/cm^2) of a Teflon-bonded platinum black electrode in 8.5N KOH (cell no. 5) at 30 °C

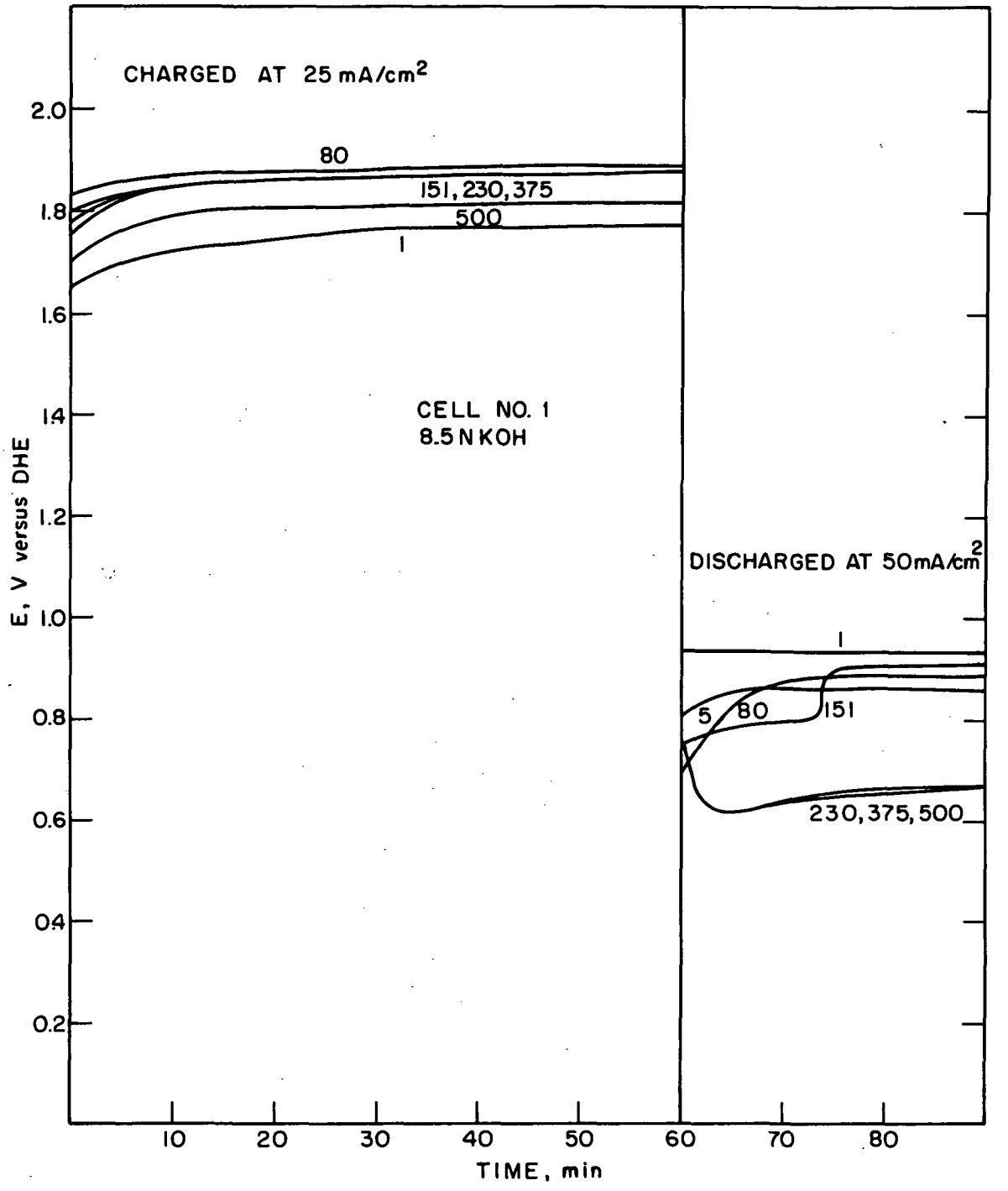

Fig. 94. Potential-time behavior during cycling of a Teflon-bonded platinum black oxygen electrode in the floating electrode configuration in 8.5N KOH (cell no. 1) at 30 °C for specified cycle numbers

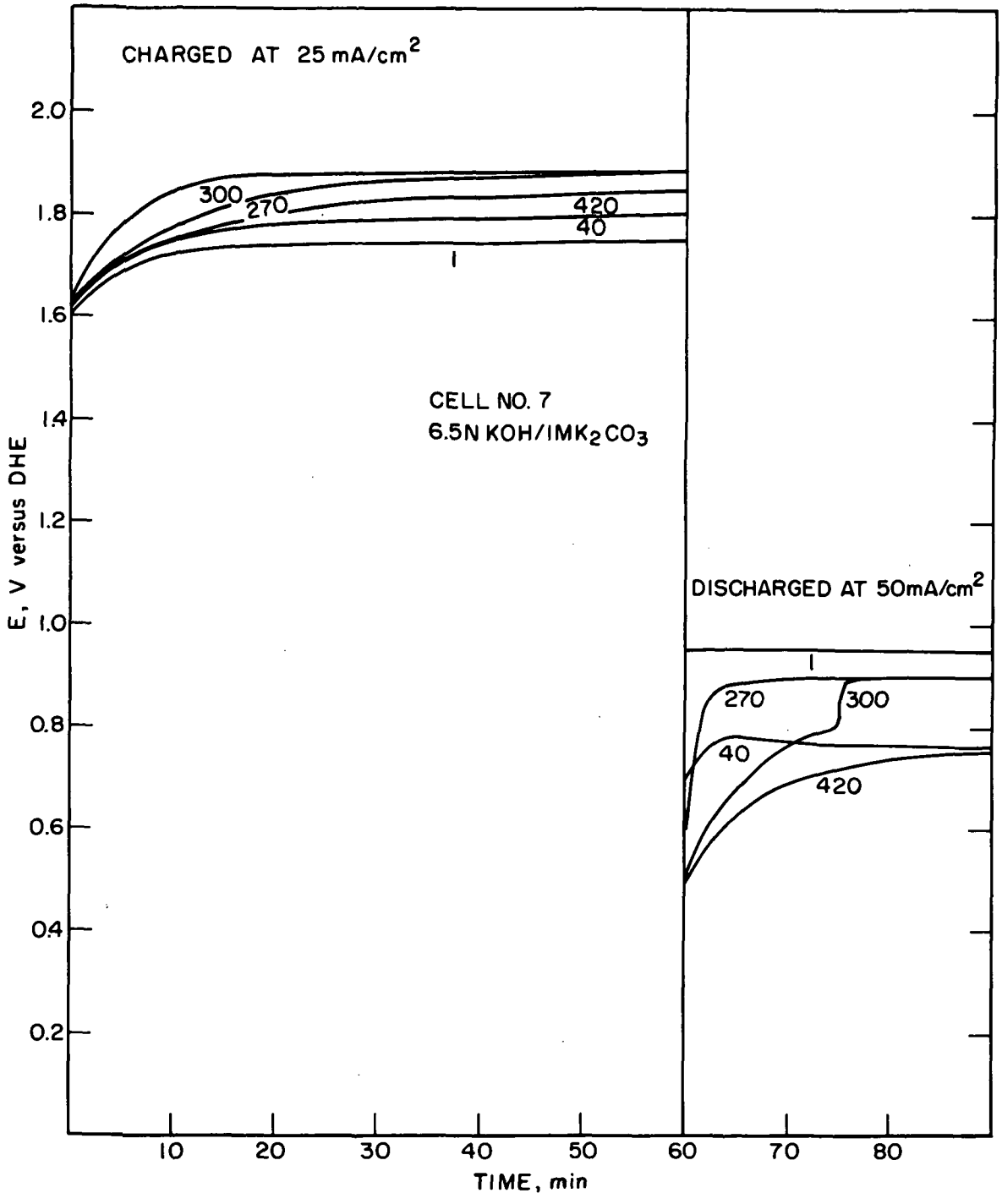

Fig. 95. Potential-time behavior during cycling of a Teflon-bonded platinum black oxygen electrode in the floating electrode configuration in 6.5N KOH/1M K_2CO_3 (cell no. 4) at 30 °C for specified cycle numbers

potential-time curves during discharge, the corresponding charging curves show fairly uniform behavior with a gradual increase in potential as the charging time increases.

It is of interest to note the improvement in discharge performance after the electrode has been removed from the cycling regime, especially after the 524th cycle. The electrodes were cycled for another 125 cycles after which testing was terminated. The observed behavior during these additional cycles for cell 1 and cell 4 is shown in Fig. 96. This apparent improvement in discharge performance is temporary and after ~50 additional cycles, the end-of-discharge potential for all cells, with the exception of the carbonate containing electrolyte is in the vicinity of ~+0.65 V. The carbonate containing cell does seem to show consistently better discharge behavior, although this again needs further verification.

Tables LV and LVI give the measured concentrations of platinum and H_2O_2 after the specified cycle. Some H_2O_2 is detectable after 5 and 47 cycles but thereafter is undetectable. The amount of dissolved platinum does build-up to a value in the vicinity of 80 to 100 μM in all cells. With an approximate electrolyte volume of 35 cc/cell, this corresponds to 0.7 mg of platinum. With a loading of 11 mg/cm^2 and an electrode area of 1.14 cm^2, this translates to a loss of 6% of the platinum loading. However, there is some further evidence to support a larger loss of platinum.

Table LV. Concentration of Dissolved Platinum in Floating Electrode Cells After Cycling

		[Pt] (μM/ℓ)				
	Cell No.	1	2	3	4	5
Cycle No.	5	Undetectable →				
	47	85*	15	12	60	38
	109	-†	60	60	190	50
	525	70	90	107	80	93

*After 67 cycles.

†Analysis not performed.

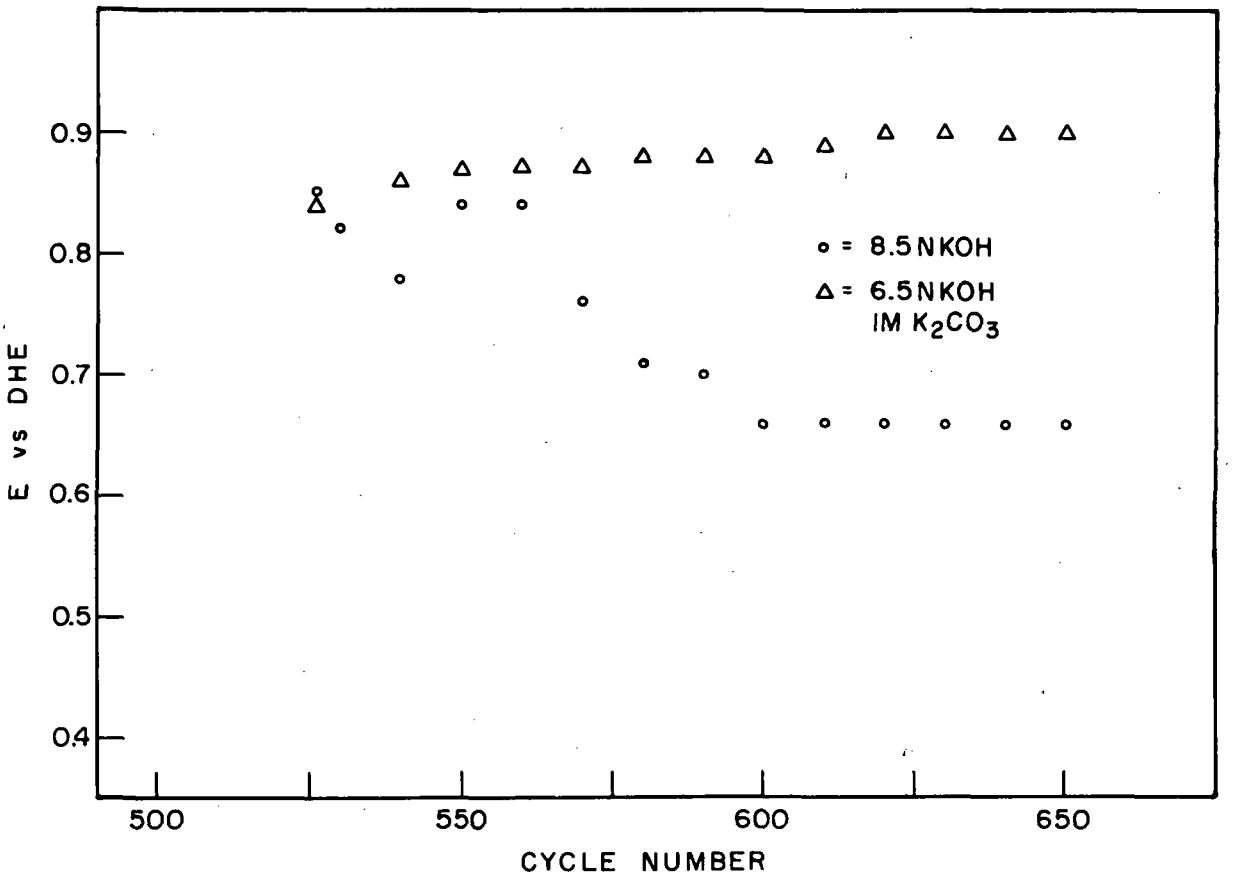

Fig. 96. Oxygen electrode potential during discharge for cycles 525-650 for cells 1 and 4 in the floating electrode configuration

Table LVI. Concentration of Dissolved H_2O_2 in Floating Electrode Cells After Cycling

		$[H_2O_2]$ ($\mu M/\ell$)				
	Cell No.	1	2	3	4	5
Cycle No.	5	80	80	50	100	50
	47	30*	60	50	80	0
	109	-†	0	0	35	25
	525	0	0	0	0	0

*After 67 cycles

†Analysis not performed.

In all cells we observed a black precipitate which may be platinum black or an insoluble or partially soluble platinum oxide or hydroxide. Table LVII summarizes the observed weight losses for the floating electrodes. With the exception of the cell containing the Johns-Manville Fuel Cell Asbestos, weight losses of greater than 10% can be observed.

Table LVII. Summary of Weight Losses of Teflon-Bonded Platinum Black Electrodes After 680 Cycles

Cell No.	% Weight Loss
1	19*
2	5
3	13
4	11
5	20

*After 525 cycles.

Estimation of the state of surface oxidation after the specified charging portion of the cycle was also made. After the glavanostatic charging portion of the cycle, the electrodes were potentiostated at +1.2 V for 6 min prior to measurement of the state of oxidation with a cathodic pulse of 50 mA/cm^2 as described earlier. Some difficulties were encountered here since it was necessary to purge any residual oxygen from the system since it would interfere with these measurements. After some experience had been gained, it was found that it was necessary to switch from oxygen to argon midway in the charging cycle to ensure sufficient

removal of oxygen. Even so, in some instances, oxygen interference was observed, particularly in cells 1 and 5. State of surface oxidation data are presented for cells 2, 3, and 4 in Table LVII.

From Table LVII, Q_H can be ssen to increase dramatically from the 5th to the 47th cycle. However, it is strange that there is not a similar increase in Q_H after a cumulative total of 109 cycles since the actual number of cycles is really comparable, i.e., 42 versus 62. After a cumulative test of 524 cycles (actually 415) both Q_{ox} and Q_H decrease quite markedly.

Table LVIII. State of Surface Oxidation Data for Teflon-Bonded Platinum Electrodes After Cycling

	Cell No.	2			3			4		
		Q_{ox}	Q_H	Q_T	Q_{ox}	Q_H	Q_T	Q_{ox}	Q_H	Q_T
Cycle No.	5	880	240	1120	750	220	970	880	250	1130
	47	880	1100	1880	750	1110	1860	940	1240	2180
	109	750	560	1310	780	530	1310	940	870	1810
	524	230	240	470	450	300	750	250	210	460

The most reliable set of surface oxidation state measurements were made on all cells after the 650th cycle and are given in Table LIX. In Table LIX, we also give the Q_H values as measured from +1.05 V/3 min, Q_H', immediately after the state of surface oxidation measurement was made. There does appear to be excess charge in the Q_H region after cycling which is 21-33% above normal value (as measured after 3 min at +1.05 V).

Table LIX. State of Surface Oxidation Measurements After 650 Cycles

Cell No.	Q_{ox}*	Q_H	Q_H'	$Q_H - Q_H'$
1	412	250	187	63
2	419	206	165	41
3	400	212	163	49
4	294	162	125	37
5	388	212	175	37

*All Q's in mcoul.

These data support the idea of the buildup of an anodic layer which is reduced at more cathodic potentials than the normal platinum- oxygen layer as our earlier results in Section IV on platinized platinum cycled under regime I suggested. Further evidence for the presence of a different type of anodic layer on cycling under this regime can be found in the displacement of the cathodic stripping curves on cycled electrodes to lower potentials as was also found for platinized platinum. It seems that the reason for the observed decrease in Q_{ox} and Q_H after the 504th cycle may be due to the lower discharge potential reached after ~200 cycles which may allow reduction of the anodic layer to occur which cannot take place at +0.8 to +0.9 V.

We have also made separate measurements of the electrochemical surface areas of the floating electrode after cycling. Table LX compares the measured surface areas as given by Q_H before and after the total of 650 cycles. With the exception of cell no. 5 whose behavior seems an anomalous, decreases of 17-38% in surface area do appear to occur. This order of magnitude of a decrease in surface area is approximately the same as that estimated by the weight loss studies.

Table LX. Comparison of Surface Area Measurements on Floating Electrodes Before and After 650 Cycles

Cell No.	Q_H, mcoul		
	Before Cycling	After Cycling	Decrease, %
1	250	183	33
2	200	166	17
3	200	163	18
4	200	125	38
5	170	175	0

In Figs. 97 through 101, we have plotted the anodic and cathodic polarization curves attained in the various cells after the specified number of cycles. There does not appear to be any noticeable effect of cycling on these E-log I curves which were obtained after the state of surface oxidation measurement was taken and thus any anodic layer would be reduced.

3. Full fuel cells

Four complete H_2-O_2 fuel cells were operated under cycling conditions similar to rechargeable H_2-O_2 fuel cells but open-ended. The main reasons for using this configuration were: (1) to ascertain if there were any significant differences in the behavior of rechargeable O_2 electrodes in this configuration as opposed to the floating electrode cells, and (2) to obtain cycled electrodes of suitable size for BET and pore size distribution measurements. Two cells contained 8.5N KOH and had 50 cm^2 electrodes (cells No. 12 and 15), while cells containing

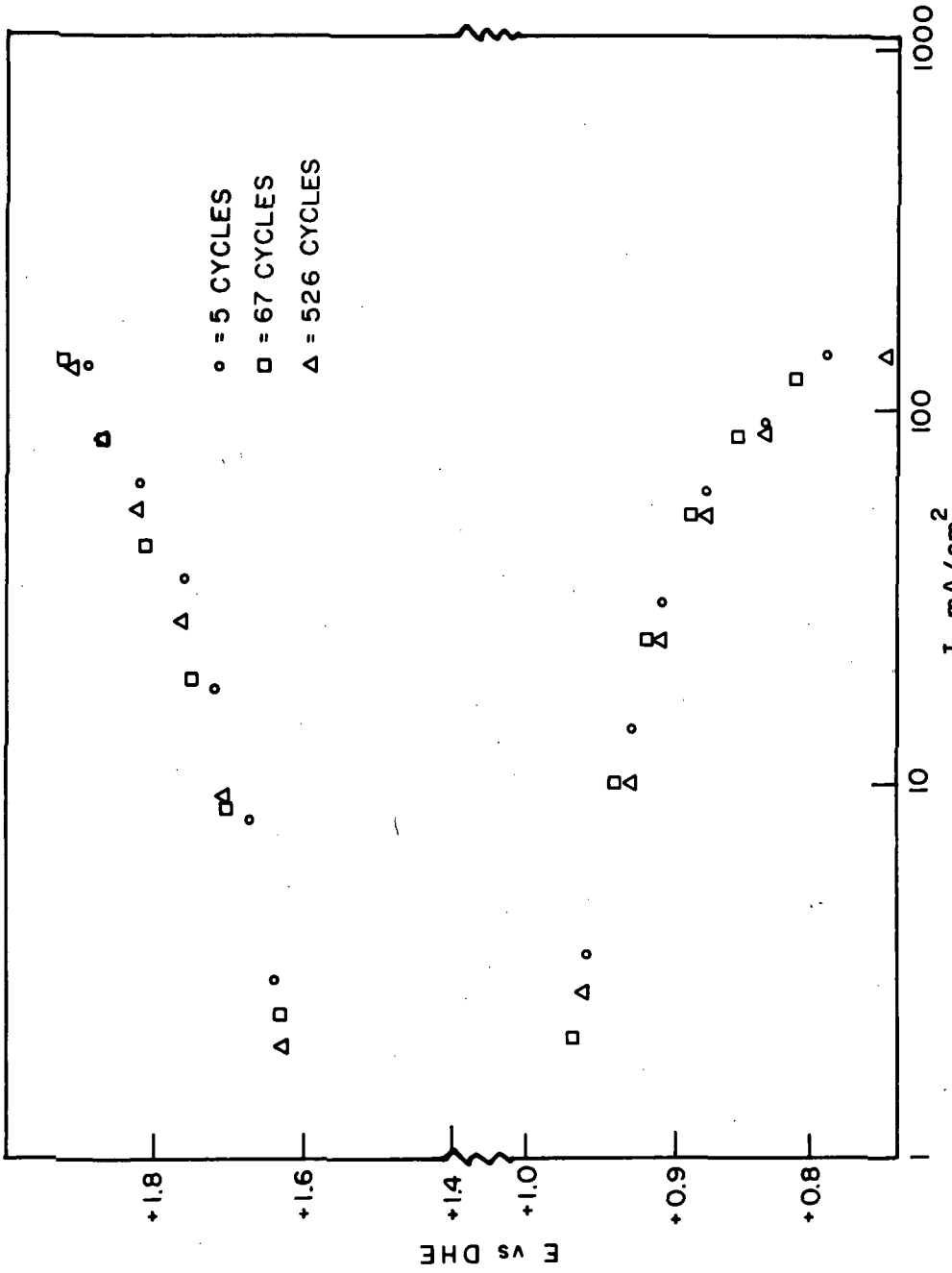

Fig. 97. Polarization behavior of Teflon-bonded platinum black floating electrodes in 8.5N KOH (cell no. 1) after cycling

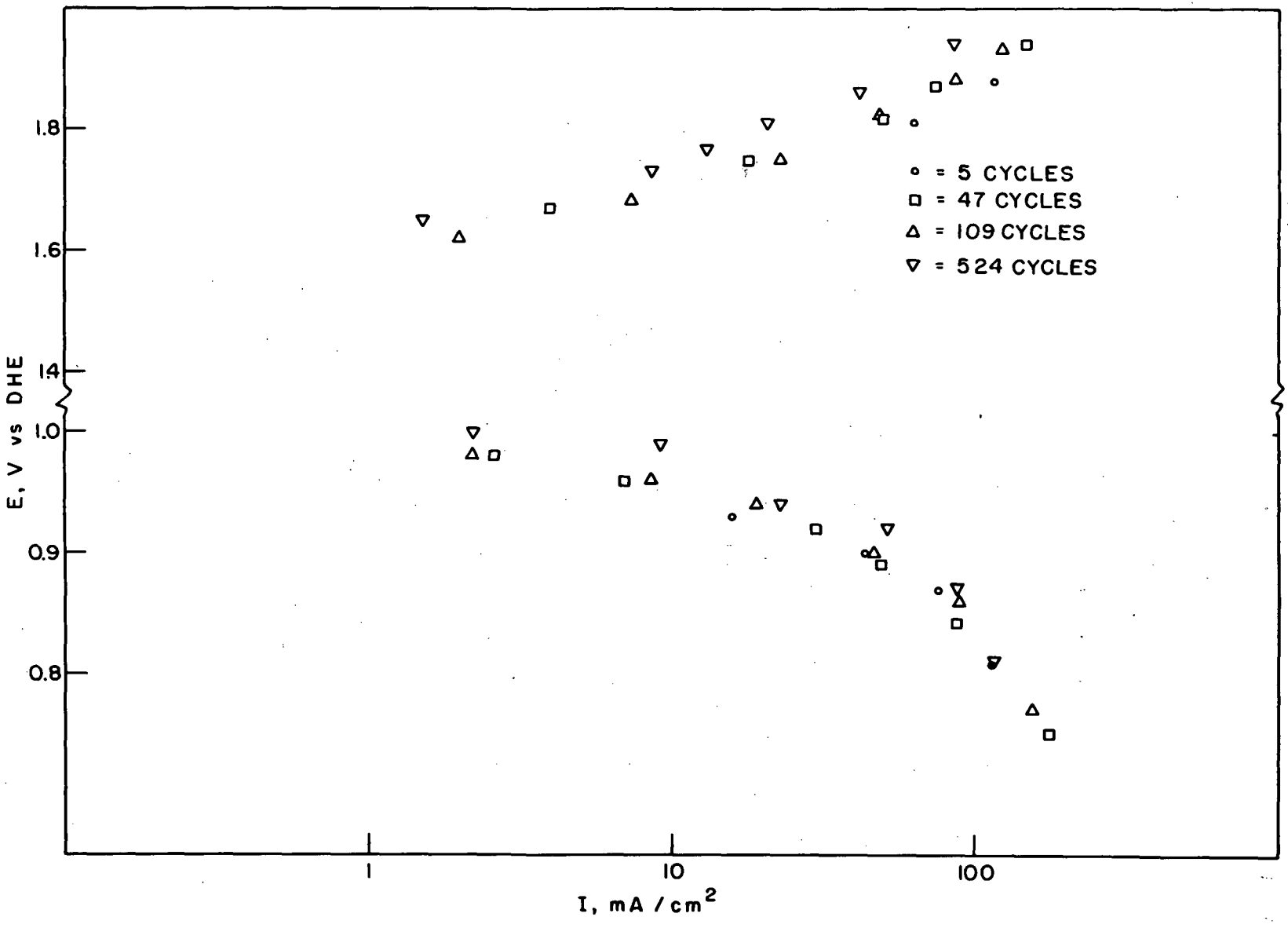

Fig. 98. Polarization behavior of Teflon-bonded platinum-black floating electrodes in 8.5N KOH saturated with Johns-Manville Fuel Cell Asbestos (cell no. 2) after cycling

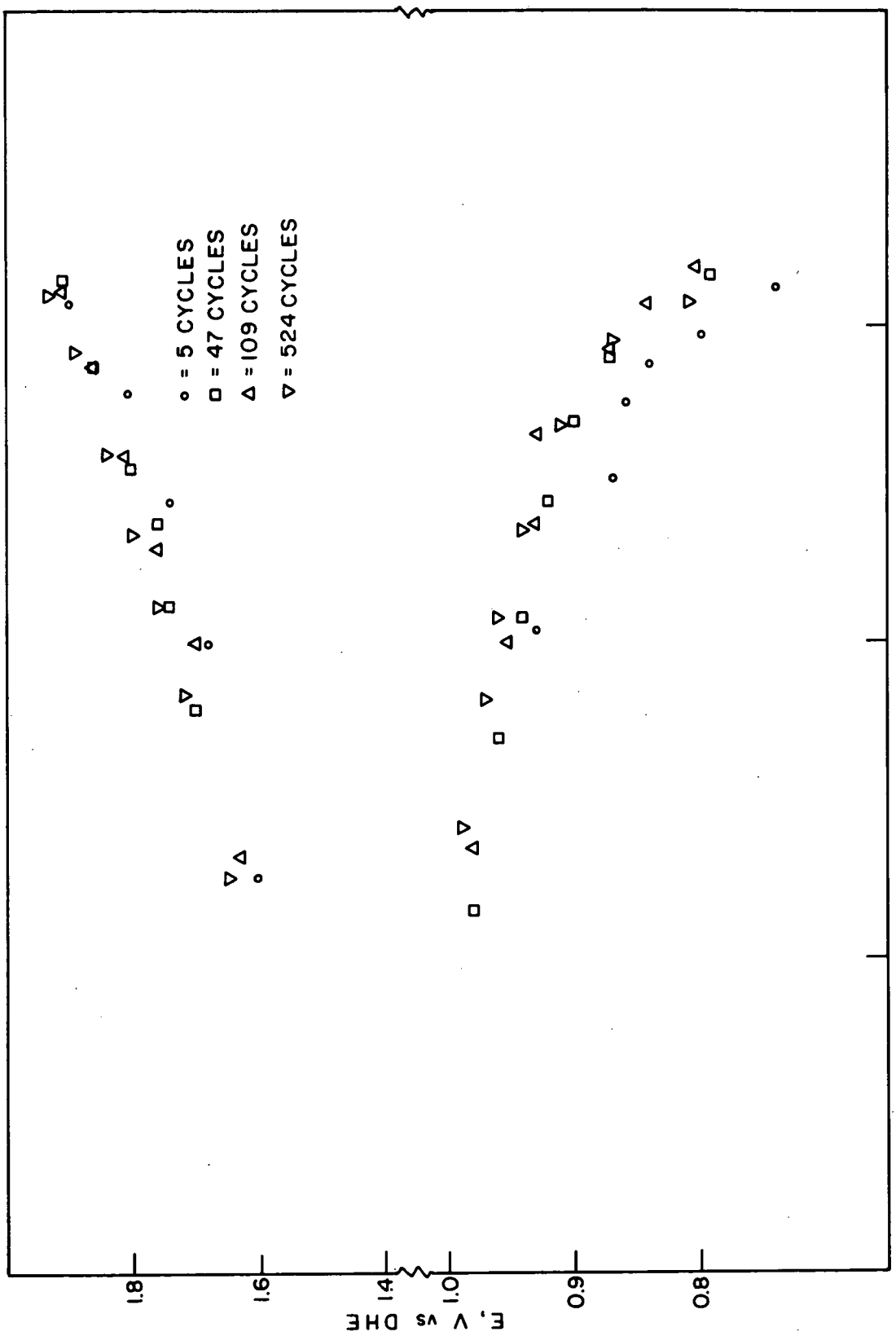

Fig. 99. Polarization behavior of Teflon-bonded platinum black floating electrodes in 8.5N KOH saturated with Fe_2O_3 (cell no. 3) after cycling

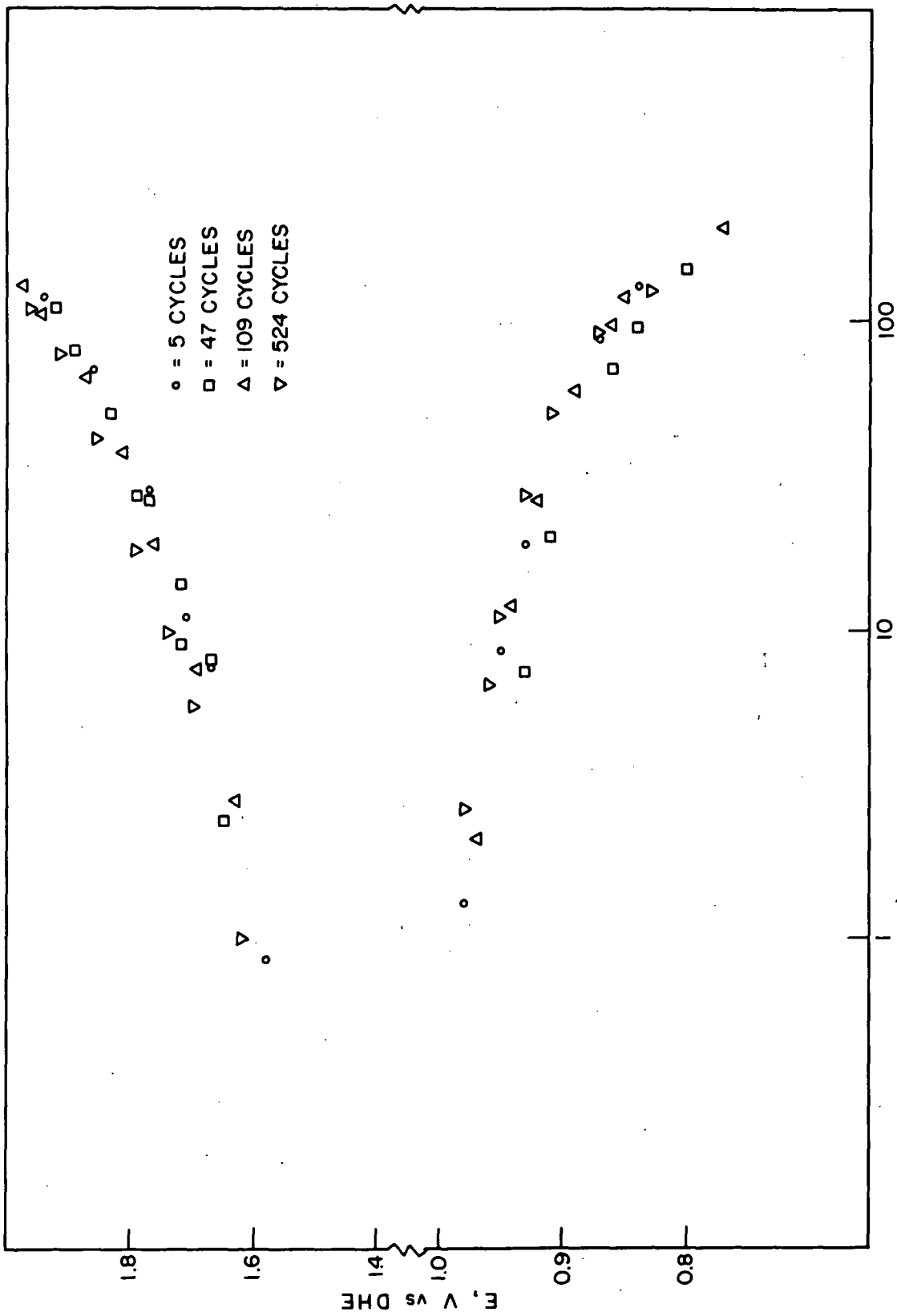

Fig. 100. Polarization behavior of Teflon-bonded platinum black floating electrodes in 6.5N KOH/1M K_2CO_3 (cell no. 4) after cycling

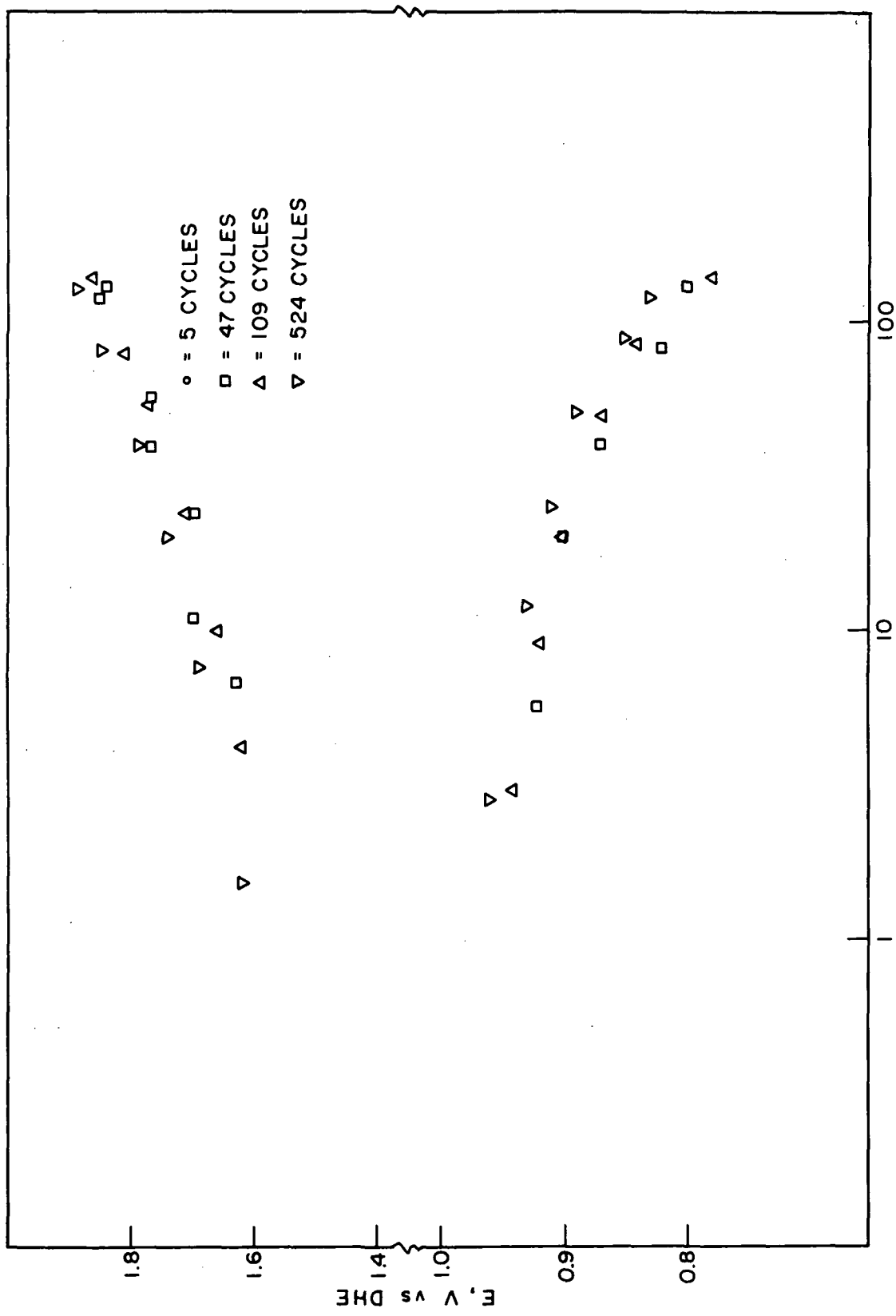

Fig. 101. Polarization behavior of Teflon-bonded platinum black floating electrodes in 8.5N KOH (cell no. 5) after cycling

6.5N KOH/1M K_2CO_3 (cell No. 21) and 8.5N KOH saturated with Fe_2O_3 (cell No. 18) used smaller electrode areas of 7 cm^2.

Considerable difficulty was encountered in the long term operation of these cells, primarily due to: (1) flooding of the O_2 electrode, and (2) shorting out of the cell through the asbestos separator. The first problem necessitated a close control of the O_2 gas flow to control any pressure differential. The occurrence of the second difficulty required replacement of the separator.

Fig. 102 shows the observed voltages for cell No. 12 containing 8.5N KOH which was cycled for 100 times. After 100 cycles, the end-of-discharge voltage has decreased from 0.7 V to a value in the vicinity of 0.5 V. Since the H_2- electrode should contribute very little polarization at these current levels, it is reasonable to attribute this decrease to increased O_2-electrode polarization.

Fig. 103 depicts the potential-time behavior during charge and discharge. During the first cycle, the discharge curve is rather flat, but as cycling proceeds shows a minimum after which the cell voltage gradually increases. On charge, as was observed with the floating electrode cells, rather uniform behavior can be seen.

Cell no. 15 also also contained 8.5N KOH. This cell failed twice during testing, at ~50 cycles and at ~270 cycles. The first failure appeared to be due to flooding since, after a time at open circuit the cell voltage recovered. A short-circuit was the cause of the second failure and the separator was replaced. From Fig. 104 the charge potentials were quite consistent at ~1.80 V, while the discharge potential were somewhat erratic but are in the vicinity of 8.5 V. The potential-time curves during charge and discharge are given in Fig. 105 and show again the tendency for an initial minimum in the discharge curve.

Cell no. 18 contained 8.5N KOH saturated with Fe_2O_3. As Fig. 106 shows, charge potentials were in the area of 1.7 V, while discharge potentials were quite low at ~0.6-0.7 V. At cycle 475, the separator was changed and it can be seen that cell performance improved. The charge and discharge curves for this cell are shown in Fig. 107.

Fig. 108 shows the end-of-charge and discharge voltages for cell no. 21 which contained 6.5N KOH/1M K_2CO_3. Charge voltages were ~1.75 V, while the average discharge voltage was ~0.7 V. At cycle 370, there was some indication that the cell was about to fail and the separator was replaced. Cell performance improved temporarily to 0.8 V on discharge but after 50 cycles had reverted to 0.7 V. The charge and discharge curves for this cell are shown in Fig. 109.

Table LXI shows the measured BET surface area of an uncycled electrode and electrodes cycled for 100 and 500 cycles. There appears to be an increase in surface area of 60% after 500 cycles, while no increase in surface area is observed after 100 cycles. This increase in surface area is confirmed by the pore size distribution plots for these three electrodes shown in Figs. 110 through 112. While no shift in the pore size distribution is observed, the number of pores of a given size (i.e., volume) have increased.

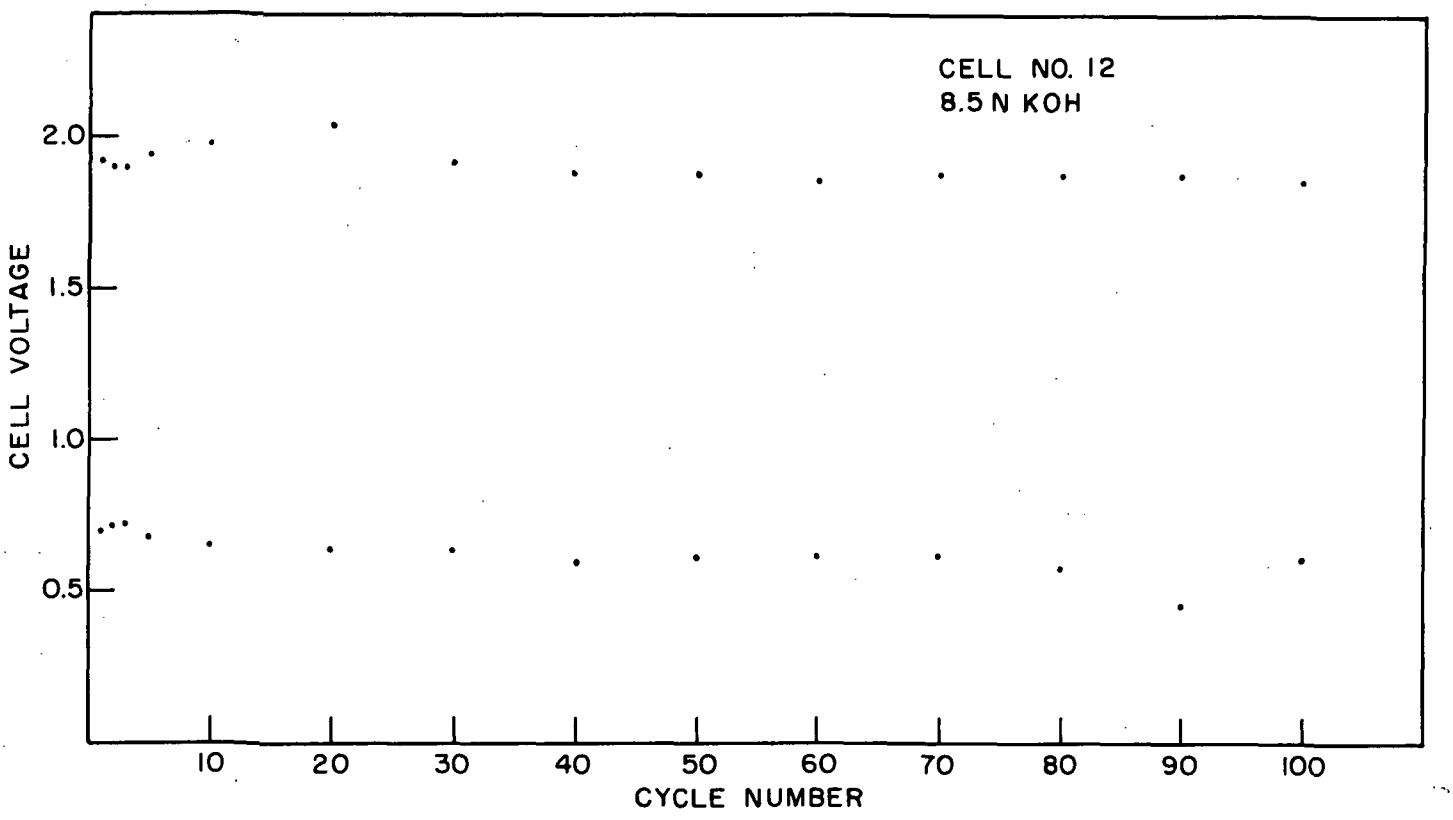

Fig. 102. End-of-charge and discharge voltage for a H_2/O_2 fuel cell (cell no. 12) operating under a cycle regime of a 60 min charge period at 25 mA/cm^2 followed by a 30 min discharge period at 50 mA/cm^2 in a 8.5N KOH electrolyte at 30°C

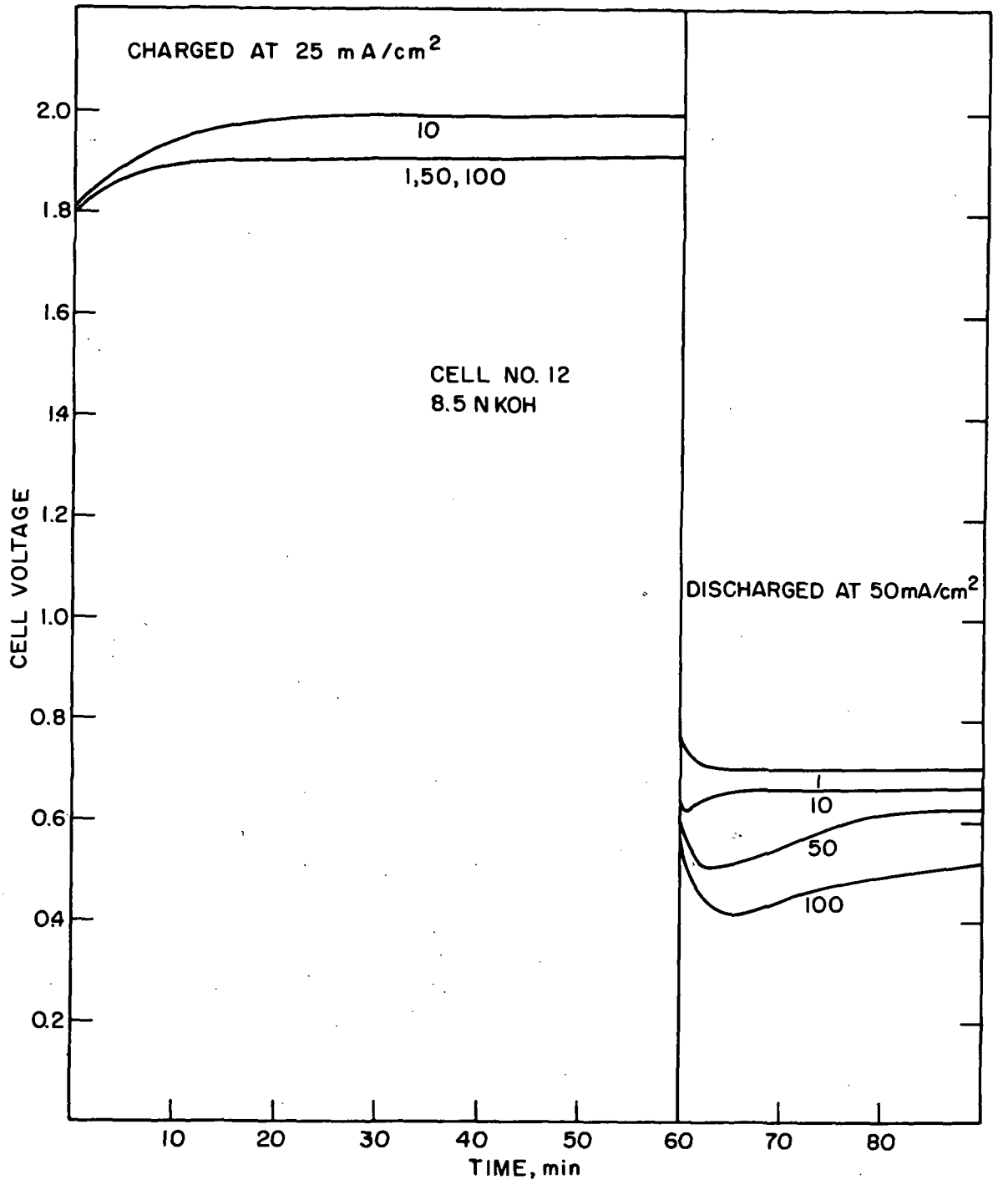

Fig. 103. Voltage-time curves for various cycles during operation of a H_2/O_2 fuel cell (cell no. 12) under a cycle regime of a 60 min charge period at 25 mA/cm^2 followed by a 30 min discharge period at 50 mA/cm^2 in a 8.5N KOH electrolyte at 30°C

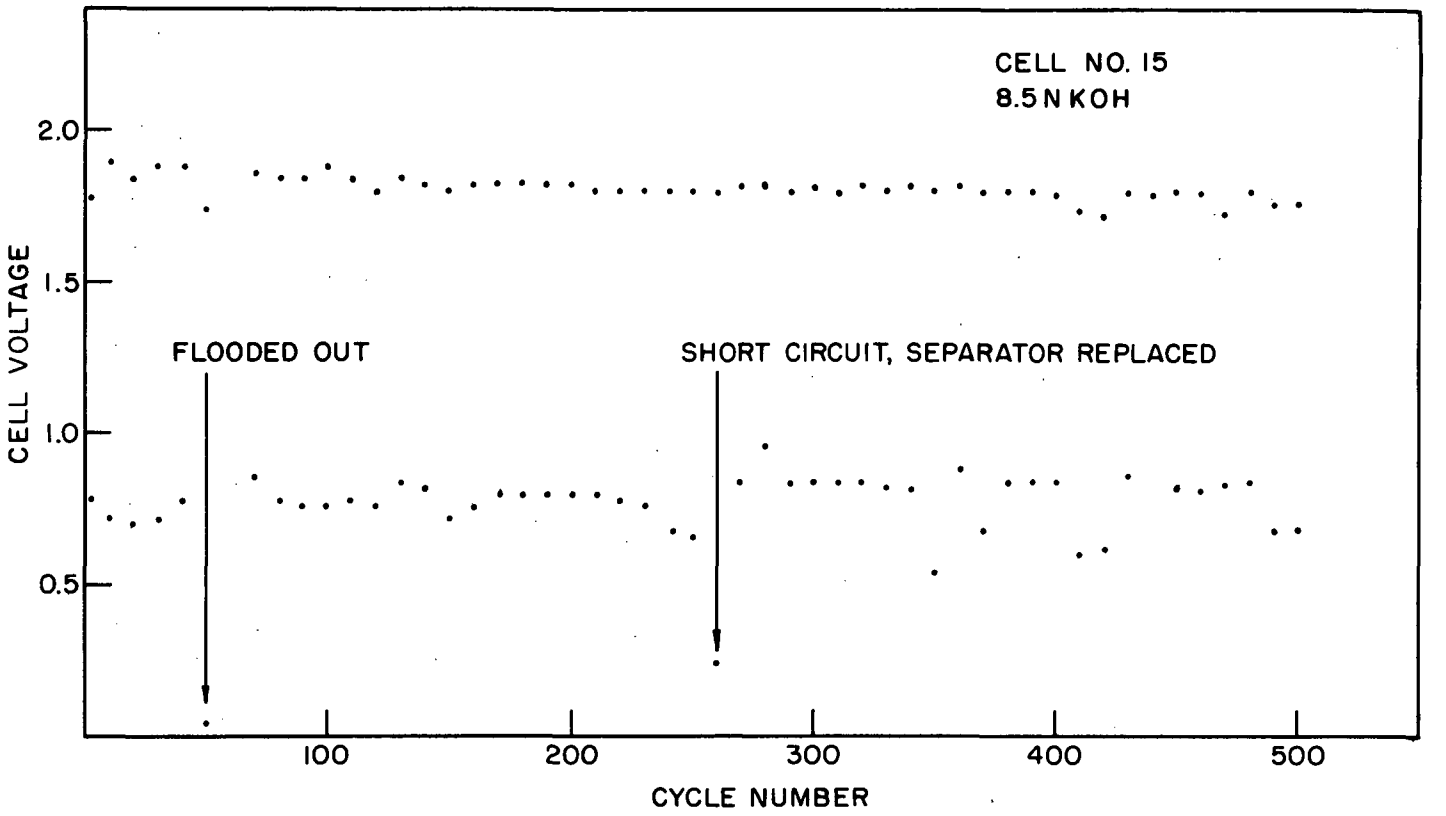

Fig. 104. End-of-charge and discharge voltages for a H_2/O_2 fuel cell (cell no. 15) operating under a cycle regime of a 60 min charge period at 25 mA/cm^2 followed by a 30 min discharge period at 50 mA/cm^2 in a 8.5N KOH electrolyte at 30°C

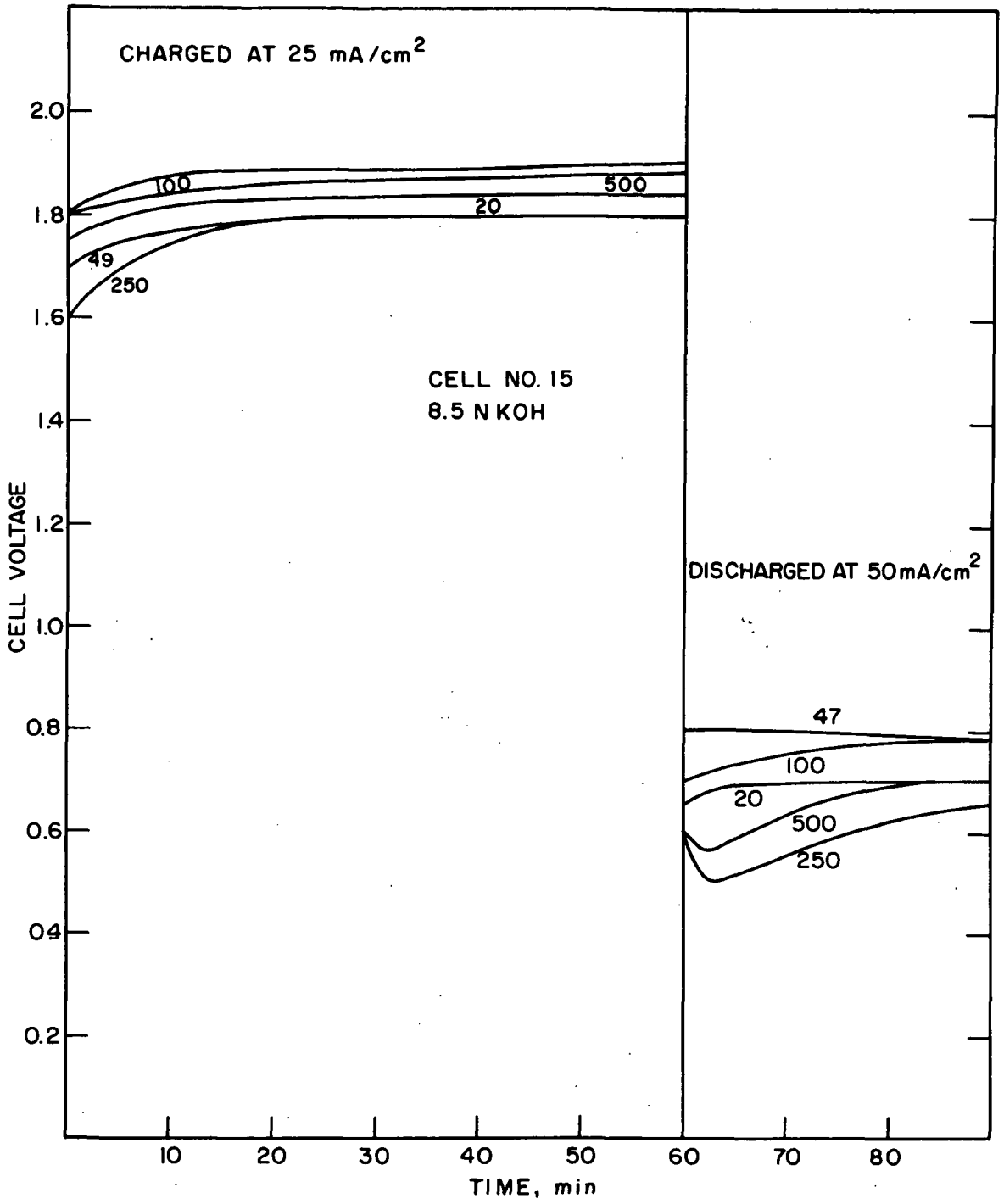

Fig. 105. Voltage-time curves for various cycles during operation of an H_2/O_2 fuel cell (cell no. 15) under a cycle regime of a 60 min charge period at 25 mA/cm^2 followed by a 30 min discharge period at 50 mA/cm^2 in a 8.5N KOH electrolyte at 30°C

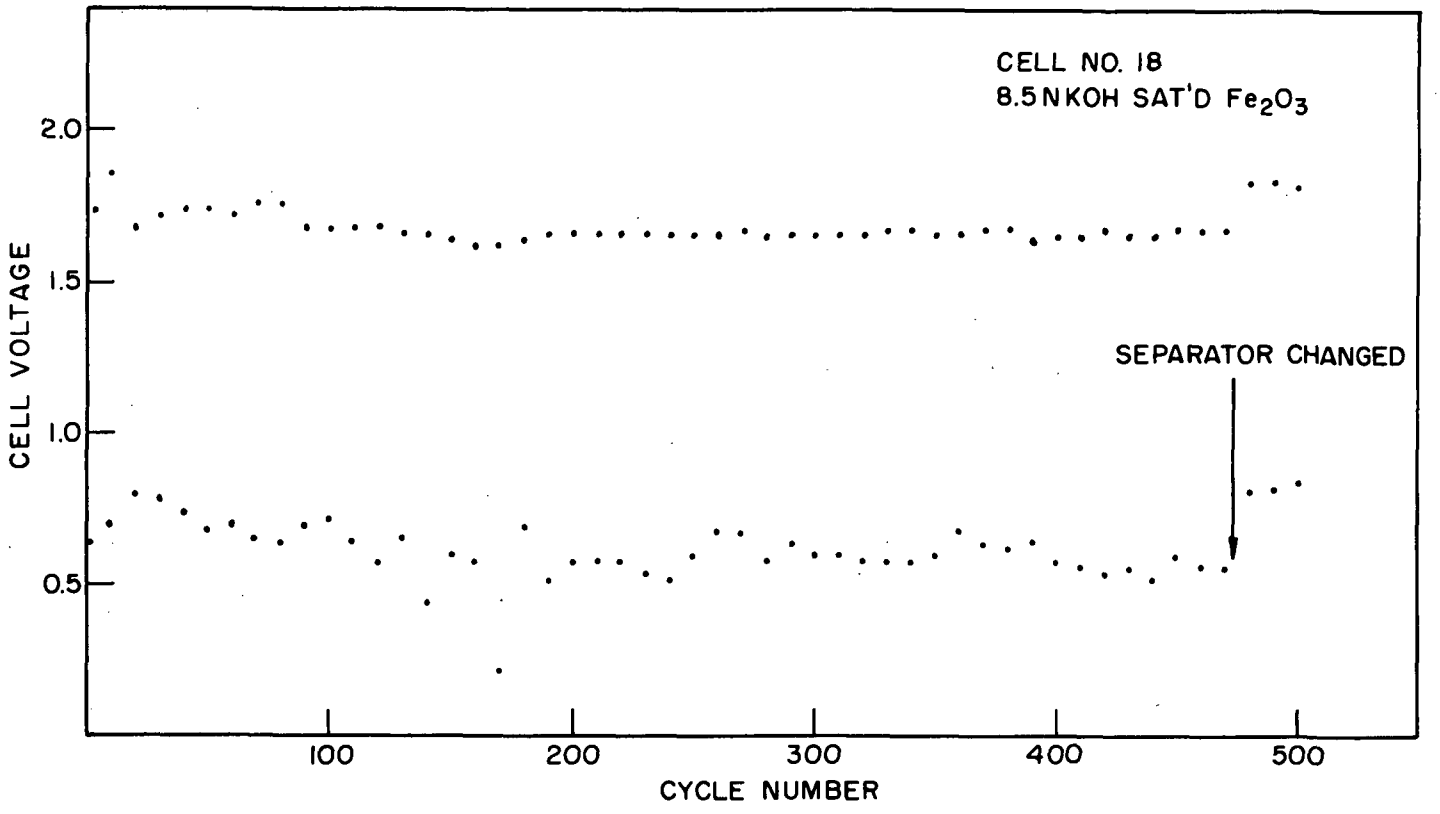

Fig. 106. End-of-charge and discharge voltages for a H_2/O_2 fuel cell (cell no. 18) operating under a cycle regime of a 60 min charge period at 25 mA/cm^2 followed by a 30 min discharge period at 50 mA/cm^2 in a 8.5N KOH electrolyte saturated with Fe_2O_3 at 30 °C

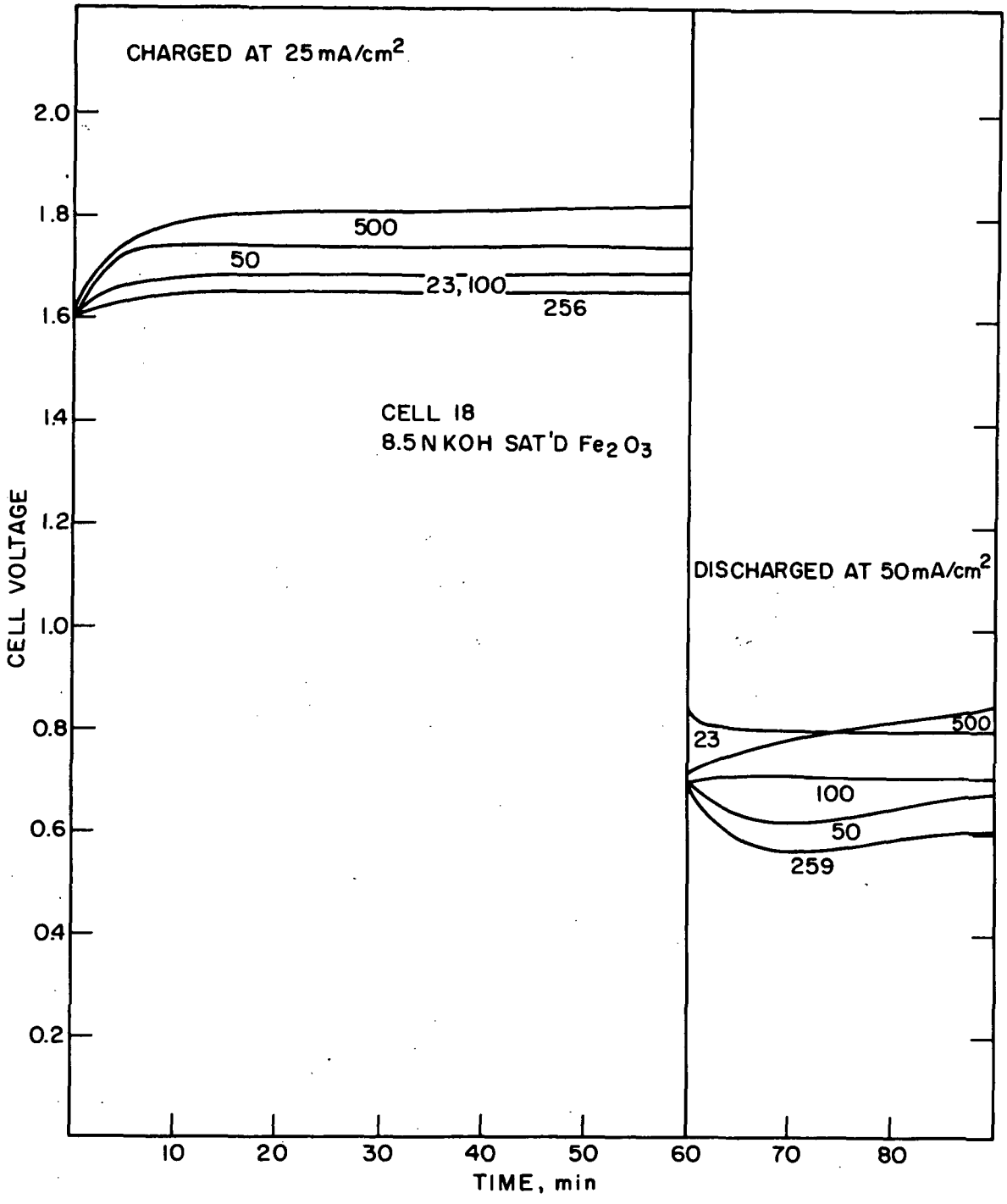

Fig. 107. Voltage-time curves for various cycles during operation of a H_2/O_2 fuel cell (cell no. 18) under a cycle regime of a 60 min charge period at 25 mA/cm^2 followed by a 30 min discharge period at 50 mA/cm^2 in a 8.5N KOH electrolyte saturated with Fe_2O_3 at 30 °C

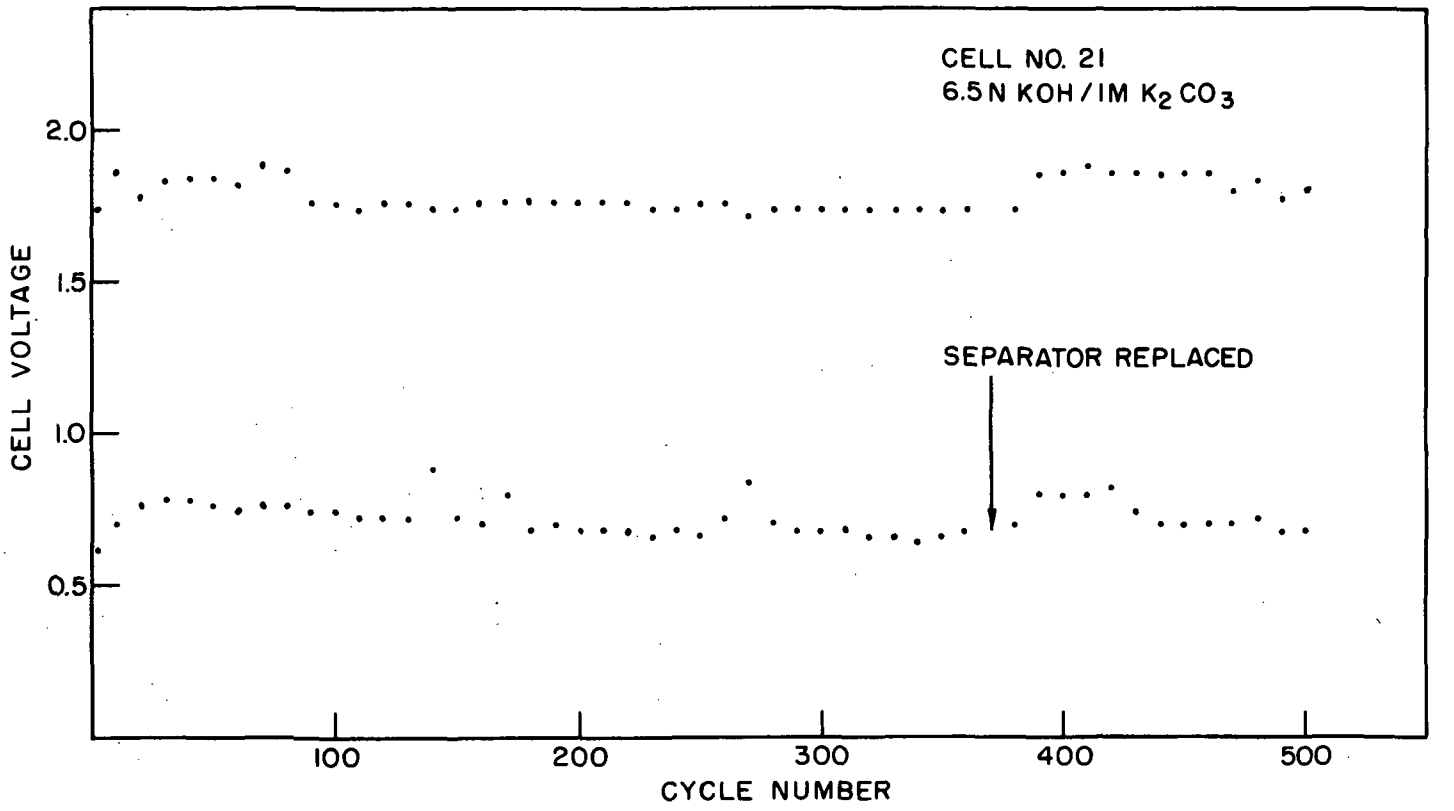

Fig. 108. End-of-charge and discharge voltages for a H_2/O_2 fuel cell (cell no. 21) operating under a cycle regime of a 60 min charge period at 25 mA/cm^2 followed by a 30 min discharge period at 50 mA/cm^2 in a 6.5N KOH/1M K_2CO_3 electrolyte at 30°C

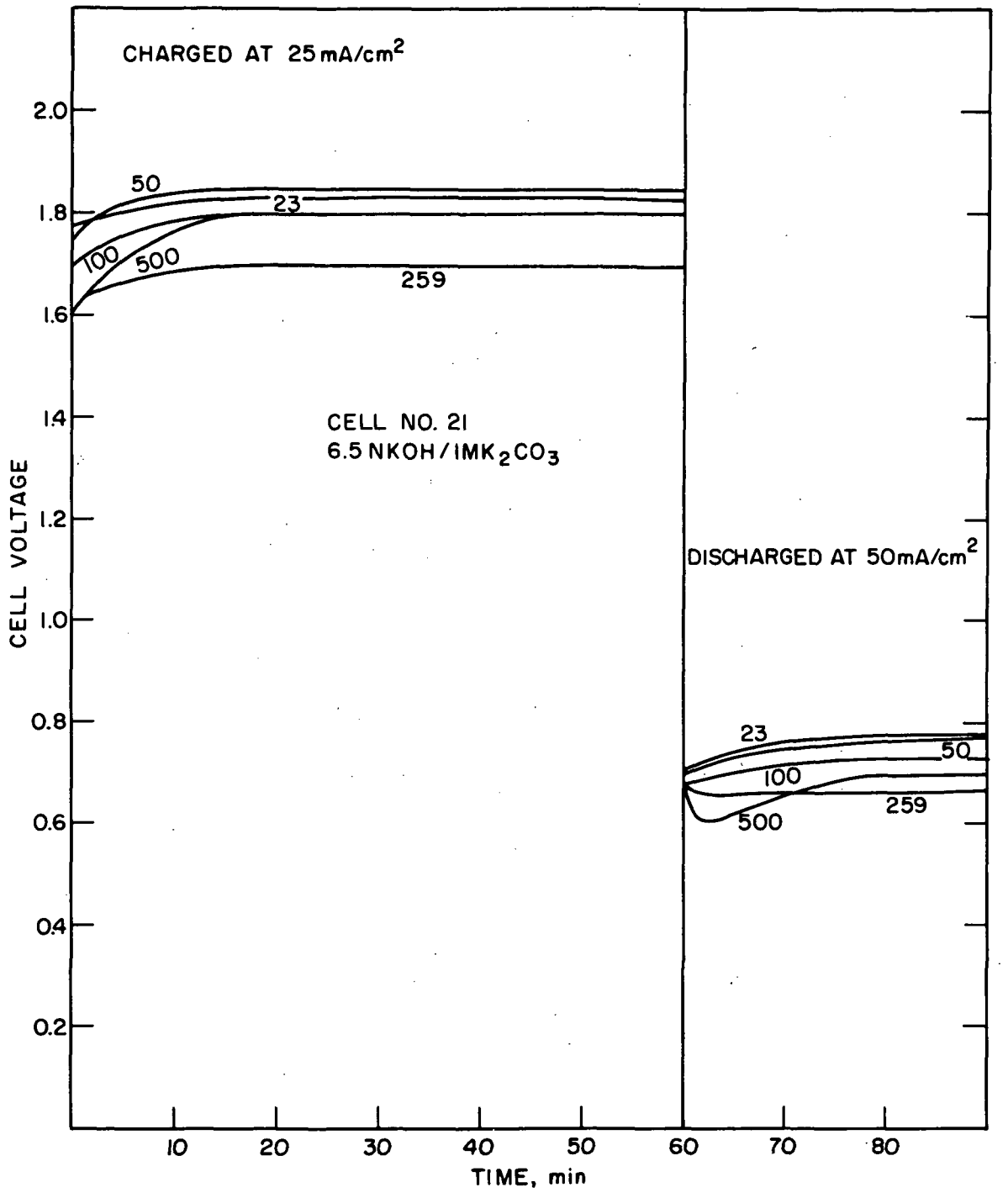

Fig. 109. Voltage-time curves for various cycles during operation of a H_2/O_2 fuel cell (cell no. 21) under a cycle regime of a 60 min charge period at 25 mA/cm^2 followed by a 30 min discharge period at 50 mA/cm^2 in a 6.5N KOH/1M K_2CO_3 electrolyte at 30 °C

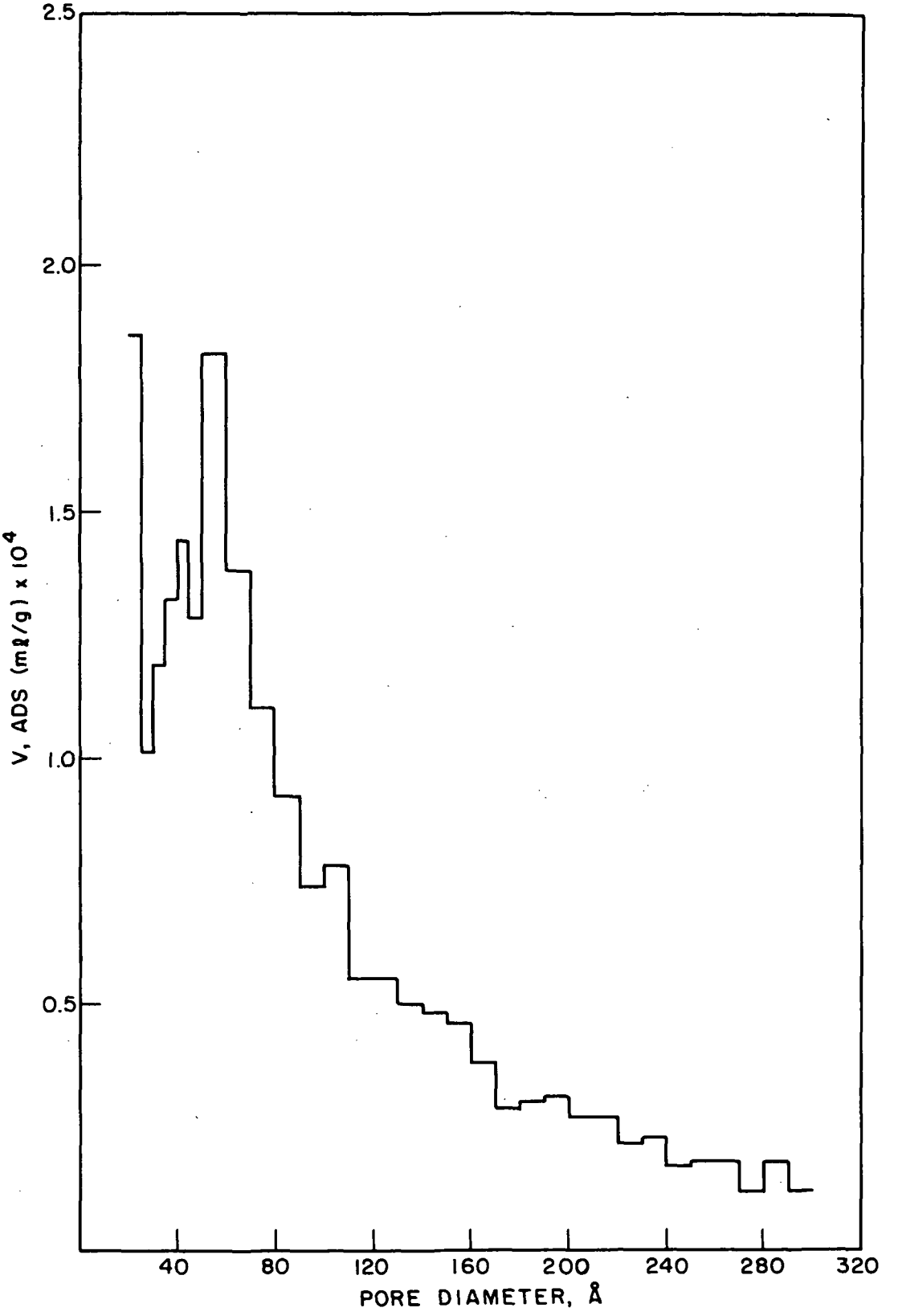

Fig. 110. Pore size distribution of uncycled Teflon-bonded platinum black electrode material

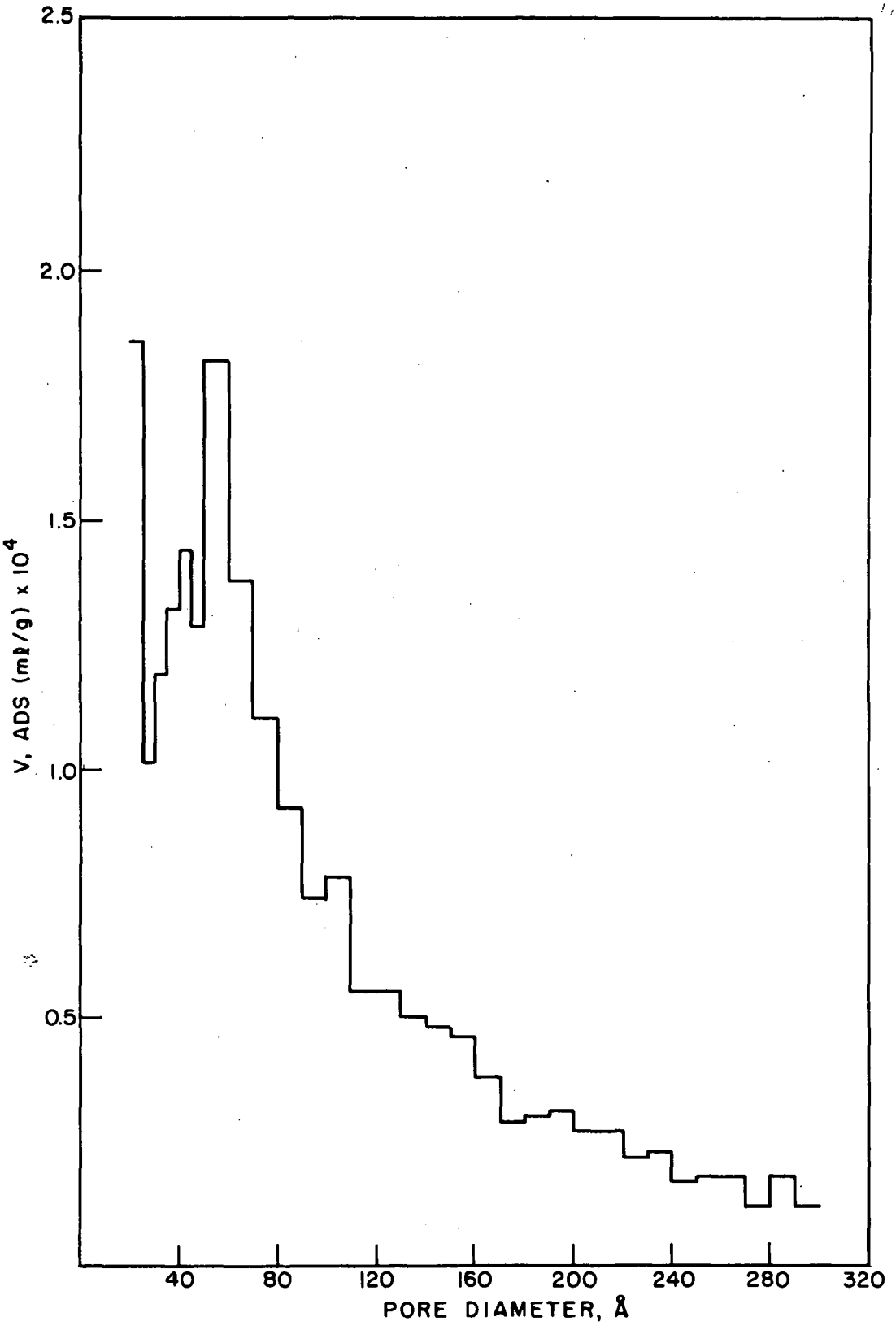

Fig. 111. Pore size distribution of Teflon-bonded platinum black electrode material after 100 cycles

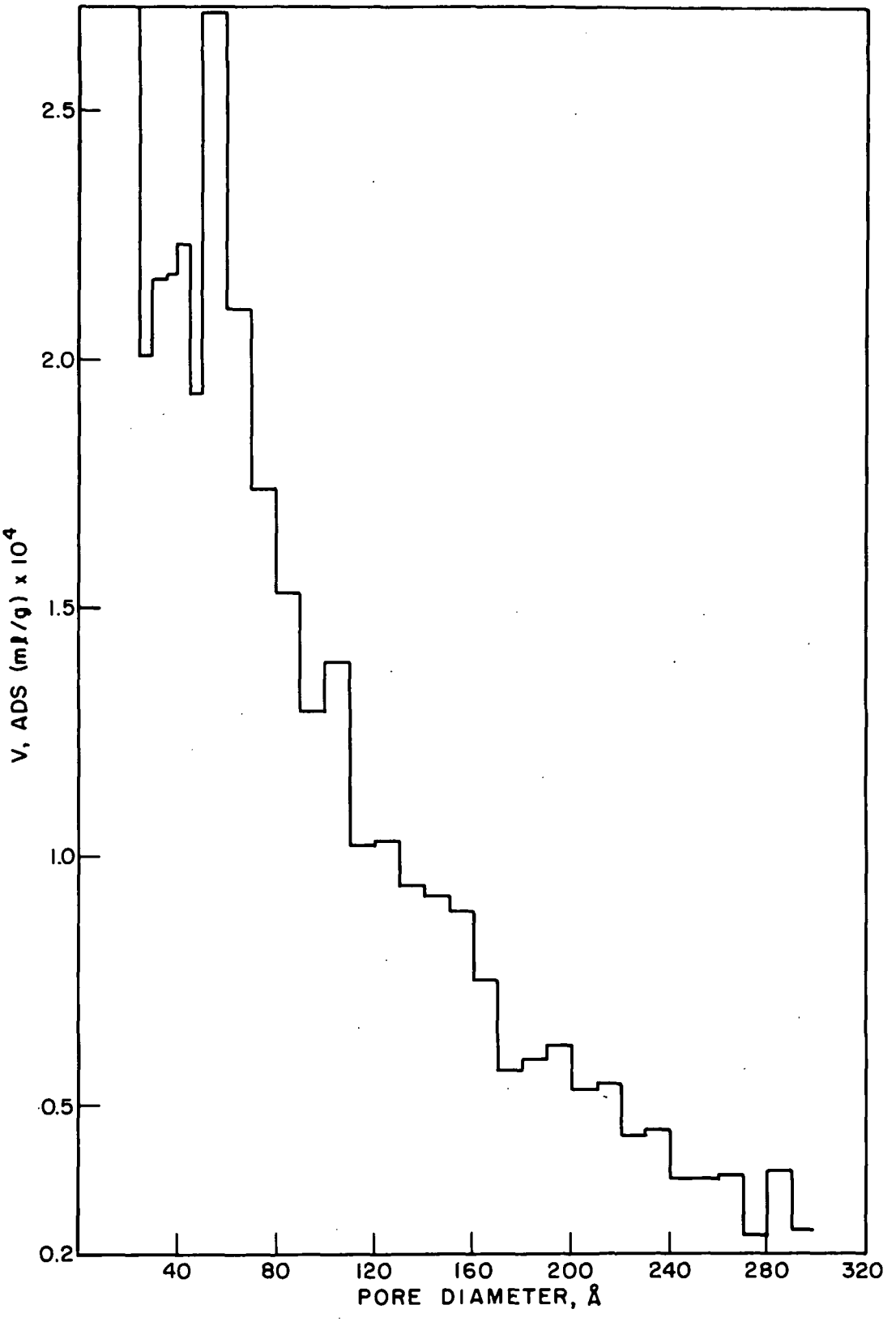

Fig. 112. Pore size distribution of Teflon-bonded platinum black electrode material after 500 cycles

Table LXI. BET Surface Area of Uncoupled Teflon-Bonded Platinum Electrode Material and Electrode Cycled 100 and 500 Times

Material	BET area, m^2/g
Uncycled	1.64
Cycled 100 times	1.63
Cycled 500 times	2.34

The average crystallite size as measured by X-ray line broadening is given in Table LXII for the uncycled electrode material and electrodes cycled 100 and 500 times. Table LXII reveals no definite indication of cyrstallite size changes with cycling within the precision of the method, ±20%. While BET surface area increases have been observed after 500 cycles, this does not necessarily lead to decreased particle size since micro-roughening of the crystallite can occur which is not detectable by X-ray line broadening.

Table LXII. Results of X-Ray Line Broadening Average Particle Size Measurements on Uncycled Teflon-Bonded Electrode Material and Electrodes Cycled 100 and 500 Times

	Average Particle Size, Å		
Reflecting Plane	Uncycled	100 Cycles	500 Cycles
<111>	190	210	180
<200>	150	200	160
<220>	160	180	145
<311>	145	160	145

We have used the scanning electron microscope in an attempt to detect changes in the microstructure of the Teflon-bonded electrodes with cycling. A major difficulty here is the problem of suitable sample preparation due to the rather soft electrode texture. This leads to smearing of the visable surface when sectioned as Fig. 113 demonstrates. Fig. 113 a and b are low magnification views (200X, 500X) of American Cyanamid AB-40 Fuel Cell electrode material which shows the loss in surface definition when sectioned at room temperature. Bending or cracking of the electrode in liquid nitrogen so as to expose the internal surface was somewhat more successful as Fig. 114 a and b demonstrate. Sectioning of the electrode in liquid nitrogen was found to be the most promising procedure.

In Fig. 115 and 116, we compare a series of micrographs of uncycled and cycled (500 times) electrode material sectioned under liquid nitrogen at magnifications up to 10K. It is

A

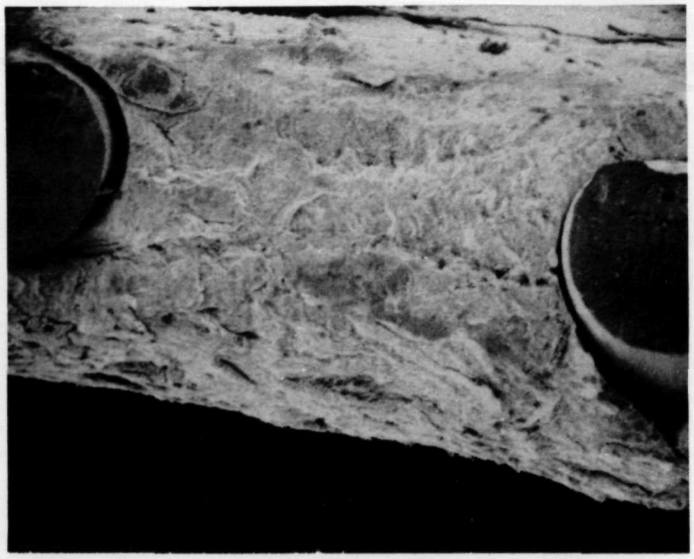

B

Fig. 113. Scanning electron micrographs of American Cyanamid Fuel Cell Electrode Material (AB-40) sectioned at room temperature (A = 200X, B = 500X)

A

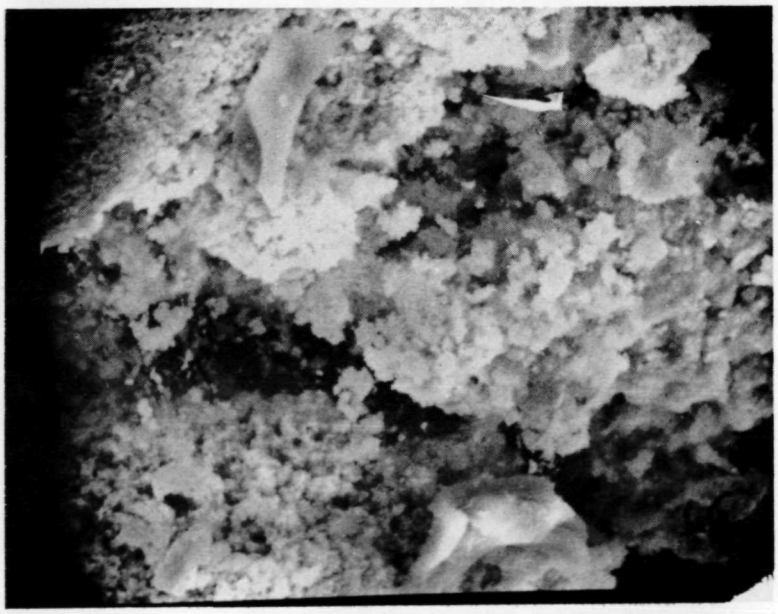

B

Fig. 114. Scanning electron micrographs of Teflon-bonded platinum black electrode material (11 mg Pt/cm^2) cracked under liquid nitrogen (A = 100X, B = 1000X)

A

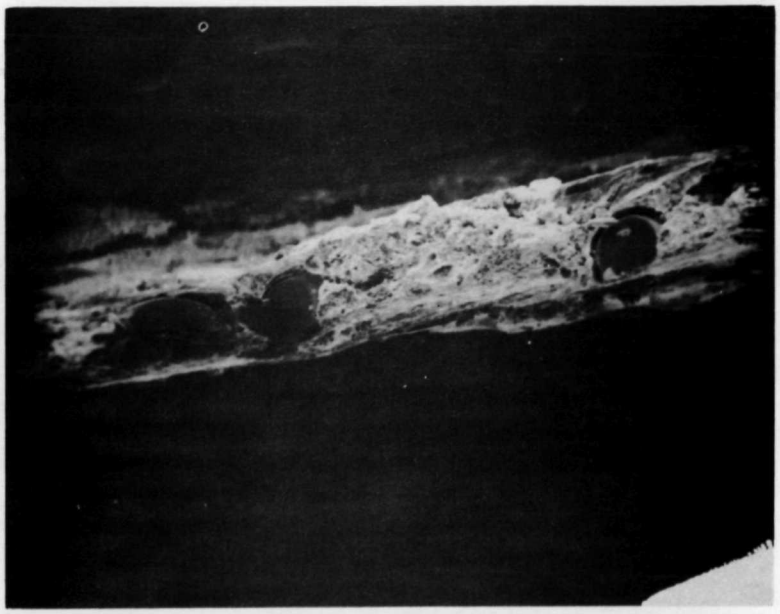

B

Fig. 115. Scanning electron microscope views of uncycled Teflon-bonded platinum black electrode material (11 mg Pt/cm^2) sectioned under liquid nitrogen (A = 100X, B = 500X)

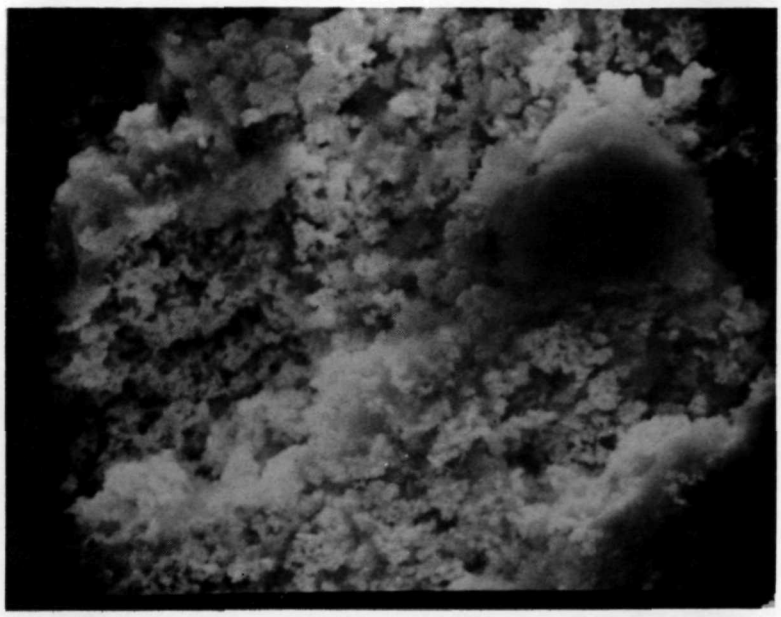

C

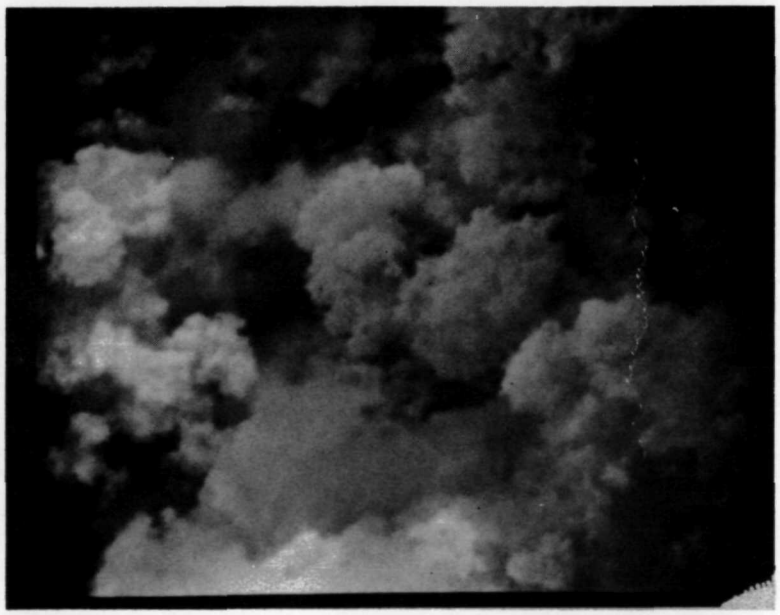

D

Fig. 115. Scanning electron microscope views of uncycled Teflon-bonded platinum black electrode material (11 mg Pt/cm^2) sectioned under liquid nitrogen (C = 2000X, D = 10,000X)

A

B

Fig. 116. Scanning electron micrographs of Teflon-bonded platinum black electrode material after 500 cycles, sectioned under liquid nitrogen (A = 100X, B = 500X)

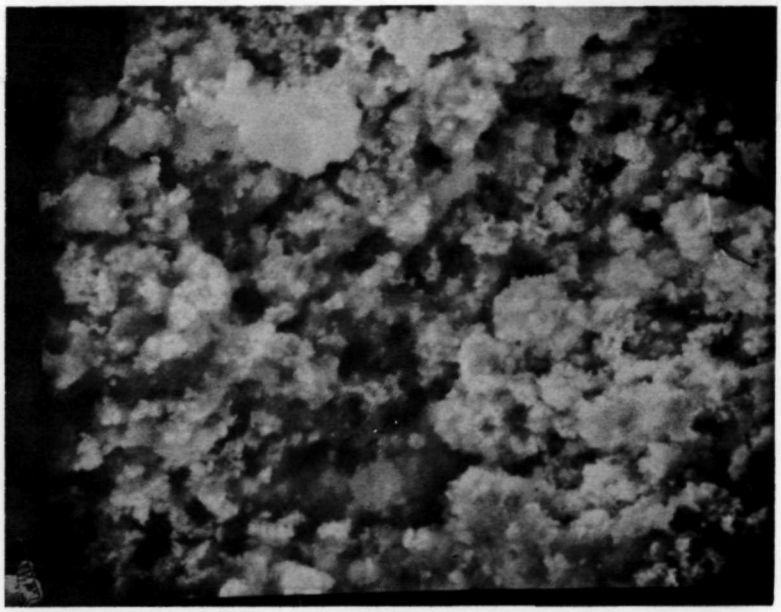

C

D

Fig. 116. Scanning electron micrographs of Teflon-bonded platinum black electrode material after 500 cycles, sectioned under liquid nitrogen (C = 2000X, D = 10,000X)

quite difficult to ascertain any specific structural difference between cycled and uncycled electrodes from these micrographs.

We have also examined the separator of those cells where shorting was encountered. In Fig. 117 a and b, we show the oxygen side and hydrogen side of a separator which was taken from cell no. 15. While little discoloration is observed on the oxygen electrode face, a greyish-blue color is distinguishable on the hydrogen side. Similar results have been reported elsewhere. This accumulation of colored material on the hydrogen side of the separator is even more strikingly depicted in Fig. 118 which shows a sectional separator. A well-defined blue-grey layer is found on the hydrogen electrode side of the separator. Analyses of the separator material for nickel, which may have resulted from the AB-40 gold-plated nickel screen electrode, were negative. A semiquantitative estimation of the platinum content of this separator was made using spectrophotometric analysis of a section of the separator and a value of ~3 mg of platinum was estimated for the complete separator. These results would seem to indicate that the losses of platinum are rather small, which would be in agreement with weight loss studies of this electrode which showed negligible weight loss.

Since it was observed that cathodic treatment seemed to rejuvenate the floating oxygen electrode test cells, some similar experiments were performed with the full fuel cells. Fig. 119 shows the effects of temporarily short-circuiting for 3 min to ~0.05 V, the cell recovered to a very respectable value of ~0.87 V. While the other cells were not behaving quite as poorly as cell no. 15, they too showed better performance after they were temporarily short-circuited. Other experiments showed that short-circuiting for times on the order of 1 sec was also effective in restoring cell voltages.

These experiments and those conducted with the floating electrodes and at the RRDE all indicated that the performance of rechargeable oxygen electrodes may be improved by temporary periods at low anodic potentials at the beginning of the discharge period. In practice, this may be effected by an initial high rate discharge period. Further work in this area is indicated especially on such factors as the discharge rates and period necessary to maintain cell performance in this manner and the thermal effects of such high rate discharges.

D. Conclusions

The deterioration in performance of rechargeable Teflon-bonded platinum-black oxygen electrodes on extended cycling appears to be largely due to the buildup of a refractory anodic layer. Removal of this anodic layer by cathodic polarization restores electrode activity. Some decrease in performance may be due to loss of platinum electrocatalyst, observed with electrodes tested in the floating electrode configuration, where a 10-20% loss of the catalyst was found. Platinum which is lost from the oxygen electrode appears to migrate through the separator to the hydrogen side of the separator and can cause short-circuits during full cell operation. No definite changes in catalyst crystallite size with cycling have been observed, although a BET surface area increase has been observed for an electrode cycled for ~900 hours. There is no

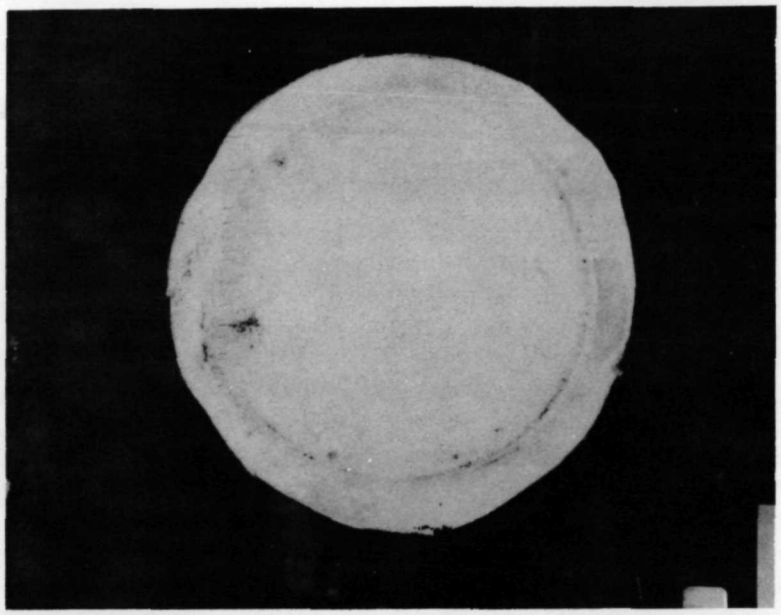

A

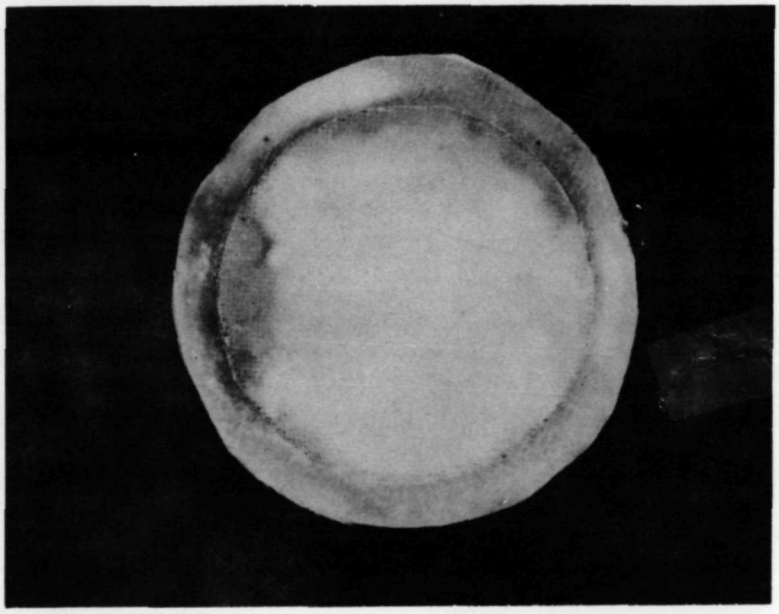

B

Fig. 117. Photographs of the asbestos separator from a shorted-out H_2/O_2 fuel cell (A = oxygen side, B = hydrogen side)

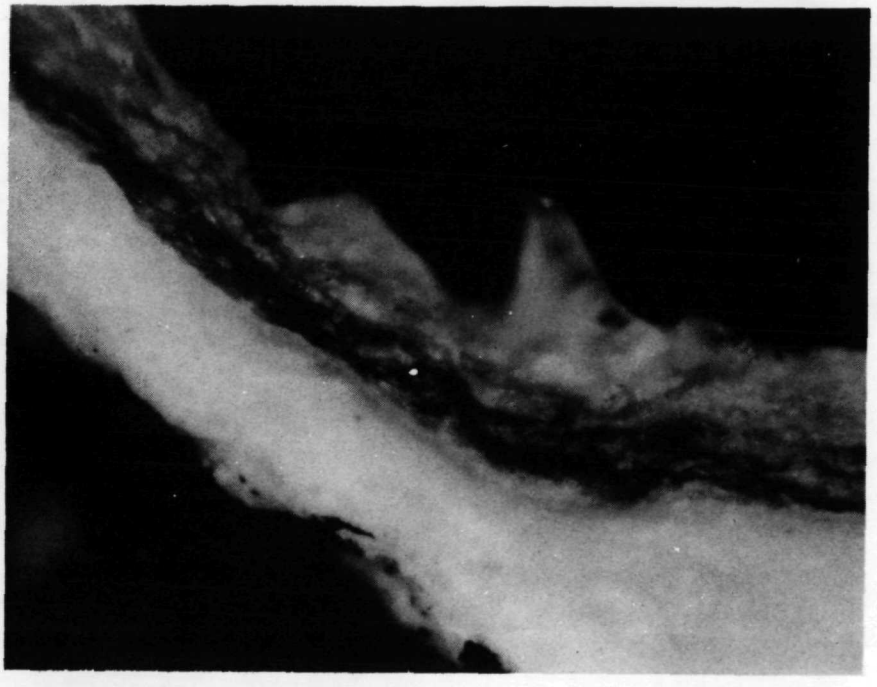

Fig. 118. Photographs of a sectioned asbestos separator from a shorted-out H_2/O_2 fuel cell at a magnification of 50X

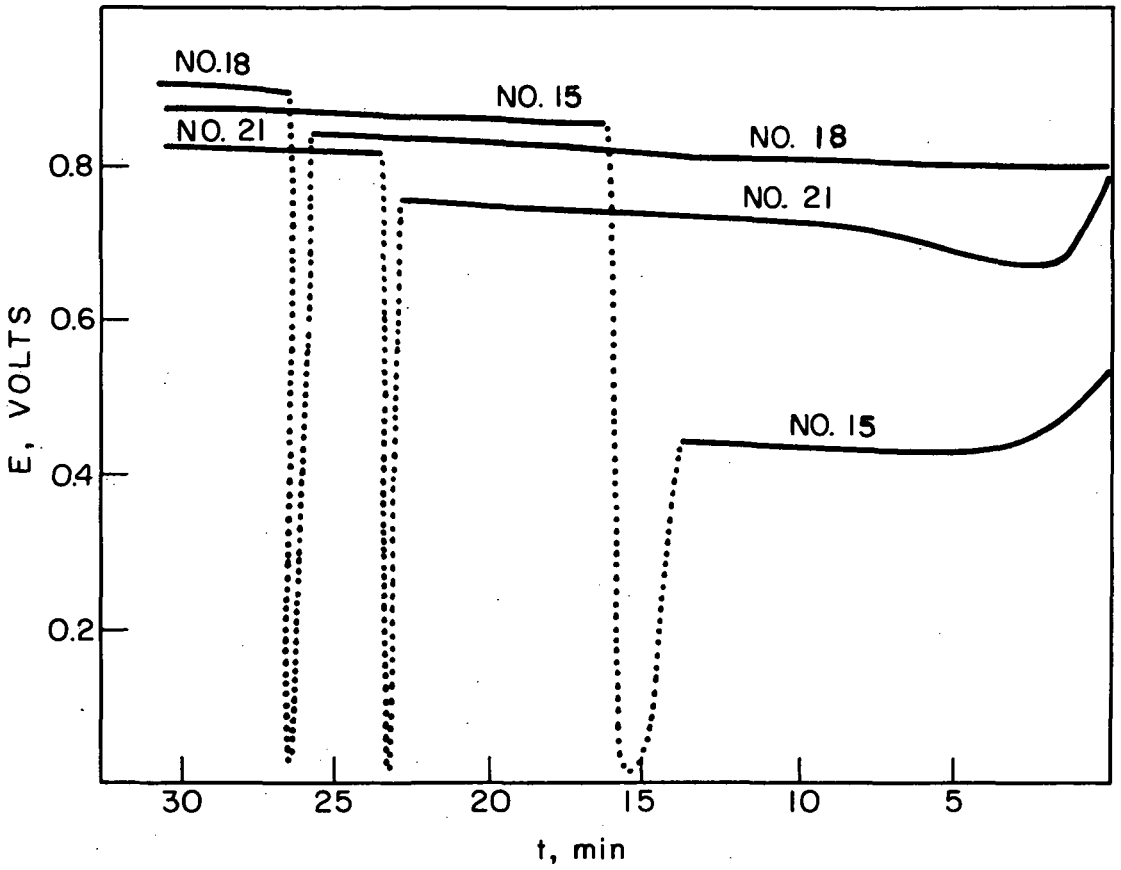

Fig. 119. Effect of temporarily short-circuiting operating H_2/O_2 fuel cells.

appreciable formation of hydrogen peroxide. There is limited evidence to indicate that carbonate is not deleterious to the operation of such fuel cells and may in fact improve performance on extended cycling. However, this effect needs further experimental verification. Ferric ion has no visible effect on cell behavior or cycle life.

IX. APPLICATION OF THE FLOODED AGGLOMERATE CONCEPT TO RECHARGEABLE OXYGEN ELECTRODES

A. Introduction

A working mechanism of the Teflon-bonded electrode, a simplified model of this electrode, and a mathematical treatment of this model have been presented elsewhere.[73] The proposed working mechanism has been confirmed by experimental determination of physical characteristics of the electrode[72] and the proposed model has been applied to the reduction of oxygen on Pt-Teflon in 30% KOH at 80°C. In this section, we will use this model to discuss the rechargeable oxygen electrode.

B. The Flooded Agglomerate Model

In the following, we will describe briefly our understanding of the Teflon-bonded electrode, the simplified model (with the assumptions used for the mathematical treatment), and the main conclusions obtained using this treatment.

We believe that, in a Teflon-bonded electrode, the catalyst particles form porous, electronically conductive agglomerates which under working conditions are completely flooded with electrolyte. These catalyst agglomerates are held together by the Teflon binder which in addition creates hydrophobic gas channels. When current is drawn from the electrode, reactant gas diffuses through the hydrophobic channels, dissolves in the electrolyte contained in the agglomerates and reacts on available sites of the catalyst particles. To treat quantitatively this working mechanism, we substitute a column of flooded agglomerates perpendicular to the electrode surface by a porous cylinder of radius r_o and length h (as shown in Fig. 120), in which catalyst particles and electrolyte are homogeneously dispersed as a continuum. (Microporosity, θ, is defined as the volume of electrolyte per total volume of cylinder.) During operation, gas arrives at the lateral surface of the cylinder and diffuses radially to its center, with simultaneous reaction on catalyst particles in the diffusion path. Ionic current is conducted in the axial direction of the cylinder.

For the mathematical treatment we further assume that:

1. The electrode is made up of a number of porous cylinders of catalyst flooded with electrolyte. These cylinders are perpendicular to the external surface of the electrode.

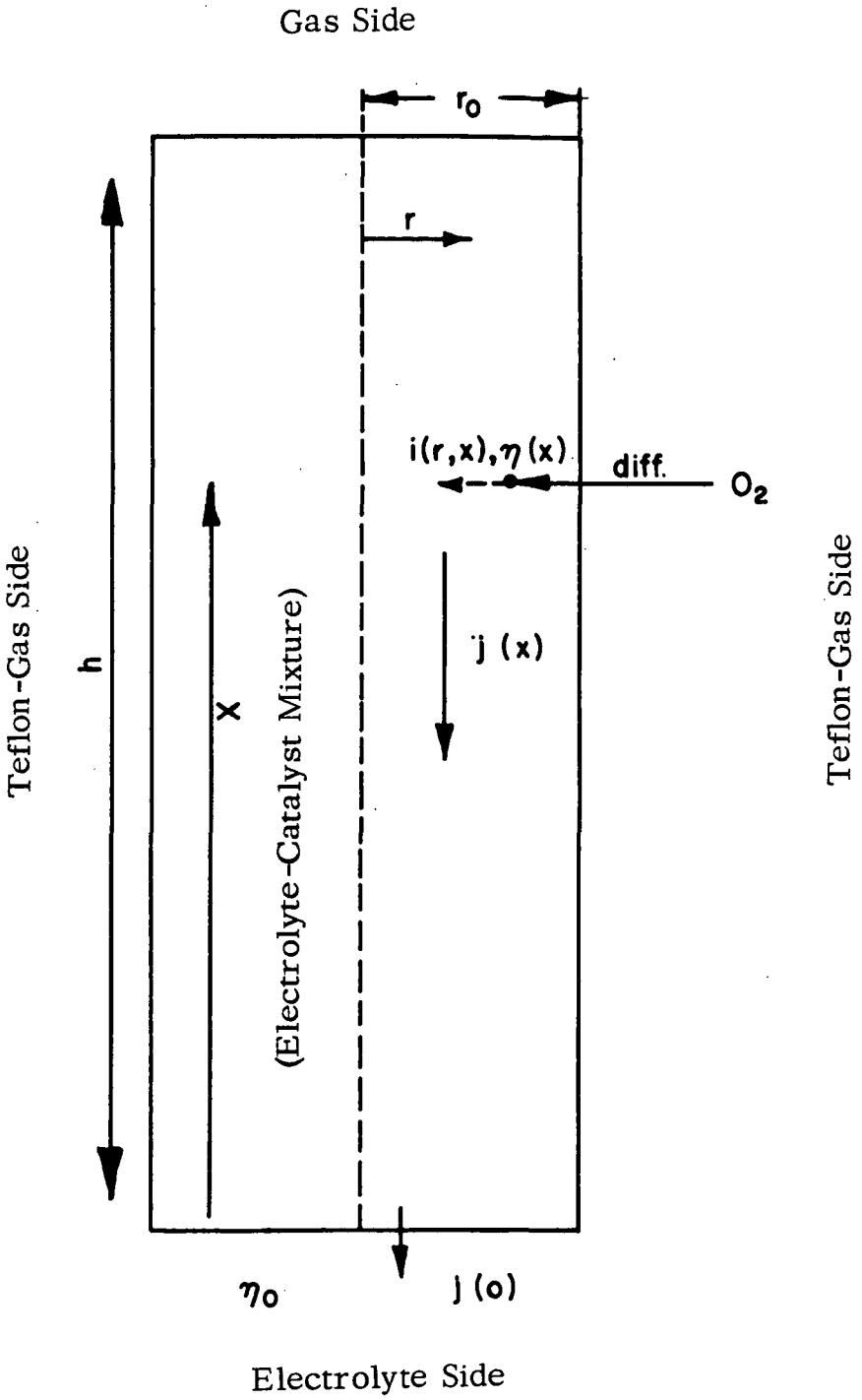

Fig. 120. Schematic representation of a flooded cylinder

2. Electrolyte and catalyst are homogeneously mixed as a continuum.

3. The intrinsic activity of the catalyst is constant throughout the cylinder.

4. Equilibration of electrolyte concentration in cylinders occurs efficiently via an evaporation-condensation process.

5. The local current density is directly proportional to the local concentration of reactant; i.e., an expression such as Eq. (1) is pertinent.

6. The voltage in the cylinder changes only in the axial direction, and diffusion of dissolved gas occurs only in the radial direction.

7. There are no transport limitations in the gas phase.

8. There are no kinetic limitations in the process of gas dissolution.

9. There is no electronic iR-drop in the cylinders.

10. Convection inside of the cylinders is low and has negligible effect on current. In order to extend the theory of a single cylinder to the complete electrode, we will further assume at this point that:

11. The radius of all porous cylinders has the same value. (Under these conditions the number of cylinders per cm^2 of electrode (N) is related to a measurable macroscopic factor, which we will call macroporosity (β), by the expression $\beta = 1 - N\pi r_o^2$).

The governing equations* are:

$$i = i_o \left[\frac{C(x, r)}{C_o} \exp\left[\alpha z \eta(x)/\phi\right] - \exp\left[-(1-\alpha) z \eta(x)/\phi\right] \right] \tag{1}$$

$$\bar{D}\left(\frac{\delta^2 C}{\delta r^2} + \frac{1}{r}\frac{\delta C}{\delta r}\right) = \frac{i\gamma}{nF} \tag{2}$$

With boundary conditions: $\frac{\delta C}{\delta r} = 0$ at $r = 0$ and $C = C_o$ at $r = r_o$

---

*For list of symbols, see page 230.

$$\frac{d\eta}{dx} = - \frac{j(x)}{\pi r_o^2 \bar{\kappa}} \tag{3}$$

and

$$- \frac{dj(x)}{dx} = 2\pi\gamma \int_o^{r_o} irdr \tag{4}$$

The solutions are:

$$C = C_o \exp\left(-\frac{z\eta}{\phi}\right) + C_o \left[1 - \exp\left(-\frac{z\eta}{\phi}\right)\right] \frac{I_o\left(q\frac{r}{r_o}\right)}{I_o(q)} \tag{5}$$

which in combination with Eq. (1) yields an equation relating the local current (i) with the radial coordinate.

In this equation, I_o is the modified Bessel function of zero order and

$$q = \left[\frac{\gamma i_o r_o^2}{nF\bar{D}C_o} \exp\frac{\alpha z\eta}{\phi}\right]^{1/2} \tag{6}$$

is the parameter of radial utilization

(This parameter is very important on the treatment of the flooded agglomerate model since it determined the utilization in depth of the agglomerates for oxygen reduction. The physical meaning of q can be understood by defining:

$$I_{act} = \gamma i_o r_o \exp\frac{\alpha z\eta}{\phi} \qquad \text{and} \qquad J_{diff} = \frac{nF\bar{D}C_o}{r_o}$$

so that:

$$q = \left(\frac{I_{act}}{I_{diff}}\right)^{1/2}$$

I_{act} is the current that would be obtained under exclusive activation control from a block with 1 cm^2 surface and r_o thickness, made of the catalyst of bulk area γ, and I_{diff} is the diffusion

limiting current density obtained if the reactant were to be consumed at one of the surfaces of the same porous block after diffusing through it. Obviously q will be large when diffusion control is more important than activation control.)

Another solution relates the local polarization to the transversal coordinate (x):

$$\frac{d^2\eta'}{dx'^2} = \frac{2nF\bar{D}C_o h^2}{\eta_o \kappa r_o^2} \left[1 - \exp\left(-\frac{z\eta_o}{\phi}\eta'\right)\right] \frac{q I_1(q)}{I_o(q)} \tag{7}$$

Boundary conditions: $\eta' = 1$ at $x' = 0$, $d\eta'/dx' = 0$ at $x' = 1$. (I_1 is the modified Bessel function of order 1).

The total current per cylinder across the surface x = constant, is

$$j(x) = -\frac{\pi \bar{\kappa} r_o^2 \eta_o}{h} \frac{d\eta'}{dx'} \tag{8}$$

The current density per unit area of electrode surface I (o) is

$$I(o) = \frac{-\bar{\kappa}\eta_o (1 - \beta)}{h} \left(\frac{d\eta'}{dx'}\right)_{x' = 0} \tag{9}$$

Using the indicated mathematical treatment, the following conclusions have been obtained (some of which concerned the specific case of reduction of oxygen in 30% KOH at 80°C):

1. The model allows one to predict not only the utilization of the catalyst across the thickness of the electrode (transversal utilization), but also the utilization of the catalyst along the radius of the flooded agglomerate. As a consequence, in addition to often studied variables such as porosity (macro- and micro-), bulk area, etc., the importance of agglomerate size is shown. A parameter (q) which determines the radial current distribution in an agglomerate is introduced and quantitatively defined as a function of diffusion coefficient, microporosity, solubility of reactant gas, exchange current, bulk surface area, local potential and agglomerate radius.

2. For the specific example of the oxygen reduction on Teflon-bonded Pt electrodes in 30% KOH at 80°C, a good radial distribution is obtained for agglomerate sizes below 1 micron and polarizations up to 300 mV. Under similar conditions the transversal utilization of the electrode is very good (very low internal iR drops).

3. For the same example, both the radial utilization of agglomerates and the transversal utilization of the electrode become poor at higher current drains ($i > 300$ mA/cm^2), and with poor structures (low microporosity and large agglomerate size).

4. For good transversal utilization of the electrode and good radial utilization of the agglomerate, the Tafel plot is obviously the same as that obtained with a smooth electrode. If, on the other hand, the transversal utilization of the electrode is good but the radial utilization of the agglomerate is very poor, a linear relationship is predicted with a Tafel slope twice that of the smooth electrode.

5. The present model and, more specifically, the parameter of radial distribution (q) introduced here can be used to design more efficient hydrophobic gas diffusion electrodes by predicting the maximum agglomerate size tolerable. When due to a high ratio of diffusion to activation control for a certain electrode reaction, high values of q are obtained for all reasonable agglomerate sizes, the model suggests the use of porous, conductive, but catalytically inactive agglomerates which have been activated with catalyst only on their periphery.

6. The proposed model cannot be used without further modification to predict quantitatively the performance of electrodes with high exchange current as the hydrogen electrode in acid electrolyte, because the parameter q becomes too large and the assumption of a continuum distribution of catalyst and electrolyte does not apply.

C. The Anodic Mode of the Oxygen Electrode

The mathematical treatment of the Teflon-bonded electrode discussed above can be extended without much modification to the case of O_2-evolution. Here, in particular, we want to consider under what conditions bubbling may occur inside of the flooded agglomerates. This is of interest because, as it has been shown in the experimental part of this work, gas bubbling in the interior of a highly developed platinized platinum surface results in significant breakage of this surface. A similar type of damage may be expected if bubbling occurs inside the platinum agglomerates of a Teflon-bonded structure. The same governing equations presented above apply also to oxygen evolution. Furthermore, under conditions of large values of $[\exp - (1 - \alpha)\, z\eta(x)/\phi]$ as one would find at E = 1.8 V, some simplifications can be performed. Thus Eq. (1) converts to:

$$i \approx - i_o \exp [- (1 - \alpha)\, z\eta(x)/\phi]$$

which says that, under these conditions, the local current is independent of the local concentration.

Eq. (2) also remains valid, but since i is negative (anodic), $\frac{i\gamma}{nF}$ is a source of oxygen instead of being a sink term.

With that, Eq. (5) can be converted to:

$$C = C_o \left[\frac{I_o (q \frac{r}{r_o})}{I_o (q)} + e^{-z\eta/\phi} \left(1 - \frac{I_o (q \frac{r}{r_o})}{I_o (q)} \right) \right] \qquad (10)$$

Since $I_o(x) \rightarrow 1$, when $x \rightarrow 0$ and $e^{-z\eta/\phi}$ is very large, the second term of Eq. (10) is an indeterminate. To solve this indeterminate, a series expansion of the Bessel function has to be performed as:

$$I_o(x) = 1 + \frac{x^2}{2^2} + \frac{x^4}{2^4 (2!)^2} + \qquad (11)$$

Using the two first terms of this series, Eq. (10) converts for small values of q into:

$$C = C_o \left[1 + e^{-z\eta/\phi} \; 1 - \frac{1 + \frac{q^2 (\frac{r}{r_o})^2}{4}}{1 + q^2/4} \right] \qquad (12)$$

or

$$C = C_o \left[1 + e^{-z\eta/\phi} \; \frac{1}{4} \; \frac{q^2 [1 - (\frac{r}{r_o})^2]}{1 + q^2/4} \right] \qquad (13)$$

or

$$C = C_o \left[1 + \frac{1}{4} \; e^{-z\eta/\phi} \; q^2 \left(1 - (\frac{r}{r_o})^2 \right) \right] \qquad (14)$$

Or substituting the value of q in Eq. (14), one obtains:

$$C = C_o \left[1 + \frac{1}{4} \; \frac{\gamma \, i_o r_o^2}{nF\bar{D}C_o} \; \exp - (1 - \alpha) \; z\eta/\phi \; \left(1 - (\frac{r}{r_o})^2 \right) \right] \qquad (15)$$

$$\frac{C - C_o}{C_o} = \frac{1}{4} \left[\frac{\gamma \, i_o r_o^2}{nF\bar{D}C_o} \; \exp - (1 - \alpha) \; z\eta/\phi \; \left(1 - (\frac{r}{r_o})^2 \right) \right] \qquad (16)$$

or

$$\frac{C - C_o}{C_o} = \frac{1}{4} \; q^2 \left(1 - (\frac{r}{r_o})^2 \right) \qquad (17)$$

$$\text{with} \qquad q' = \left[\frac{\gamma\, i_o r_o^{\,2}}{nF\bar{D}C_o} \exp - (1 - \alpha)\, z\eta/\phi \right]^{1/2} \tag{18}$$

It can be seen that q' has physical meaning similar to the previously defined parameter q of radial utilization for O_2-reduction, but it applies now to O_2-evolution. Eq. (17) can be plotted for different values of q' to show the degree of supersaturation as a function of r.

It is obvious that the maximum supersaturation occurs at the center of the cylinder at which:

$$\frac{C - C_o}{C_o} = \frac{1}{4}\, q'^2 \tag{19}$$

In order to judge the magnitude of maximum supersaturation (i.e., supersaturation at r = o), let us consider some probable values of the constant q' for 30% KOH at 30°C.

For this purpose, we can rewrite Eq. (18), if we assume a low value for the internal iR drop in the electrode (to be expected at the low current densities used for charge).

Under these conditions:

$$|I\,(o)| = h\,(1 - \beta)\,\gamma\, i_o \exp\,[-\,(1 - \alpha)\, z\eta/\phi] \tag{20}$$

where I (o) is the measured current density, h is the electrode thickness and β is the microporosity in the agglomerates, and Eq. (18) converts into:

$$q' = \left[\frac{r_o^{\,2}\; I\,(o)}{nF\bar{D}C_o\; h\,(1 - \beta)} \right]^{1/2} \tag{21}$$

Taking now into consideration that:

$$\bar{D} = \tau\,(1 - \theta)\, D \tag{22}$$

(where $\bar{D}$ and D are the effective and the actual diffusion coefficient, of O_2 in KOH at the given conditions, and τ and θ the tortuosity factor and the microporosity within the flooded agglomerate) and:

$$h\,(1 - \beta)\,(1 - \theta) = \frac{\omega}{\rho} \tag{23}$$

(where ω is the catalyst loading and ρ the density of the catalyst).

We obtain:

$$q' = \left[\frac{\rho\, r_o^{\,2}\; I\,(o)}{nFD\tau\omega C_o} \right]^{1/2} \tag{24}$$

We can now substitute in Eq. (24) the values pertinent to our operating conditions:

$\rho = 21\ g\ cm^{-2}$

$r_o \leq 10^{-4}$ cm (In ref. 73, it was concluded that, in order to explain the performance of the Teflon-bonded electrode, $r_o \leq 10^{-4}$ cm)

$|I(o)| = 2.5 \times 10^{-2}\ A\ cm^{-2}$

$n = 4\ equiv\ mol^{-1}$

$F = 96{,}500\ coul\ eq^{-1}$

$D = 0.6 \times 10^{-5}\ cm^2\ sec^{-1}$ (extrapolated from ref. 74)

$\tau = 1$ (assumption based on the high microporosity of the agglomerates and on the small size of Pt crystallites)

$\omega = 10^{-2}\ g\ cm^{-2}$

$C_o = 7.5 \times 10^{-8}\ g\ mol\ cm^{-3}$ (extrapolated from ref. 75)

Under these conditions

$$q' \leq 1.74$$

and according to Eq. (19)

$$\frac{C - C_o}{C_o} \leq 0.75$$

i.e., for 1 atm O_2 pressure the maximum supersaturation under the assumed conditions is of 0.75 atms. Supersaturations much higher than this value occur on the surface of highly activated electrodes before bubbling occurs. Thus Clamroth and Knorr[76] have reported a supersaturation corresponding to about 20 atm before H_2 bubbles are evolved on a highly activated Pd surface.

Regarding the effect of the different parameters on the degree of supersaturation (and therefore on the probability of bubbling), it is apparent that the most important factor is the agglomerate size because it appears in the equation to the second power. Thus an increase of agglomerate size from 1 μ to 10 μ would increase the theoretical supersaturation from 0.75 to 75 atm. It is obvious also that the difference $C - C_o$ is independent of C_o and therefore of the external O_2-pressure.

It should be noted here that, although "good" Teflon-bonded electrodes have a large ratio of agglomerate sizes equal to or smaller than 1 μ (otherwise one could not explain their performance), it is very probable that there are some agglomerates larger than this value. On the other hand, since the rate of oxygen evolution is independent of the depth of a catalyst surface inside of an agglomerate, oxygen evolution may cause bubbling inside of these agglomerates. How deleterious this bubbling is to the electrode structure will depend on the number of large size agglomerates and on their role in keeping the structure together. It appears, however, that homogeneity of electrode regarding agglomerate size is more important for rechargeable O_2-electrodes than for nonrechargeable oxygen cathodes.

LIST OF SYMBOLS

$C, C(r,x)$	Concentration of reactant gas at a point (r,x)
C_o	Solubility of reactant gas (mol $\times$ cm^{-1})
D	Diffusion coefficient of reactant gas in liquid (cm^2 $\times$ cm^{-1})
$\bar{D}$	Effective diffusion coefficient of reactant gas in liquid; affected by microporosity and tortuosity
F	Faraday constant
h	Thickness of electrode, cm
$i, i(r,x)$	Local real current density (A $\times$ cm^{-2})
i_o	"Real" exchange current density (A $\times$ cm^{-2})
I_o	Bessel Function of order zero
I_1	Bessel function of order one
$I(o)$	Electrode current density (A $\times$ cm^{-2})
$j, j(x)$	Current flowing through plane x of cylinder (A)
$j(o)$	Total current produced by cylinder (A)
N	Number of cylinders in one cm^2 of electrode
n	Number of electrons involved in electrode reaction
q	Parameter of radial distribution
R	Gas Constant
r	Radial coordinate in cylinder (cm)
r_o	Radius of cylinder (cm)
S	Surface area of catalyst (m^2 $\times$ g^{-1})
T	Absolute temperature (°K)
w	Catalyst load in electrode (g $\times$ cm^{-2})
x	Axial coordinate in cyclinder (also in electrode) (cm)
x'	Scaled axial coordinate
z	Stoichiometric number
α	Transfer coefficient
β	Macroporosity
γ	Surface to volume ratio, (cm^{-1}) in an agglomerate
$\eta, \eta(x)$	Overvoltage at plane (x), (volt)
η_o	Measured overvoltage, at plane x = 0, (volt)
η'	Scaled overvoltage ($\eta' = \eta/\eta_0$)
θ	Microporosity
κ	Ionic conductivity, (ohm^{-1} cm^{-1})
$\bar{\kappa}$	Effective ionic conductivity, affected by microporosity and tortuosity, (ohm^{-1} cm^{-1})
ρ	Catalyst density (g $\times$ cm^{-3})
ϕ	RT/F, (volt)

X. RECOMMENDATIONS

Based on these studies, there appears to be three main problem areas in the long-term operation of rechargeable oxygen electrodes, (1) the buildup of a refractory anodic layer on prolonged cycling which leads to a degradation in performance, (2) the dissolution and subsequent deposition of dendritic platinum in the separator leading to short-circuiting and loss of electrocatalyst, and (3) the disruptive effects of bubbling during gas evolution on charge. The effects that we have observed due to the addition of controlled amounts of impurities seem to be minimal which is not unexpected when dealing with actual fuel cell electrodes of high specific surface area. In addition, no hydrogen peroxide production is seen on such electrodes since a high activity for peroxide decomposition is maintained.

The buildup of the refractory anodic layer is not a catastrophic failure mode and it appears to be a self-regulating process. As more of this layer is formed, the oxygen electrode potential during discharge becomes more cathodic, thus increasing the rate of reduction of the layer. The process of reduction of the refractory oxide layer can be accelerated by periodic discharge at an increased rate which should result in regeneration of performance. It would be advisable to study this approach further with consideration of the duration of the regeneration period, the current densities required, the thermal effects of such a discharge, its effect on platinum dissolution, and its overall efficiency.

The problem of platinum dissolution is a more difficult one. We feel that it is intimately connected with the potentials reached during the cycling regime. Platinum appears to dissolve more readily after the platinum-oxygen layer is reduced. Therefore the Pt-O appears to impart some degree of passivity to the platinum. One approach to this problem of platinum dissolution would be to use a Pt-based noble metal alloy electrocatalyst such as Pt-Rh which may impart a greater degree of passivity to the anodic layer formed on charge. Another approach would be to decrease the surface area of the oxygen electrode catalyst by a factor of two. This would result in a corresponding decrease in the corrosion rate by a factor of two while a loss of only 40 mV polarization would result from the decreased surface area.

We have observed the disruptive effect of bubbling during gas evolution on platinized electrodes. Our work with Teflon-bonded platinum electrodes operated at 25 mA/cm^2 during charge has not shown this effect. Theory indeed predicts that this effect should be very small at this current density if the platinum agglomerates are under 1μ in size. However, the

presence of agglomerates of about 10μ could cause high internal bubbling. It seems advisable to control the agglomerate size and the homogeneity of the electrode regarding agglomerate size.

An additional comment is in order with regard to the operation of cadmium-oxygen cells. While we have shown that dissolved cadmium has no intrinsic poisoning effect on oxygen reduction, the presence of cadmiate species in the pores of the oxygen electrode seems undesirable. This is due to the large dependence of the solubility of Cd hydroxide on the KOH concentration. Thus, precipitation of $Cd(OH)_2$ in the porous oxygen electrode seems very likely and must be avoided.

XI. REFERENCES

1. R.F. Astrin and M.G. Klein, Electro-Optical Systems, Report on Contract NAS-3-10948, NASA CR-1683, November, 1970.

2. H.H. Hirsch, W.J. van der Grinten, W.N. Carson, and P.J. Moran, Report by General Electric, Technical Report ECOM-0257-3, Contract No. DAAB07-67-C-0257, April 1968.

3. Second Quarterly Report, Union Carbide Corp., Contract No. NAS5-10384, July 1-Sept. 30, 1967.

4. O.C. Wagner, Extended Abstracts, ECS Meeting, Montreal, October 1968, Abstract No. 360.

5. R. Thacker, Electrochim. Acta, 14, 433 (1969).

6. A. Damjanovic, M.A. Genshaw, and J.O'M. Bockris, J. Phys. Chem., 70, 3761 (1966).

7. A. Damjanovic, M.A. Genshaw, and J.O'M. Bockris, J. Electrochem. Soc., 114, 466 (1967).

8. L. Müller and L. Nekrasov, Electrochim. Acta, 9, 1015 (1964).

9. G. Bianchi and T. Mussini, Electrochim. Acta, 10, 445 (1965).

10. J. Giner, J. Electrochem. Soc., 111, 376 (1964).

11. W. Bold and M. Breiter, Electrochim. Acta, 5, 145 (1961).

12. N.A. Shumilova, G.V. Zhutaeva, M.R. Tarasevich, and R.Kh. Burshtein, Zh. Fiz. Khim., 39, 1012 (1965).

13. M. Breiter, J. Electroanal. Chem., 1, 38 (1964).

14. J. Giner and W.M. Krebs, Semiannual Report, Contract No. DAAB07-67-C-0447, March 1968.

15. L. Gierst, L. Vanderberghen, and E. Nicolas, J. Electroanal. Chem., 12, 462 (1966).

16. S. Gilman, in "Electroanalytical Chemistry," Vol. 2 A.J. Bard, Ed., Marcel Dekker, Inc., New York, 1967, p. 111.

17. J.P. Hoare, "The Electrochemistry of Oxygen," Interscience, New York, 1968, p. 13.

18. J. Giner, Z. Electrochem., 63, 386 (1959).

19. H.A. Laitinen and C.G. Enke, J. Electrochem. Soc., 107, 773 (1960).

20. S. Gilman, Electrochim. Acta, 9, 1025 (1964).

21. J. Giner, Electrochim. Acta, 4, 42 (1961).

22. M.W. Breiter, C.A. Knorr, and V. Volkl, Z. Electrochem., 59, 681 (1955).

23. F. Will and C. Knorr, Z. Elektrochem., 64, 258 (1960).

24. A. Reddy, M. Genshaw, and J.O'M. Bockris, J. Electroanal. Chem., 8, 406 (1964).

25. J.S. Mayell and S.H. Langer, J. Electrochem. Soc., 14, 438 (1964).

26. T. Biegler and R. Woods, J. Electroanal. Chem., 20, 73 (1969).

27. V.V. Sobol and B.I. Podlovchenko, Elektrokhimiya, 3, 1131 (1967).

28. S.B. Brummer, J. Phys. Chem., 69, 562 (1965).

29. S.B. Brummer, Report by Tyco Laboratories, Inc., Contract No. DA-44-009-AMC-410 (T), April 1965.

30. M. Becker and M.W. Breiter, Z. Elektrochem., 60, 1080 (1956).

31. T. Biegler, J. Electrochem. Soc., 116, 1131 (1969).

32. S.D. James, J. Electrochem. Soc., 116, 1681 (1969).

33. S. Shibata, Bull. Chem. Soc., Japan, 36, 525 (1963).

34. A. Kozawa, J. Electroanal. Chem., 8, 20 (1964).

35. L. Müller and L. Nekrasov, Electrochim. Acta, 9, 1015 (1964).

36. L. Müller and L. Nekrasov, J. Electroanal. Chem., 9, 282 (1965).

37. A. Damjanovic, M.A. Genshaw, and J.O'M. Bockris, J. Chem. Phys., 45, 4057 (1966).

38. A. Damjanovic, M.A. Genshaw, and J.O'M. Bockris, J. Electrochem. Soc., 114, 1107 (1967).

39. M.R. Tarasevich, Elektrokhimiya, 4, 210 (1968).

40. M.R. Tarasevich, Elektrokhimiya, 5, 713 (1969).

41. V.S. Bagotskii, V. Yu. Filinovskii, and N.A. Shumilova, Elektrokhimiya, 4, 1247 (1968).

42. V.S. Bagotskii, M.R. Tarasevich, and V.Yu. Filinovskii, Elektrokhimiya, 5, 1218 (1969).

43. Yu.B. Ivanov and V.G. Levich, Dokl. Akad, Nauk. SSR, 126, 1029 (1959).

44. V.G. Levich, "Physicochemical Hydrodynamics," Prentice Hall, Inc., Englewood Cliffs, N.J., 1962, p. 66.

45. M.R. Tarasevich, R.Kh. Burshtein, and K.A. Radyushkina, Electrokhimiya, 6, 372 (1970).

46. M. W. Breiter, "Electrochemical Processes in Fuel Cells," Springer-Verlag, Inc., New York, 1969, p. 193.

47. A. Damjanovic, M. A. Genshaw, and J. O'M. Bockris, J. Phys. Chem., 71, 3722 (1967).

48. K. F. Blurton and E. McMullin, J. Electrochem. Soc., 116, 1476 (1969).

49. J. D. E. McIntyre, J. Phys. Chem., 71, 1196 (1967).

50. J. D. E. McIntyre, J. Phys. Chem., 73, 4111 (1969).

51. B. Miller, J. Electrochem. Soc., 116, 1116 (1970).

52. A. C. Riddiford, in "Advances in Electrochemistry and Electrochemical Engineering," Vol. 4, P. Delahay, Ed., Interscience Publishers, New York, 1966, p. 96.

53. A. Damjanovic and V. Brusic, Electrochim. Acta, 12, 615 (1967).

54. A. Damjanovic, A. Dey, and J. O'M. Bockris, Electrochim. Acta, 11, 791 (1966).

55. W. F. Linke, "Solubilities of Inorganic and Metal-Organic Compounds," Vol. 1, American Chemical Society, Washington, D.C., 1958, p. 745.

56. P. C. Milner, J. Electrochem. Soc., 111, 228 (1964).

57. K. J. Vetter and D. Berndt, Z. Electrochem., 62, 378 (1958).

58. G. Grunemberg, Electrochim. Acta, 10, 339 (1965).

59. S. B. Brummer, J. Electrochem. Soc., 112, 633 (1965).

60. P. Malachesky, R. Jasinski, and B. Burrows, J. Electrochem. Soc., 114, 1104 (1967).

61. J. Giner, unpublished results.

62. A. N. Chemodanov, Ya. M. Kolotyrkin, and M. A. Dembrovskii, Elektrokhimiya, 6, 460 (1970).

63. D. C. Johnson, D. T. Napp, S. Bruckenstein, Electrochim. Acta, 15, 1493 (1970).

64. E. B. Sandell, "Colorimetric Determination of Traces of Metals," 3rd Ed., Interscience, New York, 1965, p. 726.

65. D. T. Napp, D. C. Johnson, and S. Bruckenstein, Anal. Chem., 39, 481 (1967).

66. J. Giner and S. Smith, Electrochem. Techol., 5, 61 (1967).

67. J. Giner, J. M. Parry, and L. Swette, Final Report by Tyco Laboratories, Inc. on Contract NASW-1233, June 1968.

68. R. W. Cranston and F. A. Inkley, Advances in Chemistry IX, Academic Press, New York, 1957, p. 143.

69. G. Halpert, Goddard Space Flight Center, A Fortran IV Program for Calculating and Plotting Surface Area and Pore Size Distribution Data Obtained by the BET Gas Adsorption Method.

70. M. Klug and L. Alexander, "X-Ray Diffraction Procedures," John Wiley and Sons, New York, 1961, p. 491.

71. E. B. Sandell, op. cit., p. 870.

72. J. Giner, J. M. Parry, S. Smith, and M. Turchan, J. Electrochem. Soc., 116, 1692 (1969).

73. J. Giner and C. Hunter, J. Electrochem. Soc., 116, 1124 (1969).

74. R. E. Davis, G. L. Horvath, and C. W. Tobias, Electrochim. Acta,

75. R. D. Walker, Jr., 4th Semiannual Report on NASA Research Grant NGR 10-005-022, August 31, 1967.

76. R. Clamroth and C. A. Knorr, Z. Elektrochem., 57, 399 (1953).